SYNTHESIS, STRUCTURE, AND REACTIVITY OF $\{CoNO\}^{8/9}$ SYSTEMS: DEVELOPMENT OF COBALT-BASED NITROXYL DONORS AND UNDERSTANDING THE FATE OF Co-NO

by

MELODY ANNA RHINE WALTER

(Under the Direction of Todd C. Harrop)

ABSTRACT

Metal-nitroxyl (M-HNO/M-NO^-) complexes represent critical intermediates in the global nitrogen cycle. Free nitroxyl has pharmacological and therapeutic advantages distinct from $NO^\bullet$, such as the targeting of thiols and Fe^{III}-hemes. HNO also increases heart muscle strength as a positive cardiac inotrope (increases myocardial contractility) and increases plasma levels of the calcitonin gene-related peptide (CGRP), whose cardiovascular effects include vasodilation. However, the rapid dimerization of HNO to N_2O and H_2O necessitates the use of donor molecules for HNO therapeutics. Current donors have limitations such as concomitantly releasing toxic by-products, short half-lives, and releasing $NO^\bullet$. There is a need for further development of HNO donors and improvement of our understanding of the fate of metal-nitroxyl complexes in the presence of relevant signaling agents, such as H^+, O_2, and RSH including H_2S/HS^-. Our efforts involve the rational design, synthesis, and development of $\{CoNO\}^{8/9}$ complexes with N_4 tetradentate supporting ligands for HNO delivery and investigation of the fate of Co-coordinated NO^-. Given the paucity of literature on the reactivity of $\{CoNO\}^8$ and $\{CoNO\}^9$ complexes, we have investigated their ability to react with HNO targets such as PPh_3 and [Fe(TPP)Cl] to afford

Ph_3PO/Ph_3PNH or the $\{FeNO\}^7$ porphyrin, respectively (Chapter 2). $\{CoNO\}^9$ complexes also react with a water-soluble Mn^{III}-porphyrin and metmyoglobin to afford the corresponding nitrosylated species (Chapter 3). In organic solvents, $\{CoNO\}^8$ complexes are unreactive in the presence of HNO targets; however, in the presence of a stoichiometric amount of protons, HNO reactivity is seen. In contrast, $\{CoNO\}^9$ complexes react rapidly with HNO targets in both organic and aqueous media. These results indicate that $\{CoNO\}^{8/9}$ complexes liberate HNO/NO^- and serve as a potential platform for release of this therapeutic. Finally, we show H_2S/HS^--induced release of HNO from an otherwise unreactive $\{CoNO\}^8$ complex in aqueous media (pH 7.4, 298 K; Chapter 4). These results indicate the key interplay of small molecules mediated at a metal center. Described in this dissertation are the synthesis, characterization, and reactivity studies of a series of $\{CoNO\}^{8/9}$ complexes, which indicate their utility as HNO/NO^- donors and as effective systems for investigation of metal-mediated crosstalk of known signaling agents.

INDEX WORDS: Nitroxyl, Nitroxyl donor, Cobalt, Nitric Oxide, Metal nitrosyl

SYNTHESIS, STRUCTURE, AND REACTIVITY OF $\{CoNO\}^{8/9}$ SYSTEMS: DEVELOPMENT OF COBALT-BASED NITROXYL DONORS AND UNDERSTANDING THE FATE OF Co-NO

by

MELODY ANNA RHINE WALTER

A.A., Emory University, 2007

B.S., Emory University, 2009

A Dissertation Submitted to the Graduate Faculty of The University of Georgia in Partial Fulfillment of the Requirements for the Degree

DOCTOR OF PHILOSOPHY

ATHENS, GEORGIA

2016

SYNTHESIS, STRUCTURE, AND REACTIVITY OF $\{CoNO\}^{8/9}$ SYSTEMS: DEVELOPMENT OF COBALT-BASED NITROXYL DONORS AND UNDERSTANDING THE FATE OF Co-NO

by

MELODY ANNA RHINE WALTER

Major Professor:	Todd C. Harrop
Committee:	Michael K. Johnson
	Jeffrey L. Urbauer

Electronic Version Approved:

Suzanne Barbour
Dean of the Graduate School
The University of Georgia
August 2016

ACKNOWLEDGEMENTS

I would like to express my gratitude to my Ph.D. advisor Prof. Todd C. Harrop. I appreciate all of the feedback, time, and energy that you have invested in me and all members (past, present, and future) of the Harrop lab. Your input helps us hone our scientific skills and evolve into the scientists we are. Having a Ph.D. advisor who invests so much in his students is not very common, and we are fortunate to learn from such a dedicated scientist. I am confident that I am a more insightful, purposeful scientist and person as a result of your mentorship throughout my graduate school experience.

I would also like to thank my committee members Prof. Michael K. Johnson and Prof. Jeffrey L. Urbauer for sharing their insight, expertise, and instruments during my time at UGA. Thank you for your letters of recommendation and continued support. Thank you to my college professors Prof. Heather Patrick, Prof. Brenda Harmon, Prof. Jack F. Eichler, and Prof. Cora MacBeth, for helping me to realize my interest in chemistry and chemical research as well as for sharing your valuable thoughts at each step in my professional journey. Thank you to Dr. Dongtao Cui, Dr. Greg Wyllie, and Henry Niedermaier for assistance with NMR, Dr. Pingrong Wei and Prof. Marilyn Olmstead for assistance with X-ray crystallography, and Dr. Dennis Phillips and Dr. Chau-wen Chou for assistance with MS experiments.

Thank you to my Harrop labmates, past and present: Ellen Broering, Phan Truong, Ramsey Steiner, Vivian Ezeh, Eric Gale, and Brian Sanders for all of our discussions, scientific and otherwise. Brian- thanks for all of your help in training me and for your scientific feedback, while you were at UGA and even beyond.

Thank you to Mom and Dad for giving me all of the tools I need to take on the adventure of life. Thank you to my brother Marlon and sister-in-law Nancy for all of your continued love and support. I would also like to thank the great friends I have made in graduate school, especially Briana Flaherty and Tara Bracken, who are kind enough to remind me that there is always time for pie.

Thank you to Steven, for understanding that 20 minutes of "lab time" actually means 1 – 2 hours. Thank you for all of the love, encouragement, camaraderie, and support. I am incredibly lucky that you are my life partner.

TABLE OF CONTENTS

Page

CHAPTER 1

INTRODUCTION AND LITERATURE REVIEW

1.1 Metalloenzymes of the global nitrogen cycle with a focus on NO_x (x = 1, 2) conversions

Nitrogen is an essential component of our solar system and earth's atmosphere. Indeed, for every 100 atoms of carbon that are incorporated into cellular life, between 2 and 20 nitrogen atoms will follow depending on the life form, and 79% of the atmosphere is composed of molecular nitrogen.[1] The global nitrogen cycle (GNC) encompasses the nitrogen-based transformations found on the planet and utilizes an intricate network of metalloenzymes to perform such chemistry (Figure 1.1). Despite its complexity, the GNC has been in balance prior to the substantial anthropogenic contributions from the 21st century.[2-3] This cycle is composed of five main pathways: nitrogen fixation ($N_2 \rightarrow NH_4^+$), nitrification ($NH_4^+ \rightarrow NO_3^-$), denitrification ($NO_3^- \rightarrow N_2$), nitrate reduction to ammonium ($NO_3^- \rightarrow NH_4^+$), and anaerobic ammonium oxidation to nitrogen (anammox; $NH_4^+ \rightarrow N_2$; see Figure 1.1). These pathways accomplish changes to the oxidation state of nitrogen from its most oxidized form (NO_3^-) with nitrogen in the +5 oxidation state to its most reduced form (NH_4^+) with nitrogen in in the −3 oxidation state. Enzymes found in Nature are responsible for these dramatic chemical transformations, and all of these enzymes contain active site metal ions.

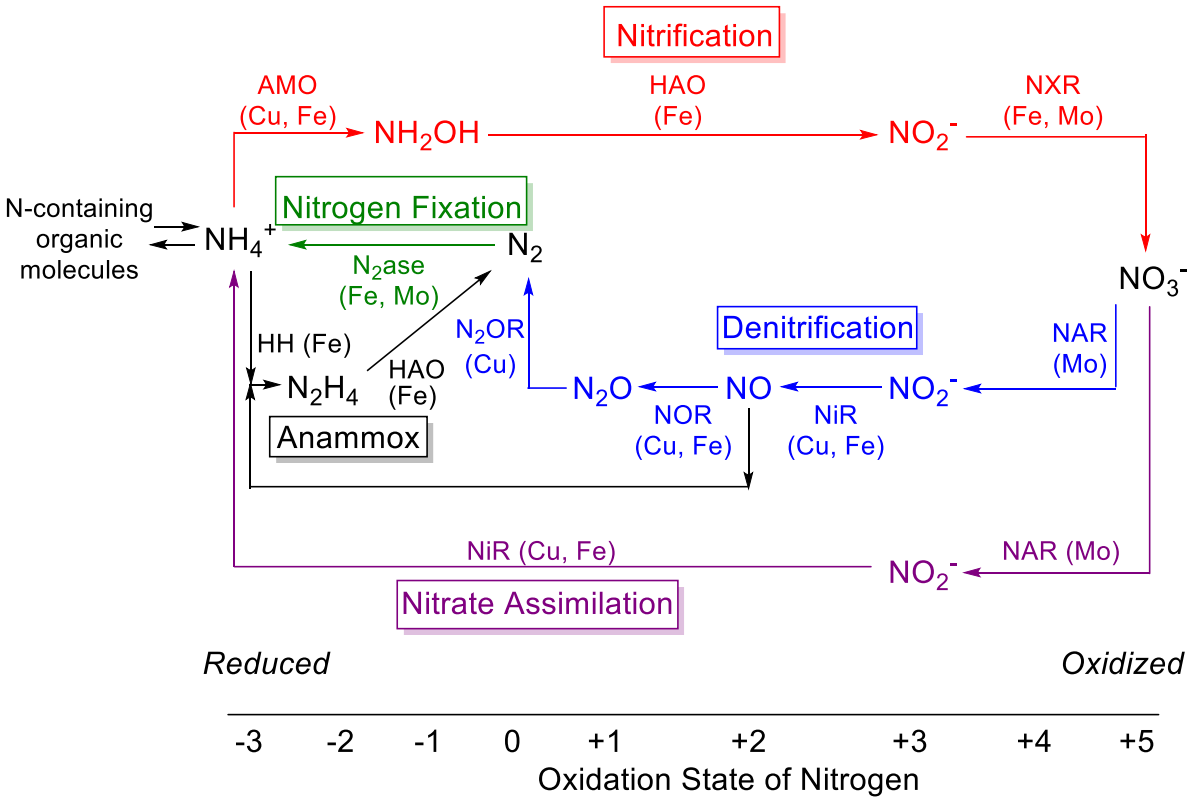

Figure 1.1. Major biological transformation pathways in the global nitrogen cycle. Color scheme: Dissimilatory denitrification (blue), nitrate assimilation (purple), nitrogen fixation (green), anaerobic ammonium oxidation or anammox (black), and nitrification (red). NO_3^-, N_2, and NH_4^+ are in black font due to participation in multiple pathways. Metals highlighted beneath each enzyme are the metals present in the metallocofactors. Metalloenzyme abbreviations: NAR = nitrate reductase; NiR = nitrite reductase; NOR = nitric oxide reductase; N_2OR = nitrous oxide reductase; N_2ase = nitrogenase; HH = hydrazine hydrolase; HAO = hydroxylamine oxidoreductase or hydrazine oxidoreductase; AMO = ammonium monooxygenase; NXR = nitrite oxidoreductase. Of the pathways depicted, nitrification ($NH_3 \rightarrow NO_3^-$) is the only pathway that is facilitated aerobically. Adapted from references 2 and 4.[2,4]

For example, nitrogen fixation involves the most formidable conversion in the fixing of free nitrogen, breaking the triple bond of N_2 (bond dissociation energy = 946 kJ/mol)[5], and performing the six-electron reduction to release two equivalents of NH_3.[6] In the process, two additional electrons are used for the production of H_2. Anaerobic bacteria are capable of such energetically costly chemistry with the metalloenzyme nitrogenase (N_2ase; Eq 1.1)

$$N_2 + 8H^+ + 16ATP + 8e^- \rightarrow 2NH_3 + H_2 + 16ADP + 16P_i \text{ (Eq. 1.1)}$$

Although there are three mechanistically-related families of N_2ase, the most extensively studied is the Mo-dependent enzyme, which utilizes two separate metal-containing proteins.[7-8] The first is the Fe protein, which contains a [4Fe-4S] cluster, and the second is the MoFe protein, which consists of the [8Fe-7S] P-cluster and FeMo-cofactor (FeMo-co; [7Fe-9S-Mo-C-homocitrate]). The proposed site of N_2 reduction is FeMo-co through a series of intermediates and proton-coupled one-electron reductions.[9-11] Large quantities of NH_3 are needed as an industrial feedstock for fertilizer in order to feed the growing worldwide population. For the US alone, 16.2 million tons of NH_3 were produced annually, 80% of which is used for fertilizer based on a 1996 estimate, and its production has grown ~1% annually since 1974.[12] As such, the Haber-Bosch process is industrially implemented to mimic the $N_2 \rightarrow NH_3$ reaction.[13-14] It accomplishes this same chemistry using high temperature (400°C to 650°C) and pressure (200 to 400 atm). In 2010, Haber-Bosch produced 133 megatons of NH_3, which helps to sustain the global population. By 2025, it is estimated that more than half of the world's food production will depend on NH_3 from the Haber-Bosch process.[15] Nature is capable of the $N_2 \rightarrow NH_3$ transformation at ambient temperature and pressure, which highlights just one example of the keen ability of finely-tuned metalloenzymes to mediate such challenging chemistry with the use of specific metal-ligand combinations.

Other nitrogen oxides (NO_x), namely NO_2^- and NO_3^-, have become increasingly prevalent in groundwater and wastewater alike,[16] and waste from industrial processes, mining, power plants, and agriculture (vide supra) have all contributed to the significant rise in levels of these potentially toxic NO_x species.[17] These particular NO_x are toxic to both the environment and human health, and as such, organizations like the EPA and World Health Organization have set limits to the levels of exposure to NO_3^- (50 mg/L) and NO_2^- (3 mg/L).[18] In fact, there are various implications of high-level exposure to NO_x ions, including coma and death,[19-20] and exposure to higher levels of NO_3^- and NO_2^- has been linked to possible increased frequency of cancer, brain tumors, leukemia, and nasopharyngeal tumors in both children and adults.[16,21-22] Environmental remediation reduces or manages the risk to human health by removing or controlling environmental pollutants,[23] and as a result of the increasing NO_x production from industrial by-products, it is imperative that methods are developed to remediate ground- and wastewater of NO_3^-/NO_2^-. In fact, anammox bacteria[24-25] and enzymes such as cytochrome P450 monooxygenases[26] are currently being used in addition to artificial systems for bioremediation. Taking a cue from Nature (vide infra), metal-based small molecules capable of NO_x reduction are a logical route for this chemistry.

Nature demonstrates the ability to reduce nitrogen oxides in bacteria and fungi in biological denitrification, in which metalloenzymes containing metals such as Fe, Cu, and Mo facilitate the reduction of NO_3^- to N_2 via four discrete steps (Figure 1.1).[27] In fact, some nitrite reductases (NiRs) and nitric oxide reductases (NORs) go through iron-nitroxyl $\{FeNO\}^8$ or $\{FeHNO\}^8$ intermediates, formally described as Fe^{II}-NO^- or Fe^{II}-HNO, in their catalytic cycle.[28] Due to the electron delocalization within metal nitrosyl bonds, the Enemark-Feltham notation $\{MNO\}^n$ is utilized to define the valence electron count within the entire metal nitrosyl moiety. In this case, n is the number of electrons in the d manifold of the metal plus the number of electrons in the π^*

orbital of the nitrosyl.[29] For example, cytochrome *c* nitrite reductase (C*c*NiR), found in denitrifying bacterial anaerobes, catalyzes the reduction of NO_2^- to NH_3 without the concomitant release of $NO^\bullet$ or NH_2OH.[30] Binding of NO_2^- to the C*c*NiR heme Fe^{II} active site leads to subsequent heterolytic cleavage of the N-O bond, forming an $\{FeNO\}^6$ intermediate and H_2O (Figure 1.2). A low-spin (LS) $\{FeHNO\}^8$ intermediate is implicated as a result of two sequential one-electron reductions of the transiently formed $\{FeNO\}^6$ and $\{FeNO\}^7$ followed by protonation (Figure 1.2). Model complexes that utilize a picket-fence porphyrin to stabilize a LS $\{FeHNO\}^8$ ($t_{1/2}$ ~5 h) support the possibility of NH_3 production as they produce high yields of NH_3 in the presence of acid upon reduction of the corresponding $\{FeNO\}^7$ species (using potentials < –1.1 V vs. ferrocenium/ferrocene (Fc^+/Fc)).[31] Although experimental insight into the mechanism of multiheme C*c*NiR is limited, computations[30] and electrochemical experiments[31-33] support the presence of an $\{FeHNO\}^8$ intermediate.

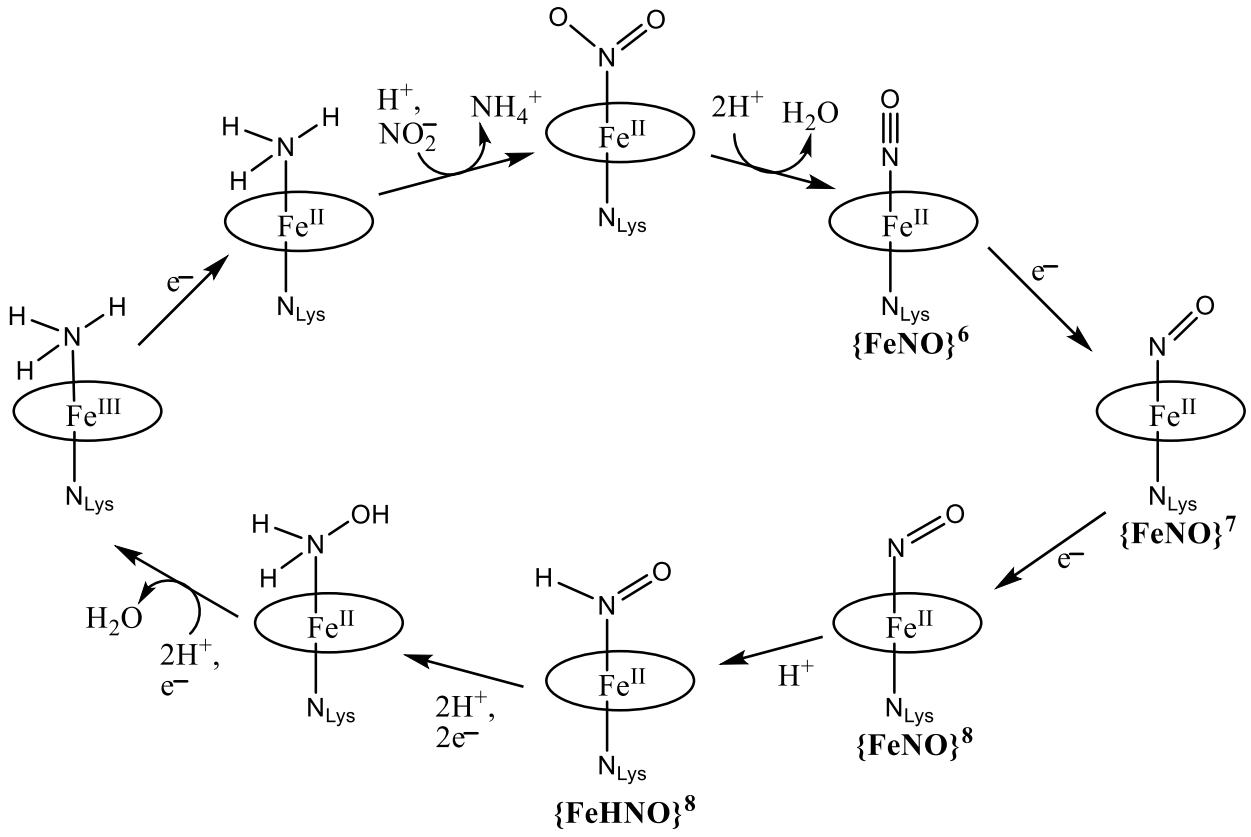

Figure 1.2. Proposed reaction mechanism for C*c*NiR. Adapted from reference 30.[30]

There are many examples of NORs in which Fe-nitroxyls are observed or implicated. Fungal respiratory NORs (rNORs), found in denitrifying organisms, are a cytochrome P450-type enzyme that binds NO• to an Fe^{III}-heme active site, forming an $\{FeNO\}^6$ species.[34] Experimental evidence shows that a direct hydride transfer from NADH forms the corresponding Fe-nitroxyl intermediate, which is then either (a) attacked by a second equivalent of NO•, thus forming the N-N bond and following protonation, forms N_2O, H_2O, and the Fe^{III}-heme or (b) first protonated to form Fe^{IV}-N(–)HOH or Fe^{III}-N(•)HOH that subsequently reacts with NO• to form the same products, to close the catalytic cycle[35] (Figure 1.3). $\{FeNO\}^8$ intermediates are also proposed for

bacterial rNORs that are cytochrome *c*-dependent (NorBC) and quinol-dependent (qNOR). In cytochrome *c* oxidases, NorBC enzymes contain an unusual dinuclear active site with a *b* heme connected via a μ-oxo bridge to a non-heme Fe (Fe_B) that is ligated with three histidines and one glutamate, with the two Fe centers being 3.9 Å apart (Figure 1.4).[27,36] When in the reduced state, the μ-oxo ligand dissociates from Fe_B which then likely moves away from heme *b* to activate the first equivalent of $NO^{\bullet}$ to generate an Fe^{II}-NO^{-} ($\{FeNO\}^8$) intermediate (Figure 1.4).[37] An alternative proposal suggests a potential bridging coordination between the two Fe centers (Fe-N-O-Fe).[38] Nearby heme *c* is a likely electron source. A bridging hyponitrite intermediate is then proposed to form after the second equivalent of $NO^{\bullet}$ reacts to form the N-N bond. Protons are then shuttled from bulk water through a channel to the active site in order to facilitate N-O bond cleavage with the resulting formation of N_2O and H_2O (Figure 1.4).[36] qNORs, which are similar to NorBC except menahydroquinone is the electron donor, are proposed to transform $NO^{\bullet}$ to N_2O in a similar fashion. However, NorBC enzymes are more likely in denitrification as qNORs are present in several pathogens that are not denitrifiers.[39]

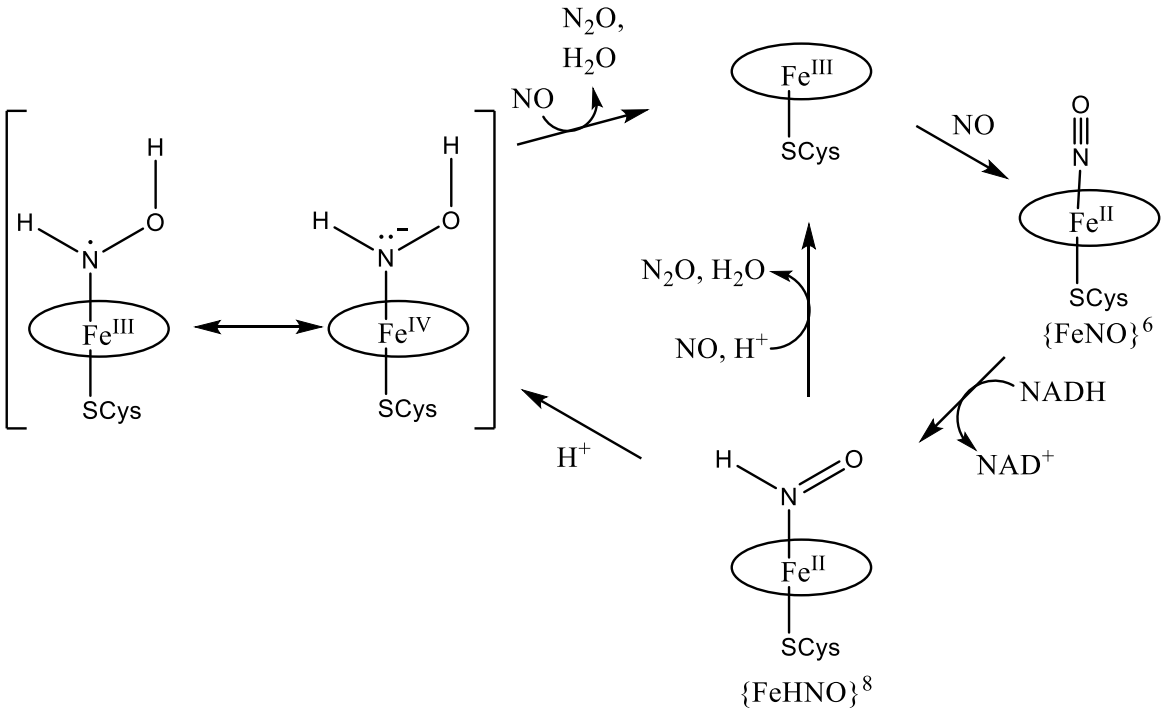

Figure 1.3. Proposed mechanism of fungal rNORs involving an $\{FeHNO\}^8$ intermediate, which forms as a result from direct hydride transfer from NADH. Adapted from reference 28.[28]

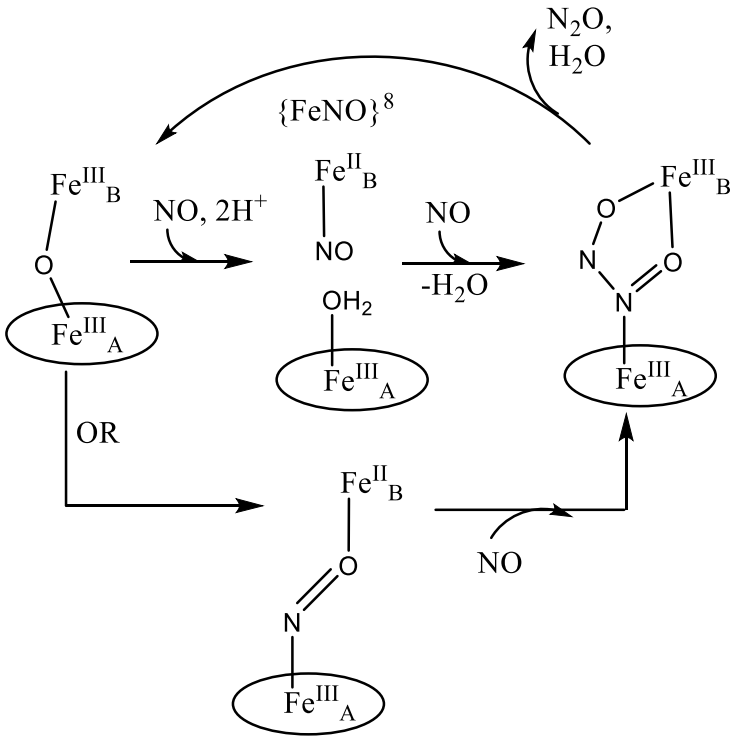

Figure 1.4. Proposed mechanism of NorBC and qNORs with heme Fe_A and non-heme Fe_B.

Similar to rNORs, flavo-diiron NO reductases (FNORs) found in pathogenic bacteria contain a non-heme diiron active site with a nearby flavin mononucleotide (FMN) cofactor less than 4 Å from the diiron site.[40] Each Fe center coordinates two His, one Glu, and one bridging Asp residue along with one bridging hydroxo, although an oxo or aqua bridge has not been conclusively eliminated.[41] With diferric ($Fe^{III}Fe^{III}$) being the resting state, the diferrous ($Fe^{II}Fe^{II}$) site is catalytically active, with reduced flavin mononucleotide ($FMNH_2$) serving as the two-electron source (Figure 1.5). Although many mechanisms have been proposed for FNORs, recent experimental evidence supports the formation of an antiferromagnetically coupled $Fe^{II}Fe^{II}$-dinitrosyl ($[\{FeNO\}^7]_2$, $S = 0$), where the NO moieties couple to release one equivalent of N_2O via formation of the $Fe^{III}Fe^{III}$-state in the rate determining step (Figure 1.5, pathway 1).[42] The $Fe^{III}Fe^{III}$-state is then reduced back to diferrrous using the two electron equivalents from the proximal $FMNH_2$; this active state can then undergo a second $2NO^{\bullet} \rightarrow N_2O$ turnover. A second "super-reduced" mechanism has been proposed involving the reduction of the $Fe^{II}Fe^{II}$-dinitrosyl ($[\{FeNO\}^7]_2$, $S = 0$) to form the corresponding $[\{FeHNO\}^8]_2$ in which HNO could dimerize to release N_2O and H_2O (Figure 1.5, pathway 2).[40,42] A third proposal, similar to the accepted rNOR mechanism, has the second equivalent of $NO^{\bullet}$ attacking the bridging (first equivalent) $NO^{\bullet}$ (Figure 1.5, pathway 3). However, pathway 1 is the most likely given experimental evidence of the $Fe^{II}Fe^{II}$ dinitrosyl ($[\{FeNO\}^7]_2$, $S = 0$).[42] In summary, biology uses metal centers to successfully transform NO_x species, often using reduced M-HNO intermediates to accomplish such feats.

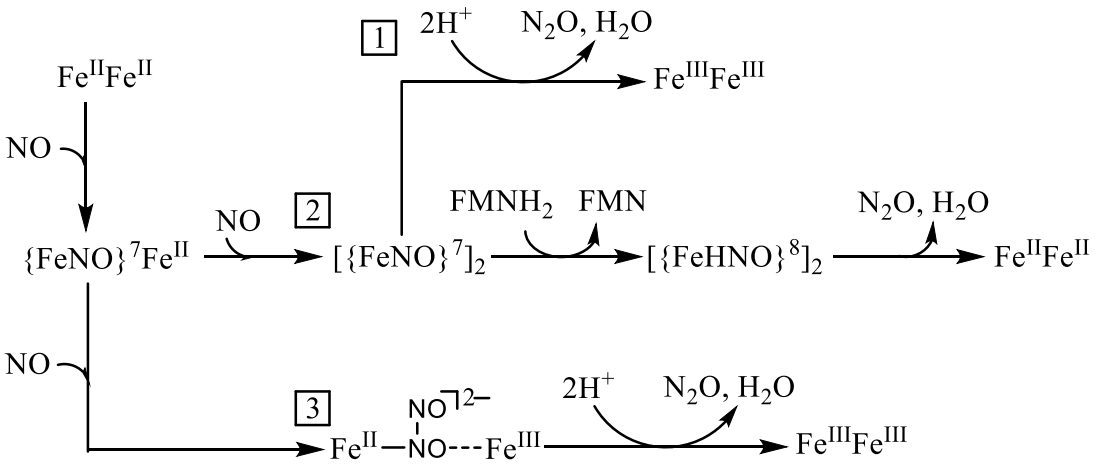

Figure 1.5. Three proposed mechanisms of FNORs, where $FMNH_2$ serves as the electron source. Based on experimental evidence, pathway 1 is most likely.[42]

1.2 Nitroxyl (HNO/NO^-) Chemistry and Pharmacology

1.2.1 Electronic features of HNO/NO^-

The role of nitric oxide ($NO^\bullet$) has been well established over the past few decades, culminating in the Nobel Prize in Physiology or Medicine for being the endothelium derived relaxing factor (EDRF).[43-46] $NO^\bullet$ serves as a gaseous signaling molecule in several physiological processes including vascular homeostasis, neurotransmitter function in both the central and peripheral nervous systems, and the immune response.[47] Given these roles, it plays a critical part in maintaining homeostatic health in the human body. Indeed, there are multiple sources of $NO^\bullet$ in physiology, including the three isoforms of NO synthase (NOS; endothelial, neuronal, and inducible)[47] and NO_2^-, whose vascular levels approach high μM quantities in vivo and serve as a reservoir for $NO^\bullet$.[48-51] $NO^\bullet$ donors such as sodium nitroprusside $Na_2[Fe(CN)_5(NO)]$ have been successful clinically as arterial and venous vasodilators and are widely used for surgeries (cardiac, vascular, pediatric), hypertensive crises, and heart failure.[52] Despite the expansive research and

utility of NO•, its one-electron reduced redox sibling nitroxyl (HNO/NO⁻, pK_a = 11.6[53]), has only recently been realized for its therapeutic potential and pharmacological implications that are distinct from NO•.[54] Before exploring these differences (vide infra), the electronic differences between NO• and its derivatives will be discussed.

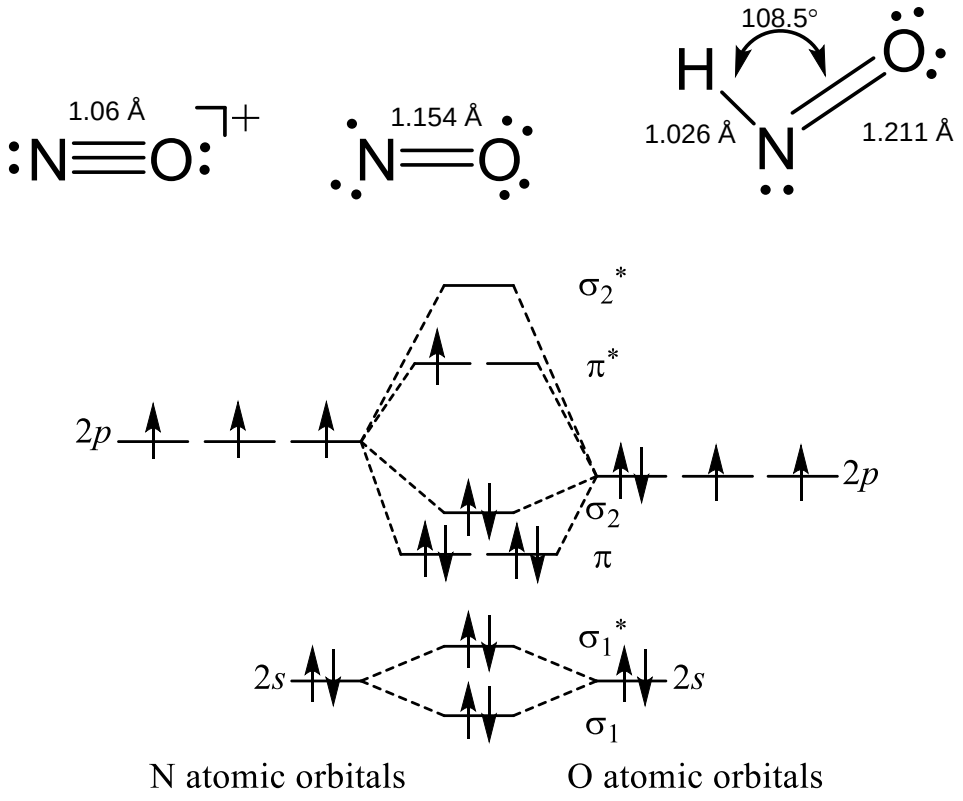

Figure 1.6. (*Top*) Structural features of NO^+, NO• and ^{1}HNO. (*Bottom*) Molecular orbital diagram of NO•. Note that the π^* HOMO will have 0, 1, or 2 electrons for NO^+, NO• and HNO respectively.

The neutral NO• contains one unpaired electron in a π^* MO, polarized towards the N atom (Figure 1.6). The radical nature governs the reactivity in which this diatom participates, and its chemistry is well-studied. Contrastingly, ^{1}HNO exhibits no unpaired electrons; however, it is either neutral when protonated as ^{1}HNO or monoanionic upon deprotonation to form $^3NO^-$. ^{1}HNO

contains two electrons in the π^* orbital and has a complicated acid-base relationship between the protonated and deprotonated states (Figure 1.7).[55] ^{1}HNO is energetically favored by 18-19 kcal/mol relative to the triplet state. On the contrary, $^3NO^-$ is the thermodynamically favored ground state by 16 kcal/mol versus the singlet isomer. Therefore, deprotonation of ^{1}HNO can occur via two pathways: (1) formation of $^1NO^-$ followed by an intersystem crossing to afford $^3NO^-$ or (2) deprotonation leading to direct formation of the energetically favored $^3NO^-$ in the absence of a $^1NO^-$ intermediate. Although an earlier proposal favored the first path,[56] experimental and theoretical evidence suggests that the ^{1}HNO/$^3NO^-$ equilibrium is more likely[53,57-61] and that this spin-forbidden process is considerably slower than typical acid-base reactions.[61]

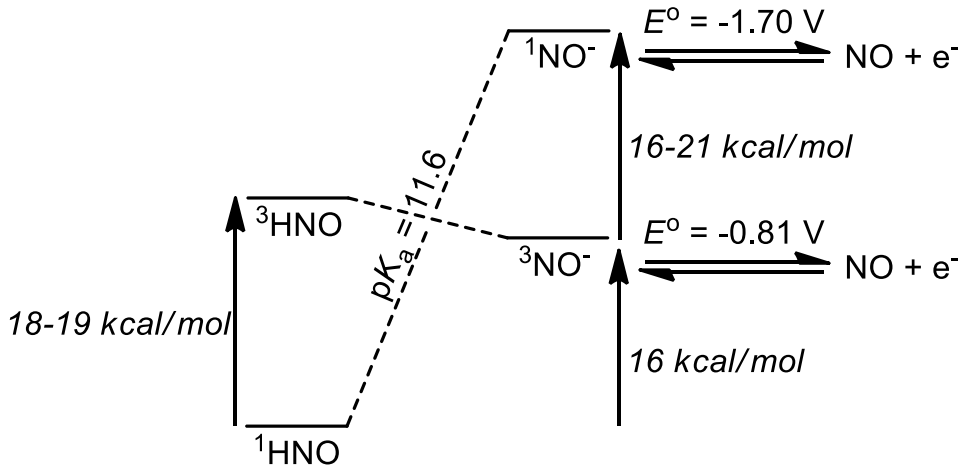

Figure 1.7. Thermochemical scheme of the acid-base and electrochemical properties (vs. NHE) of free nitroxyl. This scheme is a modified version from reference 62[62] and compiles values from references 58,[58] 63,[63] 53,[53] 64.[64] Figure reprinted with permission from reference 65.[65]

When coordinated to a metal center, the NO moiety engages in redox chemistry (termed non-innocence) and results in substantial delocalization throughout the MNO unit,[29] yet NO•,

HNO/NO^-, and nitrosonium (NO^+) may generally be distinguished from one another based on their spectroscopic and structural features. In particular, metals with a coordinated HNO/NO^- exhibit significant bending of the M-N-O bond angle and lower N-O stretching frequencies (ν_{NO}) in the FTIR spectrum due to the largest number of π^* electrons amongst NO derivatives (Figures 1.6 and 1.8).

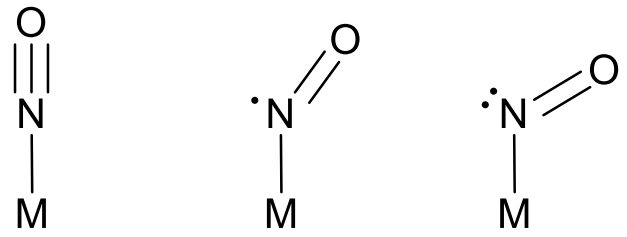

Parameters	**NO^+**	**$NO^\bullet$**	**NO^-**
e^- in π^*	0	1	2
Coordinated			
∠MNO (°)	~180	~140-150	~120
ν_{NO} (cm^{-1})	~1900	~1750	~1600-1400
Free			
ν_{NO} (cm^{-1})	2377	1875	1470

Figure 1.8. Trends of spectroscopic features for free[66-67] and metal-coordinated $NO^\bullet$, HNO/NO^-, and NO^+. The spin multiplicity of the ground states of free ^{1}HNO and $^3NO^-$ are singlet and triplet, respectively.

1.2.2 Pharmacological implications and potential sources of HNO/NO^-

Despite its structural similarity, nitroxyl has pharmacological and therapeutic advantages distinct from $NO^\bullet$ (Figure 1.9).[54-55,62-63,68-72] Such properties include the targeting of Fe^{III}-hemes and thiols. In fact, its reactivity with thiol groups to form an *N*-hydroxysulfenamide (RSNHOH) intermediate is one of the hallmark properties of HNO that is distinct from $NO^\bullet$ (vide infra). For

reference, HNO reacts with GSH ($k = 2 \times 10^6$ M^{-1} s^{-1}), which is present in mM quantities in the cytosol, 1000-times faster than NO•.[68] With respect to cardiovascular therapy, HNO exhibits a positive cardiac inotrope effect, thus increasing myocardial contractility, and elevation of levels of calcitonin gene-related peptide (CGRP), a small neuropeptide whose cardiovascular effects include vasodilation.[54,73] In fact, CGRP functions as a plasma biomarker for HNO reactivity whereas the biomarker for NO• is plasma cyclic guanosine monophosphate (cGMP), which has a negligible or negative inotropic effect. Additionally, HNO is resistant to scavenging by superoxide anion ($O_2^{\bullet-}$), a product of aerobic respiration although $^3NO^-$ does rapidly react with O_2 to form peroxynitrite ($ONOO^-$; 6×10^9 $M^{-1}s^{-1}$).[68] NO•, on the other hand, reacts with $O_2^{\bullet-}$ to form $ONOO^-$ ($4\text{-}7 \times 10^9$ $M^{-1}s^{-1}$;[74] Eqs. 1.2 and 1.3).

$$^3O_2 + {}^3NO^- \rightarrow OONO^- \qquad \text{(Eq. 1.2)}$$

$$O_2^{\bullet-} + NO^\bullet \rightarrow OONO^- \qquad \text{(Eq. 1.3)}$$

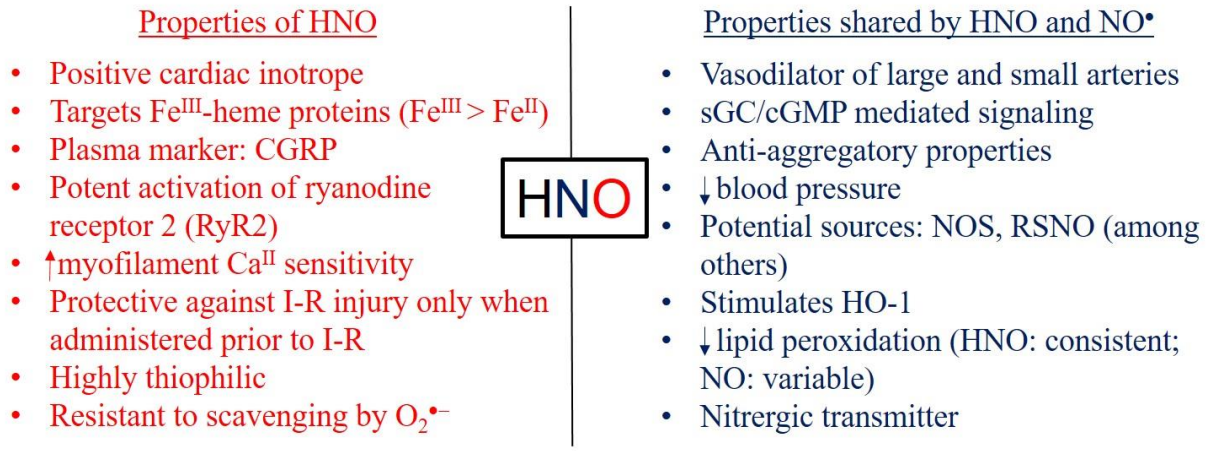

Figure 1.9. Properties of HNO relevant to the cardiovascular system that are distinct from NO• (*left*) and that are shared with NO• (*right*).

The pharmacological implications of HNO are related to cardiovascular physiology. Specifically, HNO can facilitate unloading of the myocardium through vasodilation via stimulation of soluble guanylyl cyclase (sGC) and a subsequent increase in cGMP. It is noteworthy that while HNO preferentially targets Fe^{III}- > Fe^{II}-hemes, it does stimulate Fe^{II} sGC which is an aberration from its typical Fe^{III} targets.[75] HNO is also capable of stimulating vascular smooth muscle cell ATP-sensitive and voltage-dependent K^+ channels. Although $NO^\bullet$ is capable of inducing vasodilation,[76-77] it does not induce myocardial contractions whereas HNO does. Indeed, HNO increases contractile strength of the heart muscle by prompting the release of Ca^{2+} from the sarcoplasmic reticulum (SR) through direct interactions with thiol groups of the ryanodine receptors (RyR2) in a cGMP-independent fashion.[78-79] It also encourages the reuptake of Ca^{2+} into the SR via stimulation of SR Ca^{2+}-ATPase and may play a role in anti-remodeling effects of the heart through an sGC/cGMP pathway. Finally, when administered prior to the event, HNO is protective against ischemic-reperfusion (I-R) injury, which is tissue damage that can occur after an ischemic or hypoxic event.[80] An ideal cardiovascular therapeutic, particularly for heart failure, will not only be capable of inducing vasodilation but also can induce contractions of the heart, both of which HNO is capable. Coupled with anti-aggregation (antithrombotic) and antioxidant properties, HNO could also be used for treatment of a myriad of other cardiovascular diseases such as atherosclerosis, angina, cardiomyopathy, and acute hypertensive crises. Therefore, the therapeutic potential of HNO is immense.

In spite of the vast number of pharmacological implications of HNO, its endogenous production in vivo has yet to be indisputably proven although there is in vitro evidence that it could be produced from a number of sources. Given that the redox potential of $NO^\bullet$ reduction is on the outskirts of the biological window ($E°(NO^\bullet/{}^3NO^-) = -0.81$ V vs. NHE; Figure 1.7), if HNO is

indeed endogenously produced, the widely held notion is that its source is unlikely to be NO•. However, it has been suggested that NO^- can form from the reduction of NO• facilitated by ferrocytochrome *c*,[81] and there is recent evidence of NO• being reduced by biologically relevant, moderately reducing alcohols such as ascorbate or tyrosine with the proposed mechanism being a proton-coupled nucleophilic attack to yield HNO, an alkoxyl radical, and NO_2^-.[82] The rationale is based on the redox potential of NO• to ^{1}HNO ($E°$(NO•, $H^+/^1$HNO = –0.14 V vs. NHE), given that nitroxyl is predominantly protonated at pH 7.4.[53,58] Although there is experimental evidence that this reaction is possible (N_2O quantification, trapping with a Mn^{III}-porphyrin, etc.), the percent yields of N_2O, a product of HNO self-dimerization, are mostly < 30% when testing the reactivity of four different alcohols, and the in vitro cell studies show only modest HNO formation based on the HNO sensor CuBOT1.[83-84] Notably, CuBOT1, whose turn-on is based on $Cu^{II} \rightarrow Cu^{I}$ reduction, has a substantially greater emission turn-on response from the presence of CysSH rather than from HNO. This suggests that while possible, NO• reduction is unlikely to be the principle means of HNO production physiologically.

The endogenous production of HNO has been implicated in numerous other pathways. NOS, which catalyzes the transformation of L-arginine to L-citrulline and NO• via an N^G-hydroxy-L-arginine (NHA) intermediate, has been shown to produce HNO in the absence of its cofactor tetrahydrobiopterin (BH_4; Figure 1.10) through oxidative degradation.[85-86] In fact, *N*-hydroxy guanidine compounds can release HNO or NO• depending on the oxidative conditions.[87] In a similar manner, the catalase-mediated oxidation of NHA can lead to HNO production independent of NOS.[88-89] In spite of its in vivo concentration not being well-established,[90] NH_2OH is another well-known candidate for HNO production in the presence of NO•[91] or from heme protein-mediated peroxidation,[90] although NH_2OH and HNO react together to form N_2 and two equiv of

H_2O ($k \sim 10^4$ M^{-1} s^{-1} at neutral pH).[92] HNO could also be a byproduct of drug metabolism which has already been shown with hydroxyurea, a sickle cell disease treatment,[93] and cyanamide, used as an anti-alcoholism agent[94] (vide infra). From 2010 – 2016, there have been multiple reports on the production of HNO from thiol-containing species such as hydrogen sulfide (H_2S), thionitrous acid (HSNO), or perthionitrite ($SSNO^-$) (Figure 1.10). For example, reaction of the $NO^\bullet$ donor nitroprusside with H_2S/HS^- at physiological pH leads to the production of free HNO via a transient coordinated nitrosothiol[95] (see section 1.4.2.2 for more detailed discussion, Figure 1.10). Similarly, HSNO, the smallest nitrosothiol, is produced from the interaction of H_2S and RSNO (R = glutathione or albumin), which is metabolized to then afford NO^+, $NO^\bullet$, and HNO.[96] Most recently, $SSNO^-$, which was previously considered more stable than HSNO, decomposes readily and rapidly to form HNO and elemental sulfur (S_8) in the presence of light, water, or acid (Figure 1.10).[97] However, due to its extreme instability (attributed to lengthening of the S-N bond: S-N: HSNO, 1.860 Å;[98] SSNOH (*cis*), 1.953 Å or 1.980 Å),[97] generation of $SSNO^-$ under physiological conditions is unlikely even as a transient intermediate and therefore not a candidate for endogenous HNO. Taken together, the endogenous production of HNO in mammalian cells remains to be indisputably proven; however, the therapeutic potential of this small molecule has been demonstrated (vide supra).

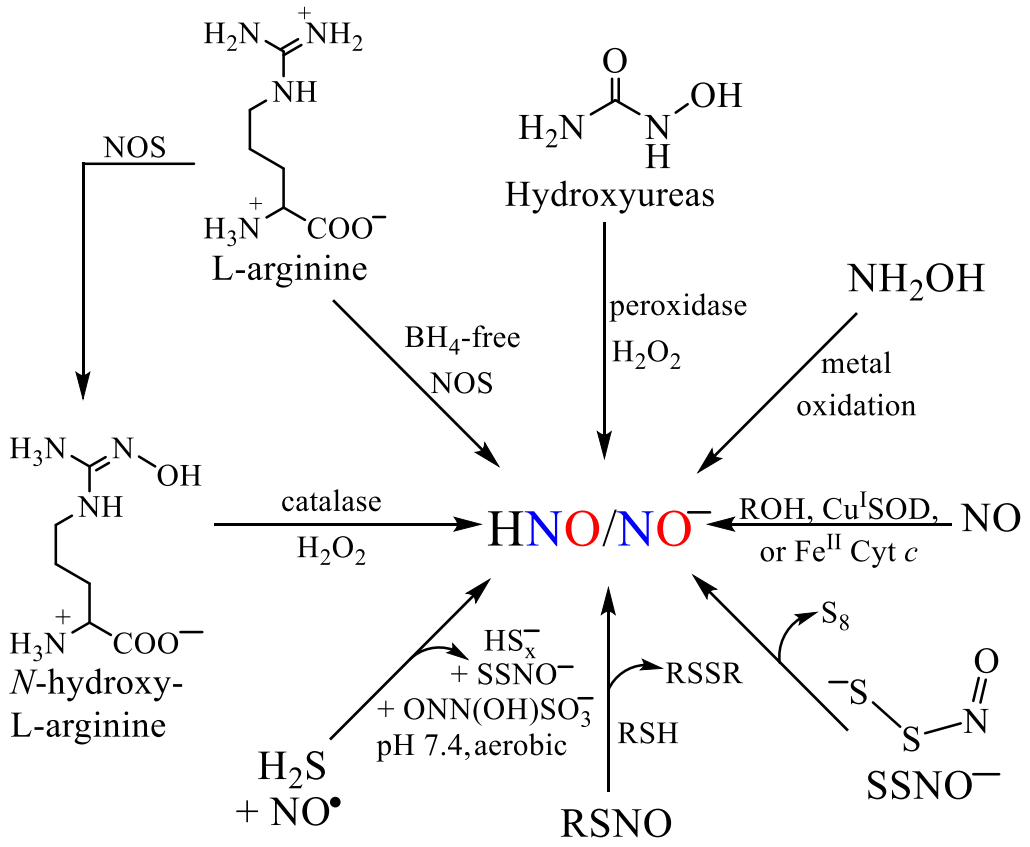

Figure 1.10. Potential sources of HNO. Note: the endogenous production of HNO has not yet been established.

1.2.3 HNO Donors

A significant obstacle in both the study and therapeutic utility of nitroxyl is the rapid dehydrative dimerization (8×10^6 M^{-1} s^{-1})[58] of HNO to nitrous oxide (N_2O) and water through the transient hyponitrous acid:[99-100]

$$2HNO \rightarrow [HONNOH] \rightarrow N_2O + H_2O \qquad \text{(Eq. 1.4)}$$

As such, studying HNO chemical biology necessitates the use of donor molecules.[62] Several classes of HNO donors, both organic and inorganic, have been employed in research and even clinically. For example, Angeli's Salt ($Na_2N_2O_3$; AS), which dissociates into HNO and NO_2^- at

physiological pH, is arguably the most well-studied and utilized nitroxyl donor (Scheme 1.1).[62,101-102] The mechanism of HNO release involves protonation followed by a slow tautomerization and subsequent heterolytic cleavage of the N-N bond. Cyanamide is an HNO donor that has been used as an anti-alcoholism agent in Europe, Canada, and Japan (Scheme 1.1);[94,103] it is oxidatively bioactivated by catalase and releases HNO and CN^- as a by-product. The understood mechanism of action is the inhibition of aldehyde dehydrogenase, a thiol-containing enzyme vital to metabolism of ethanol, resulting in elevated blood acetaldehyde levels.[103]

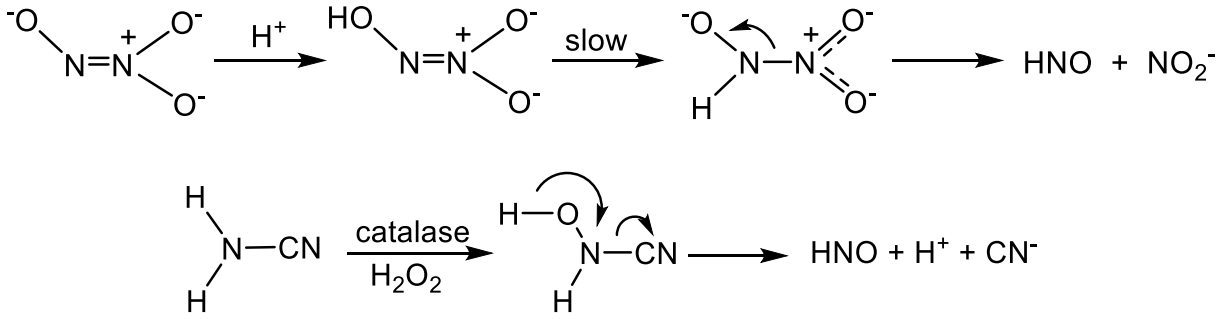

Scheme 1.1. Decomposition pathways of HNO donors Angeli's Salt (*top*) and cyanamide (*bottom*), both of which decompose to release HNO.

Although a number of nitroxyl donors have been found moderately effective, each has limitations that have hindered its widespread utility, including concomitant release of undesirable by-products (e.g., NO_2^-, CN^-), short half-lives ($t_{1/2}$ ~2.5 min), or ineffective release of HNO at physiological conditions (Table 1.1).[54,102] These by-products can complicate experiments or lead to unwelcome toxicity or chemistry.

Table 1.1. Structures, properties and limitations of current HNO donors. Adapted from reference 54.[54]

HNO Donor	Properties	Limitations	Refs
Angeli's Salt (AS) 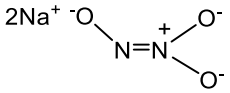	• Releases HNO between pH 4 and 8 • Only releases NO• at pH < 4	Concomitant release of NO_2^- Generates NO• at high concentrations (>10 μM) Short half-life ($t_{1/2}$ ~2.5 min)	101,104-105
Piloty's Acid 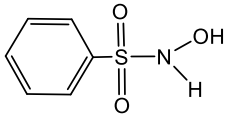	• Base-catalyzed release of HNO (requires pH > 7.4)	Releases NO• at physiological pH	102
Cyanamide 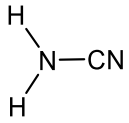	•Oxidative activation by catalase •Used as anti-alcoholism drug (Europe, Canada, Japan)	CN^- is a by-product	94
Isopropylamine NONOate (IPA/NO) 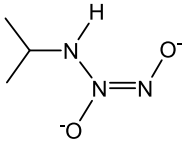	• A primary amine diazeniumdiolate • Releases HNO at physiological pH and temperature • No co-release of NO_2^- •Lead compound for the development of organic-based HNO donors	Donates NO• at pH < 7 Nitrosamine by-product (potentially toxic) Short half-life ($t_{1/2}$ ~2.3 min)	106
Acyloxy Nitroso 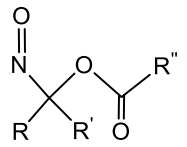	•Relaxes a pre-constricted rat aortic ring •Modifying acyl group alters rate of HNO release ($t_{1/2}$: 0.8 – 8 min)	Lower vasorelaxant potency than AS	107
Acyl Nitroso 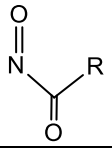	• Requires base for HNO release • Yields HNO and the corresponding amide	Formed transiently Lifetime under dilute conditions is < 1 ms	108-109
N-substituted Hydroxylamines 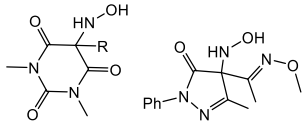 **1** **2**	• Releases HNO under physiological conditions with $t_{1/2}$ of 0.7 (**1**) and 9.5 min (**2**) • **2** and its derivatives have $t_{1/2}$ spanning min to days (based on nature of leaving group) with quantitative generation of HNO	New class of HNO donors that requires additional investigation in vitro and in vivo	110-111

To date, the majority of the findings in the HNO literature have predominantly utilized the HNO donors AS or Piloty's Acid, and their use has permitted the advancement of our understanding of

the chemical biology of HNO. With the advent of HNO donors that react under physiological conditions with longer half-lives, the field of study on both the biological implications and pharmacological applications of HNO will further develop. There is still a need for HNO donors that can overcome the aforementioned limitations, and first-row transition metals appear to be likely sites for potential endogenous generation and biological targets of HNO (vide supra).[54,62]

1.3. Reactivity of HNO/NO^-

1.3.1. Reactivity of HNO/NO^- with other small molecules

The importance of small molecules such as HNO, $NO^{\bullet}$, and H_2S, has been widely researched and documented in the literature since the discovery of $NO^{\bullet}$ as a signaling molecule,[112] and many small molecules have been realized as signaling agents in physiology. They share a significant number of common biochemical targets which can place these signaling agents in close proximity. Such targets often include redox-active metal centers (i.e. Fe and Cu) and redox-active amino acids (i.e. cysteine thiols or thiolates).[113-116] The products of such interactions exhibit distinct biochemical reactivity and properties. In spite of this, the integrated biochemistry and the subsequent implications are much less established. Table 1.2 briefly overviews the chemical interactions between HNO with other physiologically relevant nitrogen oxides and reactive oxygen species. It is clear that NO_x can be interconverted depending on what other small molecules are present in the environment. The interactions of many small molecule signaling agents ($NO^{\bullet}$, CO, H_2S) have been recently reviewed;[117] however, the integrated biological chemistry of HNO with such species is a domain that has yet to be investigated.

Table 1.2. Reactivity of ^1HNO and $^3NO^-$ with physiologically relevant NO_x and oxygen species.

Reaction	Rate Constant ($M^{-1}\ s^{-1}$)	Reference
$^1HNO + {}^1HNO \rightarrow N_2O + H_2O$	8×10^6	58
$^1HNO + NH_2OH \rightarrow N_2 + 2H_2O$	~10^4 (pH 7.2)	92
$^1HNO + NO_2^- \rightarrow HN_2O_3^-$	-	118
$^1HNO + NO^\bullet \rightleftharpoons N_2O_2^- + H^+$	5.8×10^6	58
$^3NO^- + NO^\bullet \rightleftharpoons N_2O_2^-$	2.3×10^9	58,119
$N_2O_2^- + NO^\bullet \rightarrow N_3O_3^- \rightarrow N_2O + NO_2^-$	$3\text{-}5 \times 10^6$, 2×10^4	58
$^1HNO + O_2 \rightarrow NO^\bullet + O_2^- + H^+$	$<< 3 \times 10^5$	58
$^3NO^- + O_2 \rightarrow ONOO^-$	2.7×10^9	58
$^1HNO + {}^-OH \rightarrow {}^3NO^- + H_2O$	4.9×10^4	58

The potential signaling mechanisms of such small molecule crosstalk has yet to be fully elucidated, but the physiological implications appear substantial. Using recent results pertaining to the interplay of $NO^\bullet$ and H_2S, it has been shown that levels of CGRP, the well-documented plasma marker for HNO,[54] can be the result of HNO formation from the reaction of H_2S and $NO^\bullet$.[120] The two signaling agents co-localize with transient receptor potential channel A1 (TRPA1). HNO is formed and then stimulates the sensory chemoreceptor channel TRPA1 by inducing disulfide formation of the TRPA1 cysteine residues. This leads to sustained Ca^{2+} influx and elevation of CGRP levels, resulting in subsequent local and global vasodilation. The mechanism of HNO formation has yet to be identified, although it could be related to the known reactions of H_2S with *S*-nitrosothiols[96] or metal nitrosyls,[95,121] both of which form HNO via RSNO. These results indicate that H_2S-induced vasodilation is more a result of its reactivity with $NO^\bullet$ rather than $NO^\bullet$-independent properties. Another recent example of the detailed network of S- and N-containing species that form from the $NO^\bullet/H_2S$ signaling pathway was provided through the characterization of key reaction products formed in this system.[122-123] The three major products were identified to be $SSNO^-$, polysulfides, and dinitrososulfite $[ONN(OH)SO_3]^-$. $SSNO^-$ was

found to be resistant to thiols, cyanolysis, and potently lowers blood pressure (BP). Polysulfides, which are also intermediates and products of $SSNO^-$ synthesis/decomposition, also decrease BP. Dinitrososulfite $[ONN(OH)SO_3]^-$ mainly releases N_2O upon decomposition although it is a weak $NO^\bullet$/HNO donor. It negligibly affects BP yet strongly increases myocardial contractions, an effect that is likely mediated by HNO generation. Other products from H_2S reacting with an Fe-based $NO^\bullet$ donor, including the subsequent production of HNO,[95] are detailed more thoroughly in the next section (Section 1.4.2.2; Scheme 1.7). These groundbreaking discoveries highlight that the properties attributed to a single small molecule could be the result of an upstream signaling cascade with multiple transmitters and signaling agents interacting with one another to cause significant downstream effects.

1.3.2. Reactivity of HNO/NO^- with metal centers

Many of the biological targets of these small molecules involve metal centers such as Fe or Cu. Small molecules such as HNO are transformed into other NO_x at such metals. For example, the oxidized form (Cu^{II}) of CuZn superoxide dismutase (CuZnSOD) reacts with HNO to yield free $NO^\bullet$, which is suggested to be a reversible reaction (Eq. 1.5):[124-125]

$$HNO + Cu^{II}ZnSOD \rightleftharpoons NO^\bullet + Cu^{I}ZnSOD + H^+ \qquad \text{(Eq. 1.5)}$$

Reductive nitrosylation is another well-known and documented interaction of HNO (or its anion) with higher valent metal centers such as Fe^{III}-hemes or Mn^{III}-porphyrins. A hallmark property of HNO that is distinct from $NO^\bullet$ is that it preferentially targets $Fe^{III} > Fe^{II}$ complexes and proteins like metmyoglobin (metMb) and methemoglobin (metHb) in a single step reaction forming the corresponding $\{FeNO\}^7$:[126-128]

$$HNO + Fe^{III} \rightarrow Fe^{II}\text{-}NO^\bullet + H^+ \qquad \text{(Eq. 1.6)}$$

This is in contrast to a stepwise electron-transfer followed by nitrosylation ($NO^{\bullet}$) or nitrosation (NO^{+}) of the ferrous species, which has been previously eliminated as the reaction mechanism based on spectroscopic studies.[126] One of the most important reactions of HNO is with Fe^{III}-hemes and is a defining property distinct from other nitrogen oxides because it is often used as an HNO detection method. MetHb is rarely used for this purpose due to allosteric interactions[128] and competitive reactions of HNO to the β-93 cysteine residues.[126] In fact, the kinetics of the HNO/Fe^{III}-heme reaction are greatly affected by the protein environment and active site. For example, the active site of cytochrome *c* (cyt *c*) contains a ferric heme coordinated by an axial histidine (His18) and methionine (Met80). HNO must displace an axial ligand in order to reductively nitrosylate the active site.[129] This leads to a 20-fold decrease in the rate constant ($k = 4 \times 10^4$ M^{-1} s^{-1}) compared to the reductive nitrosylation of a relatively unhindered active site, such as metMb ($k = 8 \times 10^5$ M^{-1} s^{-1}).[68]

The next section highlights a great deal of thiol reactivity, including H_2S/HS^{-}, with sodium nitroprusside, an $NO^{\bullet}$ donor which is formally an $\{FeNO\}^6$ complex containing a linear NO^{+} moiety. This is the most well-studied system for its H_2S interactions, although due to the challenging nature of this emerging field, there have been controversial findings pertaining to this chemistry (vide infra). There has yet to be a detailed investigation of the chemistry of an M-NO^{-} complex (where M = Fe, Co, etc.) with H_2S and the resulting species, and therefore biological significance may be vastly different relative to those observed in the $\{FeNO\}^6/H_2S$ reactive pathway. It is critical to understand the integrated chemistry and biochemistry of HNO with relevant small molecules (H_2S, $NO^{\bullet}$, O_2, $O_2^{\bullet-}$, CO, etc.) because many of these signaling molecules, including HNO, share biological targets and therefore are in close proximity to engage in additional chemistry. The crosstalk of H_2S and $NO^{\bullet}$ highlights the overlap between signaling

molecules, and a continued gap in knowledge will be detrimental because the chemical biology of such molecules is understood to have a significant effect on the physiological homeostasis in mammals.

1.4 Overview of Thiol Reactivity with Coordinated NO in {FeNO}$^{6/7}$ complexes[1]

1.4.1 Introduction of the reactivity of free NO$^{+/0/-}$ with RSH[130]

Reactive nitrogen species (RNS) such as nitric oxide ($NO^{\bullet}$) and nitrite (NO_2^-) are recognized as key players in the global nitrogen cycle and also for their biological properties in mammalian physiology. For example, the gaseous free radical $NO^{\bullet}$ is one of the more well-studied RNS and is known for its role in cardiovascular maintenance.[47] Other biological properties of $NO^{\bullet}$ include its ability to promote smooth muscle contraction[131] and to protect against ischemic-reperfusion injury.[132] The interactions of NO with biological targets is significantly complicated by the three oxidation states and corresponding N-O bond order (BO) of this diatom, e.g., nitrosonium cation (NO^+, BO = 3), neutral $NO^{\bullet}$ (BO = 2.5) and nitroxyl or nitroxyl anion (HNO/NO^-, pK_a 11.6, BO = 2).[53] Although bearing some similarities, these three NO_x species are considered to have pharmacological properties distinct from each other. For example, HNO is well-documented to be a positive cardiac inotrope due to its ability to increase myocardial contractility whereas $NO^{\bullet}$ is a negligible or negative cardiac inotrope.[54] HNO is also known to have a high proclivity toward thiols (RSH) (Eq. 1.7). On the other hand, $NO^{\bullet}$ exhibits negligible direct thiol reactivity in aerobic conditions[133-135] or in the absence of an oxidant.[136] Indeed, the fate of $NO^{\bullet}$ and its derivatives in biology or the environment is closely tied with its oxidation state.

[1] Melody A. Rhine, Brian C. Sanders, Ashis K. Patra, and Todd C. Harrop. *Inorg. Chem.* **2015**, *54*, 9351 – 9366. Reprinted (adapted) with permission from the American Chemical Society. Copyright 2015 American Chemical Society.

As the reaction of NO_x with RSH are implicated in the biological activity of these species, we elaborate more on this chemistry. For example, the products of HNO and RSH are formed through an *N*-hydroxysulfenamide (RSNHOH) intermediate (Eq. 1.7) whose fate is condition-dependent. In the presence of excess RSH, the reaction affords disulfide (RSSR) and hydroxylamine (NH_2OH) (Eq. 1.8).[126,137] When the concentration of RSH is lower, the *N*-hydroxysulfenamide rearranges to a sulfinamide ($RS(O)NH_2$) intermediate that hydrolyzes to yield sulfinic acid (RSO_2H) and NH_3 (Eqs. 1.9 and 1.10).[138]

$$HNO + RSH \rightarrow RSNHOH \qquad \text{(Eq. 1.7)}$$

$$RSNHOH + RSH \rightarrow RSSR + NH_2OH \qquad \text{(Eq. 1.8)}$$

$$RSNHOH \rightarrow RS(O)NH_2 \qquad \text{(Eq. 1.9)}$$

$$RS(O)NH_2 + H_2O \rightarrow RSOOH + NH_3 \qquad \text{(Eq. 1.10)}$$

The oxidized NO species, $NO^{\bullet}$ and NO^{+}, react differently with RSH but ultimately form the same *S*-nitrosothiol (RSNO) product. For instance, under anaerobic conditions, $NO^{\bullet}$ reacts with low molecular weight thiolates (RS^{-}) to afford RSSR via an *S*-nitrosothiol anion ($RSNO^{\bullet-}$) intermediate (Eq. 1.10) that also forms hyponitrous acid (HON=NOH) (Eq. 1.11), which decomposes to N_2O and H_2O:[139]

$$RS^{-} + NO^{\bullet} \rightarrow RSNO^{\bullet-} \qquad \text{(Eq. 1.10)}$$

$$RSNO^{\bullet-} + H^{+} \rightarrow RSNOH^{\bullet} \rightarrow 0.5RSSR + 0.5HON{=}NOH \qquad \text{(Eq. 1.11)}$$

Contrastingly, in aerobic conditions, $NO^{\bullet}$ does not interact directly with RSH groups. Indeed, it is the reaction of NO with molecular O_2 followed by reaction with another equiv of NO that leads to the reactive N_2O_3 species (Eq. 1.12 – 1.14):[140-141]

$$2NO^{\bullet} + O_2 \rightarrow 2NO_2 \qquad \text{(Eq. 1.12)}$$

$$^{\bullet}NO_2 + NO^{\bullet} \rightarrow N_2O_3 \qquad \text{(Eq. 1.13)}$$

$N_2O_3 + RSH \rightarrow RSNO + NO_2^- + H^+$ (Eq. 1.14)

When RSH = GSH, even the presence of 1% O_2 can lead to GSNO formation,[142] but GSNO is not typically observed anaerobically.[141,143-145] Unlike $NO^\bullet$, the reaction of NO^+ with thiols is straightforward yielding the expected RSNO product (Eq. 1.15):[146-147]

$NO^+ + RSH \rightarrow RSNO + H^+$ (Eq. 1.15)

The reactivity of free NO_x species with thiols is relatively well understood. However, NO_x/RSH interactions are often mediated at metal centers and the fate of these species when coordinated to a first-row transition metal (e.g. Fe, Co) in the presence of biomolecules deserves further investigation. Some metal-bound NO_x moieties (especially NO^+) have been more thoroughly investigated than others (NO^-) regarding their fate in the presence of thiol biomolecules, such as glutathione (GSH) or cysteine (CysSH). For example, sodium nitroprusside (SNP) $Na_2[Fe(CN)_5(NO)]$, used clinically as a vasodilator, has been studied extensively with regard to its reactivity with various thiols such as CysSH, GSH, and hydrogen sulfide (H_2S). The products of these reactions are often conditionally dependent on pH, O_2, and concentration (vide infra). Some studies have shown that release of $NO^\bullet$ is mediated by RSH molecules leading to the formation of the corresponding RSSR via transient *S*-nitrosothiols, yet the mechanism of NO release from the nitroprusside anion (NP) $[Fe(CN)_5(NO)]^{2-}$ has yet to be fully understood.[52,148] On the other hand, it is well established that one of the most facile and biologically significant reactions of HNO is with thiols.[62] However, thiol reactivity of metal nitrosyls assigned to have coordinated HNO or NO^- has not been extensively studied. The varying oxidation states of a coordinated nitrosyl as well as the condition-dependent nature of thiol reactions allude to the complexity of NO_x/RSH interactions.

This section will start by reviewing the fundamental reaction chemistry of thiols and/or thiolates with low molecular weight metal-nitrosyl complexes. Because an extensive amount of literature has been dedicated to RSH interactions with SNP, we initiate our overview with select examples from the most recent SNP literature (2000-present) where examples of N-O bond activation from coordinated *S*-nitrosothiols has been observed. We next describe RSH reactions of iron-sulfur complexes containing one or two coordinated nitrosyls that don't typically result in N-O bond activation.

1.4.2 Overview of Thiol Reactions with Metal Nitrosyls[130]

1.4.2.1 Thiol/thiolate reactions with SNP

SNP is the clinical nomenclature for $Na_2[Fe(CN)_5(NO)]$, an $\{FeNO\}^6$ complex,[29] whose NO moiety has electrophilic NO^+ character (formally LS-Fe^{II}-NO^+). Initially discovered in 1849 by Playfair,[149] SNP has been widely used clinically as an arterial and venous vasodilator to lower blood pressure for the past 40 years.[52,150] Since 1929 when SNP was first recognized as a hypotensive agent,[151] SNP has been used in cardiac, vascular, and pediatric surgery as well as hypertensive crises, heart failure, and other acute applications.[52] The interaction of thiol groups with SNP can lead to the release of NO•, the diatom to which the vasodilatory properties of SNP are attributed. However, NO• release from SNP is condition-dependent and its thiol reactivity profile under a range of conditions will be discussed here. Due to the considerable literature on SNP, we will limit our discussion and forward interested readers to comprehensive reviews on SNP in medicine[52,150] and other SNP reactivity.[148,152-155]

In 1975, Mulvey and Waters proposed that the reaction of SNP and thiolate anions (RS^-) yields the pink *S*-nitrosothiol (RSNO, coordination through N) product $[Fe(CN)_5N(O)SR]^{3-}$ (λ_{max}

= 522 nm, abbreviated **RP** due to being referred to as the "red product", Scheme 1.2), which decomposes to the $\{FeNO\}^7$ complex $[Fe(CN)_5(NO)]^{3-}$ with the concomitant production of disulfide (RSSR) via thiyl radical ($RS^{\bullet}$) formation.[156] Under anaerobic conditions, the intensity of the pink color was weak at pH 8 whereas it was much stronger at pH 10, indicating that **RP** forms from nucleophilic attack of RS^- (versus RSH) on the NO^+ of SNP. A three-line electron paramagnetic resonance (EPR) signal (g = 2.024, a(N) = 14.9 G) was obtained from the pink solution anaerobically (but not aerobically) that persisted even after the full disappearance of the pink color. The mechanism of the physiological activity of SNP remains to be fully elucidated; however, reactions between SNP and thiols have been extensively studied.[95,148,152-153,155] In 2002, Butler summarized how the interaction of SNP with thiols led to $NO^{\bullet}$ release with respect to in vivo action of SNP, augmenting the schemes previously proposed by Mulvey,[156] Butler,[157] Kowaluk,[158] and Stasicka.[159] It is generally accepted that **RP** is the RSNO complex $[Fe(CN)_5N(O)SR]^{3-}$ resulting from the nucleophilic attack of RS^- on the NO^+ of NP.[160] UV-vis spectroscopy has been the primary means of characterizing **RP** with $\lambda_{max}(\varepsilon)$: 522-527 nm ($10^3$-$10^4$ M^{-1} cm^{-1}); 320 nm (10^2-10^3 M^{-1} cm^{-1}).[161] Once formed, **RP** undergoes homolytic cleavage to afford EPR-active $\{FeNO\}^7$ species $[Fe(CN)_5(NO)]^{3-}$ and $RS^{\bullet}$, the latter of which will dimerize to RSSR (Scheme 1.2). The former can be oxidized by O_2 to reform the $[Fe(CN)_5(NO)]^{2-}$ ion or can interact with membrane-bound proteins or enzymes to release NO. With earlier findings discussed in previous reviews,[148,155] we will emphasize some of the recent highlights in SNP/RSH reactivity and characterization (vide infra).

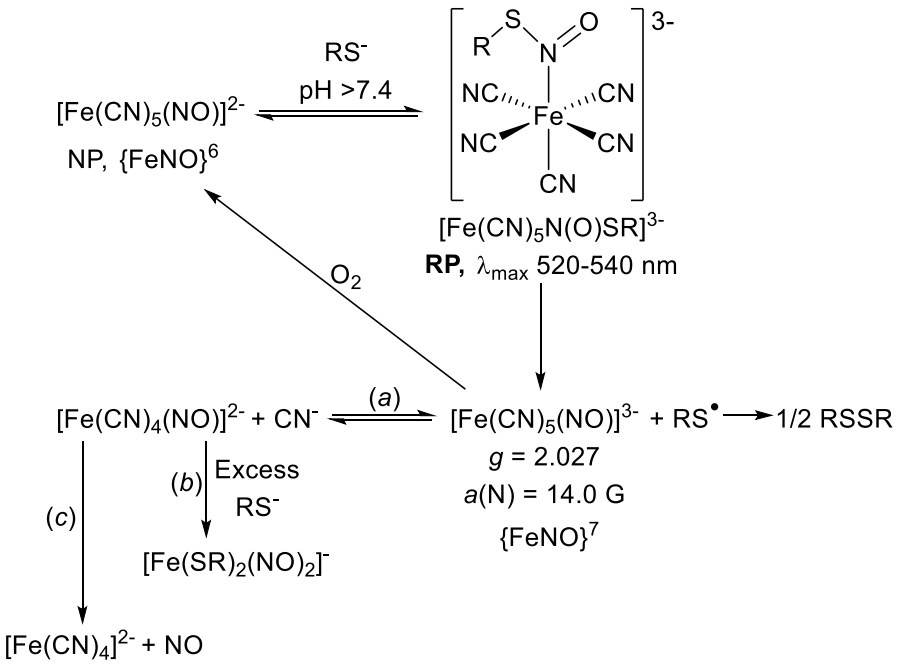

Scheme 1.2. Reactions of SNP with thiolates under basic conditions.

In 2002, Ashby and coworkers conducted a FTIR investigation of the intermediates formed in the anaerobic reaction of SNP with EtS^- in D_2O buffer (pD: 5.0-11.0).[162] Consistent with the summary from Butler,[148] SNP was shown to be reduced by one electron to form $[Fe(CN)_5(NO)]^{3-}$, but previous pulse radiolysis studies of the aqueous reduction of NP suggested that $[Fe(CN)_5(NO)]^{3-}$ rapidly loses CN^- to yield a five-coordinate (5C) $[Fe(CN)_4(NO)]^{2-}$ complex.[163] These FTIR studies identified a band at 1380 cm^{-1} that correlates with the loss of **RP** color in the UV-vis at 520 nm. Using ^{15}NO-labeled NP, this band shifts to 1350 cm^{-1} (Δ_{NO}: 30 cm^{-1}) and was assigned as the ν_{NO} of **RP**. Given that free RSNO compounds typically exhibit ν_{NO} ~1500 cm^{-1},[164] the **RP** intermediate was assigned as the RSNO compound $[Fe(CN)_5N(O)SR]^{3-}$. As the ν_{NO} at 1380 cm^{-1} decreased, a new ν_{NO} band at 1648 cm^{-1} increased, which is assigned to the 6C $\{FeNO\}^7$ complex $[Fe(CN)_5(NO)]^{3-}$. Previous work has observed NP to be a catalyst for the oxidation of

thiols to disulfides under aerobic conditions[157,165] and the results of this FTIR investigation are certainly consistent with prior reports.

Stasicka and coworkers showed that the lifetime of **RP**, now assigned as $[Fe(CN)_5N(O)SR]^{3-}$, was contingent upon a number of variables including type of thiol, pH, reactant concentrations, and the nature and concentration of the countercations.[161] For example, the **RP** lifetime significantly depended upon the nature of the thiolate: an electron-rich group close to the thiol-SH (NH_2) *destabilizes* **RP**; electron-withdrawing groups (COOH) *stabilizes* **RP**. This effect can be seen in the trend of the **RP** half-life ($t_{1/2}$; pH 10): 2-aminoethanethiol ($t_{1/2}$ = 20 s); 3-mercaptopropionate ($t_{1/2}$ = 8.3 min); mercaptosuccinic acid ($t_{1/2}$ > 36 h). In all cases with aliphatic thiolates, **RP** was generated very fast, consistent with a second-order rate constant $k_{RS^-} = 3 \times 10^3$ - 4×10^4 M^{-1} s^{-1}.[156,165-167] This report was followed by an investigation into the products and kinetics of the decomposition of **RP** in the reaction of SNP and RSH (RSH = CysSH, *N*-acetylcysteine, EtSH, and GSH) in alkaline, anaerobic conditions.[168] Consistent with previous studies,[156,165] the products formed were highly condition-dependent.[168-169] In acidic or non-aqueous conditions, the blue $[Fe(CN)_4(NO)]^{2-}$ ion results from the corresponding loss of one CN^- ligand. In basic media, the brown $[Fe(CN)_5(NO)]^{3-}$ ion (λ_{max} = 350, 440(sh) nm) is favored, indicating that pH and $[CN^-]$ induce an interconversion of the species (Scheme 1.2, path a).[163] EPR studies revealed the generation of only one stable paramagnetic species that has spectral parameters (g = 2.027; a(N) = 14.0 G) congruous with those reported for $[Fe(CN)_5(NO)]^{3-}$.[156,161,165,168,170]

The mechanism of $NO^\bullet$ release from SNP in vivo had been hypothesized to involve interaction with thiols such as GSH and CysSH, leading to the corresponding disulfides, *S*-nitrosothiols, $NO^\bullet$, and free CN^-. However, much ambiguity had yet to be resolved regarding the species involved. Grossi studied this mechanism in 2005 with the goal of elucidating both radical

and nonradical species involved through EPR, UV-vis, and IR spectroscopies.[171] As such, anaerobic experiments involving SNP and RSH (RSH = GSH, CysSH) in distilled water (pH 7) and phosphate buffered solutions (pH 7.4, 6.86, 6.4, and 5.0) were carried out. The reduced SNP $\{FeNO\}^7$ radical $[Fe(CN)_5(NO)]^{3-}$ was detected by EPR at t_{rxn} = 1 min generating a three-line EPR signal (g = 2.0255; a(N) = 14.8 G) consistent with the previously reported EPR of this $\{FeNO\}^7$ complex (vide supra). By reacting SNP with GSH directly in the cavity of the EPR at RT, signal was monitored continuously over an extended period of time, leading to no evidence of any EPR-active species other than $[Fe(CN)_5(NO)]^{3-}$. The reversible reaction: $[Fe(CN)_5(NO)]^{2-}$ (NP) ↔ $[Fe(CN)_5(NO)]^{3-}$ ($\{FeNO\}^7$) was studied in deoxygenated DMF using sodium naphthalenide in the IR cell. Upon introduction of reductant, the IR-active stretches of NP diminished as those of the reduced NP $\{FeNO\}^7$ radical increased. Upon introduction of air to the IR cell, the peaks from NP $\{FeNO\}^6$ reappeared and those of reduced NP $\{FeNO\}^7$ radical diminished. It was concluded that a direct electron transfer between the reactants occurred with no possible involvement of intermediates. Given the literature precedent of NO$^\bullet$ release and elimination of CN^- ligand(s),[52,150] it was hypothesized that reaction of a GSH radical cation ($GSH^{\bullet+}$) with $[Fe(CN)_5(NO)]^{3-}$ would lead to an Fe^{II}-complex, HCN, and GSNO, the latter of which could form disulfide GSSG and free NO$^\bullet$ (Scheme 1.3).

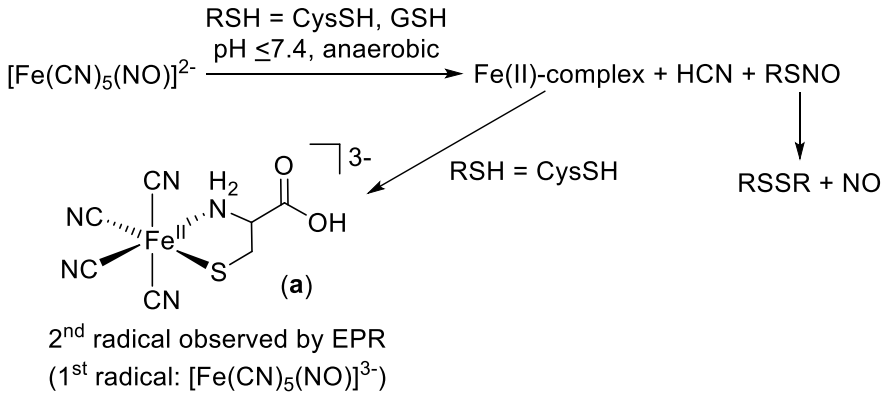

Scheme 1.3. Reactions of SNP with CysSH or GSH under neutral-to-acidic conditions.

In spite of only one detectable radical forming in the reaction of SNP and GSH, reacting SNP with CysSH led to the formation of a second EPR-active species (g = 2.0297), which is present at t_{rxn} = 5 min and 25 min.[171] One proposal is that the Fe^{II}-complex formed after reacting with one-equiv CysSH may interact with a second equiv of CysSH to form a paramagnetic 6C radical species **a** (Scheme 1.3). This is the first evidence of the involvement of a second radical, consistent with the electron being delocalized on the S, N donors of Cys. The arrangement of 6C **a** was further confirmed by repeating the experiment with 2-aminothiophenol, an aromatic thiol with an NH_2 group positioned *ortho* to SH. EPR provided evidence of a paramagnetic species with g = 2.0027 that was dominant in the reaction mixture at t_{rxn} = 5 min. Only one single EPR-active species (consistent with $[Fe(CN)_5(NO)]^{3-}$) was seen in SNP/RSH studies (where RSH = GSH, benzyl thiol, 3-mercaptopropionic acid) under these conditions (anaerobic, pH ≤ 7.4), which is indicative of the need for an amino group close to -SH and minimal sterics to form radical species **a**.

In many cases in the SNP/RSH literature, reactivity was attributed to the thiolate only.[153,157,165-166,168] These experiments were mostly performed in alkaline media with the pH well

above physiological conditions (pH ≥ 10). Although the thiolate may indeed be the reactive species under basic conditions, Grossi conducted the previously discussed experiments in buffered acidic solutions (pH = 6.86, 6.4, and 5.0) and attributed the observed reactivity to the possibility of the thiol group itself serving as the reducing species.[171] The percentage of thiolate is estimated to be 85, 30, and 1%, respectively, for the aforementioned pH values, and the reduced NP radical was "*straightforwardly detectable by EPR*" in each acidic medium. Given that at least one or more radical species forms in acidic conditions, including the $\{FeNO\}^7$ NP radical anion $[Fe(CN)_5(NO)]^{3-}$, the involvement of thiols (not only thiolates) cannot be excluded as possible reductants of SNP.

1.4.2.2 H_2S/HS^- reactions with SNP

The reaction of Na_2S or K_2S and SNP was first published in 1966 by Rock and Swinehart, whose studies indicated the formation of isolable salts of $[Fe(CN)_5N(O)S]^{4-}$ under alkaline conditions (pH = 10.2-12.6).[172] In 2011, Olabe conducted studies on the reactivity of H_2S/HS^- with SNP (pH = 8.5-12.5; anaerobic),[173] and, using stopped-flow UV-vis, EPR, and FTIR, showed evidence for generation of the HSNO complex $[Fe(CN)_5N(O)SH]^{3-}$ (**I**, $\lambda_{max} \approx 570$ nm, pK_a = 10.5 ± 0.1 at 25 °C, I = 1 M) as the initial adduct (Scheme 1.4). Deprotonation of **I** led to $[Fe(CN)_5N(O)S]^{4-}$ (**II**, λ_{max} = 535 nm). The pH (10, 11, 12) and HS^-/NP ratios (3.9/1; 13/1) were varied and under all these conditions, **I** and **II** form the $\{FeNO\}^7$ complex $[Fe(CN)_5(NO)]^{3-}$ through elimination of $HS_2^{\bullet 2-}$ (Scheme 1.4).

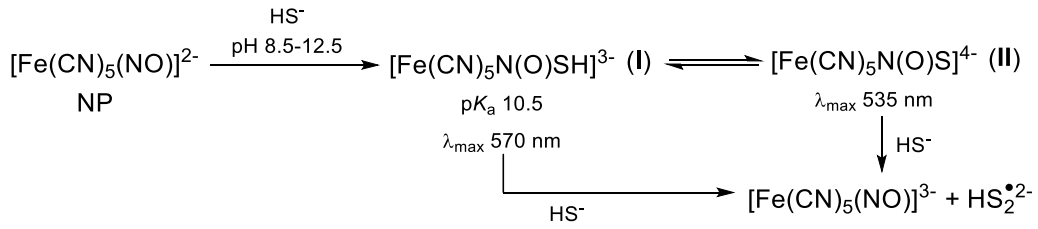

Scheme 1.4. Reactions of NP with H_2S/HS^- under basic and anaerobic conditions.

For each condition, N_2O was also observed and quantified by GC-MS headspace analysis (mole fraction N_2O (χ_{N2O}) = 0.67-1.0), and in solution, a nearly constant production of NH_3 was also observed. It is important to point out that these reactions are competing with the major path involving formation of **I** as described above. Nonetheless, they do suggest that HSNO/SNO compounds **I** and **II** do result in N-O bond activation under these conditions. To account for the multi-electron reduction to form NH_3, a series of intermediates were proposed based on density functional theory (DFT) calculations at pH = 9.5 and 11.5, with the reducing equivalents coming from excess HS^-. At pH 9.5, the initial HSNO adduct **I** ($\lambda_{max} \approx 570$ nm) appeared but then diminished as two bands increased in intensity that are attributed to $\{FeNO\}^7$ $[Fe(CN)_5(NO)]^{3-}$ (λ_{max} = 345, 430 nm), a compound that is unreactive toward excess HS^-. The current proposal involves a fast, spontaneous homolytic cleavage of **I** and, under excess HS^- conditions, a second intermediate leads to a series of reductions to form NH_3 ($k_{obs} = 1.6 \pm 0.1 \times 10^{-3}$ s^{-1}) via a bis-thiolated hydroxylamine intermediate $(HS)_2N$-OH (Scheme 1.5).

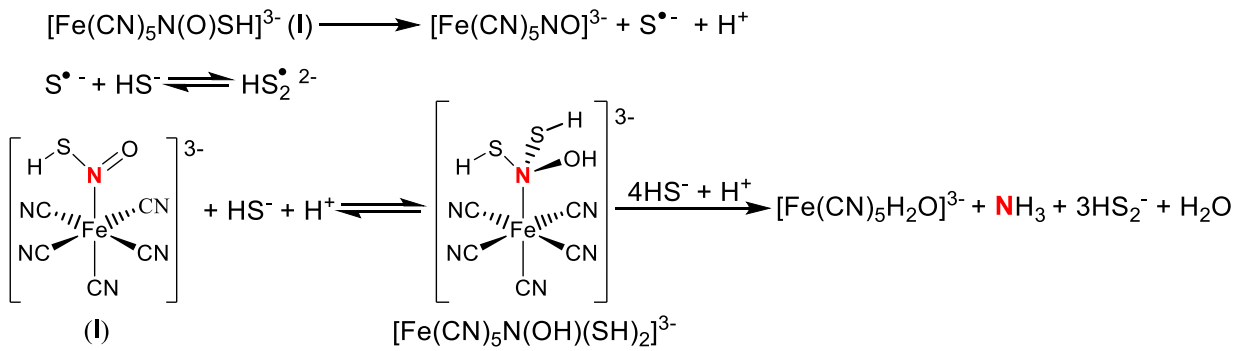

Scheme 1.5. Reactions of NP with excess HS^- at pH 9.5; intermediates proposed by DFT.

At pH 11.5, two processes occur (as monitored by UV-vis), the first of which is a first-order kinetic process (k_{obs} 1.2 ± 0.2 × 10^{-2} s^{-1}) whereas the second process decays more slowly (k ≈ 5 × 10^{-5} s^{-1}). This slower rate for the latter process indicates the formation of a stable intermediate until the generation of N_2O and NH_3 is complete (Scheme 1.6). Formation of NH_3 then occurs via a similar pathway as was proposed at pH 9.5 (vide supra).[173]

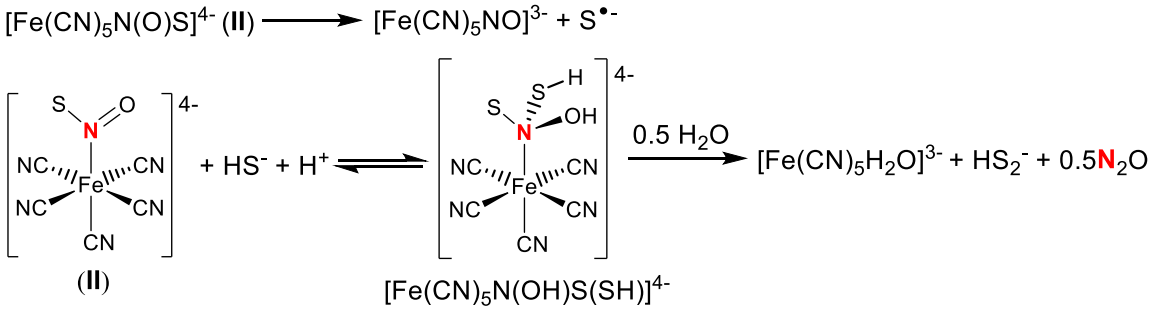

Scheme 1.6. Reactions of NP with excess HS^- at pH 11.5; intermediates proposed by DFT.

Olabe also proposed that the representative EPR spectrum arising from the SNP/HS^- reaction was a result of $[Fe(CN)_4(NO)]^{2-}$ through loss of one CN^- ligand from the $\{FeNO\}^7$ $[Fe(CN)_5(NO)]^{3-}$ complex. The EPR indicates a 1:1:1 triplet with g = 2.025 and a(N) = 14.8 G,

which has been previously assigned to the 6C $[Fe(CN)_5(NO)]^{3-}$ ion.[168] After the decay of this signal, a second EPR signal was observed with a similar morphology (1:1:1 triplet, $g = 2.0235$ and $a(N) = 46$ G), which the authors assign to be a 4C dinitrosyl iron complex (DNIC) $[Fe(SH)_2(NO)_2]^-$ (Scheme 1.2, path b).

As has been common in the field of NP/RSH reactivity, ambiguity often leads to more questions. Filipovic and Ivanović-Burmazović followed up the Olabe study[173] seeking to further clarify the kinetics and intermediates formed in the SNP/H_2S reaction.[174] They determined that the reaction of SNP with Na_2S results in a short-lived red-violet species **I** ($\lambda_{max} = 535$ nm), presumably HSNO complex **I**, that rapidly turned to a dark blue product ($\lambda_{max} = 570$ nm). In order to avoid uncertainty, studies carried out in this report were performed at pH 7.4, given the estimated pK_a value of 10.5 for **I**;[173] however, it is noted that these results remained consistent under various conditions (pH ≥ 7.4; aerobic and anaerobic).[174] Accordingly, the SNP/H_2S reaction occurred in three reaction steps: (i) formation of the $\lambda_{max} = 535$ nm intermediate (complete within ~20 s); (ii) transformation of **I** into the species with a $\lambda_{max} = 570$ nm (~20 s < t_{rxn} < ~60 s); and (iii) decomposition of the 570 nm complex. Many questions surrounding the complexities of the reactivity pathway of SNP and H_2S remained unanswered, as was clear in this correspondence.

In 2013, Ivanović-Burmazović and co-workers clarified many of these questions surrounding the reactivity of SNP and H_2S under physiological conditions.[95] Firstly, *$NO^\bullet$ is not released* from the reaction of SNP and H_2S using an $NO^\bullet$-specific electrode. This implies that free $NO^\bullet$ nor a free RSNO is produced in the reaction as RSNOs are known to release $NO^\bullet$ upon decomposition.[175] Additionally, the quick and complete consumption of H_2S in < 500 s was observed after mixing equimolar solutions of SNP with H_2S. There was strong evidence for HNO formation directly, with an HNO-specific fluorescent sensor, and indirectly, through GC-MS

detection of N_2O (*m/z* 44) and HNO-induced calcitonin gene-related peptide (CGRP) release (ex vivo). Finally, SNP was shown to function as a rhodanese, a mitochondrial enzyme that converts CN^- to SCN^-, given the detection of SCN^- by real-time FTIR, GC-MS, and ^{15}N NMR experiments. Consistent with their previous report,[174] three main reaction steps were observed using stopped-flow kinetics studies under pseudo first order, physiological conditions: (i) formation of pink $[Fe(CN)_5N(O)SH]^{3-}$ (**I**) with a λ_{max} = 535 nm; (ii) mixture of Prussian-blue-type species and transient $[Fe(CN)_5(HNO)]^{3-}$ with λ_{max} = 720 nm and 440 nm, respectively; and (iii) formation of the final product $[Fe^{II}(CN)_{5-x}(SCN)_x(H_2O)]^{3-}$ with λ_{max} = 575 nm (Scheme 1.7). Increasing $[H_2S]$ and $[O_2]$ resulted in faster kinetics. The generation of nitroxyl (HNO/NO^-) and the ability of SNP to react as a rhodanese were two additional pivotal discoveries in this work.

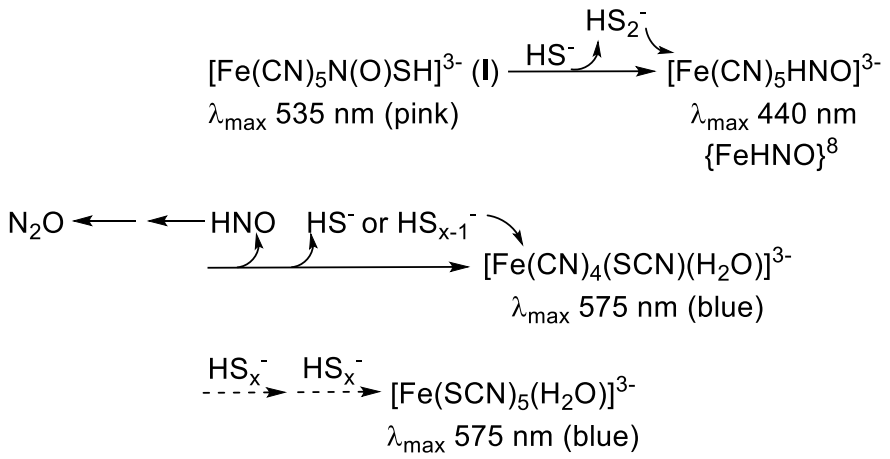

Scheme 1.7. Reactions of NP with excess H_2S/HS^- under physiological conditions.

These experiments allowed logical mechanistic insights into the SNP/H_2S reaction pathway under more relevant biological conditions, some of which had yet to be proposed until this study.[95] The reaction of H_2S with SNP affords the HSNO complex **I**, the short-lived pink

intermediate. Upon introduction of a second equivalent of HS^-, $\{FeHNO\}^8$ complex $[Fe(CN)_5(HNO)]^{3-}$ and HS_2^- form; the former releases HNO, which can then dimerize to lead to N_2O and H_2O, and the latter interacts with O_2 to become a polysulfide HS_x^- ion. The complex ion $[Fe^{II}(CN)_{5-x}(SCN)_x(H_2O)]^{3-}$ is formed through interaction of the Fe species with HS^- or HS_{x-1}^-, which after a series of steps ultimately forms the blue thiocyanate-bound product $[Fe^{II}(SCN)_5(H_2O)]^{3-}$ (Scheme 1.7). In a minor side reaction, the presence of O_2 complicates the mechanism by reacting with $[Fe^{II}(CN)_{5-x}(SCN)_x(H_2O)]^{3-}$ to form mixed valent Fe^{II}/Fe^{III} Prussian blue type compounds. These are short-lived and react further with polysulfides to also form $[Fe^{II}(SCN)_5(H_2O)]^{3-}$. These careful and insightful studies have significantly contributed to elucidating the reaction pathway of SNP and H_2S and more broadly, augments the prevailing literature surrounding RSH reactivity with small molecule metal complexes.

Kostka and coworkers highlight another interesting path that has been seen in SNP/RSH reactions, which is the formation of peroxynitrite ($OONO^-$) and hydroxyl radical ($^{\bullet}OH$) during thiol-mediated reduction of SNP.[176] Under aerobic conditions (pH 7.4), equimolar concentrations of SNP and dithiothreitol (DTT) led to a concentration-dependent increase in the rate of oxidation of dihydrorhodamine-123 (DHR), whose oxidation is mediated by $OONO^-$, $^{\bullet}OH$, or $^{\bullet}NO_2$.[177-179] Dimethyl sulfoxide (DMSO), a known $^{\bullet}OH$ scavenger, partially suppressed the DHR oxidation rate, implying reactive species other than $^{\bullet}OH$. In the presence of O_2 and CN^- ions, $[Fe(CN)_4(NO)]^{2-}$ is known to reform NP and superoxide ($O_2^{\bullet-}$) (Eq. 1.16),[157] and $O_2^{\bullet-}$ can then react with an NO moiety to form $OONO^-$ (Eq. 1.17). DHR oxidation rates diminished significantly and were almost completely eliminated in the presence of Cu/Zn superoxide dismutase (SOD; 20 U/mL). The authors rationalized these results by hypothesizing the stabilization of the intermediate(s) of SNP reduction (λ_{max} = 450 nm) when in the presence of SOD. This reactivity

trends accordingly with other biologically relevant thiols, such as CysSH and GSH, which has important implications for products of the decomposition of reduced NP radical anion under aerobic conditions.[176]

$[Fe(CN)_4(NO)]^{2-} + CN^- + O_2 \rightarrow [Fe(CN)_5(NO)]^{2-} + O_2^{\bullet-}$ (Eq. 1.16)

$O_2^{\bullet-} + NO \rightarrow ONOO^-$ (Eq. 1.17)

1.4.2.3 Reactions of Other Iron Nitrosyls with Thiols/Thiolates

First proposed in 1965,[180] $\{Fe(NO)_2\}^9$ tetrahedral dinitrosyl iron complexes (DNICs, Scheme 1.8) have distinct spectroscopic signatures including: (i) a characteristic RT EPR signal at $g = 2.03$; (ii) low-energy bands in the UV-vis at ~470 nm and ~800 nm; and (iii) the ν_{NO} region of the IR displays two strong peaks at ~1690/~1740 cm^{-1}.[148,181-182] An abundance of reactivity studies of DNICs with RSH (e.g. H_2S, $HSCPh_3$),[183-185] RS^- (e.g. EtS^-, PhS^-),[184,186] S_8,[184] and RSSR (e.g. $(Me_2NCS_2)_2$), $(Et_2NCS_2)_2$)[187-188] have been extensively investigated. Liaw and coworkers have published an account of this work in 2015 detailing both characterization of various DNIC and dinuclear Roussin's red ester (RRE, Scheme 1.8) complexes, as well as a report of the biological and catalytic roles of DNICs.[181] There is also an example of trinitrosyl iron species (TNICs) synthesized by Darensbourg that engage in exchange reactions with RS^- (e.g. PhS^-) to form the corresponding S-bound DNIC via thiolate displacement of the coordinated NO.[189] As the bulk of this chemistry involves thiolate exchange reactions without any noted activation of the N-O bond, we will limit our discussion to a few selected examples. For additional information on DNICs, we refer the reader to the most recent review by Liaw[181] and the work of Kim[190-192] and Lippard.[193-197]

In 2015, Ford demonstrated the complicated dynamics involved between the DNIC $[Fe(SCys)_2(NO)_2]^-$ and RRE $[Fe_2(\mu\text{-}SCys)_2(NO)_4]$ with CysSH in deaerated aqueous solution.[198] DNICs are formed by the reaction of chelatable Fe^{II} pools with NO and biological thiols such as CysSH,[199-200] and as such, $FeSO_4$, CysSH, and NO were used in the study of this equilibrium. Consistent with the results of Vanin,[201-202] the dinuclear RRE was favored under acidic conditions (pH = 5.0) and lower [CysSH] at pH 7.4 (Scheme 1.8). The mononuclear DNIC was favored at basic pH (≥ 10) and higher [CysSH] at pH 7.4 (Scheme 1.8). Thus, rapid biological formation of DNICs can be explained by the readily occurring transformation of RRE to DNIC under high [RSH] and the high concentration of thiols in cells, for example [GSH] = 0.5-10 mM.[203] Notably, the Fe-NO bond remains intact in the DNIC ↔ RRE interconversion. Both products are formed via a common 3C $\{FeNO\}^8$ intermediate, namely $[Fe(SCys)_2(NO)]^-$, the rate-determining step of which is proposed to be the spontaneous reduction of the Fe^{II} center of the 3C $[Fe(SCys)_2(NO)]^-$ to yield the $\{FeNO\}^8$ Fe^I intermediate [Fe(SCys)(NO)] and $CysS^\bullet$ radical, the latter of which ultimately affords CysSSCys. Similar transformations of RREs to DNICs in the presence of excess thiolates have been reported by Lippard[204] and Liaw.[205] Flash photolysis studies of the RRE formed at pH 5.0 led to reversible dissociation of the NO moiety, with a fast second-order back reaction ($k_{NO} = 6.9 \times 10^7\ M^{-1}\ s^{-1}$). Rather than NO dissociation, flash photolysis studies of the DNIC formed at pH 10.0 released $CysS^\bullet$ through a reversible photo-induced redox reaction. This recent work highlights the complex nature of the RRE/DNIC equilibrium and how biologically relevant conditions, such as changes in pH or [RSH] is likely to determine the fate of the Fe-NO species. Overall, the rates of the RRE/DNIC interconversion process are dependent upon [CysSH] and on pH; increasing [CysSH] favors DNIC formation (seen at pH 7.4) and decreasing pH rapidly increases the transformation to RRE (Scheme 1.8).[198] Additionally, thiol-containing DNICs have

been implicated in the safe storage and trafficking of NO, which details their physiological importance as well as possible therapeutic utility.[206-207] These results are indicative of the biological relevance of the reaction of DNICs with thiol-containing groups as well as the decomposition of S-bound DNICs and their implication in the fate of NO/RSH crosstalk.

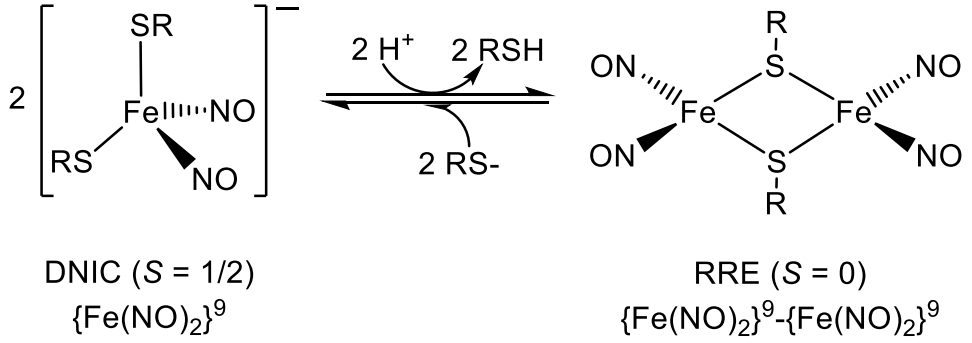

DNIC (S = 1/2)
$\{Fe(NO)_2\}^9$

RRE (S = 0)
$\{Fe(NO)_2\}^9$-$\{Fe(NO)_2\}^9$

Scheme 1.8. Interconversion of DNIC and RRE.

In contrast to SNP/RSH reactivity, the relationship between other mononitrosyl iron complexes (MNICs) and thiols is one that has only been recently studied. For example, the nitrosylation of biological and synthetic [Fe-S] clusters or $[Fe(SR)_4]^{2-}$ complexes to yield DNIC has long been established, but the isolation of the $\{FeNO\}^7$ MNIC $[Fe(SR)_3(NO)]^-$ evoked in this transformation first occurred in 2006.[193] DNIC ultimately results from the reductive elimination of one coordinated thiolate/sulfide to give disulfide (for $[Fe(SR)_4]^{2-}$) or elemental S (for [Fe-S] clusters) upon formation of the second Fe-NO bond (Scheme 1.9).

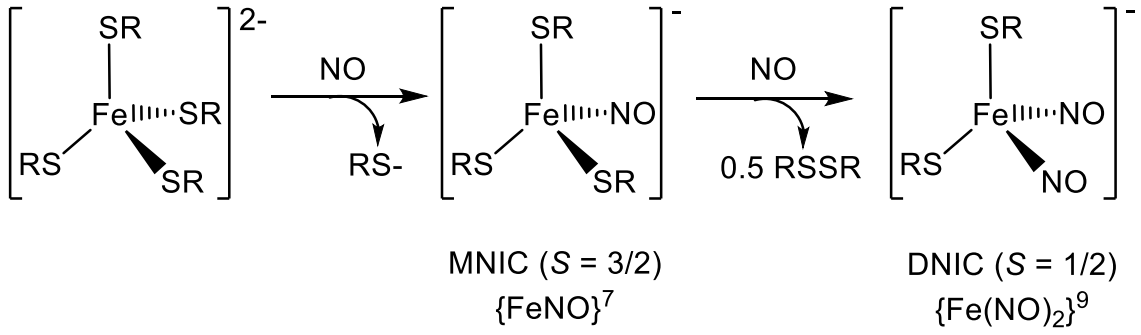

Scheme 1.9. Reaction of $[Fe(SR)_4]^{2-}$ complexes with $NO^{\bullet}$(g).

There are already significant implications for MNICs in the repair of NO-damaged [2Fe-2S] clusters, and the role of $NO^{\bullet}$ in the degradation of [Fe-S] clusters has been well-documented.[190-191] In 2014, Kim reported the transformation of MNIC (PPN)[Fe(S^{t}Bu)$_3$(NO)] (PPN = μ-nitrido-bis(triphenylphosphorus)) to [2Fe-2S] cluster through the addition of 20 equiv of methyl 3-mercaptopropionate (MMP, a cysteine analogue).[192] This reaction resulted in two Fe-containing products: (i) a [2Fe-2S] cluster employing MMP thiolates $(PPN)_2[Fe_2S_2(SR)_4]$, and (ii) the $\{Fe(NO)_2\}^9$ complex $(PPN)[Fe(SR)_2(NO)_2]$ (R = MMP). Indeed, the only NO-containing product was the $\{Fe(NO)_2\}^9$ complex $(PPN)[Fe(SR)_2(NO)_2]$. No other product containing NO was detected, and N_2O was not observed in the headspace of the reaction mixture. The evidence supports the formation of the DNIC and the [2Fe-2S] cluster in a 2:1 stoichiometry. The first step involves disproportionation of the unstable MNIC into two equivs of the DNIC $[Fe(SR)_2(NO)_2]^-$ and one equiv of $[Fe_2S_2(SR)_4]^{2-}$ per two equiv of $[Fe(SR)_3(NO)]^-$ complex (Scheme 1.10). Elimination of MMP disulfide provides the source of sulfide ion to generate the [2Fe-2S] cluster and RSR thioether (verified by ^{34}S-labelling). First suggested in 2006 by Lippard[193] and more recently corroborated by Ford,[198] MNICs may indeed serve as intermediates in reaction pathways

leading to DNIC in environments rich in sulfur, which indicates that MNICs may have a substantial biological role.

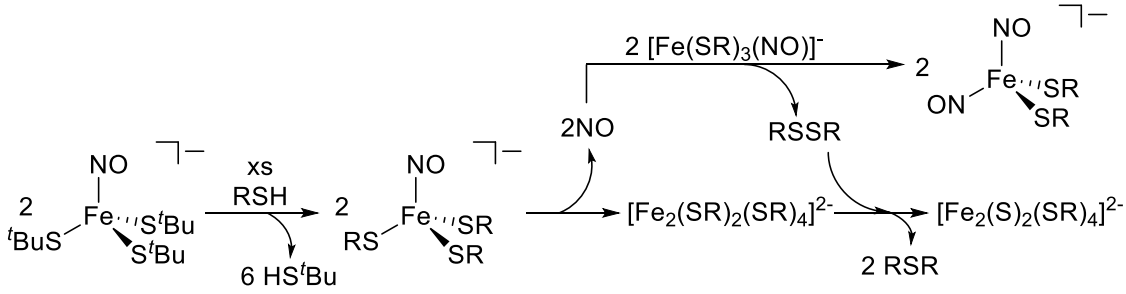

Scheme 1.10. Transformation of MNIC into DNIC and [2Fe-2S] cluster. RSH = methyl 3-mercaptopropionate.

Additional examples of thiol-induced reactivity of other iron nitrosyls include photolytic conversion of DNICs to [2Fe-2S] clusters in the presence of elemental sulfur.[186,194] Although these examples used reagents and reaction conditions differing from those found in biology, they do provide keen insight into [Fe-S] cluster repair through a pathway analogous to the cysteine desulfurase-mediated repair of DNICs. Furthermore, an MNIC intermediate has been proposed in the reductive activation of coordinated NO_2^- on heme Fe with H_2S.[121] It has also been shown by Warren that *S*-nitrosothiols (RSNO) react with Cu^I mononitrosyls to form Cu^{II}-SR and release two equiv of $NO^{\bullet}$.[208] This transformation highlights the importance of crosstalk between NO- and S-containing species. Each of these examples highlights the relevance of the MNIC/RSH reactivity, which until recently was not considered a significant biological pathway.

1.5 Cobalt and NO in biology

1.5.1 Structural and electronic properties of nitrosylcobalamin (NOCbl)

Although used less frequently in biology than other first-row transition metals, cobalt and cobalt-containing enzymes are required for mammalian life.[209-210] Cobalamin (Cbl), also known as vitamin B_{12}, is used as a cofactor in two metalloenzymes found in humans: methionine synthase (MetH), which catalyzes the synthesis of methionine from homocysteine, and methylmalonyl-CoA mutase (MMCM), which catalyzes the isomerization of methylmalonyl-CoA to succinyl-CoA. This is an important intermediate in the citric acid cycle.[211] Cbls have a cobalt center that is ligated with the four nitrogen ligands of a tetraazamacrocyclic corrin ring. Corrins are similar to porphyrin rings although they have only one central deprotonatable proton rather than two. Cbls often bear an N-donor ligand from a 5,6-dimethylbenzimidazole (DMB) nucleotide covalently bonded to the corrin ring in the lower axial position (Figure 1.11). Ligands in the position above the corrin ring of Cbls are more variable, with four ligands being the most common: methyl- (L = CH_3, Figure 1.11) and adenosylcobalamin (L = Ado, Figure 1.11), which both serve as biological cofactors (isomerases, methyltransferases, and dehalogenases), and aquo- and cyanocobalamin (L = H_2O or CN^- respectively, Figure 1.11).[212] Glutathionyl, hydroxo, nitro, and nitroso are also observed axial ligands,[213-214] and glutathionylcobalamin is proposed as a precursor to MeCbl and AdoCbl.[213,215]

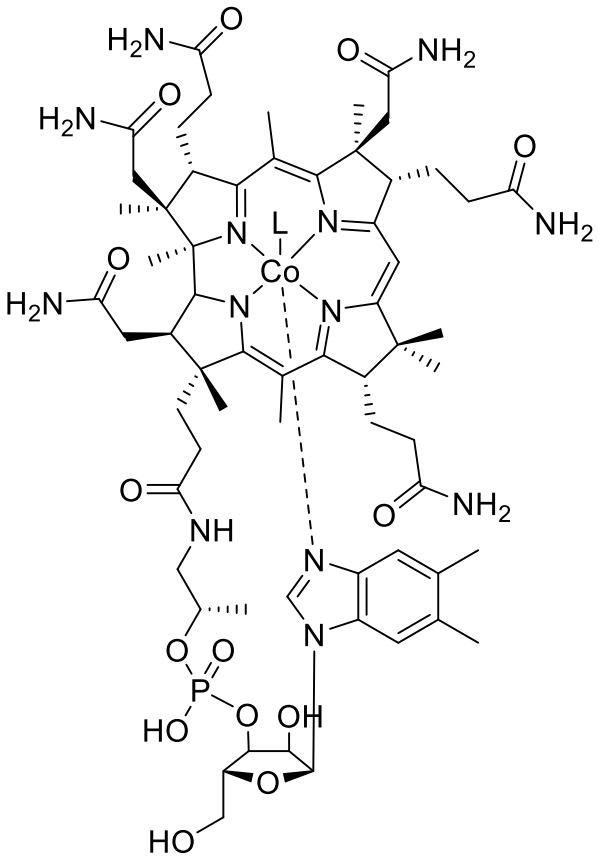

Figure 1.11. Chemical structure of cobalamin (Cbl). Dotted line signifies the coordination at the lower axial position of pendant DMB group, which is absent in cobinamide (Cbi^{+}). L = ligand at the upper axial position; methyl or adenosyl for the active forms of Cbl.

Both Cbl-dependent enzymes MetH and MMCM are known to interact with $NO^{\bullet}$ (vide infra) to form nitrosylcobalamin (NOCbl), of which the only difference is NO at the upper axial position.[216] NOCbl is a $\{CoNO\}^{8}$ species, also termed nitroxylcobalamin, given the overall oxidation state of Co^{III}-NO^{-}, and consistent with the typical assignment for $\{CoNO\}^{8}$ complexes.[217-218] There is a plethora of experimental evidence corroborating the formation of NOCbl,[219-220] and its structural features have received attention for their departure from the structure of typical Cbls. The crystal structure of NOCbl indicates a highly bent Co-N-O bond

angle (118.9 - 120.3°), an N-O bond distance of 1.12-1.14 Å, a Co-N(O) distance of 1.91-1.94 Å, and an exceptionally long Co-N(DMB) (2.32-2.35 Å), which is ~0.1 Å longer than that of all other Cbl structures.[216] The base-on form of NOCbl refers to the DMB nitrogen coordinating to Co in the lower axial position whereas base-off implies that the DMB nitrogen is dissociated from the Co center. Based on NMR studies, the base-on form of NOCbl is favored (67%) over the base-off form (33%) at neutral pH.[221]

In 2014, the electronic and spectral nature of NOCbl was elucidated. Due to the ambiguity of the electronic features of NOCbl responsible for the long Co-N(DMB) bond, Brunold and co-workers launched a thorough spectroscopic investigation of NOCbl.[222] The low-temperature (4.5 K) absorption spectrum of the base-on form exhibits a feature at ~500 nm, which is characteristic of Co^{III}Cbl species and known to be highly sensitive to changes in axial ligands.[223] These so-called α/β bands are attributed to a corrin $\pi \rightarrow \pi^*$ transition.[224] This spectrum is consistent with Co^{III}Cbl species that are axially coordinated to an alkyl ligand such as -CH_3 or -Ado. There are also broader, more intense bands around 323 nm and a shoulder at 357 nm, which represent electronic transitions distinct from typical Co^{III}Cbl spectra. The rR data (77 K, λ_{ex}: 488.0 nm) show four strong features between 1450 cm^{-1} and 1650 cm^{-1}, all of which can be assigned to corrin-based vibrational frequencies based on a previous report.[225] When NOCbl was compared with isotopically labeled ^{15}NOCbl, a low-energy isotope-sensitive band shifted from 532 cm^{-1} to 496 cm^{-1} ($\Delta\nu_{Co\text{-}N}$ = 36 cm^{-1}). Deconvolution of the bands reveals two distinct features at 515 cm^{-1} (base-on) and 532 cm^{-1} (base-off) which shifts to 500 ($\Delta\nu_{Co\text{-}N}$ = 15 cm^{-1}) and 521 cm^{-1} ($\Delta\nu_{Co\text{-}N}$ = 11 cm^{-1}) upon isotopic substitution respectively. These features show that the Co-N(O) bond is stronger for base-off NOCbl as a result of decreased electron donation into σ^* molecular orbitals. A DFT vibrational frequency analysis predicts an isotope-sensitive IR-active band at 1688 cm^{-1} (assigned ν_{NO}), yet

this stretching mode is very weak in the experimental rR spectrum, which was explained by the lack of coupling between the N-O and corrin ring stretches (mechanically) and the NO moiety and corrin π system (electronically). This low intensity is not unprecedented for heme-containing NO complexes and could be a result of a broad band with a small polarizability component. The similarities in rR data between base-on and base-off NOCbl indicate that β ligand substitution from DMB → H_2O does not substantially alter the Co-N(O) bonding interaction,[222] which could be a consequence of the elongated Co-N(DMB) bond. DFT and natural bond order analyses (NBO) shed multiple insights into the electronic structure of both forms of NOCbl. Firstly, NO, which exerts a strong trans influence, is a stronger σ-donor than other alkyl groups that bind to Cbl (i.e. CH_3, Ado). Increasing σ-donor strength of the β axial ligand results in increased $3d_{z2}$ character in the HOMO and increased antibonding interactions with Co-N(DMB) σ^*. This is in line with experimental observations in the long Co-N(DMB) bond in NOCbl (MeCbl: 2.16 Å;[226] NOCbl: 2.35 Å).[216] For reference, $3d_{z2}$ contributes as much as 29% to the NOCbl HOMO (in addition to 40% NO π^* character), compared with only 7% in MeCbl.[224] Secondly, DMB → H_2O ligand substitution leads to a stabilization of MOs that contain significant contributions from $3d_{z2}$ orbitals. Lastly, a more accurate description of NOCbl is a hybrid of the Co^{III}-NO^- ↔ Co^{II}-$NO^\bullet$ resonance structures resulting from the substantial NO^- to Co^{III} charge donation. $NO^\bullet$ is known to inhibit Cbl-dependent enzymes MetH and MMCM through binding to the Co^{II}Cbl active site (vide infra). The summary of these detailed experiments and computations is that the Co $3d_{z2}$ orbital participates in significant covalent bonding with the NO p_z orbital and that the Co-N(O) bond is further strengthened by π-backbonding interactions. These interactions are distinct to NOCbl and are not yet observed in any other Co^{III}Cbl species. The primary biological implication of the structural and electronic features of NOCbl, including the strength of the Co-N(O) bond and lengthening of the

Co-N(DMB) bond, is that in order to reactivate the nitrosylated enzymes, NOCbl removal from the active site and subsequent Cbl replacement rather than simple NO dissociation may be required.

1.5.2 Cobalamin-dependent enzymes in humans and their interactions with NO•

There has been substantial controversy over the years regarding the interaction of NO• with cobalamins,[214,220] which could be attributed to the varying oxidation states (+3, +2, +1) of the cobalt center in Cbl throughout catalytic cycles (Cbl^{III}/Cbl^{II}: 0.20 V; Cbl^{II}/Cbl^{I}: -0.61 V, both vs. SHE).[227-228] MMCM and MetH are chemically unreactive with NO• in their diamagnetic Co^{III} (d^6) resting states, but the Co^{II}Cbl (d^7) intermediates formed in cofactor reactivation (for MetH) or during catalysis (MMCM) react readily with NO•,[220] given that both have unpaired electrons. In fact, NO• reacts with Co^{II}Cbl to form NOCbl with a formation constant of $1 \pm 0.5 \times 10^8$ at pH 7, and therefore, it is likely that the Co^{II}Cbl species (vitamin B_{12r}; reduced form of Cbl) is the cobalamin form that most effectively binds NO• in biological systems.[220,223] Despite the known stability of $\{CoNO\}^8$ complexes, NOCbl is then capable of transferring NO^+ to Hb accompanied by the reduction of Co^{III} to Co^{II} in vitro.[219] There is also a report on NO• inhibiting MetH in vivo which most likely involves its reaction with Co^{I}Cbl, leading to a disrupted carbon flow through the folate pathway.[229] However, there is no convincing evidence to support the binding of NO• to cobalamin in the +3 oxidation state (Co^{III}Cbl). Earlier reports claimed that Co^{III}Cbl reacted with NO•, but van Eldik later determined that any observed Co^{III}Cbl/NO• reactivity was a result of NO_2^- impurities, thus forming nitrocobalamin (NO_2Cbl).[230] The Co^{III}Cbl/NO_2^- reaction has been known since the mid-20th century.[231] Interestingly, Brasch and coworkers have shown that as-isolated H_2O-Co^{III}Cbl reacts directly with HNO after Angeli's Salt (AS) decomposes at pH > 10.80. At

lower pH (< 9.90), it instead reacts through an HNO donor-Cbl interaction.[232] In spite of the different mechanisms of reaction, both lead to formation of the corresponding {CoNO}^{8} NOCbl. They have also shown that $Co^{I}Cbl$, which is present in the catalytic pathway of MetH, can react with NO_2^- and NO_3^-.[233] The former reacts with $Co^{I}Cbl$ to form $Co^{III}Cbl$ and HNO (eq. 1.18), which further reacts with $Co^{I}Cbl$ to ultimately afford $Co^{II}Cbl$ and NH_2OH (Eqs. 1.18-1.20; overall reaction: eq. 1.21). NO_3^- reacts with $Co^{I}Cbl$ to afford $Co^{II}Cbl$ and NH_4^+ under strongly acidic conditions (Eq. 1.22), but unfortunately the rate of the $Co^{I}Cbl/NO_3^-$ reaction is slower than the rate of $Co^{I}Cbl$ decomposition to accurately determine the stoichiometry at higher pH values.[233]

$$2H^+ + Co^{I}Cbl^- + HNO_2 \rightarrow H_2OCo^{III}Cbl + HNO \quad \text{(Eq. 1.18)}$$

$$2H^+ + Co^{I}Cbl^- + HNO + H_2O \rightarrow H_2OCo^{III}Cbl + NH_2OH \quad \text{(Eq. 1.19)}$$

$$2H^+ + 2Co^{I}Cbl^- + H_2OCo^{III}Cbl \rightarrow 4Co^{II}Cbl + 2H_2O \quad \text{(Eq. 1.20)}$$

$$4H^+ + 4Co^{I}Cbl^- + HNO_2 \rightarrow 4Co^{II}Cbl + NH_2OH + H_2O \quad \text{(Eq. 1.21)}$$

$$8Co^{I}Cbl^- + NO_3^- + 10H^+ \rightarrow 8Co^{II}Cbl + NH_4^+ + 3H_2O \quad \text{(Eq. 1.22)}$$

Interactions with $NO^{\bullet}$ can lead to the inhibition of MMCM and MetH,[229,234] and inhibition of these enzymes and even Cbl deficiency, sometimes induced by NO-binding, is implicated in multiple disease states. Inhibition of MMCM results in methylmalonic aciduria, an autosomal disorder that is often fatal in infants,[235] and $NO^{\bullet}$ has been shown to inhibit MMCM activity in rodent cell extracts within minutes by reacting with the Cbl^{II} cofactor.[234] However, no direct link of methylmalonic aciduria resulting from Cbl/$NO^{\bullet}$ interactions in vivo has yet been reported. Additionally, inhibition of MetH leads to hyperhomocysteinemia, which is characterized by abnormally high plasma levels of homocysteine (>15 μmol/L) leading to higher risk of cardiovascular disease, thrombosis, and neurological disorders such as Alzheimer's Disease.[236] Severe inhibition of MetH results in megaloblastic anemia and even degeneration of the spinal

cord along with lower intracellular folate levels and a redistribution of folate derivatives.[237] $NO^{\bullet}$ has been shown to inhibit MetH activity in vivo,[229] likely through interaction with Co^{I}Cbl which would form a transient $\{CoNO\}^{9}$ complex. Similarly, elevated levels of $NO^{\bullet}$ are observed in megaloblastic anemia.[238] Finally, there are many disease states associated with Cbl deficiency. In humans, deficiency of Cbl is a major cause of reversible megaloblastic anemia and neurobehavioral abnormalities, such as myelopathy and dementia.[239-240] $NO^{\bullet}$ exposure can cause Cbl deficiency which results from its inactivity and is known to produce impaired neurological functions.[241-242] However, $NO^{\bullet}$ toxicity resulting from MetH Cbl-interactions more often leads to hematological responses (e.g., megaloblastic anemia) rather than neurological pathologies.[243-244]

1.5.3 Implications of interactions of $NO^{\bullet}$ with cobalamin as a treatment for disease

Given the known affinity of Co^{II}Cbl for $NO^{\bullet}$, this interaction has been targeted for various medicinal purposes. Cbls show potential in treating pathologies that are associated with elevated $NO^{\bullet}$ levels by serving as $NO^{\bullet}$ scavengers.[245-246] For example, cyanocobalamin replacement therapy can scavenge the increased levels of $NO^{\bullet}$ in patients with megaloblastic anemia in the early phase of treatment and thus restore $NO^{\bullet}$ levels.[238] Cobinamide, a cobalamin precursor (Cbi, Figure 1.11), similarly binds $NO^{\bullet}$ with high affinity and is an effective intra- and extracellular $NO^{\bullet}$ scavenger, as it prevents $NO^{\bullet}$-induced vasodilation and NO-induced smooth muscle contraction.[245] A widely used treatment for hyperhomocysteinemia, a common downstream result of inhibited MetH, is a combination therapy of folic acid, B_6- and B_{12}-vitamins, which may have a role in preventing osteoporosis-induced bone fractures in high risk patients.[236] This treatment is partially in response to the homocysteine-induced $NO^{\bullet}$ production in vascular smooth muscle cells by activation of an NOS isoform.[247] In addition to Cbl and Cbi, NOCbl has also been proposed as a chemotherapeutic

agent to treat cancer due to its potent ability to inhibit growth via S-nitrosylation and subsequent induction of apoptosis in several human cancer cell lines.[248] NOCbl can also serve as a treatment of inflammatory and hyperproliferative skin disease.[249] Finally, nitrosyl-cobinamide (NOCbi) has been used an NO•-releasing agent that is stable in H_2O and was shown to increase coronary flow much more potently than other known NO• donors such as nitroglycerin.[250] Unrelated to NO_x but pertinent to another biologically occurring small molecule, Cbi has also been shown to effectively scavenge H_2S/HS^- and serve as an H_2S/HS^- antidote in a rabbit model,[251] which further emphasizes its role in RNS and RSS biology.

1.6 Co-L Reactivity

Further support for the utility of Co in NO_x chemistry is found in their ability to transform and release other small molecules. Indeed, Co complexes, many of which contain N_4 ancillary ligands, have been successful in facilitating NO_2^- reduction,[252] H_2 evolution,[253-261] and the reductive activation of other small molecules of biological/industrial interest such as N_2[262-263] and CO_2.[264] For example, the heterobimetallic CoMg complex **3** reduces NO_2^- to N_2O through a proton-coupled electron transfer (PCET) to the coordinated NO_2^- (Figure 1.12; Eq. 1.23).[252]

$$2NO_2^- + 4e^- + 6H^+ \rightarrow N_2O + 3H_2O \qquad \text{(Eq. 1.23)}$$

In the process, a $\{CoNO\}^8$ complex (ν_{NO} = 1636 cm^{-1}; Co-N-O = 122°; $E_{1/2}$ = -0.65 V vs. SCE) is formed and then reduced to afford a transient $\{CoNO\}^9$ intermediate (ν_{NO} = 1691 cm^{-1}). Immediate addition of $Et_3N{\cdot}HCl$ produced N_2O as the favored product. A series of stoichiometric reactions and bulk electrolysis experiements intimated the possibility of **3** to facilitate multiple turnovers, although a turnover number (TON) has was not reported. The ability to reduce NO_2^- to N_2O without release of other NO_x indicates the preference for the denitrification pathway. This

highlights the utility of reduced M-NO systems in the reduction of NO_x such as NO_2^- in model complexes in addition to known biological enzymes.

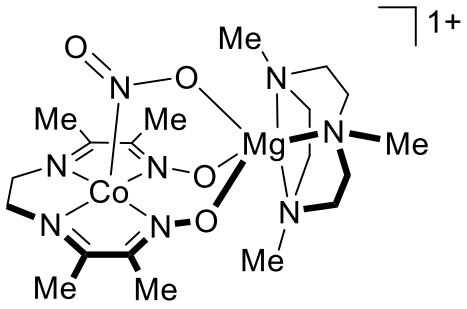

Figure 1.12. Co-N_4 complex **3** known to participate in nitrite reduction via generation of a cobalt nitrosyl.[252]

The Peters and Gray groups have pioneered families of Co small molecules that contain N_4 equatorial donor sets that are capable of electrocatalytic H_2 evolution.[254-255,265-271] Gray and coworkers have principally focused on Co^{II}-diglyoxime complexes that have low overpotentials and whose H_2 evolution is initiated upon reduction to Co^{I}.[255,265-267] Reacting with a proton donor leads to the formation of a Co^{III}-hydride intermediate that either protonates or reacts with another Co^{III}-hydride species, both of which subsequently release H_2. Another promising H_2-evolving complex is cobalt bis(iminopyridine) complex **4** that exhibits high Faradaic efficiency (H_2 yields up to 87 ± 10%) in constant potential electrolyses (-1.4 V vs. SCE) with an apparent second order rate constant of $\leq 10^7$ M^{-1} s^{-1} (Figure 1.13).[254] Peters and coworkers have published diimine-dioxime cobalt complexes such as **5** that generate H_2 at pH 2 in ~80% yield in controlled-potential electrolyses (-0.93 V vs. SCE) with a turnover number (TON) of 23 over 2 h (k_{obs} = 295 s^{-1}; Figure 1.13).[253] The Nocera group has reported Co^{II} hangman porphyrins, including [CoHPX-CO_2H] (**6**), which incorporate an acid/base moiety linked to a xanthene or furan backbone attached to a redox-

active porphyrin. Complex **6** releases H_2 from acidic MeCN solutions, and the acid/base functionality adjoined to the ligand scaffolds facilitates the PCET necessary for such a reaction.[259-261] Co-porphyrins such as **6** are an excellent example of the use of secondary sphere interactions to modulate reactivity at metal centers. Based on these H_2-evolving model complexes, notable commonalities are the presence of four equatorial nitrogen donors, accession of multiple Co oxidation states, and a vacant coordination site in the axial position(s), controlled by the energy of the d_{z2} orbital.

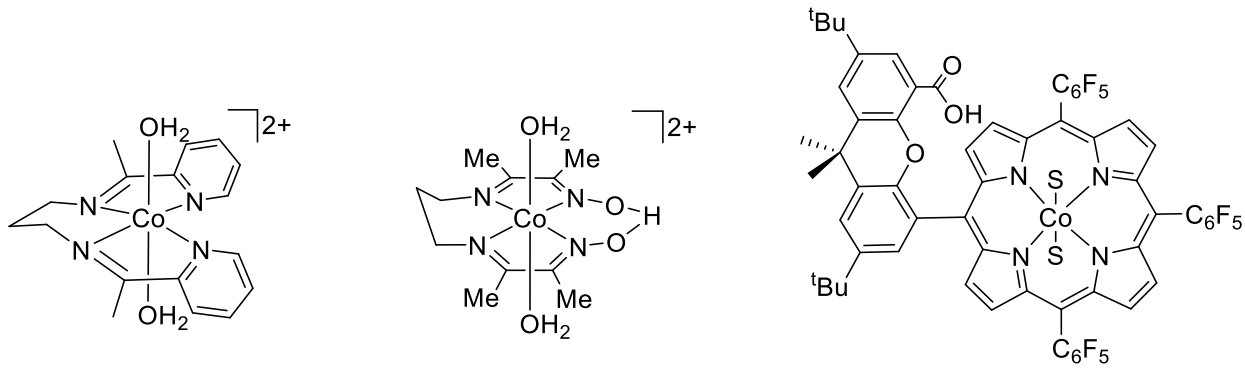

4
Bis(iminopyridine) scaffold

5
Diimine-dioxime scaffold

CoHPX-CO_2H (**6**)
Hangman porphyrin

Figure 1.13. Examples of Co-N_4 complexes known to participate in hydrogen evolution (**4**,[254] **5**,[253] and **6**[260]).

1.7 Overview of the Properties of {CoNO}^{8} Complexes

1.7.1 Structure and Spectroscopic properties of {CoNO}^{8} Complexes

The most common Enemark-Feltham notation for cobalt nitrosyls is {CoNO}^{8}. The predominant oxidation state assignment in {CoNO}^{8} systems evokes a LS Co^{III} d^6 ion with a coordinated $^1NO^-$ resulting in a diamagnetic (S_{tot} = 0) complex. While a reduced nitrogen oxide ligand is postulated in these constructs, very little has been reported with respect to the reactivity of the putative $^1NO^-$ although it should be noted that the less stable singlet state of the nitroxyl

anion is stabilized on Co^{III} and relatively non-reactive (vide infra). Perhaps this non-reactivity should be expected as a result of the kinetically-inert Co^{III} center. Additionally, the structural properties, especially the severely bent Co-N-O angle, appear to support this assignment although the Co^{II}-$NO^{\bullet}$ resonance structure has also been proposed.[272] The first structurally characterized metalloporphyrin nitrosyl was the 5C $\{CoNO\}^8$ complex [Co(TPP)(NO)] (**7**) (TPP = tetraphenylporphyrin) reported by Scheidt's group in 1973.[273] It was synthesized by purging purified $NO^{\bullet}$(g) into a degassed CH_2Cl_2 solution of [Co(TPP)] in the presence of piperidine. Since then, many other $\{CoNO\}^8$-P (P = porphyrin) complexes have been characterized and display the following average structural and vibrational parameters: Co–N(O) = 1.84 ± 0.00719 Å, N–O = 1.13 ± 0.0379 Å, Co-N-O = 124 ± 0.995°; ν_{NO} = 1675-1696 cm^{-1} (KBr or Nujol).[274-275]

There are relatively fewer structurally characterized non-P $\{CoNO\}^8$ complexes, but many of the trends observed in the P systems are also noted in the non-P analogs. Six-coordinate (6C) $[Co(en)_2(Cl)(NO)]ClO_4$ (en = ethylenediamine) (**8**) was synthesized in 1970 by Weaver and coworkers by bubbling NO(g) into a solution with $[Co(H_2O)_6]Cl_2$ and en for ~ 1 h.[276] Filtering and cooling the filtrate afforded a crystalline solid.[277] This complex represents the first structure of a 6C $\{CoNO\}^8$ complex with two bidentate ligands. There is very little displacement of Co from the N_4 plane of the en ligands (0.09 Å), and the Co-N(O) and N-O bond distances of 1.820 Å and 1.109 Å respectively as well as Co-N-O bond angle of 124.4° are consistent with metric trends in $\{CoNO\}^8$-P. Vibrational analysis shows an N-O stretching frequency of 1611 cm^{-1}.[278] Given the tendency for disorder and thermal vibrations in the N-O unit, the authors noted the difficulty in accurately determining the N-O bond distance. Notably, the Co-Cl bond is 2.576 Å, highlighting the strong trans influence of the NO group on the Cl ligand. The complex $[Co(en)_2(OClO_3)(NO)]ClO_4$ (**9**) was later reported to have similar structural features as **8** except a

longer N-O bond (1.15 Å) and a Co-O(ClO_3) bond distance of 2.360 Å (Table 1.3).[278] The trans influence of the axial NO is also noted in $[Co(NH_3)_5(NO)]Cl_2$ (**10**) with a significantly longer Co-N_{trans} bond of 2.28 Å than the Co-N_{equat} bonds of 1.93 Å.[279] Given the ability of NO^- to serve as a strong σ-donor and poor π-acceptor, it is not surprising that the majority of structurally characterized $\{CoNO\}^8$ complexes are five-coordinate (5C; vide infra). Conversely, NO^+ and $NO^\bullet$ are relatively good π-acceptors.

A family of $\{CoNO\}^8$ complexes bearing a tropocoronand ligand (TC) with varying lengths of the polymethylene chain linker were synthesized by Lippard and coworkers.[280-281] Purging NO(g) into a THF (*n* = 3, 4 for complexes **11**, **12** respectively) or CH_2Cl_2 (*n* = 5, complex **13**) solutions of $[Co^{II}(TC\text{-}n,n)]$ afforded the corresponding [Co(TC-*n*,*n*)(NO)] complexes. [Co(TC-*n*,*n*)(NO)] (*n* = 4, 5) exhibit diamagnetic behavior, indicative of the typical assignment of LS Co^{III}-NO^-, with ν_{NO} being ~1600 cm^{-1}. The structural features further support a coordinated NO^- with the bent Co-N-O angle (~129°) and an N-O bond distance (~1.16 Å) that lies between that which is reported for $NO^\bullet$ and ^1HNO (1.15 and 1.21 Å, respectively). Interestingly, [Co(TC-3,3)(NO)] (**11**) was originally reported as paramagnetic,[280] which deviated from the typical *S* = 0 ground state for these systems. A DFT study and experimental reinvestigation elucidated that **11** is indeed diamagnetic and has a substantial singlet-triplet gap of ~0.5 eV.[282] The initial paramagnetic interpretation was likely due to difficulty obtaining sufficient quantities of **11**. On the other hand, an NO(g) purge into a solution [Co(TC-6,6)] afforded the corresponding $\{Co(NO)_2\}^{10}$ and [Co(TC-6,6)(η^2-O_2N)] species. The mononitrosyl has not yet been isolated, likely a result of low-energy, thermally accessible triplet states.[282] The electrochemistry of this family has not yet been probed, although it is expected that a reversible electrochemical event

would be observed for the $\{CoNO\}^{8/9}$ with an $E_{1/2}$ lying close to that of other $\{CoNO\}^{8}$ complexes bearing dianionic ligands (Table 1.3).

Another 5C $\{CoNO\}^{8}$ system involved the N_2S_2 ligand bme-dach (*N*,*N*′-Bis(2-mercaptoethyl)-1,4-diazacycloheptane) by Darensbourg.[283] Purging NO(g) into a 60 °C MeOH solution of dimeric $[Co(bme\text{-}dach)]_2$ followed by a CH_2Cl_2/pentane crystallization resulted in $[Co(N_2S_2)(NO)]$ (**14**) as dark purple solid in 58% yield. X-ray crystallography of **14** revealed the square-pyramidal geometry of the Co center. The Co-N(O), N-O and Co-N-O metric parameters are in line with other $\{CoNO\}^{8}$ complexes (1.787 Å, 1.187 Å, 123.8° respectively). Addition of a $[W(CO)_4]$ adduct to **14** formed $[Co(N_2S_2)(NO)][W(CO)_4]$ (**15**) via S,S-binding of the W fragment. This modification negligibly impacted the structural/geometric features yet dramatically influenced the electronic features, which is most easily observed in the $\{CoNO\}^{8/9}$ redox couple. Similar to $\{FeNO\}^{7}$ systems, some $\{CoNO\}^{8}$ complexes also display diffusion-controlled electrochemical waves arising from what has been assigned as the $\{CoNO\}^{8/9}$ redox couple. Complex **14** exhibits an $E_{1/2}$ of -1.08 V (vs. Fc^{+}/Fc) which shifts by +0.49 V upon introduction of the $[W(CO)_4]$ adduct in **15**. This highlights the significant effect of peripheral ligands on the redox potential of the MNO unit.

An additional example of a heterobimetallic $\{CoNO\}^{8}$ complex with a similar $E_{1/2}$ (of -0.65 V vs. Fc^{+}/Fc) is $[(NO)(Cl)Co(^{Me}doen)Mg(Me_3TACN)(H_2O)](BPh_4)$ (**16**) (where ^{Me}doen = a diimine-dioxime ligand and Me_3TACN = 1,4,7-trimethyl-1,4,7-triazacyclononane).[252] Complex **16** was synthesized as a spectroscopic standard for the intermediate formed in nitrite reduction to form N_2O using this platform (Figure 1.12, Eq. 1.23). As an intermediate, **16** forms from the reduction of a conserved μ-(η^1-N:η^1-O)-NO_2 in the presence of TEA·HCl and is then reduced to form a putative $\{CoNO\}^{9}$ complex. Protonation of the reduced species leads to the presumed

elimination of N_2O. Complex **16** is isolated from the reaction of the μ-(η^1-N:η^1-O)-NO_2 complex with two equivs of TEA·HCl in THF for 6 h followed by a counterion exchange with $NaBPh_4$. Pentane diffusion into THF afforded **16** as a red crystalline solid. The FTIR spectrum exhibited ν_{NO} at 1636 cm^{-1} (ATR), and despite the significantly bent Co-N-O angle of 122.1° and diamagnetism, the relatively long Co-N distance of 1.856 Å and shorter N-O distance of 1.149 Å are more in line with Co^{II}-$NO^{\bullet}$ in resonance with Co^{III}-NO^{-} (Table 1.3). Thorough characterization of the chemically reduced $\{CoNO\}^9$ analog of **16** has been precluded due to instability of the reduced species. However, when generated in situ, the addition of stoichiometric protons led to the liberation of 0.5 equiv of free N_2O.

The $\{CoNO\}^8$ complex [Co(LN_4^{Pr})(NO)] bearing an N_4 tetradentate non-macrocyclic ligand was published by Harrop and coworkers in 2012 (**17**; where LN_4^{Pr} = dianion of (*N*^{1}*E*,*N*^{3}*E*)-*N*^{1},*N*^{3}-bis((1H-pyrrol-2-yl)methylene)-propane-1,3-diamine).[272] Complex **17** was synthesized by purging NO(g) into an MeCN solution of $(Et_4N)_2$[Co(LN_4^{Pr})$(Cl)_2$] for 1.5 min under dark conditions. Workup of the dark red crude reaction mixture with THF afforded **17** in 75% yield. Diffusion of Et_2O into a THF solution of **17** at -20 °C led to X-ray quality crystals. The dianionic nature of LN_4^{Pr2-} leads to a negative redox potential of **17** at -1.40 V (vs. Fc^+/Fc). The N-O stretching frequency (ν_{NO}) is 1645 cm^{-1} and in line with other P and non-P ν_{NO} values (Table 1.3). The structure of **17** highlights that the metric parameters are consistent with those reported for similar Co-NO compounds (Co-N, 1.7890 Å; N-O, 1.1551 Å; Co-N-O, 125.97°; Table 1.3.)

In 2015 and 2016, Nam and coworkers reported a family of $\{CoNO\}^8$ complexes bearing neutral TMC ligands $[Co(n\text{-TMC})]^{2+}$ (where TMC = 1,4,7,10-tetramethyl-1,4,7,10-tetraazacyclam, where *n* = 12, 13, or 14).[284-285] The common route of purging excess NO(g) into an MeCN solution of the precursor $[Co^{II}(n\text{-TMC})]^{2+}$ was found to be an effective nitrosylation

method for *n* =12 (**18**), 13 (**19**). Layering the MeCN solutions with Et_2O resulted in pink colored crystals after slow diffusion over several days. For *n* = 14, stoichiometric NO(g) was added to an MeCN solution of $[Co^{II}(14\text{-TMC})]^{2+}$ at -40 °C resulting in $[Co(14\text{-TMC})(NO)]^{2+}$ (**20**). In spite of the differences in ligand size, the ν_{NO} of **18, 19,** and **20** are 1712, 1716, and 1715 cm^{-1} respectively. The experimentally determined metric parameters within the Co-NO unit of **18** and **19** are similar (**18**: Co-N, 1.7844 Å; N-O, 1.155 Å; Co-N-O, 128.50°; **19**: Co-N, 1.797 Å; N-O, 1.159 Å; Co-N-O, 124.4°).[285] The geometry optimized structure of **20** is in good agreement with the structural features of **18** and **19,** except for an elongated Co-N(O) bond of 1.907 Å. This elongation leads to increased lability of the NO in **20** and can be attributed to the spin-state of the $[Co(n\text{-TMC})]^{2+}$ starting material. $[Co(n\text{-TMC})]^{2+}$ for complexes **18** (*n* = 12) and **20** (*n* = 14) has a Co center with *S* = 1/2 and 3/2, respectively. The LS Co^{II} center and smaller ring size of 12-TMC are the two principle factors that lead to a higher affinity for $NO^{\bullet}$, as noted in the relatively shorter Co-N(O) bond of the resulting complex **18** (1.7844 Å vs. 1.907 Å for **20**). The structures of **18, 19**, and **20** fall in-line with the trends of non-porphyrin $\{CoNO\}^8$ systems (Co–N(O) = 1.796 Å, N–O = 1.159 Å, Co-N-O = 126.2°), although the ν_{NO} is higher by ~70 cm^{-1} ($\{CoNO\}^8$ avg ν_{NO} = 1645 cm^{-1}), likely a result of diminished electron donation from the neutral TMC ligands into the NO π^* orbital (see Figure 1.14 and Table 1.3). Given the small deviation of the metric parameters within $\{CoNO\}^8$ complexes, the ν_{NO} is a more effective measure of the electronic nature of Co-NO.

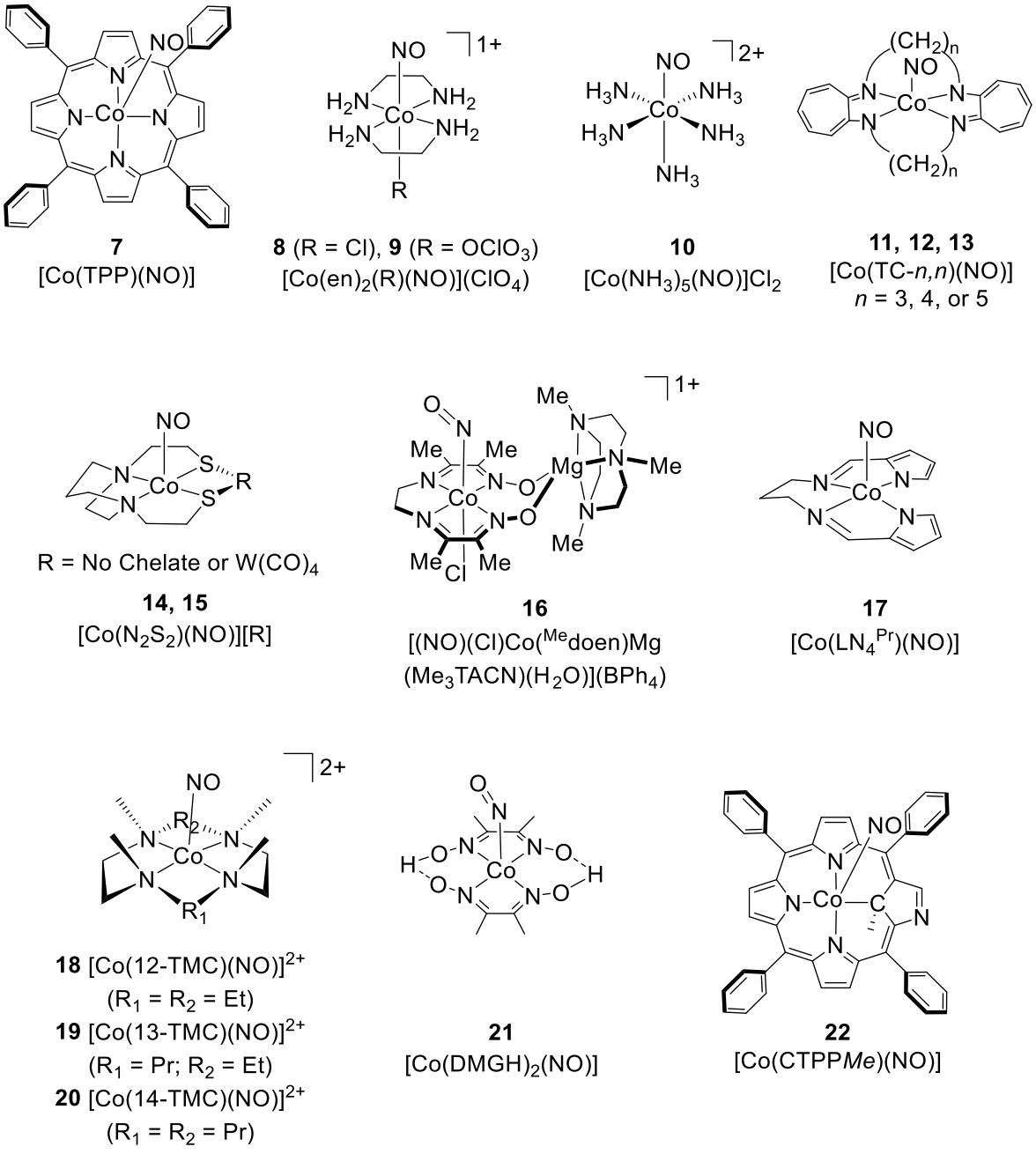

Figure 1.14. Structurally characterized non-porphyrin {CoNO}^{8} complexes. [Co(TPP)(NO)] is used as reference given the numerous structurally characterized porphyrin-based {CoNO}^{8} complexes.[286] [Co(CTPP*Me*)(NO)] (**22**) is included given its relevance to {CoNO}^{9} reactivity (vide infra).[287] Otherwise, non-porphyrin {CoNO}^{8} complexes are highlighted. See Table 1.3 for structural and electrochemical parameters.

Table 1.3. Summary of data for select structurally characterized $\{CoNO\}^8$ complexes.

$\{CoNO\}^8$ Complex	$E_{1/2}$ **(V)**[a]	ν_{NO} **(cm^{-1})**	**Co-N (Å)**	**N-O (Å)**	**∠CoNO (°)**	**Ref**
[Co(TPP)(NO)] (**7**)	-1.58[b]	1689[e]	1.833	1.01	135.2	273,288
[Co(OEP)(NO)]	-1.66[b]	1677[e]	1.8444	1.1642	122.70	289-290
$[Co(en)_2(Cl)(NO)]ClO_4$[m] (**8**)	--	1611[h]	1.820	1.109	124.4	276
$[Co(en)_2(OClO_3)(NO)]ClO_4$[m] (**9**)	--	1668[h]	1.805	1.15	122.7	278
$[Co(NH_3)_5(NO)]Cl_2$ (**10**)	--	1620[e]	1.99	1.26	~180	279,291
[Co(TC-3,3)(NO)][h] (**11**)	--	1656[e]	1.785	1.137	127.3	280
[Co(TC-4,4)(NO)][h] (**12**)	--	1584[e]	1.779	1.151	128.9	280
[Co(TC-5,5)(NO)][h] (**13**)	--	1622[e]	1.7856	1.177	129.48	281
$[Co(N_2S_2)(NO)]$ (**14**)	-1.08[c]	1604[f]	1.787	1.187	123.8	283
$[Co(N_2S_2)(NO)][W(CO)_4]$ (**15**)	-0.59[c]	1638[f]	1.80	1.21	123.1	283
[(NO)(Cl)Co(^{Me}doen)Mg (Me_3TACN)(H_2O)]BPh_4 (**16**)	-0.65[d]	1636[g]	1.856	1.149	122.1	252
$[Co(LN_4^{Pr})(NO)]$ (**17**)	-1.40[d]	1645[e]	1.7890	1.1551	125.97	272
$[Co(12\text{-}TMC)(NO)](ClO_4)_2$[j] (**18**)	--	1712[e]	1.7844	1.155	128.50	285
$[Co(13\text{-}TMC)(NO)](ClO_4)_2$[j] (**19**)	--	1716[e]	1.797	1.159	124.4	285
$[Co(14\text{-}TMC)(NO)](ClO_4)_2$[j,k] (**20**)	--	1715[e]	1.901	1.152	129.35	284
$[Co(DMGH)_2(NO)]$ (**21**)[n]	--	1641[h]	1.800	1.110	128.5	292-293
[Co(CTPP*Me*)(NO)][l] (**22**)	-0.835[f]	1620[e]	1.7886	1.187	125.62	287
Avg for 5C non-P complexes[o]	--	1645 ± 41.8	1.796 ± 0.0221	1.159 ± 0.0275	126.2 ± 2.69	

[a]Represents the $E_{1/2}$ value for the $\{CoNO\}^{8/9}$ redox couple normalized to Fc^+/Fc based on the information found in the literature.[294] [b] butyronitrile, [c] DMF, [d] MeCN, [e] KBr, [f] CH_2Cl_2, [g] ATR, [h] Nujol mull, [j]12-TMC = 1, 4, 7, 10-tetramethyl-1, 4, 7, 10-tetraazacyclododecane; 13-TMC = 1, 4, 7, 10-tetramethyl-1, 4, 7, 10-tetraazacyclotridecane; 14-TMC = 1, 4, 8, 11-tetramethyl-1, 4, 8, 11-tetraazacyclotetradecane. [k] DFT geometry optimized structure. [l] CTPP*Me* = an *N*-confused porphyrin; 2-aza-21-methyl-5,10,15,20-tetraphenyl-21-carbaporphyrin. [m] en = ethylenediamine; the coordinated ClO_4^- is in the *trans* position relative to the nitrosyl. [n] Values averaged over 3 discrete molecules in unit cell. [o] Only 5C, non-P, experimentally determined structures **11 -19** and **21** included in averages and standard deviations. There are other examples of structurally characterized $\{CoNO\}^8$ complexes that are P_2Cl_2-,[295] As_4- or As_4N-,[296] S_4-,[297] N_4,[298] or N_2O_2-ligated.[299]

1.7.2 {CoNO}^{8} Reactivity with O_2, $O_2^{\bullet-}$, and $NO^{\bullet}$

Another perspective of HNO/NO^- reactivity is the fate of a metal-coordinated HNO/NO^- in the presence of small molecules. Given the paucity in the literature of isolated M-HNO and M-NO^- complexes,[300-301] it is no surprise that this reactivity has yet to be investigated. However, the fate of M-NO^- in the presence of known signaling agents is a small yet emerging field, and there are examples of the reactivity of {CoNO}^{8} complexes with the exogenously added small molecules O_2 and $O_2^{\bullet-}$[284-285,302-305] (Figures 1.15 and 1.16) in addition to the known $NO^{\bullet}$ disproportionation with coordinated Co-NO.[306-314] Brasch and coworkers have highlighted the reactivity of NOCbl, a biologically occurring {CoNO}^{8} species, with O_2.[302] Their detailed investigation showed that the aquocobalamin (H_2OCbl^+) and *N*-bound nitrocobalamin (NO_2Cbl) products form through a common Co^{III}-peroxynitrite intermediate, and the O_2/NOCbl reactivity significantly increases with the presence of a strong axial σ-donor such as the 5,6-dimethylbenzimidazole (DMB) ligand present at the lower axial site of base-on Cbl (vide supra; Figure 1.11).[302] The proposed mechanism for this reaction is consistent with the mechanism of oxidation of non-corrinoid cobalt nitrosyls containing tetradentate dianionic Schiff base ligands.[304]

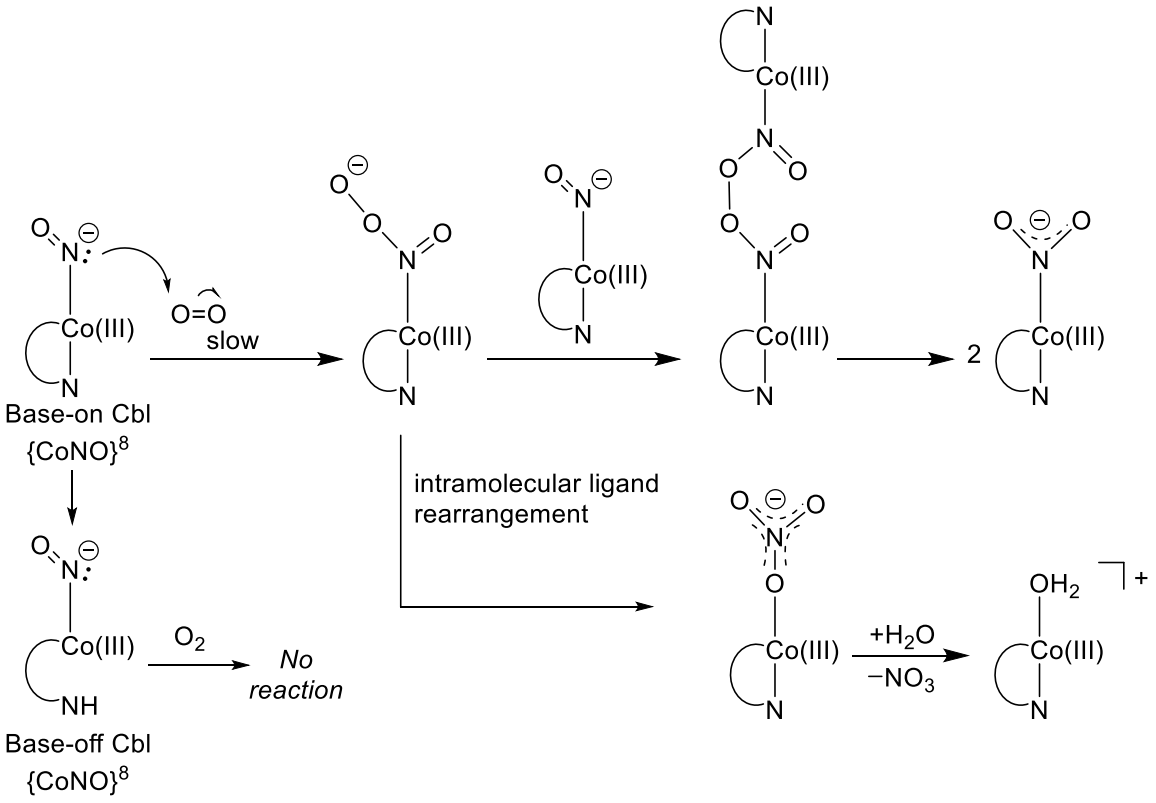

Figure 1.15. Proposed reaction mechanism for the formation of NO_2Cbl from the reaction of NOCbl and O_2. Adapted from references 302[302] and 304.[304]

A peroxynitrite intermediate is also proposed in the oxidation of oxymyoglobin (MbO_2) by free $NO^{\bullet}$ that has dissociated from a 5- to 15-fold excess of $[Co(DMGH)_2(NO)]$ (**21**) (where DMGH = dimethylglyoximate; $[Co(DMGH)_2(L)_x]^{n+}$ = cobaloxime).[315] In the process, free NO_3^-, metMb, and $[Co^{II}(DMGH)_2]$ form with $k = 3.1 \times 10^7$ M^{-1} s^{-1} at 10 °C. The resulting Co^{II}-L can serve as an effective trap for exogenous O_2, rapidly forming a μ-superoxo or μ-superoxo dimer $[(DMGH)_2Co(\mu\text{-}O_2)Co(DMGH)_2]$ that is capable of oxidizing deoxyMb, although this is not a dominant process in the above reaction. The oxidation of cobaloxime nitrosyls and their derivatives by O_2 has also been shown to form the corresponding nitrato- (>50%) and nitro- (<50%) species with reactions completed in 15 s.[305] These trends are further apparent with

oxycoboglobin models [Co^{II}(Por)(NH_3)(O_2)] (where Por = *meso*-tetraphenyl- and *meso*-tetra-*p*-tolylporphyrinato dianions) and their reactions with $NO^{\bullet}$. An η^1-peroxynitrite intermediate forms then rearranges to the thermally unstable η^1-ONO_2 nitrato species, which ultimately affords dissociated NO_3^- and the corresponding oxidized complex [Co^{III}(Por)(NH_3)$_n$] (*n* = 1, 2).[316] The instability of the six-coordinate (6C) nitrato species is consistent with what is observed with Hb, Mb, and other model Fe-porphyrins.

In 2016, Nam and coworkers documented the reactivity of three {CoNO}^{8} complexes **18-20** bearing TMC ligands ([Co(*n*-TMC)(NO)]$^{2+}$, *n* = 12 (**18**), 13 (**19**), 14 (**20**)). Complexes **18** and **19** react with $O_2^{\bullet-}$ to form the corresponding [Co(*n*-TMC)(η^2-O_2N)]$^{2+}$ complexes (*n* =12, 13), and complex **20** reacts with O_2 to form the corresponding [Co(14-TMC)(η^2-O_2NO)]$^{2+}$. The three NO_x products all form via a Co^{II}-peroxynitrite intermediate (Figure 1.16).[284-285] [Co(14-TMC)(NO)]$^{2+}$ (**20**) is dioxygenated by O_2 with a k_{obs} of 7.6(7) × 10^{-4} s^{-1} to form exclusively one product: the O,O-chelated nitrato species [Co(14-TMC)(η^2- O_2NO)]$^{2+}$ verified crystallographically and by spectral monitoring of this reaction (Co-O distances: 2.234 and 2.225 Å). The ν_{NO} of the {CoNO}^{8} species at 1715 cm^{-1} disappears upon the appearance of an N-O stretch at 1302 cm^{-1} attributed to the coordinated NO_3^-. Based on isotopically labeled $^{18}O_2$, it was determined that two of the three O atoms in η^2-O_2NO originate from O_2, and the peroxynitrite intermediate was confirmed through a phenol ring nitration assay. In contrast to the reactivity observed in [Co(14-TMC)(NO)]$^{2+}$ (**20**), NOCbl, and other small molecules, no reaction occurs between [Co(12-TMC)(NO)]$^{2+}$ (**18**) or [Co(13-TMC)(NO)]$^{2+}$ (**19**) and O_2.[285] These complexes do, on the other hand, react with $O_2^{\bullet-}$ to form the corresponding nitrito species in ~85% yield with concomitant production of 0.5 equiv of O_2. The FTIR once again shows the disappearance of the {CoNO}^{8} ν_{NO} at 1712 cm^{-1} and the concurrent appearance of bands at 1261 and 1300 cm^{-1}, consistent with η^2-O_2N coordination.

Using crystals grown from diffusion of Et_2O into MeCN solutions of the corresponding η^2-O_2N complexes, X-ray crystallography confirmed the formation of the Co^{II} nitrito complexes [Co(12-TMC)(η^2-O_2N)]$^{2+}$ and [Co(13-TMC)(η^2-O_2N)]$^{2+}$ with Co-O bond distances of ~2.22 and ~2.13 Å. The N-O bond distances lengthen between the {CoNO}^{8} complex and [Co(*n*-TMC)(η^2-O_2N)]$^{2+}$ from ~1.16 Å to ~1.26 Å for both systems (*n* = 12, 13). Taken together, these results highlight the general reactivity of {CoNO}^{8} complexes with O_2 and $O_2^{\bullet-}$ to form the corresponding NO_2^- and NO_3^- complexes, often through an $ONOO^-$ intermediate.

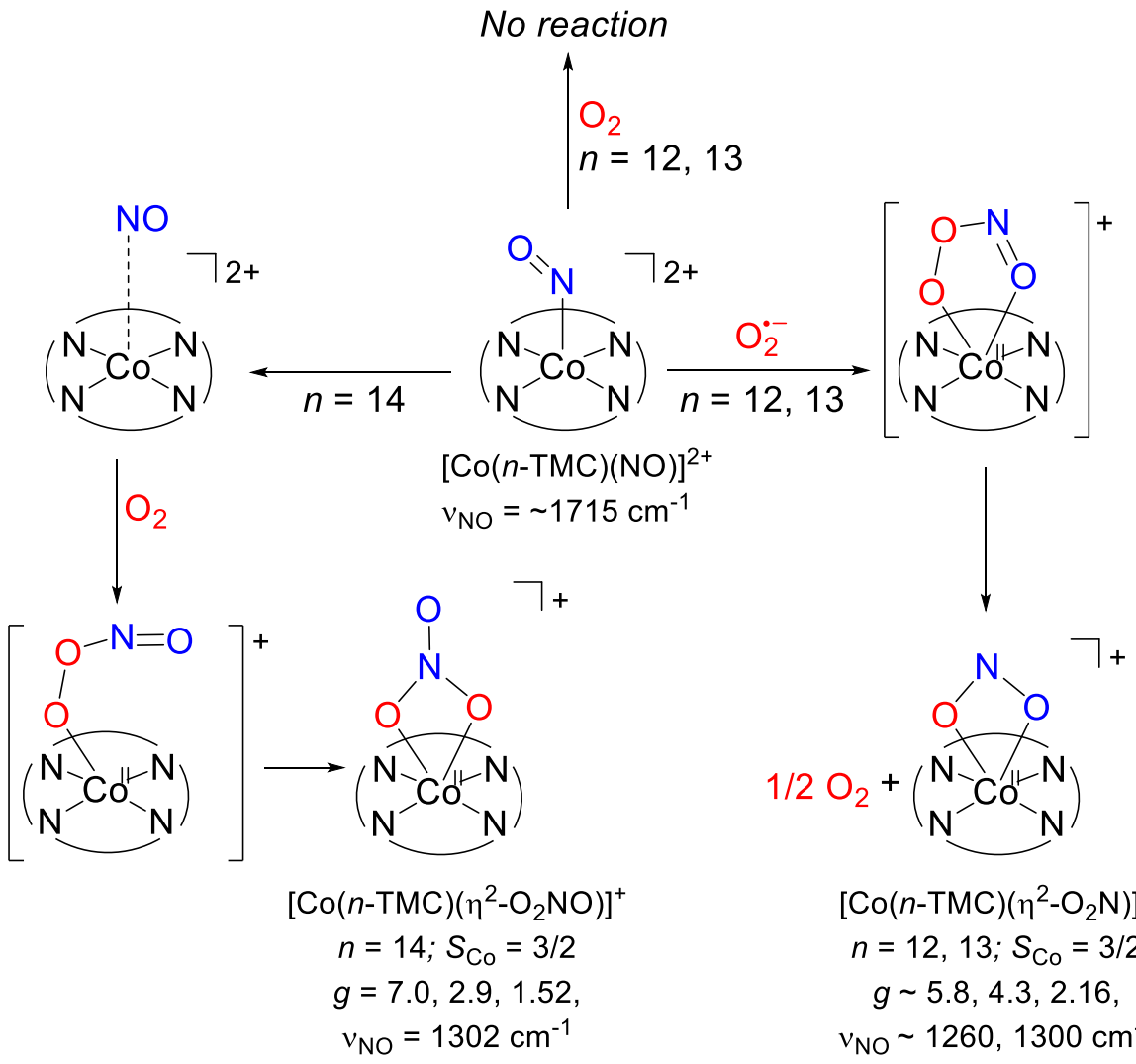

Figure 1.16. Mechanism for oxygenation of cobalt nitrosyls bearing TMC ligands in the presence of O_2 and $O_2^{\bullet-}$, compiled from references 285[285] and 284.[284] Compounds in brackets have not been spectroscopically observed, but support of their formation is found in the phenol ring nitration of 2,4-di-*tert*-butylphenol.

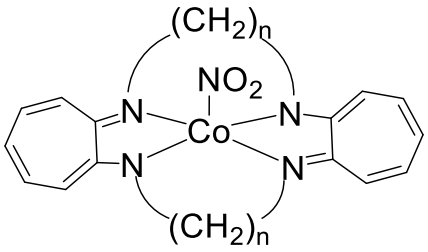

23

[Co(TC-*n,n*)(η^2-NO_2)]

Figure 1.17. Example of Co^{III}-η^2-O_2N (**23**) complex shown to react with NO•.[317] TC = tropocoronand.

The reactivity of Co^{III} nitrito complexes bearing a dianionic tetraazamacrocyclic ring have also been investigated with NO•.[317] Depending on the length of the tropocoronand (TC) polymethylene chain linker, [Co(TC-*n,n*)(η^2-O_2N)] affords the corresponding $\{CoNO\}^8$ **12** (*n* = 4), $\{CoNO\}^8$ **13** (*n* = 5), and/or $\{Co(NO)_2\}^{10}$ species (*n* = 5, 6) (Figure 1.14). This reactivity may correlate to the reactivity of Co^{III}-nitrito species present in biology, such as NO_2Cbl. Contrastingly, [Co(TC-6,6)(NO)] has eluded isolation, likely due to the low singlet-triplet gap which allows for the triplet state to be thermally accessed.[282] This could promote NO dissociation or further reactivity to form [Co_2(TC-6,6)$(NO)_4$].[281] There are also several examples of the disproportionation of NO• with cobalt nitrosyls to form NO_2 and N_2O, often requiring the presence of base in order to destabilize the coordinated nitrosyl.[306-314] Gwost and Caulton first reported such a phenomenon using [$Co(en)_2(NO)]Cl_2$ and [$Co(DMGH)_2(NO)]\cdot CH_3OH$ (**21·CH_3OH**) (Figure 1.18). In summary, the reactivity of these cobalt nitrosyls with oxygen and nitrogen species highlights the anionic nature of the NO moiety; however, the physiological consequences of such reactivity have yet to be investigated.

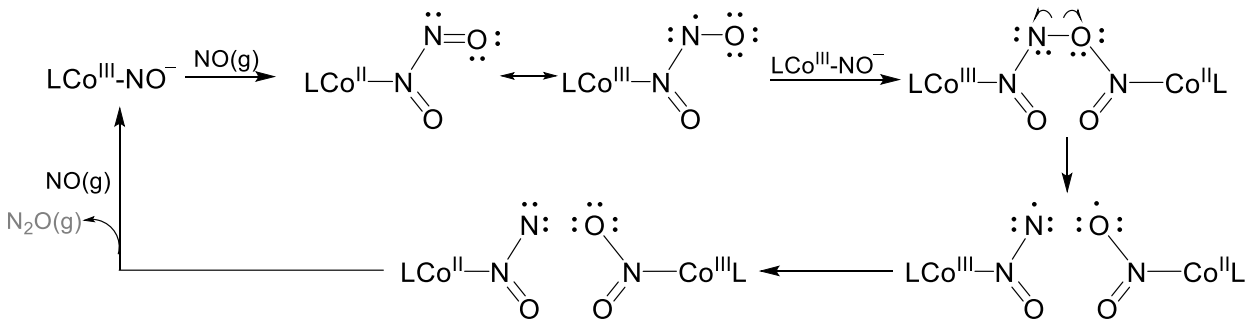

Figure 1.18. Mechanism of oxidation of coordinated nitric oxide by free NO•. Adapted from references 308[308] and 217.[217]

1.7.3 NO^n transfer from {CoNO}^{8} complexes

While the release and transfer of the nitrosyl ligand from {CoNO}^{8} complexes has not been extensively explored, a few earlier studies and one recent investigation report such activity under several conditions.[284,318-321] Armor first showed the release of NO from $[Co(NH_3)_5(NO)]Cl_2$ to Cr^{II} for the quantitative formation of $Cr^{II}NO$ under acidic conditions (0.1 M HCl).[318] This reaction was hypothesized to occur through an associative mechanism but was later determined to release free NO• upon decomposition in aqueous conditions. Ungermann and Caulton later established that the {CoNO}^{8} cobaloxime, namely $[Co(DMGH)_2(NO)]$ (**21**), could transfer NO• to a series of low-valent, coordinatively unsaturated, and halogen-bound complexes (Fe, Co, Ni, and Ru).[321] This reaction was hypothesized to occur through a net NO• for X• exchange (X = Cl).[321] Interestingly, reaction of **21** with Fe^{I}- or Fe^{II}-complexes resulted in dinitrosyl iron complexes (DNICs) as the primary NO-containing product. In a more bio-relevant study, Doyle showed the feasibility of NO• transfer from several {CoNO}^{8} complexes, including **21**, $[Co(en)_2(Cl)(NO)]ClO_4$ (**8**) (en = ethylenediamine), and $[Co(NH_3)_5(NO)]Cl_2$ (**10**) to Fe^{II}-heme proteins such as hemoglobin,

myoglobin and cytochrome *c*.[320] These studies involved the release of NO• from the $\{CoNO\}^8$ complexes to the in situ generated Fe^{II}-heme proteins using dithionite as reducing agent. No reaction occurred between $[Co(DMGH)_2(NO)]$ (**21**) or $[Co(en)_2(Cl)(NO)]ClO_4$ (**8**) with the Fe^{III}-heme proteins even with 10- to 20-fold excess $\{CoNO\}^8$. Notably, $[Co(NH_3)_5(NO)]Cl_2$ (**10**) reacts with both Fe^{II}- and Fe^{III}-hemes; however, the complex decomposes in H_2O leading to the release of free NO• which can then rapidly diffuse to a heme protein with the same selectivity as free NO•. In a follow-up publication from Doyle, rapid loss of NO• to deoxyhemoglobin (Hb) is observed when Hb and **21** are treated with dithionite.[319] The $\{CoNO\}^9$ complex, which is a likely NO-releasing agent, may be generated under these conditions.

In 2016, Nam and coworkers reported the transfer of NO• from $\{CoNO\}^8$ complex $[Co(14\text{-}TMC)(NO)]^{2+}$ (**20**) to $[Co^{II}(12\text{-}TMC)]^{2+}$ via a dissociative mechanism with an overall $k_{obs} = 8.2(7) \times 10^{-4}$ s^{-1} (Figure 1.14).[284] Contrastingly, the opposite NO• transfer reaction in which the cobalt nitrosyl bearing the smaller TMC ring $[Co(12\text{-}TMC)(NO)]^{2+}$ (**18**) would transfer to $[Co^{II}(14\text{-}TMC)]^{2+}$ does not occur. This difference in reactivity is attributed to the spin state of the two corresponding Co^{II} species. The X-band EPR spectra of $[Co^{II}(12\text{-}TMC)]^{2+}$ and $[Co^{II}(14\text{-}TMC)]^{2+}$ exhibit *g* vales at [2.34, 2.31, 2.05] and [7.41, 2.17, 1.50], which are consistent with LS $S = 1/2$ and HS $S = 3/2$ Co^{II}, respectively. These differences facilitate a proclivity to react with NO• when the tetraazamacrocyclic ring is smaller in size, i.e., when Co^{II} is $S = 1/2$; therefore, as the TMC ring size increases, the affinity for NO• decreases and conversely, the reactivity of the $\{CoNO\}^8$ complexes increases. These trends are observed in the O_2 reactivity with $[Co(n\text{-}TMC)(NO)]^{2+}$ (n = 12, 13, 14; Figure 1.16). Although scarce, there are a few examples of the liberation of the NO moiety from $\{CoNO\}^8$ complexes; however, their potential utility as HNO/NO^- donors when in the presence of known HNO/NO^- targets such as Fe^{III}-hemes was not studied.

1.8 {CoNO}^{9} coordination complexes[2,65]

Analogous to the {FeNO}^{8} notation for iron, {CoNO}^{9} is rare for cobalt nitrosyls with {CoNO}^{8} being the most common EF designation[274-275,322] and a number of {CoNO}^{8} complexes have been synthesized and extensively characterized (vide supra).[274] However, there is only one report on the isolation and structural characterization of a discrete {CoNO}^{9} complex among the 5C systems described above. The known 4C distorted tetrahedral and 5C porphyrinoid {CoNO}^{9} systems will thus serve as a point of reference; however, reports of these types of {CoNO}^{9} complexes are scarce and very much preliminary as of 2016.

Although the {CoNO}^{9} notation is elusive, it dates back nearly 100 years to the early 1930s in the synthesis of the tetrahedral organometallic complex, [$Co(CO)_3$(NO)] (**24**).[323-324] Numerous subsequent publications on the synthesis and properties of **24** also appeared over the next 50 years. This organometallic cobalt nitrosyl will not be discussed in detail; however, its corresponding structural and spectroscopic properties (Table 1.4) will serve as the benchmark of comparison for the 4C tetrahedral {CoNO}^{9} complexes that will be described. As of 2016, the synthesis and structural characterization of only four isolated {CoNO}^{9} complexes have been reported.[287,325-327]

[2] Melody A. Rhine, Brian C. Sanders, Ashis K. Patra, and Todd C. Harrop. *Inorg. Chem.* **2015**, *54*, 9351 – 9366. Reprinted (adapted) with permission from the American Chemical Society. Copyright 2015 American Chemical Society.

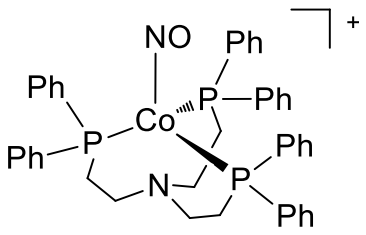

Figure 1.19. Structure of the $\{CoNO\}^9$ complex, $[Co(NO)(np_3)]^+$ (**25**).[325]

Sacconi and coworkers reported the synthesis and structure of the first non-organometallic $\{CoNO\}^9$ species, namely $[Co(NO)(np_3)]BPh_4$ (**25**), where np_3 = tris(2-diphenylphosphinoethyl)amine (Figure 1.19).[325,328] Complex **25** was obtained as a green crystalline material via NO(g) purge to a CH_2Cl_2 solution of the Co^I-hydrido complex, $[Co(np_3)H]$, containing $NaBPh_4$ in the reaction medium.[325] The 4C Co center in **25** was determined to be in a distorted tetrahedral geometry arising from the three tertiary phosphines and the nitrosyl to afford a NP_3 coordination sphere. The notable structural data indicated a Co-N-O bond angle of 165° with Co-N(O) and N-O bond distances of 1.83 Å and 1.14 Å, respectively. These values were somewhat atypical of cobalt nitrosyls; however, the low quality crystal data presumably explains the noted deviation. A ν_{NO} IR peak for **25** was observed at 1680 cm^{-1} (Nujol), which is significantly lower than that observed in $[Co(CO)_3(NO)]$ (**24**) ν_{NO} = 1818 cm^{-1} (Ar matrix, 7 K).[325,329] The π-donating phosphines seemingly account for significant back-donation into the NO of **25** whereas the three CO ligands of **24** effectively compete for this electron density to result in the higher ν_{NO}. Solid-state magnetic susceptibility measurements indicated a μ_{eff} of 1.98 μ_B at 293 K, which is close to the spin-only value for one unpaired electron, thus indicating an S_{tot} = 1/2 ground state for **25**. Solutions of **25** in 1,2-dichloroethane display shoulders at λ_{max} of 575 nm (ε = 400 M^{-1} cm^{-1}) and 1399 nm (ε = 51 M^{-1} cm^{-1}) in the electronic absorption spectrum which are attributed to a Co-

to-ligand MLCT transition and a ligand-field $^2E \leftarrow {}^2A_1$ transition, respectively. Although further analysis of **25** was lacking, this report offered the first insight into the structural and spectroscopic properties expected of non-organometallic 4C tetrahedral $\{CoNO\}^9$ complexes.

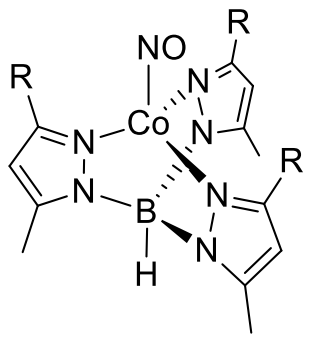

Figure 1.20. Structure of $\{CoNO\}^9$ complexes, with the hydrotris(3-R-5-methylpyrazolyl)borato ligand where R = *t*-butyl in **26**[326] and CH_3 in **27.**[327]

Analogous to the np_3 supporting ligand of **25**, two other $\{CoNO\}^9$ complexes have been reported that utilize the N_3 chelate of tris-pyrazolyl borate derivatized ligands (Figure 1.20).[326-327] Theopold and coworkers synthesized the green crystalline $\{CoNO\}^9$ complex, $[Tp^{t\text{-}Bu,Me}Co(NO)]$ (**26**) (where $Tp^{t\text{-}Bu,Me}$ = hydrotris(3-tert-butyl-5-methylpyrazolyl)borato), in 60% yield by purging NO(g) through a pentane solution of $[(Tp^{t\text{-}Bu,Me})Co(N_2)]$.[326] Quite in contrast to **25**, the corresponding Co-N(O) and N-O distances are much shorter in **26**, 1.671 Å and 1.071 Å, respectively. Additionally, the Co-N-O angle was perfectly linear and reported to be 180.000°. The idealized bond angle and short N-O bond length are not consistent with the $\{CoNO\}^9$ notation and is likely the result of positional disorder of the O-atom in the NO ligand, which has been observed in a variety of metal nitrosyls.[273,330] A strong ν_{NO} IR peak was observed at 1736 cm^{-1} (KBr), which is blue-shifted by 56 cm^{-1} from the ν_{NO} of **25**. The π-donor nature of the phosphine

ligands in **25** appears to have a dramatic influence on ν_{NO} in these otherwise isostructural $\{CoNO\}^9$ complexes. Several ligand-field bands were also observed in the UV-vis spectrum of **26** at λ_{max} (ε, M^{-1} cm^{-1}) of 449 (117), 554 (31), and 656 (76) nm in THF. While spectroscopic studies were available at this point, a more thorough investigation of the electronic structure and possible oxidation state assignments were lacking. However, an in-depth theoretical in conjunction with experimental paper was reported in 2011 for a near identical CoTp $\{CoNO\}^9$ species.

Wieghardt described a more detailed account of a similar 4C $\{CoNO\}^9$ complex utilizing a methylated version of the Tp ligand, namely $[Co(Tp^*)(NO)]^-$ (**27**) (Figure 1.20) (where Tp* = hydrotris(3,5-dimethylpyrazolyl)borato).[327] Complex **27** was synthesized via a ligand exchange reaction in THF with the cobalt dinitrosyl complex, $[(TMEDA)Co(NO)_2]BPh_4$ (TMEDA = *N,N,N′N′*-tetramethylethylenediamine), and KTp* to yield the dark green product in 45% yield. Like **25** and **26**, complex **27** exhibited a pseudotetrahedral coordination geometry about Co with Co-N(O) and N-O distances of 1.625 Å and 1.161 Å, respectively. The Co-N-O bond angle was reported to be 173.5(6)°. Unlike **26**, severe disorder of the NO oxygen was not observed in **27**, thus providing a more reliable handle on the metric parameters expected for a tetrahedral 4C $\{CoNO\}^9$ complex. Vibrational measurements on **27** revealed a single ν_{NO} peak at 1732 cm^{-1} (KBr), which is consistent with the IR data for **26** considering the extreme structural similarities between these compounds. Four predominant features were also observed in the UV-vis at λ_{max}, nm (ε, M^{-1} cm^{-1}) of 438 (234), 493 (183), 658 (141), and 1620 (14). The distribution of the 1620 nm peak precluded a determination of the vibronic origin of the signal; however, the higher energy peaks were assigned as *d-d* transitions. The spin-state assignments were supported by EPR, which was lacking in **26**. The EPR spectrum of **27** displayed an anisotropic signal with resonances at g_x = 1.814, g_y = 1.910, g_z = 3.505 with an especially large hyperfine coupling of the g_z component to

the I = 7/2 nucleus of Co (A_x = 28.2 × 10^{-4} cm^{-1}, A_y = 29.0 × 10^{-4} cm^{-1}, A_z = 213.0 × 10^{-4} cm^{-1}) indicative of primarily metal-centered spin density. This spectrum is suggestive of a ground state doublet (S_{tot} = 1/2) for **27**, and the assignment of a HS Co^{II} center (S_{Co} = 3/2) antiferromagnetically coupled to $^3NO^-$ (S_{NO} = 1) for the CoNO unit in **27**. DFT (B3LYP/CP(PPP)) and CASSCF calculations further confirm this description and predict a non-bonding d_{xy} orbital (98% Co-based) as the SOMO suggesting that the $\{CoNO\}^9$-to-$\{CoNO\}^8$ transformation should be relatively facile in these 4C complexes. Complex **27** has been shown to coordinate an additional NO ligand to form a $Co(NO)_2$ dinitrosyl, which appears to activate olefins.[327] Thus, the $\{CoNO\}^9$ state in 4C tetrahedral Co complexes is accessible and sufficiently stable as evidenced by the isolation of the aforementioned systems. Furthermore, the $\{CoNO\}^9$ frontier MOs demonstrate non-bonding character making redox transformations and their associated reaction chemistry (such as nitroxyl donation) a considerable possibility for the future applications of such constructs.

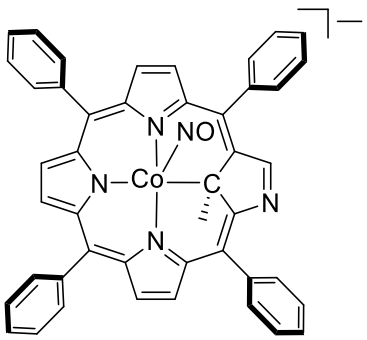

Figure 1.21. Structure of a $\{CoNO\}^9$ complex bearing an *N*-confused porphyrin, $[Co(Cp^*)_2][Co(CTPPMe)(NO)]$ (**28**).[287]

In 2016, Liaw, Hung, and coworkers established the first example of a $\{CoNO\}^9$ complex utilizing a *N*-confused porphyrin, $[Co(Cp^*)_2][Co(CTPPMe)(NO)]$ (**28**) (where CTPP*Me* = 2-aza-

21-methyl-5,10,15,20-tetraphenyl-21-carbaporphyrin).[287] Although this account lacks a detailed structural or theoretical description of **28**, this is the first example of a 5C $\{CoNO\}^9$ porphyrinoid complex and the first example of such a species converting $NO^{\bullet}$ to N_2O. Complex **28** was synthesized by reducing the parent $\{CoNO\}^8$ complex [Co(CTPP*Me*)(NO)] (**22**) ($E_{1/2}$ = -0.835 V vs. SCE) with 1.2 equiv of $[Co(Cp^*)_2]$ in THF in 90% yield. Vibrational measurements on **28** revealed a single ν_{NO} peak at 1537 cm^{-1} (KBr), which shifted by 83 cm^{-1} from the parent $\{CoNO\}^8$ complex and to 1510 cm^{-1} upon isotopic substitution of $\{Co^{15}NO\}^9$ **28-^{15}NO**. The UV-vis profile of this species exhibited a single peak at 434 nm (ε = 91,200 $M^{-1}\,cm^{-1}$) which has a much higher molar absorptivity relative to its tetrahedral $\{CoNO\}^9$ counterparts, likely a result of the $\pi \rightarrow \pi^*$ transitions present within the porphyrin. One of the principle highlights of this account was that the addition of MeOH or H_2O to THF solutions of **28** (ROH:THF, 1:1) led to the generation of N_2O, identified by GC-MS and IR analysis, and could be generated through five iterations of the $NO^{\bullet}$-to-N_2O conversion cycle. Catalytic production of N_2O was ascribed to NOR-like activity, with H^+ donation from the protic solvent. This H-bonding interaction facilitated N-N bond formation via a proposed $[Co(CTPPMe)]_2(N_2O_2)$ intermediate (FTIR, MS) and subsequent N-O bond cleavage. However, further studies need to be conducted in order to carefully examine the nature of this intermediate, the electronic structure of the metal nitrosyl unit in $\{CoNO\}^9$, and alternative mechanisms (HNO self-dimerization can not be excluded).

Table 1.4. Spectroscopic and Structural Data of $\{CoNO\}^9$ Systems.

$\{CoNO\}^9$	$E_{1/2}$ (V)[a]	ν_{NO} (cm^{-1})	S_{tot}	Co-N, N-O (Å)	∠CoNO (°)	Ref
$[Co(CO)_3(NO)]$ (**24**)	-	1818[f]	-	1.665, 1.165	180.0	329
$[Co(np_3)(NO)]BPh_4$ (**25**)	-	1680[g]	1/2	1.83, 1.14	165	325,328
$[Co(Tp^{t\text{-}Bu,Me})(NO)]$ (**26**)	-	1736[e]	-	1.671, 1.071	180.000	326
[Co(Tp*)(NO)] (**27**)	-	1732[e]	1/2	1.625, 1.161	173.5	327
$[Co(Cp^*)_2][Co(CTPPMe)(NO)]$ (**28**)	-	1537[e]	-	-	-	287

[a] Data represents the $E_{1/2}$ value for the $\{CoNO\}^{8\text{-}9}$ redox couple normalized to the saturated calomel reference electrode (SCE) based on information found in [294]. [b] CH_2Cl_2, [c] DMF, [d] MeCN, [e] KBr. [f] Ar matrix. [g] Nujol mull.

1.9 Research Objectives and Purpose

This research includes the investigation of the structural and electronic properties of $\{CoNO\}^{8/9}$ systems and their capability to serve as HNO donors. The driving forces behind this research include the therapeutic potential of HNO/NO^-, limitations of current donors, the prevalence of metal centers as implicated biological HNO/NO^- targets, and the known reactivity of Co-centered cobalamins with NO_x species. $\{FeNO\}^{7/8}$ systems have been shown to function as potential HNO sources; however they react with HNO targets immediately.[272,331] This precedent is indicative of the possible utility and advantageous properties that could be found in cobalt-centered HNO/NO^- donating platforms: first-row transition metal, biologically relevant, tunable, and more controllable properties (e.g., kinetics). These complexes can facilitate release of HNO/NO^- on a slower timescale, which would overcome a limitation of many current HNO donors that exhibit short half-lives ($t_{1/2}$ ~2.5 min). There are very few $\{CoNO\}^9$ complexes that have been

published to date,[287,325-327] none of which have been used as HNO/NO^- donors. There are three principle goals of this research: (i) Synthesize and characterize 5C $\{CoNO\}^{8/9}$ complexes bearing non-corrin, non-macrocyclic N4 ligand scaffolds and establish their spectroscopic and structural benchmarks, as $\{CoNO\}^9$ systems remain a rare and elusive species; (ii) investigate the potential for HNO/NO^- donation of both $\{CoNO\}^8$ and $\{CoNO\}^9$ complexes when in the presence of known HNO targets ([Fe(TPP)Cl], PPh_3, metMb) in both organic and aqueous (pH 7.4) media and determine the Co and Co-NO species that form from such reactivity; and (iii) explore the fate and mechanism of release of M-bound HNO/NO^- in the presence of small molecule signaling agents (i.e. H^+, H_2S/RSH, O_2) present in the biological milieu in an effort to elucidate the potential crosstalk between signaling pathways. In doing so, we expect to shed insights on mechanisms of HNO-release and enhance our understanding of the fate of M-HNO/NO^- in biology.

We investigate this chemistry with two different platforms: the first involves $\{CoNO\}^{8/9}$ complexes that contain a diimine-dipyrrolide donor set. The 2– charge of the deprotonated ligand leads to neutral $\{CoNO\}^8$ and monoanionic $\{CoNO\}^9$ species. The majority of the characterization and reactivity data reported in this dissertation utilizes this framework, and we show that these complexes can be used as HNO/NO^- donors in organic and aqueous media. However, the $\{CoNO\}^8$ species exhibit poor water solubility and negative $\{CoNO\}^{8/9}$ redox potentials on the outskirts of the biological window (see Chapters 2 and 3). The second generation of complexes involves a diimine-diimidazole donor set in which the ligand bears a neutral charge, leading to charged $\{CoNO\}^{8/9}$ complexes. The overall 2+ or 1+ charge of these cobalt nitrosyls affords enhanced water solubility and a more positive redox potential by ~800 mV for the $\{CoNO\}^{8/9}$ couple ($E_{1/2}$ ~ –500 mV vs. Fc^+/Fc). Both of these properties increase the biological utility of these species and expand our knowledge of water-soluble cobalt nitrosyls and their interactions with

other small molecules. We expect that the $\{CoNO\}^{8/9}$ complexes presented herein will not only serve as electronic and structural benchmarks for non-macrocyclic cobalt nitrosyls but also will highlight the viability of these complexes to serve as HNO donors under physiological conditions and shed insights into the fate of M-HNO/NO^- that traverse biology. In doing so, we can elucidate the factors that govern NO_x transformation and/or release in enzymatic pathways found in the global nitrogen cycle.

1.10 References

(1) Sterner, R. W.; Elser, J. J., *Ecological Stoichiometry: The Biology of the Elements from Molecules to the Biosphere*. Princeton Univ. Press: Princeton, NJ, 2002.

(2) Canfield, D. E.; Glazer, A. N.; Falkowski, P. G. *Science* **2010**, *330*, 192.

(3) Fowler, D.; Coyle, M.; Skiba, U.; Sutton, M. A.; Cape, J. N.; Reis, S.; Sheppard, L. J.; Jenkins, A.; Grizzetti, B.; Galloway, J. N.; Vitousek, P.; Leach, A.; Bouwman, A. F.; Butterbach-Bahl, K.; Dentener, F.; Stevenson, D.; Amann, M.; Voss, M. *Phil. Trans. R. Soc. B.* **2013**, *368*, 20130164.

(4) Bertini, I.; Gray, H. B.; Stiefel, E. I.; Valentine, J. S., *Biological Inorganic Chemistry: Structure and Reactivity*. University Science Books: Sausalito, 2007.

(5) Dean, J. A., Properties of Atoms, Radicals, and Bonds. In *Lange's Handbook of Chemistry, 15th ed.*, McGraw-Hill, Inc.: New York, 1999.

(6) Spatzal, T.; Aksoyoglu, M.; Zhang, L.; Andrade, S. L. A.; Schleicher, E.; Weber, S.; Rees, D. C.; Einsle, O. *Science* **2011**, *334*, 940.

(7) Seefeldt, L. C.; Dance, I. G.; Dean, D. R. *Biochemistry* **2004**, *43*, 1401.

(8) Dos Santos, P. C.; Dean, D. R.; Hu, Y.; Ribbe, M. W. *Chem. Rev.* **2004**, *104*, 1159.

(9) Hoffman, B. M.; Dean, D. R.; Seefeldt, L. C. *Acc. Chem. Res.* **2009**, *42*, 609.

(10) Hoffman, B. M.; Lukoyanov, D.; Dean, D. R.; Seefeldt, L. C. *Acc. Chem. Res.* **2013**, *46*, 587.

(11) Burgess, B. K.; Lowe, D. J. *Chem. Rev.* **1996**, *96*, 2983.

(12) Chemical Manufacturers Association, **1996**. "U.S. Chemical Industry Statistical Handbook," CMA, Arlington, VA.

(13) Erisman, J. W.; Sutton, M. A.; Galloway, J.; Klimont, Z.; Winiwarter, W. *Nat. Geosci.* **2008**, *1*, 636.

(14) Pool, J. A.; Laobkovsky, E.; Chirik, P. J. *Nature* **2004**, *427*, 527.

(15) Smil, V. *World Agriculture* **2011**, *2*, 9.

(16) Nitrates and Nitrites. In *U.S. Environmental Protection Agency*, Toxicity and Exposure Assessment for Children's Health (TEACH): 2007; pp 1.

(17) Tavares, P.; Pereira, A. S.; Moura, J. J. G.; Moura, I. *J. Inorg. Biochem.* **2006**, *100*, 2087.

(18) In *Ch. 12 Chemical Fact Sheets*, World Health Organization: pp 307.

(19) "Consumer Factsheet on: Nitrates/Nitrites". U.S. Environmental Protection Agency Ground Water and Drinking Water. http://www.epa.gov/safewater/dwh/c-ioc/nitrates.html: 2006.

(20) Case Studies in Environmental Medicine: Nitrate/Nitrite Toxicity. U.S. Agency for Toxic Substances and Diseases Registry: 2001.

(21) Sanchez-Echaniz, J.; Benito-Fernández, J.; Mintegui-Raso, S. *Pediatrics* **2001**, *107*, 1024.

(22) Ward, M. H.; Pan, W.-H.; Cheng, Y.-J.; Li, F.-H.; Brinton, L. A.; Chen, C.-J.; Hsu, M.-M.; Chen, I.-H.; Levine, P. H.; Yang, C.-S.; Hildesheim, A. *Int. J. Cancer* **2000**, *86*, 603.

(23) Holland, K. S. *Environ. Sci. Technol.* **2011**, *45*, 7116.

(24) Pennisi, E. *Science* **2012**, *337*, 674.

(25) Pennisi, E. *Science* **2012**, *337*, 675.

(26) Alcalde, M.; Ferrer, M.; Plou, F. J.; Ballesteros, A. *Trends Biotechnol.* **2006**, *24*, 281.

(27) Wasser, I. M.; de Vries, S.; Moënne-Loccoz, P.; Schroder, I.; Karlin, K. D. *Chem. Rev.* **2002**, *102*, 1201.

(28) Speelman, A. L.; Lehnert, N. *Acc. Chem. Res.* **2014**, *47*, 1106.

(29) Enemark, J. H.; Feltham, R. D. *Coord. Chem. Rev.* **1974**, *13*, 339.

(30) Einsle, O.; Messerschmidt, A.; Huber, R.; Kroneck, P. M. H.; Neese, F. *J. Am. Chem. Soc.* **2002**, *124*, 11737.

(31) Goodrich, L. E.; Roy, S.; Alp, E. E.; Zhao, J.; Hu, M. Y.; Lehnert, N. *Inorg. Chem.* **2013**, *52*, 7766.

(32) Murphy, W. R., Jr.; Takeuchi, K. J.; Meyer, T. J. *J. Am. Chem. Soc.* **1982**, *104*, 5817.

(33) Liu, Y.; Ryan, M. D. *J. Electroanal. Chem.* **1994**, *368*, 209.

(34) Nakahara, K.; Tanimoto, T.; Hatano, K.-i.; Usuda, K.; Shoun, H. *J. Biol. Chem.* **1993**, *268*, 8350.

(35) Lehnert, N.; Praneeth, V. K. K.; Paulat, F. *J. Comput. Chem.* **2006**, *27*, 1338.

(36) Hino, T.; Matsumoto, Y.; Nagano, S.; Sugimoto, H.; Fukumori, Y.; Murata, T.; Iwata, S.; Shiro, Y. *Science* **2010**, *330*, 1666.

(37) Berto, T. C.; Speelman, A. L.; Zheng, S.; Lehnert, N. *Coord. Chem. Rev.* **2013**, *257*, 244.

(38) Blomberg, M. R. A.; Siegbahn, P. E. M. *Biochemistry* **2012**, *51*, 5173.

(39) Hendriks, J.; Oubrie, A.; Castresana, J.; Urbani, A.; Gemeinhardt, S.; Saraste, M. *Biochim. Biophys. Acta* **2000**, *1459*, 266.

(40) Kurtz, D. M., Jr. *Dalton Trans.* **2007**, 4115.

(41) Silaghi-Dumitrescu, R.; Coulter, E. D.; Das, A.; Ljungdahl, L. G.; Jameson, G. N. L.; Huynh, B. H.; Kurtz, D. M., Jr. *Biochemistry* **2003**, *42*, 2806.

(42) Caranto, J. D.; Weitz, A.; Hendrich, M. P.; Kurtz, D. M., Jr. *J. Am. Chem. Soc.* **2014**, *136*, 7981.

(43) Furchgott, R. F. *Angew. Chem. Int. Ed.* **1999**, *38*, 1870.

(44) Ignarro, L. J. *Angew. Chem. Int. Ed.* **1999**, *38*, 1882.

(45) Ignarro, L. J., *Nitric Oxide Biology and Pathobiology*. Academic Press: San Diego, 2000.

(46) Murad, F. *Angew. Chem. Int. Ed.* **1999**, *38*, 1856.

(47) Moncada, S.; Higgs, E. A. *Br. J. Pharmacol.* **2006**, *147*, S193.

(48) Maia, L. B.; Moura, J. J. G. *Chem. Rev.* **2014**, *114*, 5273.

(49) Pattillo, C. B.; Bir, S.; Rajaram, V.; Kevil, C. G. *Cardiovasc. Res.* **2011**, *89*, 533.

(50) Dezfulian, C.; Raat, N.; Shiva, S.; Gladwin, M. T. *Cardiovasc. Res.* **2007**, *75*, 327.

(51) Duranski, M. R.; Greer, J. J. M.; Dejam, A.; Jaganmohan, S.; Hogg, N.; Langston, W.; Patel, R. P.; Yet, S.-F.; Wang, X.; Kevil, C. G.; Gladwin, M. T.; Lefer, D. J. *J. Clin. Invest.* **2005**, *115*, 1232.

(52) Hottinger, D. G.; Beebe, D. S.; Kozhimannil, T.; Prielipp, R. C.; Belani, K. G. *J. Anaesthesiol. Clin. Pharmacol.* **2014**, *30*, 462.

(53) Bartberger, M. D.; Liu, W.; Ford, E.; Miranda, K. M.; Switzer, C.; Fukuto, J. M.; Farmer, P. J.; Wink, D. A.; Houk, K. N. *Proc. Natl. Acad. Sci. U.S.A.* **2002**, *99*, 10958.

(54) Irvine, J. C.; Ritchie, R. H.; Favaloro, J. L.; Andrews, K. L.; Widdop, R. E.; Kemp-Harper, B. K. *Trends Pharmacol. Sci.* **2008**, *29*, 601.

(55) Fukuto, J. M.; Dutton, A. S.; Houk, K. N. *ChemBioChem* **2005**, *6*, 612.

(56) Stanbury, D. M. *Adv. Inorg. Chem.* **1989**, *33*, 69.

(57) Bartberger, M. D.; Fukuto, J. M.; Houk, K. N. *Proc. Natl. Acad. Sci. U.S.A.* **2001**, *98*, 2194.

(58) Shafirovich, V.; Lymar, S. V. *Proc. Natl. Acad. Sci. U.S.A.* **2002**, *99*, 7340.

(59) Janaway, G. A.; Zhong, M.; Gatev, G. G.; Chabinye, M. L.; Brauman, J. I. *J. Am. Chem. Soc.* **1997**, *119*, 11697.

(60) Janaway, G. A.; Brauman, J. I. *J. Phys. Chem. A.* **2000**, *104*, 1795.

(61) Shafirovich, V.; Lymar, S. V. *J. Am. Chem. Soc.* **2003**, *125*, 6547.

(62) Miranda, K. M. *Coord. Chem. Rev.* **2005**, *249*, 433.

(63) Farmer, P. J.; Sulc, F. *J. Inorg. Biochem.* **2005**, *99*, 166.

(64) Benderskii, V. A.; Krivenko, A. G.; Ponomarev, E. A. *Elektrokhimiya* **1990**, *26*, 318.

(65) Sanders, B. C.; Rhine, M. A.; Harrop, T. C. *Struct. Bond.* **2014**, *160*, 57.

(66) McCleverty, J. A. *Chem. Rev.* **2004**, *104*, 403 and references therein.

(67) Dalby, F. W. *Can. J. Phys.* **1958**, *36*, 1336.

(68) Miranda, K. M.; Paolocci, N.; Katori, T.; Thomas, D. D.; Ford, E.; Bartberger, M. D.; Espey, M. G.; Kass, D. A.; Feelisch, M.; Fukuto, J. M.; Wink, D. A. *Proc. Natl. Acad. Sci. U.S.A.* **2003**, *100*, 9196.

(69) Fukuto, J. M.; Bianco, C. L.; Chavez, T. A. *Free Rad. Biol. Med.* **2009**, *47*, 1318.

(70) Fukuto, J. M.; Bartberger, M. D.; Dutton, A. S.; Paolocci, N.; Wink, D. A.; Houk, K. N. *Chem. Res. Toxicol.* **2005**, *18*, 790.

(71) Miranda, K. M.; Nims, R. W.; Thomas, D. D.; Espey, M. G.; Citrin, D.; Bartberger, M. D.; Paolocci, N.; Fukuto, J. M.; Feelisch, M.; Wink, D. A. *J. Inorg. Biochem.* **2003**, *93*, 52.

(72) Miranda, K. M.; Espey, M. G.; Paolocci, N.; Bartberger, M. D.; Colton, C. A.; Wink, D. A. *Free Rad. Biol. Med.* **2001**, *31*, S72.

(73) Paolocci, N.; Saavedra, W. F.; Miranda, K. M.; Martignani, C.; Isoda, T.; Hare, J. M.; Espey, M. G.; Fukuto, J. M.; Feelisch, M.; Wink, D. A.; Kass, D. A. *Proc. Natl. Acad. Sci. U.S.A.* **2001**, *98*, 10463.

(74) Pryor, W. A.; Squadrito, G. L. *Am. J. Physiol.* **1995**, *268*, L699.

(75) Miller, T. W.; Cherney, M. M.; Lee, A. J.; Francoleon, N. E.; Farmer, P. J.; King, S. B.; Hobbs, A. J.; Miranda, K. M.; Burstyn, J. N.; Fukuto, J. M. *J. Biol. Chem.* **2009**, *284*, 21788.

(76) Ellis, A.; Li, C. G.; Rand, M. J. *Br. J. Pharmacol.* **2000**, *129*, 315.

(77) Wanstall, J. C.; Jeffrey, T. K.; Gambino, A.; Lovren, F.; Triggle, C. R. *Br. J. Pharmacol.* **2001**, *134*, 463.

(78) Tocchetti, C. G.; Wang, W.; Froehlich, J. P.; Huke, S.; Aon, M. A.; Wilson, G. M.; Di Benedetto, G.; O'Rourke, B.; Gao, W. D.; Wink, D. A.; Toscano, J. P.; Zaccolo, M.; Bers, D. M.; Valdivia, H. H.; Cheng, H. P.; Kass, D. A.; Paolocci, N. *Circ. Res.* **2007**, *100*, 96.

(79) Cheong, E.; Tumbev, V.; Abramson, J.; Salama, G.; Stoyanovsky, D. A. *Cell Calcium* **2005**, *37*, 87.

(80) Pagliaro, P.; Mancardi, D.; Rastaldo, R.; Penna, C.; Gattullo, D.; Miranda, K. M.; Feelisch, M.; Wink, D. A.; Kass, D. A.; Paolocci, N. *Free Rad. Biol. Med.* **2003**, *34*, 33.

(81) Sharpe, M. A.; Cooper, C. E. *Biochem. J.* **1998**, *332*, 9.

(82) Suarez, S. A.; Neuman, N. I.; Muñoz, M.; Álvarez, L.; Bikiel, D. E.; Brondino, C. D.; Ivanović-Burmazović, I.; Miljkovic, J. L.; Filipovic, M. R.; Martí, M. A.; Doctorovich, F. *J. Am. Chem. Soc.* **2015**, *137*, 4720.

(83) Rosenthal, J.; Lippard, S. J. *J. Am. Chem. Soc.* **2010**, *132*, 5536.

(84) Royzen, M.; Wilson, J. J.; Lippard, S. J. *J. Inorg. Biochem.* **2013**, *118*, 162.

(85) Pufahl, R. A.; Wishnok, J. S.; Marletta, M. A. *Biochemistry* **1995**, *34*, 1930.

(86) Clague, M. J.; Wishnok, J. S.; Marletta, M. A. *Biochemistry* **1997**, *36*, 14465.

(87) Fukuto, J. M.; Wallace, G. C.; Hszieh, R.; Chaudhuri, G. *Biochem. Pharmacol.* **1992**, *43*, 607.

(88) Fukuto, J. M.; Hobbs, A. J.; Ignarro, L. J. *Biochem. Biophys. Res. Commun.* **1993**, *196*, 707.

(89) Fukuto, J. M.; Chiang, K.; Hszieh, R.; Wong, P.; Chaudhuri, G. *J. Pharmacol. Exp. Ther.* **1992**, *263*, 546.

(90) Donzelli, S.; Espey, M. G.; Flores-Santana, W.; Switzer, C. H.; Yeh, G. C.; Huang, J. M.; Stuehr, D. J.; King, S. B.; Miranda, K. M.; Wink, D. A. *Free Rad. Biol. Med.* **2008**, *45*, 578.

(91) Cooper, J. N.; Chilton, J. E., Jr.; Powell, R. E. *Inorg. Chem.* **1970**, *9*, 2303.

(92) Bonner, F. T.; Dzelzkalns, L. S.; Bonucci, J. A. *Inorg. Chem.* **1978**, *17*, 2487.

(93) Kim-Shapiro, D. B.; King, S. B.; Bonifant, C. L.; Kolibash, C. P.; Ballas, S. K. *Biochim. Biophys. Acta* **1998**, *1380*, 64.

(94) Nagasawa, H. T.; DeMaster, E. G.; Redfern, B.; Shirota, F. N.; Goon, D. J. W. *J. Med. Chem.* **1990**, *33*, 3120.

(95) Filipovic, M. R.; Eberhardt, M.; Prokopovic, V.; Mijuskovic, A.; Orescanin-Dusic, Z.; Reeh, P.; Ivanović-Burmazović, I. *J. Med. Chem.* **2013**, *56*, 1499.

(96) Filipovic, M. R.; Miljkovic, J. L.; Nauser, T.; Royzen, M.; Klos, K.; Shubina, T.; Koppenol, W. H.; Lippard, S. J.; Ivanović-Burmazović, I. *J. Am. Chem. Soc.* **2012**, *134*, 12016.

(97) Wedmann, R.; Zahl, A.; Shubina, T. E.; Dürr, M.; Heinemann, F. W.; Bugenhagen, B. E. C.; Burger, P.; Ivanović-Burmazović, I.; Filipovic, M. R. *Inorg. Chem.* **2015**, *54*, 9367.

(98) Ivanova, L. V.; Anton, B. J.; Timerghazin, Q. K. *Phys. Chem. Chem. Phys.* **2014**, *16*, 8476.

(99) Kohout, F. C.; Lampe, F. W. *J. Am. Chem. Soc.* **1965**, *87*, 5795.

(100) Smith, P. A. S.; Hein, G. E. *J. Am. Chem. Soc.* **1960**, *82*, 5731.

(101) Angeli, A.; Angelico, F.; Scurti, F. *Chem. Zentralbl.* **1902**, *73*, 691.

(102) Paolocci, N.; Jackson, M. I.; Lopez, B. E.; Miranda, K.; Tocchetti, C. G.; Wink, D. A.; Hobbs, A. J.; Fukuto, J. M. *Pharmacol. Ther.* **2007**, *113*, 442.

(103) DeMaster, E. G.; Redfern, B.; Nagasawa, H. T. *Biochem. Pharmacol.* **1998**, *55*, 2007.

(104) Irvine, J. C.; Favaloro, J. L.; Kemp-Harper, B. K. *Hypertension* **2003**, *41*, 1301.

(105) Angeli, A. *Gazz. Chim. Ital.* **1903**, *33*, 245.

(106) Miranda, K. M.; Katori, T.; de Holding, C. L. T.; Thomas, L.; Ridnour, L. A.; MeLendon, W. J.; Cologna, S. M.; Dutton, A. S.; Champion, H. C.; Mancardi, D.; Tocchetti, C. G.; Saavedra, J. E.; Keefer, L. K.; Houk, K. N.; Fukuto, J. M.; Kass, D. A.; Paolocci, N.; Wink, D. A. *J. Med. Chem.* **2005**, *48*, 8220.

(107) Sha, X.; Isbell, T. S.; Patel, R. P.; Day, C. S.; King, S. B. *J. Am. Chem. Soc.* **2006**, *128*, 9687.

(108) Atkinson, R. N.; Storey, B. M.; King, S. B. *Tetrahedron Lett.* **1996**, *37*, 9287.

(109) Cohen, A. D.; Zeng, B.-B.; King, S. B.; Toscano, J. P. *J. Am. Chem. Soc.* **2003**, *125*, 1444.

(110) Guthrie, D. A.; Kim, N. Y.; Siegler, M. A.; Moore, C. D.; Toscano, J. P. *J. Am. Chem. Soc.* **2012**, *134*, 1962.

(111) Guthrie, D. A.; Ho, A.; Takahashi, K.; Collins, A.; Morris, M.; Toscano, J. P. *J. Org. Chem.* **2015**, *80*, 1338.

(112) Moncada, S.; Palmer, R. M. J.; Higgs, E. A. *Pharmacol. Rev.* **1991**, *43*, 109.

(113) Li, L.; Moore, P. K. *Biochem. Soc. Trans.* **2007**, *35*, 1138.

(114) Mustafa, A. K.; Gadalla, M. M.; Snyder, S. H. *Sci. Signaling* **2009**, *2*, 1.

(115) Olsen, K. R.; Donald, J. A. *Acta Histochem.* **2009**, *111*, 244.

(116) Fukuto, J. M.; Collins, M. D. *Curr. Pharm. Des.* **2007**, *13*, 2952.

(117) Fukuto, J. M.; Carrington, S. J.; Tantillo, D. J.; Harrison, J. G.; Ignarro, L. J.; Freeman, B. A.; Chen, A.; Wink, D. A. *Chem. Res. Toxicol.* **2012**, *25*, 769.

(118) Akhtar, M. J.; Lutz, C. A.; Bonner, F. T. *Inorg. Chem.* **1979**, *18*, 2369.

(119) Seddon, W. A.; Young, M. J. *Can. J. Chem.* **1970**, *48*, 393.

(120) Eberhardt, M.; Dux, M.; Namer, B.; Miljkovic, J.; Cordasic, N.; Will, C.; Kichko, T. I.; de la Roche, J.; Fischer, M.; Suárez, S. A.; Bikiel, D.; Dorsch, K.; Leffler, A.; Babes, A.; Lampert, A.; Lennerz, J. K.; Jacobi, J.; Martí, M. A.; Doctorovich, F.; Högestätt, E. D.; Zygmunt, P. M.; Ivanovic-Burmazovic, I.; Messlinger, K.; Reeh, P.; Filipovic, M. R. *Nature Commun.* **2014**, *5*, 4381.

(121) Miljkovic, J. L.; Kenkel, I.; Ivanović-Burmazović, I.; Filipovic, M. R. *Angew. Chem. Int. Ed.* **2013**, *52*, 12061

(122) Cortese-Krott, M. M.; Kuhnle, G. G. C.; Dyson, A.; Fernandez, B. O.; Grman, M.; DuMond, J. F.; Barrow, M. P.; McLeod, G.; Nakagawa, H.; Ondrias, K.; Nagy, P.; King, S. B.; Saavedra, F. E.; Keefer, L. K.; Singer, M.; Kelm, M.; Butler, A. R.; Feelisch, M. *Proc. Natl. Acad. Sci. U.S.A.* **2015**, *112*, E4651.

(123) Bianco, C. L.; Fukuto, J. M. *Proc. Natl. Acad. Sci. U.S.A.* **2015**, *112*, 10573.

(124) Liochev, S. I.; Fridovich, I. *J. Biol. Chem.* **2001**, *276*, 35253.

(125) Murphy, M. E.; Sies, H. *Proc. Natl. Acad. Sci. U.S.A.* **1991**, *88*, 10860.

(126) Doyle, M. P.; Mahapatro, S. N.; Broene, R. D.; Guy, J. K. *J. Am. Chem. Soc.* **1988**, *110*, 593.

(127) Bazylinski, D. A.; Goretski, J.; Hollocher, T. C. *J. Am. Chem. Soc.* **1985**, *107*, 7986.

(128) Bazylinski, D. A.; Hollocher, T. C. *J. Am. Chem. Soc.* **1985**, *107*, 7982.

(129) Sanishvili, R.; Volz, K. W.; Westbrook, E. M.; Margoliash, E. *Structure* **1995**, *3*, 707.

(130) Rhine, M. A.; Sanders, B. C.; Patra, A. K.; Harrop, T. C. *Inorg. Chem.* **2015**, *54*, 9351.

(131) Ignarro, L. J.; Buga, G. M.; Wood, K. S.; Byrns, R. E.; Chaudhuri, G. *Proc. Natl. Acad. Sci. U.S.A.* **1987**, *84*, 9265.

(132) Bolli, R. *J. Mol. Cell. Cardiol.* **2001**, *33*, 1897.

(133) Pino, R. Z.; Feelisch, M. *Biochem. Biophys. Res. Commun.* **1994**, *201*, 54.

(134) Fukuto, J. M.; Jackson, M. I.; Kaludercic, N.; Paolocci, N. *Methods Enzymol.* **2008**, *440*, 411.

(135) Donzelli, S.; Espey, M. G.; Thomas, D. D.; Mancardi, D.; Tocchetti, C. G.; Ridnour, L. A.; Paolocci, N.; King, S. B.; Miranda, K. M.; Lazzarino, G.; Fukuto, J. M.; Wink, D. A. *Free Radical Biol. Med.* **2006**, *40*, 1056.

(136) Koppenol, W. H. *Inorg. Chem.* **2012**, *51*, 5637.

(137) Wong, P. S.-Y.; Hyun, J.; Fukuto, J. M.; Shirota, F. N.; DeMaster, E. G.; Shoeman, D. W.; Nagasawa, H. T. *Biochemistry* **1998**, *37*, 5362.

(138) Miranda, K. M.; Ridnour, L.; Esprey, M.; Citrin, D.; Thomas, D.; Mancardi, D.; Donzelli, S.; Wink, D. A.; Katori, T.; Tocchetti, C. G.; Ferlito, M.; Paolocci, N.; Fukuto, J. M. *Prog. Inorg. Chem.* **2005**, *54*, 349.

(139) Pryor, W. A.; Church, D. F.; Govindan, C. K.; Crank, G. *J. Org. Chem.* **1982**, *47*, 156.

(140) Kharitonov, V. G.; Sundquist, A. R.; Sharma, V. S. *J. Biol. Chem.* **1995**, *270*, 28158.

(141) Wink, D. A.; Nims, R. W.; Darbyshire, J. F.; Christodoulou, D.; Hanbauer, I.; Cox, G. W.; Laval, F.; Laval, J.; Cook, J. A.; Krishna, M. C.; DeGraff, W. G.; Mitchell, J. B. *Chem. Res. Toxicol.* **1994**, *7*, 519.

(142) Jourd'heuil, D.; Jourd'heuil, F. L.; Feelisch, M. *J. Biol. Chem.* **2003**, *278*, 15720.

(143) Folkes, L. K.; Wardman, P. *Free Radical Biol. Med.* **2004**, *37*, 549.

(144) DeMaster, E. G.; Quast, B. J.; Redfern, B.; Nagasawa, H. T. *Biochemistry* **1995**, *34*, 11494.

(145) Goldstein, S.; Czapski, G. *J. Am. Chem. Soc.* **1996**, *118*, 3419.

(146) Stamler, J. S.; Singel, D. J.; Loscalzo, J. *Science* **1992**, *258*, 1898.

(147) Stamler, J. S.; Jaraki, O.; Osborne, J.; Simon, D. I.; Keaney, J.; Vita, J.; Singel, D.; Valeri, C. R.; Loscalzo, J. *Proc. Natl. Acad. Sci. U.S.A.* **1992**, *89*, 7674.

(148) Butler, A. R.; Megson, I. L. *Chem. Rev.* **2002**, *102*, 1155.

(149) Playfair, L. *Phil. Trans. R. Soc. Lond.* **1849**, *139*, 477.

(150) Friederich, J. A.; Butterworth, J. F. *Anesth. Analg.* **1995**, *81*, 152.

(151) Johnson, C. C. *Arch. Int. Pharmacodyn. Ther.* **1929**, *35*, 489.

(152) Swinehart, J. H. *Coord. Chem. Rev.* **1967**, *2*, 385.

(153) Butler, A. R.; Glidewell, C. *Chem. Soc. Rev.* **1987**, *16*, 361.

(154) Roncaroli, F.; Videla, M.; Slep, L. D.; Olabe, J. A. *Coord. Chem. Rev.* **2007**, *251*, 1903.

(155) Szaciłowski, K.; Chmura, A.; Stasicka, Z. *Coord. Chem. Rev.* **2005**, *249*, 2408.

(156) Mulvey, D.; Waters, W. A. *J. Chem. Soc. Dalton Trans.* **1975**, 951.

(157) Butler, A. R.; Calsy-Harrison, A. M.; Glidewell, C. *Polyhedron* **1988**, *7*, 1197.

(158) Kowaluk, E. A.; Seth, P.; Fung, H.-L. *J. Pharmacol. Exp. Ther.* **1992**, *262*, 916.

(159) Szaciłowski, K.; Oszajca, J.; Stochel, G.; Stasicka, Z. *J. Chem. Soc. Dalton Trans.* **1999**, 2353.

(160) Manoharan, P. T.; Gray, H. B. *J. Am. Chem. Soc.* **1965**, *87*, 3340.

(161) Szaciłowski, K.; Stochel, G.; Stasicka, Z.; Kisch, H. *New J. Chem.* **1997**, *21*, 893.

(162) Schwane, J. D.; Ashby, M. T. *J. Am. Chem. Soc.* **2002**, *124*, 6822.

(163) Cheney, R. P.; Simic, M. G.; Hoffman, M. Z.; Taub, I. A.; Asmus, K.-D. *Inorg. Chem.* **1977**, *16*, 2187.

(164) Williams, D. L. H. *Acc. Chem. Res.* **1999**, *32*, 869.

(165) Morando, P. J.; Borghi, E. B.; de Schteingart, L. M.; Blesa, M. A. *J. Chem. Soc. Dalton Trans.* **1981**, 435.

(166) Johnson, M. D.; Wilkins, R. G. *Inorg. Chem.* **1984**, *23*, 231.

(167) Reglinski, J.; Butler, A. R.; Glidewell, C. *Appl. Organomet. Chem.* **1994**, *8*, 25.

(168) Szaciłowski, K.; Wanat, A.; Barbieri, A.; Wasielewska, E.; Witko, M.; Stochel, G.; Stasicka, Z. *New J. Chem.* **2002**, *26*, 1495.

(169) Bates, J. N.; Baker, M. T.; Guerra, R., Jr.; Harrison, D. G. *Biochem. Pharmacol.* **1991**, *42*, S157.

(170) Carapuça, H. M.; Simao, J. E. J.; Fogg, A. G. *J. Electroanal. Chem.* **1998**, *455*, 93.

(171) Grossi, L.; D'Angelo, S. *J. Med. Chem.* **2005**, *48*, 2622.

(172) Rock, P. A.; Swinehart, J. H. *Inorg. Chem.* **1966**, *5*, 1078.

(173) Quiroga, S. L.; Almaraz, A. E.; Amorebieta, V. T.; Perissinotti, L. L.; Olabe, J. A. *Chem. Eur. J.* **2011**, *17*, 4145.

(174) Filipovic, M. R.; Ivanovic-Burmazovic, I. *Chem. Eur. J.* **2012**, *18*, 13538.

(175) Williams, D. L. H. *Methods Enzymol.* **1996**, *268*, 299.

(176) Aleryani, S.; Milo, E.; Kostka, P. *Biochim. Biophys. Acta* **1999**, *1472*, 181.

(177) Kooy, N. W.; Royall, J. A.; Ischiropoulos, H.; Beckman, J. S. *Free Radical Biol. Med.* **1994**, *16*, 149.

(178) Aleryani, S.; Milo, E.; Rose, Y.; Kostka, P. *J. Biol. Chem.* **1998**, *273*, 6041.

(179) Miles, A. M.; Bohle, D. S.; Glassbrenner, P. A.; Hansert, B.; Wink, D. A.; Grisham, M. B. *J. Biol. Chem.* **1996**, *271*, 40.

(180) McDonald, C. C.; Phillips, W. D.; Mower, H. F. *J. Am. Chem. Soc.* **1965**, *87*, 3319.

(181) Tsai, M.-L.; Tsou, C.-C.; Liaw, W.-F. *Acc. Chem. Res.* **2015**, *48*, 1184.

(182) Lu, T.-T.; Chiou, S.-J.; Chen, C.-Y.; Liaw, W.-F. *Inorg. Chem.* **2006**, *45*, 8799.

(183) Lu, T.-T.; Huang, H.-W.; Liaw, W.-F. *Inorg. Chem.* **2009**, *48*, 9027.

(184) Tsou, C.-C.; Lin, Z.-S.; Lu, T.-T.; Liaw, W.-F. *J. Am. Chem. Soc.* **2008**, *130*, 17154.

(185) Tsou, C.-C.; Chiu, W.-C.; Ke, C.-H.; Tsai, J.-C.; Wang, Y.-M.; Chiang, M.-H.; Liaw, W.-F. *J. Am. Chem. Soc.* **2014**, *136*, 9424.

(186) Tsai, M.-L.; Chen, C.-C.; Hsu, I.-J.; Ke, S.-C.; Hsieh, C.-H.; Chiang, K.-A.; Lee, G.-H.; Wang, Y.; Chen, J.-M.; Lee, J.-F.; Liaw, W.-F. *Inorg. Chem.* **2004**, *43*, 5159.

(187) Lu, T.-T.; Chen, C.-H.; Liaw, W.-F. *Chem. Eur. J.* **2010**, *16*, 8088.

(188) Tsai, F.-T.; Lee, Y.-C.; Chiang, M.-H.; Liaw, W.-F. *Inorg. Chem.* **2013**, *52*, 464.

(189) Hsieh, C.-H.; Darensbourg, M. Y. *J. Am. Chem. Soc.* **2010**, *132*, 14118.

(190) Tran, C. T.; Kim, E. *Inorg. Chem.* **2012**, *51*, 10086.

(191) Tran, C. T.; Williard, P. G.; Kim, E. *J. Am. Chem. Soc.* **2014**, *136*, 11874.

(192) Fitzpatrick, J.; Kalyvas, H.; Filipovic, M. R.; Ivanović-Burmazović, I.; MacDonald, J. C.; Shearer, J.; Kim, E. *J. Am. Chem. Soc.* **2014**, *136*, 7229.

(193) Harrop, T. C.; Song, D.; Lippard, S. J. *J. Am. Chem. Soc.* **2006**, *128*, 3528.

(194) Harrop, T. C.; Song, D.; Lippard, S. J. *J. Inorg. Biochem.* **2007**, *101*, 1730.

(195) Harrop, T. C.; Tonzetich, Z. J.; Reisner, E.; Lippard, S. J. *J. Am. Chem. Soc.* **2008**, *130*, 15602.

(196) Tonzetich, Z. J.; Wang, H.; Mitra, D.; Tinberg, C. E.; Do, L. H.; Jenney, F. E., Jr.; Adams, M. W. W.; Cramer, S. P.; Lippard, S. J. *J. Am. Chem. Soc.* **2010**, *132*, 6914.

(197) Tonzetich, Z. J.; McQuade, L. E.; Lippard, S. J. *Inorg. Chem.* **2010**, *49*, 6338.

(198) Pereira, J. C. M.; Iretskii, A. V.; Han, R.-M.; Ford, P. C. *J. Am. Chem. Soc.* **2015**, *137*, 328.

(199) Li, Q.; Li, C.; Mahtani, H. K.; Du, J.; Patel, A. R.; Lancaster, J. R., Jr. *J. Biol. Chem.* **2014**, *289*, 19917.

(200) Bosworth, C. A.; Toledo, J. C., Jr.; Zmijewski, J. W.; Li, Q.; Lancaster, J. R., Jr. *Proc. Natl. Acad. Sci. U.S.A.* **2009**, *106*, 4671.

(201) Vanin, A. F.; Poltorakov, A. P.; Mikoyan, V. D.; Kubrina, L. N.; Burbaev, D. S. *Nitric Oxide* **2010**, *23*, 136.

(202) Borodulin, R. R.; Kubrina, L. N.; Mikoyan, V. D.; Poltorakov, A. P.; Shvydkiy, V. O.; Burbaev, D. S.; Serezhenkov, V. A.; Yakhontova, E. R.; Vanin, A. F. *Nitric Oxide* **2013**, *29*, 4.

(203) Maher, P. *Ageing Res. Rev.* **2005**, *4*, 288.

(204) Tinberg, C. E.; Tonzetich, Z. J.; Wang, H.; Do, L. H.; Yoda, Y.; Cramer, S. P.; Lippard, S. J. *J. Am. Chem. Soc.* **2010**, *132*, 18168.

(205) Lu, T.-T.; Tsou, C.-C.; Huang, H.-W.; Hsu, I.-J.; Chen, J.-M.; Kuo, T.-S.; Wang, Y.; Liaw, W.-F. *Inorg. Chem.* **2008**, *47*, 6040.

(206) Lok, H. C.; Rahmanto, Y. S.; Hawkins, C. L.; Kalinowski, D. S.; Morrow, C. S.; Townsend, A. J.; Ponka, P.; Richardson, D. R. *J. Biol. Chem.* **2012**, *287*, 607.

(207) Rahmanto, Y. S.; Kalinowski, D. S.; Lane, D. J. R.; Lok, H. C.; Richardson, V.; Richardson, D. R. *J. Biol. Chem.* **2012**, *287*, 6960.

(208) Zhang, S.; Çelebi-Ölçüm, N.; Melzer, M. M.; Houk, K. N.; Warren, T. H. *J. Am. Chem. Soc.* **2013**, *135*, 16746.

(209) Marsh, E. N. G. *Essays in Biochem.* **1999**, *34*, 139.

(210) Odaka, M.; Kobayashi, M., Cobalt Proteins, Overview. In *Encyclopedia of Metalloproteins*, Kretsinger, R. H.; Uversky, V. N.; Permyakov, E. A., Eds. Springer: 2013; Vol. 1, pp 670.

(211) Ludwig, M. L.; Matthews, R. G. *Annu. Rev. Biochem.* **1997**, *66*, 269.

(212) Banerjee, R.; Ragsdale, S. W. *Annu. Rev. Biochem.* **2003**, *72*, 209.

(213) Suarez-Moreira, E.; Hannibal, L.; Smith, C. A.; Chavez, R. A.; Jacobsen, D. W.; Brasch, N. E. *Dalton Trans.* **2006**, 5269.

(214) Brown, K. L. *Chem. Rev.* **2005**, *105*, 2075.

(215) Pezacka, E.; Green, R.; Jacobsen, D. W. *Biochem. Biophys. Res. Commun.* **1990**, *169*, 443.

(216) Hassanin, H. A.; El-Shahat, M. F.; DeBeer, S.; Smith, C. A.; Brasch, N. E. *Dalton Trans.* **2010**, *39*, 10626.

(217) McCleverty, J. A. *Chem. Rev.* **1979**, *79*, 53.

(218) Duffin, P. A.; Larkworthy, L. F.; Mason, J.; Stephens, A. N.; Thompson, R. M. *Inorg. Chem.* **1987**, *26*, 2034.

(219) Brouwer, M.; Chamulitrat, W.; Ferruzzi, G.; Sauls, D. L.; Weinberg, J. B. *Blood* **1996**, *88*, 1857.

(220) Zheng, D.; Birke, R. L. *J. Am. Chem. Soc.* **2001**, *123*, 4637.

(221) Hassanin, H. A.; Hannibal, L.; Jacobsen, D. W.; El-Shahat, M. F.; Hamza, M. S. A.; Brasch, N. E. *Angew. Chem. Int. Ed.* **2009**, *48*, 8909.

(222) Pallares, I. G.; Brunold, T. C. *Inorg. Chem.* **2014**, *53*, 7676.

(223) Wolak, M.; Zahl, A.; Schneppensieper, T.; Stotchel, G.; van Eldik, R. *J. Am. Chem. Soc.* **2001**, *123*, 9780.

(224) Stich, T. A.; Brooks, A. J.; Buan, N. R.; Brunold, T. C. *J. Am. Chem. Soc.* **2003**, *125*, 5897.

(225) Park, K.; Brunold, T. C. *J. Phys. Chem. B.* **2013**, *17*, 5397.

(226) Perry, C. B.; Marques, H. M. *S. Afr. J. Sci.* **2004**, *100*, 368.

(227) Selçuki, C.; van Eldik, R.; Clark, T. *Inorg. Chem.* **2004**, *43*, 2828.

(228) Lexa, D.; Saveant, J.-M. *Acc. Chem. Res.* **1983**, *16*, 235.

(229) Danishpajooh, I. O.; Gudi, T.; Chen, Y.; Kharitonov, V. G.; Sharma, V. S.; Boss, G. R. *J. Biol. Chem.* **2001**, *276*, 27296.

(230) Wolak, M.; Stochel, G.; Hamza, M.; van Eldik, R. *Inorg. Chem.* **2000**, *39*, 2018.

(231) Firth, R. A.; Hill, H. A. O.; Pratt, J. M.; Thorp, R. G.; Williams, R. J. P. *J. Chem. Soc. A* **1969**, 381.

(232) Subedi, H.; Hassanin, H. A.; Brasch, N. E. *Inorg. Chem.* **2014**, *53*, 1570.

(233) Plymale, N. T.; Dassanayake, R. S.; Hassanin, H. A.; Brasch, N. E. *Eur. J. Inorg. Chem.* **2012**, 913.

(234) Kambo, A.; Sharma, V. S.; Casteel, D. E.; Woods, V. L., Jr.; Pilz, R. B.; Boss, G. R. *J. Biol. Chem.* **2005**, *280*, 10073.

(235) Brooks, A. J.; Vlasie, M.; Banerjee, R.; Brunold, T. C. *J. Am. Chem. Soc.* **2004**, *126*, 8167.

(236) Maron, B. A.; Loscalzo, J. *Annu. Rev. Biochem.* **2009**, *60*, 39.

(237) Banerjee, R. V.; Matthews, R. G. *FASEB J.* **1990**, *4*, 1450.

(238) Erkurt, M. A.; Aydogdu, I.; Bayraktar, N.; Kuku, I.; Kaya, E. *Turk. J. Hematol.* **2009**, *26*, 197.

(239) Stabler, S. P.; Brass, E. P.; Marcell, P. D.; Allen, R. H. *J. Clin. Invest.* **1991**, *87*, 1422.

(240) Beck, W. S., Metabolic features of cobalamin deficiency in man. In *Cobalamin: biochemistry and pathophysiology*, Babior, B. M., Ed. John Wiley & Sons: New York, 1975.

(241) Stollhoff, K.; Schulte, F. J. *Eur. J. Pediatr.* **1987**, *146*, 201.

(242) Hall, C. A. *Amer. J. Hemat.* **1990**, *34*, 121.

(243) Qureshi, G. A.; Memon, S. A.; Collin, C.; Parvez, S. H. *Biogenic Amines* **2004**, *18*, 117.

(244) Seneff, S.; Davidson, R. M.; Liu, J. *Entropy* **2012**, *14*, 2265.

(245) Broderick, K. E.; Singh, V.; Zhuang, S.; Kambo, A.; Chen, J. C.; Sharma, V. S.; Pilz, R. B.; Boss, G. R. *J. Biol. Chem.* **2005**, *280*, 8678.

(246) Sharma, V. S.; Pilz, R. B.; Boss, G. R.; Magde, D. *Biochemistry* **2003**, *42*, 8900.

(247) Welch, G. N.; Upchurch, G. R., Jr.; Farivar, R. S.; Pigazzi, A.; Vu, K.; Brecher, P.; Keaney, J. F., Jr.; Loscalzo, J. *Proc. Assoc. Am. Physicians* **1998**, *110*, 22.

(248) Tang, Z.; Bauer, J. A.; Morrison, B.; Lindner, D. J. *Mol. Cell. Biol.* **2006**, *26*, 5588.

(249) Melnik, B. Treatment of Inflammatory and Hyperproliferative Skin Disease. U.S. Patent EP2322188 A1. **2011**.

(250) Broderick, K. E.; Alvarez, L.; Balasubramanian, M.; Belke, D. D.; Makino, A.; Chan, A.; Woods, V. L., Jr.; Dillmann, W. H.; Sharma, V. S.; Pilz, R. B.; Bigby, T. D.; Boss, G. R. *Exp. Biol. Med.* **2007**, *232*, 1432.

(251) Brenner, M.; Benavides, S.; Mahon, S. B.; Lee, J.; Yoon, D.; Mukai, D.; Viseroi, M.; Chan, A.; Jiang, J.; Narula, N.; Azer, S. M.; Alexander, C.; Boss, G. R. *Clin. Toxicol.* **2014**, *52*, 490.

(252) Uyeda, C.; Peters, J. C. *J. Am. Chem. Soc.* **2013**, *135*, 12023.

(253) McCrory, C. C. L.; Uyeda, C.; Peters, J. C. *J. Am. Chem. Soc.* **2012**, *134*, 3164.

(254) Stubbert, B. D.; Peters, J. C.; Gray, H. B. *J. Am. Chem. Soc.* **2011**, *133*, 18070.

(255) Valdez, C. N.; Dempsey, J. L.; Brunschwig, B. S.; Winkler, J. R.; Gray, H. B. *Proc. Natl. Acad. Sci. U.S.A.* **2012**, *109*, 15589.

(256) Zee, D. Z.; Chantarojsiri, T.; Long, J. R.; Chang, C. J. *Acc. Chem. Res.* **2015**, *48*, 2027 and references therein.

(257) Kelley, P.; Day, M. W.; Agapie, T. *Eur. J. Inorg. Chem.* **2013**, 3840.

(258) Basu, D.; Mazumder, S.; Niklas, J.; Baydoun, H.; Wanniarachchi, D.; Shi, X.; Staples, R. J.; Poluektov, O.; Schlegel, H. B.; Verani, C. N. *Chem. Sci.* **2016**, *7*, 3264.

(259) Roubelakis, M. M.; Bediako, D. K.; Dogutan, D. K.; Nocera, D. G. *Energy Environ. Sci.* **2012**, *5*, 7737.

(260) Lee, C. H.; Dogutan, D. K.; Nocera, D. G. *J. Am. Chem. Soc.* **2011**, *133*, 8775.

(261) Solis, B. H.; Maher, A. G.; Honda, T.; Powers, D. C.; Nocera, D. G.; Hammes-Schiffer, S. *ACS Catal.* **2014**, *4*, 4516.

(262) Ding, K.; Brennessel, W. W.; Holland, P. L. *J. Am. Chem. Soc.* **2009**, *131*, 10804.

(263) Betley, T. A.; Peters, J. C. *J. Am. Chem. Soc.* **2003**, *125*, 10782.

(264) Chapovetsky, A.; Do, T. H.; Haiges, R.; Takase, M. K.; Marinescu, S. C. *J. Am. Chem. Soc.* **2016**, *138*, 5765.

(265) Baffert, C.; Artero, V.; Fontecave, M. *Inorg. Chem.* **2007**, *46*, 1817.

(266) Dempsey, J. L.; Brunschwig, B. S.; Winkler, J. R.; Gray, H. B. *Acc. Chem. Res.* **2009**, *42*, 1995 and references therein.

(267) Dempsey, J. L.; Winkler, J. R.; Gray, H. B. *J. Am. Chem. Soc.* **2010**, *132*, 1060.

(268) Hu, X. H.; Brunschwig, B. S.; Peters, J. C. *J. Am. Chem. Soc.* **2007**, *129*, 8988.

(269) Lin, T.-P.; Peters, J. C. *J. Am. Chem. Soc.* **2013**, *135*, 15310.

(270) Hu, X.; Cossairt, B. M.; Brunschwig, B. S.; Lewis, N. S.; Peters, J. C. *Chem. Commun.* **2005**, 4723.

(271) Berben, L. A.; Peters, J. C. *Chem. Commun.* **2010**, *46*, 398.

(272) Patra, A. K.; Dube, K. S.; Sanders, B. C.; Papaefthymiou, G. C.; Conradie, J.; Ghosh, A.; Harrop, T. C. *Chem. Sci.* **2012**, *3*, 364.

(273) Scheidt, W. R.; Hoard, J. L. *J. Am. Chem. Soc.* **1973**, *95*, 8281.

(274) McCleverty, J. A. *Chem. Rev.* **2004**, *104*, 403.

(275) Wyllie, G. R. A.; Scheidt, W. R. *Chem. Rev.* **2002**, *102*, 1067.

(276) Snyder, D. A.; Weaver, D. L. *Inorg. Chem.* **1970**, *9*, 2760.

(277) Feltham, R. D.; Nyholm, R. S. *Inorg. Chem.* **1965**, *4*, 1334.

(278) Johnson, P. L.; Enemark, J. H.; Feltham, R. D.; Swedo, K. B. *Inorg. Chem.* **1976**, *15*, 2989.

(279) Hall, D.; Taggart, A. A. *J. Chem. Soc.* **1965**, 1359.

(280) Franz, K. J.; Doerrer, L. H.; Spingler, B.; Lippard, S. J. *Inorg. Chem.* **2001**, *40*, 3774.

(281) Kozhukh, J.; Lippard, S. J. *J. Am. Chem. Soc.* **2012**, *134*, 11120.

(282) Hopmann, K. H.; Conradie, J.; Tangen, E.; Tonzetich, Z. J.; Lippard, S. J.; Ghosh, A. *Inorg. Chem.* **2015**, *54*, 7362.

(283) Hess, J. L.; Conder, H. L.; Green, K. N.; Darensbourg, M. Y. *Inorg. Chem.* **2008**, *47*, 2056.

(284) Kumar, P.; Lee, Y.-M.; Hu, L.; Chen, J.; Park, Y. J.; Yao, J.; Chen, H.; Karlin, K. D.; Nam, W. *J. Am. Chem. Soc.* **2016**, *138*, 7753.

(285) Kumar, P.; Lee, Y.-M.; Park, Y. J.; Siegler, M. A.; Karlin, K. D.; Nam, W. *J. Am. Chem. Soc.* **2015**, *137*, 4284.

(286) Wyllie, G. R. A.; Scheidt, W. R. *Chem. Rev.* **2002**, *102*, 1067 and references therein.

(287) Chuang, C.-H.; Liaw, W.-F.; Hung, C.-H. *Angew. Chem. Int. Ed.* **2016**, *55*, 5190.

(288) Kadish, K. M.; Mu, X. H.; Lin, X. Q. *Inorg. Chem.* **1988**, *27*, 1489.

(289) Ellison, M. K.; Scheidt, W. R. *Inorg. Chem.* **1998**, *37*, 382.

(290) Fujita, E.; Chang, C. K.; Fajer, J. *J. Am. Chem. Soc.* **1985**, *107*, 7665.

(291) Bertin, E. P.; Mizushima, S.-I.; Lane, T. J.; Quagliano, J. V. *J. Am. Chem. Soc.* **1959**, *81*, 3821.

(292) Tamaki, M. M., I.; Shinra, K. *Bull. Chem. Soc. Jpn.* **1972**, *45*, 171.

(293) Englert, U.; Strähle, J. *Gazz. Chim. Ital.* **1988**, *118*, 845.

(294) Connelly, N. G.; Geiger, W. E. *Chem. Rev.* **1996**, *96*, 877.

(295) Brock, C. P.; Collman, J. P.; Dolcetti, G.; Farnham, P. H.; Ibers, J. A.; Lester, J. E.; Reed, C. A. *Inorg. Chem.* **1973**, *12*, 1304.

(296) Enemark, J. H.; Feltham, R. D.; Riker-Nappier, J.; Bizot, K. F. *Inorg. Chem.* **1975**, *14*, 624.

(297) Enemark, J. H.; Feltham, R. D. *J. Chem. Soc. Dalton Trans.* **1972**, 718.

(298) Görls, H.; Reck, G.; Jäger, E.-G.; Müller, K.; Seidel, D. *Cryst. Res. Technol.* **1990**, *25*, 1277.

(299) Groombridge, C. J.; Larkworthy, L. F.; Marécaux, A.; Povey, D. C.; Smith, G. W.; Mason, J. *J. Chem. Soc. Dalton Trans.* **1992**, 3125.

(300) Hu, B.; Li, J. *Angew. Chem. Int. Ed.* **2015**, *54*, 10579.

(301) Pellegrino, J.; Bari, S. E.; Bikiel, D. E.; Doctorovich, F. *J. Am. Chem. Soc.* **2010**, *132*, 989.

(302) Subedi, H.; Brasch, N. E. *Inorg. Chem.* **2013**, *52*, 11608.

(303) Rhine, M. A.; Rodrigues, A. V.; Bieber Urbauer, R. J.; Urbauer, J. L.; Stemmler, T. L.; Harrop, T. C. *J. Am. Chem. Soc.* **2014**, *136*, 12560.

(304) Clarkson, S. G.; Basolo, F. *Inorg. Chem.* **1973**, *12*, 1528.

(305) Trogler, W. C.; Marzilli, L. G. *Inorg. Chem.* **1974**, *13*, 1008.

(306) Rossi, M.; Sacco, A. *Chem. Commun.* **1971**, 694.

(307) Maejima, T.; Miki, E.; Tanaka, M.; Tezuka, H.; Mizumachi, K.; Ishimori, T. *Bull. Chem. Soc. Jpn.* **1990**, *63*, 1596.

(308) Gwost, D.; Caulton, K. G. *Inorg. Chem.* **1974**, *12*, 414.

(309) Gargano, M.; Giannoccaro, P.; Rossi, M.; Sacco, A.; Vasapollo, G. *Gazz. Chim. Ital.* **1975**, *105*, 1279.

(310) Miki, E. *Chem. Lett.* **1980**, 835.

(311) Miki, E.; Ishimaru, K.; Mizumachi, K.; Ishimori, T.; Tanaka, M. *Bull. Chem. Soc. Jpn.* **1985**, *58*, 962.

(312) Miki, E.; Saito, K.; Mizumachi, K.; Ishimori, T. *Bull. Chem. Soc. Jpn.* **1983**, *56*, 3515.

(313) Miki, E.; Tanaka, M.; Mizumachi, K.; Ishimori, T. *Bull. Chem. Soc. Jpn.* **1986**, *59*, 3275.

(314) Miki, E.; Tanaka, M.; Saito, K.; Maejima, T.; Mizumachi, K.; Ishimori, T. *Bull. Chem. Soc. Jpn.* **1985**, *58*, 1642.

(315) Doyle, M. P.; Pickering, R. A.; Cook, B. R. *J. Inorg. Biochem.* **1983**, *19*, 329.

(316) Kurtikyan, T. S.; Eksuzyan, S. R.; Hayrapetyan, V. A.; Martirosyan, G. G.; Hovhannisyan, G. S.; Goodwin, J. A. *J. Am. Chem. Soc.* **2012**, *134*, 13861.

(317) Kozhukh, J.; Lippard, S. J. *Inorg. Chem.* **2012**, *51*, 9416.

(318) Armor, J. *Inorg. Chem.* **1973**, *12*, 1959.

(319) Doyle, M. P.; Pickering, R. A.; Dykstra, R. L.; Cook, B. R. *J. Am. Chem. Soc.* **1982**, *104*, 3392. The species responsible for release of the NO moiety may be a reduced cobalt nitrosyl given the presence of excess reductant.

(320) Doyle, M. P.; Van Doornik, F. J.; Funckes, C. L. *Inorg. Chim. Acta* **1980**, *46*, L111. $[Co(NH_3)_5(NO)]Cl_2$ reacts with both Fe^{III}- and Fe^{II}-heme proteins.

(321) Ungermann, C. B.; Caulton, K. G. *J. Am. Chem. Soc.* **1976**, *98*, 3862.

(322) Richter-Addo, G. B.; Legzdins, P., *Metal Nitrosyls*. Oxford University Press: New York, 1992.

(323) Blanchard, A. A.; Rafter, J. R.; Adams, W. B., Jr *J. Am. Chem. Soc.* **1934**, *56*, 16.

(324) Coleman, G. W.; Blanchard, A. A. *J. Am. Chem. Soc.* **1936**, *58*, 2160.

(325) Di Vaira, M.; Ghilardi, C. A.; Sacconi, L. *Inorg. Chem.* **1976**, *15*, 1555.

(326) Thyagarajan, S.; Incarvito, C. D.; Rheingold, A. L.; Theopold, K. H. *Inorg. Chim. Acta.* **2003**, *345*, 333.

(327) Tomson, N. C.; Crimmin, M. R.; Petrenko, T.; Rosebrugh, L. E.; Sproules, S.; Boyd, W. C.; Bergman, R. G.; DeBeer, S.; Toste, F. D.; Wieghardt, K. *J. Am. Chem. Soc.* **2011**, *133*, 18785.

(328) Feltham, R. D.; Enemark, J. H., *Structures of Metal Nitrosyls*. Wiley: New York, 1981; Vol. 12, p 155.

(329) Wang, X.; Andrews, L. *J. Phys. Chem. A.* **2001**, *105*, 4403.

(330) Scheidt, W. R.; Frisse, M. E. *J. Am. Chem. Soc.* **1975**, *97*, 17.

(331) Sanders, B. C.; Patra, A. K.; Harrop, T. C. *J. Inorg. Biochem.* **2013**, *118*, 115.

CHAPTER 2

PROTON-INDUCED REACTIVITY OF NO^- FROM A $\{CoNO\}^8$ COMPLEX[1]

[1] Rhine, M.A.; Rodrigues, A.V.; Bieber Urbauer, R.J.; Urbauer, J.L.; Stemmler, T.L.; Harrop, T.C. *J. Am. Chem. Soc.* **2014**, *136*, 12560 – 12563. http://pubs.acs.org/doi/full/10.1021/ja5064444.

2.1 Abstract

Research on the one-electron reduced analogue of NO, namely nitroxyl (HNO/NO^-), has revealed distinguishing properties regarding its utility as a therapeutic. However, the fleeting nature of HNO requires the design of donor molecules. Metal nitrosyl (MNO) complexes could serve as potential HNO donors. The synthesis, spectroscopic/structural characterization, electrochemical and HNO donor properties of a $\{CoNO\}^8$ complex in a pyrrole/imine ligand frame are reported. The $\{CoNO\}^8$ complex $[Co(LN_4^{PhCl})(NO)]$ (**1**) does not react with established HNO targets such as Fe^{III} hemes or Ph_3P. However, in the presence of stoichiometric H^+ **1** behaves as an HNO donor. Complex **1** readily reacts with [Fe(TPP)Cl] or Ph_3P (THF, 298 K) to afford the $\{FeNO\}^7$ porphyrin or $Ph_3P{=}O$/$Ph_3P{=}NH$, respectively. In the absence of an HNO target, the $\{Co(NO)_2\}^{10}$ dinitrosyl (**3**) is the end product. Complex **1** also reacts with O_2 to yield the corresponding Co^{III}-η^1-ONO_2 (**2**) nitrato analogue. This report is the first to suggest an HNO donor role for $\{CoNO\}^8$ with biotargets. These studies indicate that $\{CoNO\}^8$ complexes can function as HNO/NO^- donors and exhibit such reactivity with known HNO/NO^- targets.

2.2 Introduction

Amongst the many biochemical and physiological roles of NO•,[1] its redox chemistry to reduced analogues such as nitroxyl (HNO/NO$^-$, pK_a = 11.6)[2] has not been extensively studied. This is primarily due to the rapid dimerization and dehydration of HNO to N_2O and H_2O ($k = 10^6$ M^{-1} s^{-1})[3] that makes this particular nitrogen oxide difficult to study. Despite its analogous structure, nitroxyl has demonstrated pharmacological and therapeutic advantages distinct from NO•.[4] Such properties include specific targeting of biological thiols and Fe^{III} heme proteins, increasing the plasma concentration of calcitonin gene-related peptide (CGRP - a small neuropeptide involved in vasodilation), and its positive cardiac inotrope effect (heart muscle contraction). These properties have driven the field to better understand the chemical biology of HNO through the design and synthesis of controllable donor molecules.[5-6] The most common donors include diazeniumdiolates such as $Na_2N_2O_3$ (Angeli's salt)[7] and *N*-hydroxysulfonamide derivatives (R-SO_2-NH-OH) such as Piloty's acid.[6,8] While reliable as HNO donors, these compounds are limited as they release other potentially reactive species or function at pH > 9.[5-6] Clearly, the development of better HNO donors is needed.

Metal nitrosyls (MNO) could serve as an alternative platform for HNO/NO$^-$ delivery. Indeed, the heme enzyme responsible for NO synthesis (NO synthase) has been shown to release HNO via an Fe-bound *N*-hydroxy-L-arginine intermediate in the absence of its biopterin cofactor.[9-10] Due to the variable redox states of NO when coordinated to metals (i.e. NO$^+$, NO•, NO$^-$), descriptions of bonding typically resort to the Enemark-Feltham (EF) notation as a result of extensive electron delocalization within the MNO moiety.[11] We reported the synthesis and properties of non-heme {FeNO}^{8} complexes (a rare EF notation),[12-13] one which demonstrates nitroxyl-like reactivity with equine skeletal metmyoglobin under pseudo-physiological

conditions.[12] Due to the inherent reactivity of the $\{FeNO\}^8$ systems, we have now synthesized isoelectronic $\{CoNO\}^8$ complexes with more electron-deficient supporting ligands as the next logical step in our goal of customizing an HNO/NO^- delivery vehicle with more controllable properties. Herein we describe the synthesis and properties of a non-porphyrin-based $\{CoNO\}^8$ complex, the H^+-induced formation of the fleeting HNO donor intermediate, and its nitroxyl-like reaction with an Fe^{III}-heme model complex and Ph_3P.

2.3 Results and Discussion

The $\{CoNO\}^8$ complex $[Co(LN_4^{PhCl})(NO)]$ (**1**) (LN_4^{PhCl} = dianion of (N^1E,N^2E)-N^1,N^2-bis((1H-pyrrol-2-yl)methylene)-4,5-dichlorobenzene-1,2-diamine; Chart 2.1) was synthesized by purging NO(g) into an MeCN solution of in situ prepared $(Et_4N)_2[Co(LN_4^{PhCl})Cl_2]$ at 60 °C. The resulting dark-brown microcrystalline product precipitated from the reaction mixture and was isolated as analytically pure material in 72% yield. Complex **1** is stable to air, moisture, and vacuum in the solid-state. Solution samples (THF, MeCN) of **1** also demonstrate similar stability; however, slow air exposure (one week) to an MeCN/THF solution of **1** afforded the corresponding nitrato complex $[Co(LN_4^{PhCl})(MeCN)(\eta^1\text{-}ONO_2)]$ (**2**) as single crystals (see Chart 2.1 and Scheme 2.1). This result parallels what is seen in other $\{CoNO\}^8/O_2$ reactions[14] and highlights the nucleophilic nature of the NO ligand in **1** which is suggestive of its NO^- character.

Chart 2.1.

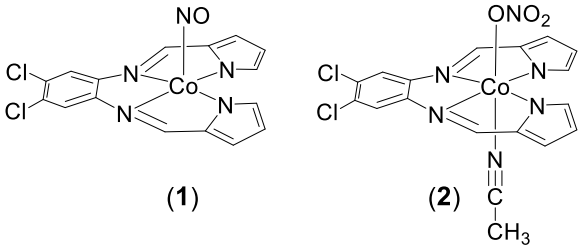

Recrystallization of the $\{CoNO\}^8$ complex from 2-MeTHF/Et_2O afforded X-ray quality crystals of **1**, which revealed a square-pyramidal Co center originating from the diimine-dipyrrolide N_4-ligand (basal plane) with NO in the apical position (Figure 2.1). Relevant X-ray data and metric parameters are provided in Tables 2.S1 and 2.S2 (see the Supporting Information = SI). The near-perfect square-pyramidal geometry in **1** is indicated by its low trigonal distortion parameter ($\tau = 0.08$) and is due to the extreme planarity of the N_4-ligand[15] with Co displaced by 0.264 Å out of the N_4 plane and towards NO. The Co-N_{imine} (avg: 1.895 Å) and Co-$N_{pyrrole}$ (avg: 1.919 Å) distances are comparable to Co-N bonds in other non-porphyrin $\{CoNO\}^8$ complexes[16-19] and also in Co^{III} complexes without NO ligands such as the nitrato complex **2** (avg. Co-N_{imine}: 1.893 Å; avg. Co-$N_{pyrrole}$: 1.926 Å; SI, Figure 2.1). This comparison suggests a Co^{III} oxidation state for **1**, which was further verified by X-ray absorption spectroscopic (XAS) measurements (vide infra). The Co-N(O) (1.798(3) Å) and bent Co-N-O angle (124.4(3)°) are also representative metrics of five-coordinate $\{CoNO\}^8$ complexes.[19] The bent nature of the Co-N-O unit in solution is further supported by the large downfield shift of the NO nitrogen in the ^{15}N NMR spectrum (δ: 688 ppm vs. CH_3NO_2 in THF-d_8, Figure 2.S2).[20] Additionally, the N-O bond distance (1.172(4) Å) is in between that reported for ^1HNO (1.21 Å)[21] and NO (1.15 Å), but more like the latter.[19] Consistent with this observation is the solid-state FTIR spectrum of **1**, which exhibits ν_{NO} at 1667 cm^{-1} that shifts to 1638 cm^{-1} ($\Delta\nu_{NO}$: 29 cm^{-1}) after isolating [Co(LN_4^{PhCl})(^{15}NO)] (**1-^{15}NO**) using

^{15}NO(g) in the synthesis (Figure 2.S3). The ν_{NO} and diamagnetic ground state (see ^{1}H NMR, Figure 2.S1) is typical for this class of Co nitrosyls.[19,22]

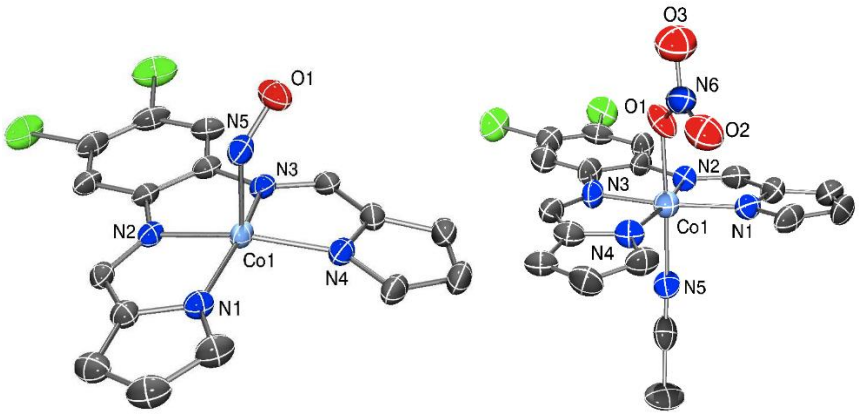

Figure 2.1. X-ray structures of [Co(LN$_4^{PhCl}$)(NO)] (**1**) (*left*) and [Co(LN$_4^{PhCl}$)(MeCN)(η^1-ONO$_2$)] (**2**) (*right*) (50% probability level). H atoms and distorted THF solvent of crystallization for **1** have been omitted for clarity.

XAS measurements support the crystallographic results obtained for **1**. The X-ray absorption near edge spectrum (XANES) shows a large pre-edge feature centered at 7710.6 eV, characteristic of Co^{III} 1s→3d electronic transitions; the measured peak area (0.387 eV) confirms the metal is coordinated in a non-centrosymmetric ligand environment (Figure 2.2). The first inflection energy in the XANES spectrum occurs at 7721.3 eV, as in other XAS-characterized Co^{III} compounds.[23-24] Simulations of the extended X-ray absorption fine structure (EXAFS) spectral region are consistent with Co^{III} in a five-coordinate ligand environment constructed of five O/N ligands at an average distance of 1.88 Å (Figure S4). These results compare favorably to distances obtained from X-ray diffraction (avg: 1.89 Å). Taken together, these results suggest the MNO unit in **1** is best described as low-spin Co^{III} ($S = 0$) bound to singlet nitroxyl anion (^{1}NO^{-}; $S = 0$).

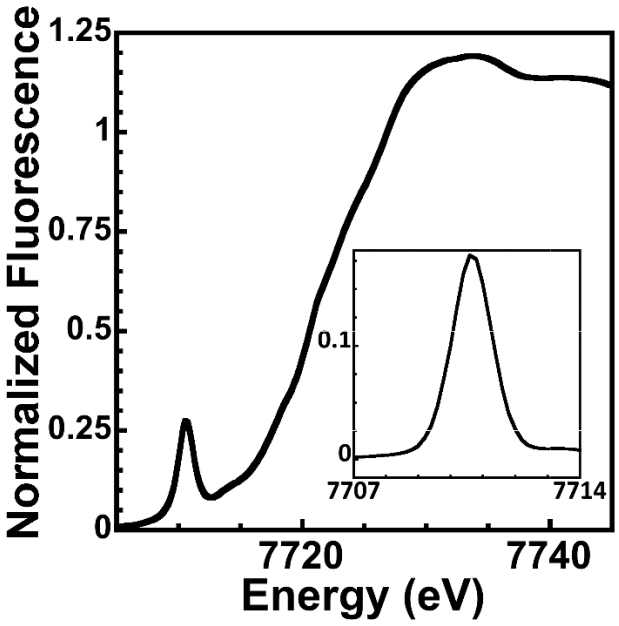

Figure 2.2. XANES spectrum for $\{CoNO\}^8$ **1**. *Inset*: The baseline subtracted pre-edge features for **1**.

Despite the formal assignment of the NO ligand as $^1NO^-$ in other $\{CoNO\}^8$ systems,[25-26] we were surprised that their chemical reactivity had not been explored in detail given their potential as HNO donors. Indeed, complexes with the $\{CoNO\}^8$ notation are generally designated as low-spin Co^{III} coordinated to $^1NO^-$ to yield $S_{tot} = 0$.[25-26] Perhaps this paucity is due to the well-known kinetic inertness of low-spin d^6 metals such as Co^{III}.[27] One common and sensitive test for an HNO donor involves its reaction with Fe^{III}-porphyrins[28-29] or Fe^{III}-heme proteins[30-33] to afford the corresponding $\{FeNO\}^7$ derivatives. Thus, the capability of **1** to reductively nitrosylate the Fe^{III}-heme model [Fe(TPP)Cl] (TPP = dianion of tetraphenylporphyrin) was explored. When a stoichiometric amount of **1** was added to the Fe^{III} heme in THF at 298 K, *no reaction* was observed even after 24 h (Scheme 2.1). Similarly, increasing the temperature to 310 K and monitoring over the same 24 h time period resulted in *no reaction*. However, when the reaction was repeated in the

presence of one mol-equiv of an organic-soluble H^+ donor (HBF_4•Et_2O), an entirely different reaction resulted (Scheme 2.1). In this case, [Fe(TPP)Cl] was almost immediately consumed within 4 min of H^+ addition (monitored by UV-vis, FTIR) to afford the corresponding $\{FeNO\}^7$ heme analogue [Fe(TPP)NO] (ν_{NO}: 1698 cm^{-1} in KBr). Bulk reaction studies further confirmed the near stoichiometric NO transfer between **1** and [Fe(TPP)Cl] (88% yield; Figure 2.S7 for FTIR/EPR of the [Fe(TPP)NO] product). Using isotopically-labeled **1-^{15}NO** resulted in the corresponding shift of ν_{NO} in the IR spectrum of the [Fe(TPP)^{15}NO] product (ν_{NO}: 1667 cm^{-1} in KBr, $\Delta\nu_{NO}$: 31 cm^{-1}) as well as the expected triplet-to-doublet hyperfine structural change in its X-band EPR spectrum (Figure 2.S7).

Scheme 2.1. Reactivity of **1**. HNO-derived products highlighted.

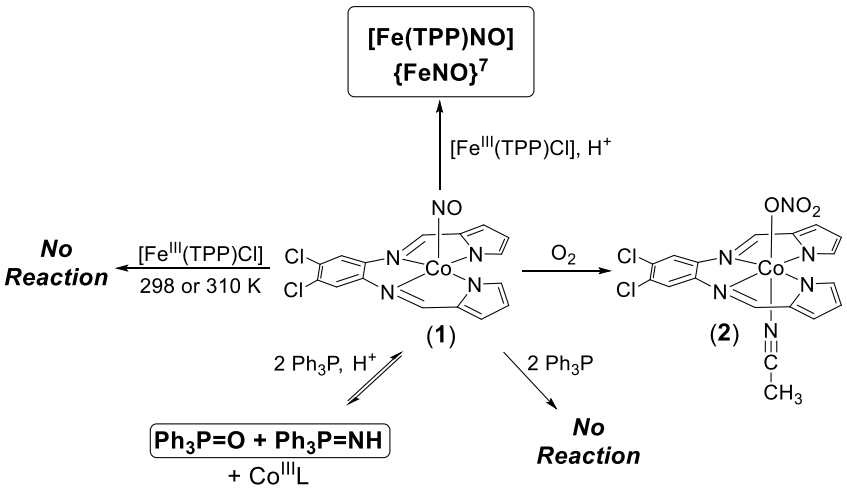

Further insight regarding the mechanism of the reductive nitrosylation of [Fe(TPP)Cl] with **1** and HBF_4•Et_2O come from electrochemical measurements. In THF, **1** displays a quasi-reversible $\{CoNO\}^9/\{CoNO\}^8$ wave at $E_{½}$ = -1.46 V vs. Fc^+/Fc in THF (Figure 2.S5). One possible route to

[Fe(TPP)NO] is via reduction of [Fe(TPP)Cl] from **1** to yield a $\{CoNO\}^7$ complex that would release NO$^{\bullet}$ to the Fe^{II}-heme model. An irreversible E_{ox} peak at 0.75 V is observed suggesting the $\{CoNO\}^7$ complex is unstable and likely results in loss of NO$^{\bullet}$. Since the $Fe^{III/II}$ couple of [Fe(TPP)Cl] is -0.90 V in THF (vs. Fc^+/Fc),[34] it is doubtful that **1** can reduce Fe^{III} to Fe^{II} in this reaction. It is possible that HNO transfer is taking place upon H^+ addition to **1**. Support for this hypothesis comes from reactions performed with DNICs (mononuclear tetrahedral dinitrosyl iron complexes) and Fe^{III}-porphyrins by Darensbourg and coworkers.[35] In these studies, addition of H^+ *greatly enhances* the rate of HNO transfer to form the corresponding $\{FeNO\}^7$ analogues (72 h without H^+; 9 h with 0.25 equiv of H^+). This rate enhancement of HNO transfer/release from the DNICs has been attributed to the "carrier effect" of H^+ for NO^- as the neutral HNO should be more mobile in non-polar aprotic solvents such as CH_2Cl_2 or THF.

Additional proof that **1** behaves as an HNO donor in the presence of stoichiometric H^+ stem from its reaction with Ph_3P. King established that triarylphosphines (R_3P) react selectively with HNO donors to yield the corresponding phosphine oxide (R_3P=O) and aza-ylide (R_3P=NH): HNO + $2R_3P \rightarrow$ R_3P=O + R_3P=NH.[36-37] These molecules represent unique and quantifiable products as markers of HNO, which is measured by the amount of R_3P=O formed (R_3P=NH is reactive and hydrolyzes to R_3P=O). Accordingly, addition of two equiv of Ph_3P to the red-brown **1**/H^+ mixture resulted in a lightening of this solution to a yellow-tinted transparent brown after 24 h. ^{31}P NMR analysis of this mixture clearly indicated the presence of Ph_3P=O (δ: 26.3 ppm), Ph_3P=NH (δ: 20.6 ppm), and unreacted Ph_3P (-6.0 ppm) (Figure 2.S16). Additional support for Ph_3P=NH derives from using **1-^{15}NO**, which afforded identical ^{31}P NMR features except for the doublet splitting of the 20.6 ppm peak arising from the ^{15}N nucleus ($^1J_{P\text{-}N}$: 135 Hz). *This result is definitive proof that **1** in the presence of H^+ is an HNO donor*. Control experiments with Ph_3P and **1** indicated no

reaction. To evaluate the extent to which **1**/H^+ donates HNO, the amount of Ph_3P was quantified by HPLC (SI), which was determined to be 33% (2 equiv Ph_3P) after 24 h. Utilizing excess (10 equiv) Ph_3P improved the yield to 37% (Figure 2.S19). Other peaks in the chromatogram were identified as **1** and free ligand (SI), which may account for the ~40% yield of Ph_3P=O. R_3P-based reactions with established HNO donors have also been less than stoichiometric.[37] Collectively, these results offer strong support that **1** and H^+ generate a compound that is capable of releasing HNO.

In an effort to verify the actual species responsible for the HNO donor property, we attempted in situ characterization of intermediates utilizing high-resolution MS. For example, the MS of the **1** and HBF_4 (1/1.3; 30 min) mixture generate a major peak at *m/z*: 418.974(1) that is assigned to a reduced and doubly protonated cation of general formula $[Co(LN_4^{PhCl}H_2)(NO)]^+$ (Figure 2.3).[38-39] This peak remains even after 24 h mixing. Fragmenting this peak afforded one signal at *m/z*: 388.976(1) corresponding to loss of NO (30 amu) and formation of $[Co(LN_4^{PhCl}H_2)]^+$. Experiments with **1-^{15}NO** provided analogous results with loss of 31 amu (^{15}NO) (Figure 2.S14). In contrast, **1** reveals no significant peaks in the MS, consistent with its neutral charge. FTIR and ^{1}H NMR measurements reveal additional benchmarks that may be assigned to this intermediate (isotope-sensitive ν_{NO}: 1544 cm^{-1}; δ_{NH}: 11.5 ppm, Figures 2.S8-2.S13). A $\{[Co(LN_4^{PhCl})(HNO)] + H\}^+$ $\{CoHNO\}^9$ formulation is consistent with the MS; however, the absence of ^{15}N coupling (I = ½) to the 11.5 ppm peak in the NMR (using **1-^{15}NO**) suggest this signal to arise from protonated ligand. Overall, these observations implicate a three-coordinate, protonated pyrrole-NH and imine-N bound $\{CoNO\}^8$ (**4**) as the first intermediate formed in the **1**/H^+ reaction (Scheme 2.2). After 24 h mixing, a new species corresponding to $[Co(LN_4^{PhCl}H_2)(NO)_2]BF_4$ (**3**) is observed. Spectroscopic analysis of the reaction mixture confirm this assignment with ^{15}N-sensitive ν_{NO} (1869, 1793 cm^{-1})

and *m/z*: 448.972 (Figures 2.S9, 2.S15). These parameters are consistent with independently synthesized and characterized **3** and other neutral N-bound $\{Co(NO)_2\}^{10}$ complexes (Figures 2.S20-2.S23).[40] A significant portion of **1** and **4** also remain and implicate the equilibrium depicted in Scheme 2.2.[41]

Scheme 2.2. Reactivity of **1** with H^+.

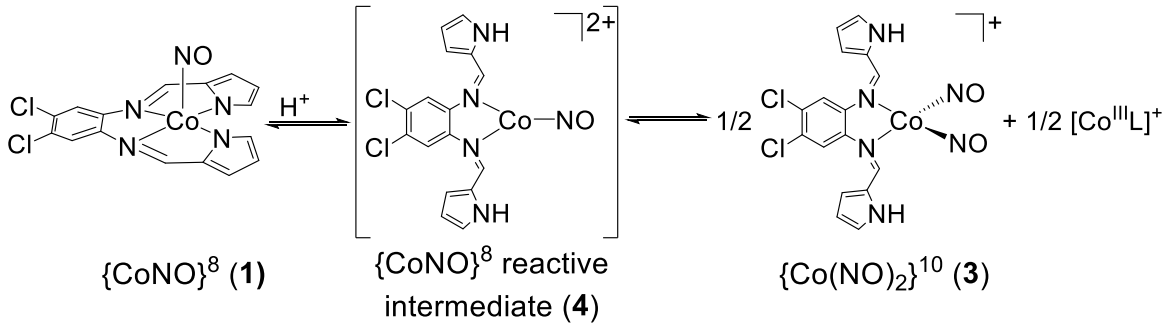

The results obtained provide insight into the potential paths traversed with **1**/H^+. In the absence of HNO targets, **4** appears as the first CoNO intermediate after H^+ addition, providing strong support that this species is likely responsible for the observed reaction chemistry based on IR, MS, and NMR. While this proposal does not completely eliminate a transient Co-HNO, none of the current evidence supports its formation. Indeed, the lack of definitive proof for Co-HNO is not too surprising as the isolation and characterization of first-row M-HNO adducts have met with limited success due to the reactive nature of the nitroxyl ligand.[42-45] Attempts to isolate **4** either from the reaction mixture or directly have not been successful.[46,47] One hypothesis for the reductive nitrosylation of [Fe(TPP)Cl] is the generation of a bridging {Co(μ-NO)(μ-Cl)Fe} intermediate where trans-nitroxylation occurs to yield the $\{FeNO\}^7$ heme, a route suggested for the isoelectronic $\{FeNO\}^8$ complex.[13] H^+ addition simply enhances the rate of nitroxyl transfer as

suggested for DNICs.[35] Such bridging intermediates have also been proposed in the dismutation of $\{CoNO\}^8$ species to $\{Co(NO)_2\}^{10}$ and Co^{III} indicative of formal NO^- transfer.[48] This result is analogous to the fate of **1** to give **3** in the absence of HNO-reactive molecules (Scheme 2.2). The reaction with Ph_3P may take place from **4** (via tautomerization) or a transient Co-HNO intermediate structurally similar to **1**. Both free and coordinated Ph_3P represent viable possibilities as well. More detailed studies were precluded by the complexity of the process and the difficulty in isolating and detecting every reaction product. Regardless, the observed results are consistent with an HNO donor property for **1**/H^+.

While the release and transfer of the nitrosyl ligand from $\{CoNO\}^8$ complexes have not been extensively explored, a few earlier reports exist.[49-52] In the most bio-relevant study, Doyle showed the feasibility of NO transfer from several $\{CoNO\}^8$ complexes including $[Co(DMG)_2(NO)]$ (DMG = dimethylglyoximate) to hemoglobin and myoglobin.[51] These reactions involved the release of $NO^{\bullet}$ from the $\{CoNO\}^8$ complex to the Fe^{II}-heme proteins using dithionite as reducing agent. *No reaction occurred with Fe^{III}-heme proteins even with 10- to 20-fold excess $\{CoNO\}^8$, a benchmark property of HNO donors*.[31] It is possible that a dithionite-generated $\{CoNO\}^9$ species is the NO-releasing agent. Indeed, rapid loss of NO is observed when $[Co(DMG)_2(NO)]$ is treated with dithionite.[50] In comparison, this account reports the isolation of a $\{CoNO\}^8$ complex that functions like an HNO donor with Fe^{III}-heme and Ph_3P targets.

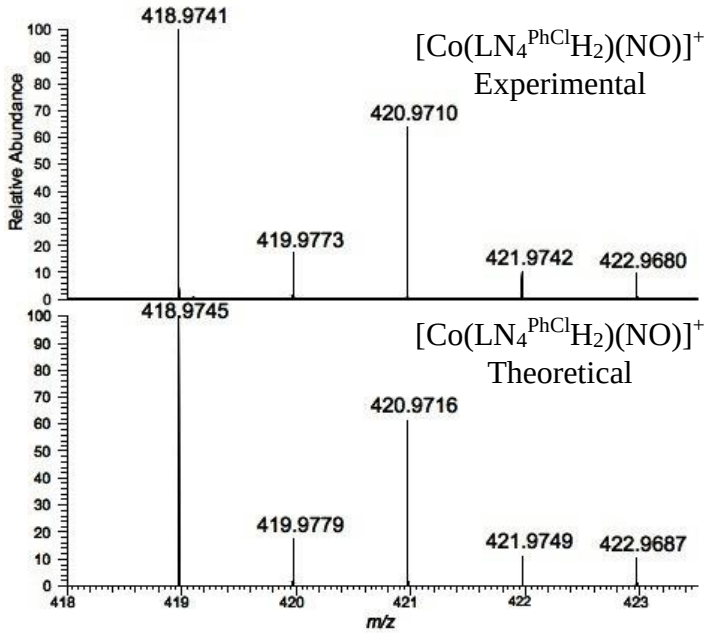

Figure 2.3. *Top*: High-resolution ESI-MS (positive mode) of the reaction of **1** + HBF_4•Et_2O. *Bottom*: Theoretical isotopic distribution.

2.4 Reactivity of a {CoNO}^{8} Complex with *p*-chlorobenzenethiol (*p*-Cl-PhSH)[2]

As an isoelectronic analogue to {FeNO}^{8}, {CoNO}^{8} complex have been used as a comparison regarding electronic structure and reactivity in this mostly elusive EF notation for Fe-nitrosyls.[12] Experimental proof for the oxidation state of Co and NO in these complexes has come from X-ray absorption spectroscopy where a low-spin (d^6) Co^{III} ($S = 0$) coordinated to $^1NO^-$ ($S = 0$) assignment has been verified (vide supra).[53] As such, the reactivity of {CoNO}^{8} complex [Co(LN_4^{Pr})(NO)] (**5**; LN_4^{Pr} = dianion of (N^1E,N^3E)-N^1,N^3-bis((1H-pyrrol-2-yl)methylene)-propane-1,2-diamine), which contains a propyl linker rather than the dichlorophenylene linker in **1,** with a stoichiometric amount of *p*-Cl-PhSH was also investigated under the same conditions as

[2] Rhine, M.A; Sanders, B.C.; Patra, A.K.; Harrop, T.C. *Inorg. Chem.* **2015**, *54*, 9351 – 9366. Reprinted with permission from the American Chemical Society. Copyright 2015 American Chemical Society.

with the $\{FeNO\}^{7/8}$ systems with the identical ligand.[54] In this case mixing the thiol with **5** in MeCN did not result in any dramatic color change of the red-brown reaction mixture after 24 h, a likely indicator of an incomplete reaction as observed with the analogous $\{FeNO\}^{7}$ complex. Indeed, the strong ν_{NO} of **5** at 1657 cm^{-1} remained predominant in the FTIR spectrum of the reaction mixture. However, two additional peaks appeared in the ν_{NO} region at 1778 and 1726 cm^{-1} (~25% the intensity of the ν_{NO} of **5**), consistent with a new $\{Co(NO)_2\}$ species (Figure 2.4). We assigned this complex as the thiolate-bound $\{Co(NO)_2\}^{10}$ complex $[Co(SPh\text{-}p\text{-}Cl)_2(NO)_2]^-$ (anion of **6**) based on FTIR, ^1H NMR, and ESI-MS(–) evidence and comparison to independently synthesized **6** as the Et_4N^+ salt (see Figures 2.S24-2.S26). Much fewer in number than DNICs, mononuclear/S-bound/anionic $\{Co(NO)_2\}^{10}$ dinitrosyls tend to exhibit symmetric and asymmetric ν_{NO} stretches that are lower in energy than the more common N-bound and cationic cobalt dinitrosyls.[55] This shift in ν_{NO} is due to additional electron density in the π^* orbital of the NO moiety. For example, the higher ν_{NO} values of $[Co(LN_4^{Pr}H_2)(NO)_2]Cl$ (**7**) (1839, 1755 cm^{-1}) eliminates this *N-bound* $\{Co(NO)_2\}^{10}$ complex as a product in the **5** and *p*-Cl-PhSH reaction (Figure 2.S27). Although the corresponding reduced Roussin's red ester (rRRE) and Roussin's red ester (RRE) is formed in the reaction of $\{FeNO\}^{7/8}$ complexes containing the LN_4^{Pr} ligand with *p*-Cl-PhSH, respectively, it is unlikely that a Co analogue forms given the small separation of the symmetric and asymmetric ν_{NO} bands ($\Delta\nu_{NO}$) ~15-38 cm^{-1} for such compounds,[56-57] as $\Delta\nu_{NO}$ for the **5**/RSH reaction mixture is 52 cm^{-1} (Figure 2.4). Additionally, there is no compelling evidence in the ESI-MS(+/–) for this kind of species. However, there is strong evidence in the ESI-MS of the reaction mixture for $\{$**6** - $NO\}^-$ (calcd. *m/z* = 374.9; found *m/z* = 374.8; Figure 2.S29), and it is common for $\{M(NO)_2\}^n$ species to lose one or both nitrosyls in MS experiments.[58] The ESI-MS(+) of the bulk reaction also exhibits a strong peak at *m/z* = 515.3 that is consistent with a 2:1 complex with protonated ligand

$LN_4^{Pr}H_2$ coordinated through the imine-N to a Co(I) center, i.e., $[Co(LN_4^{Pr}H_2)_2]^+$ (calcd. *m/z* = 515.2). Thus, the complete formula for **6** is $[Co(LN_4^{Pr}H_2)_2][Co(SPh\text{-}p\text{-}Cl)_2(NO)_2]$. Previous studies in our group have indicated the possibility of protonating the pyrrolide nitrogens of LN_4^{2-} ligands when stoichiometric protons are added to a $\{CoNO\}^8$ complex, ultimately affording $[Co(LN_4H_2)(NO)_2]^+$ (analogous to **7**) and $[Co^{III}(LN_4)]^+$ complexes.[53] Separation and isolation of all products was problematic due to similar solubility; however, species present in the equilibrium at t = 24 h were quantified based on NMR integration with an internal standard. The ^{1}H NMR spectrum provides evidence of unreacted $\{CoNO\}^8$ **5** (31%) and thiol (45%) as well as $\{Co(NO)_2\}^{10}$ **6** (17%) and the disulfide *p*-Cl-PhSSPh-*p*-Cl (8%), as confirmed by authentic synthesis. While the product distribution does not change, the amount of unreacted **5** (46%) is greater when the reaction is performed in non-polar solvents such as THF. The difference between unreacted thiol and **5** can be explained by unforeseen reaction paths of **5** with other species present in the reaction mixture that have yet to be defined. Indeed, the ~50% of unreacted thiol better represents the relatively inert nature of the **5**/RSH reaction in comparison to **1** and **2**. The oxidation of RSH to RSSR is consistent with affording the reduced Co(I) complex. In contrast to the $\{FeNO\}^7$/thiol reaction where disulfide is also observed, there is no cogent support for $LN_4^{Pr}H_2$ in the ^{1}H NMR nor ESI-MS. As such, the reaction depicted in Scheme 2.3 is the most logical proposal although other unidentified species are also present in small amounts according to ^{1}H NMR (Figures 2.S29-2.S30).

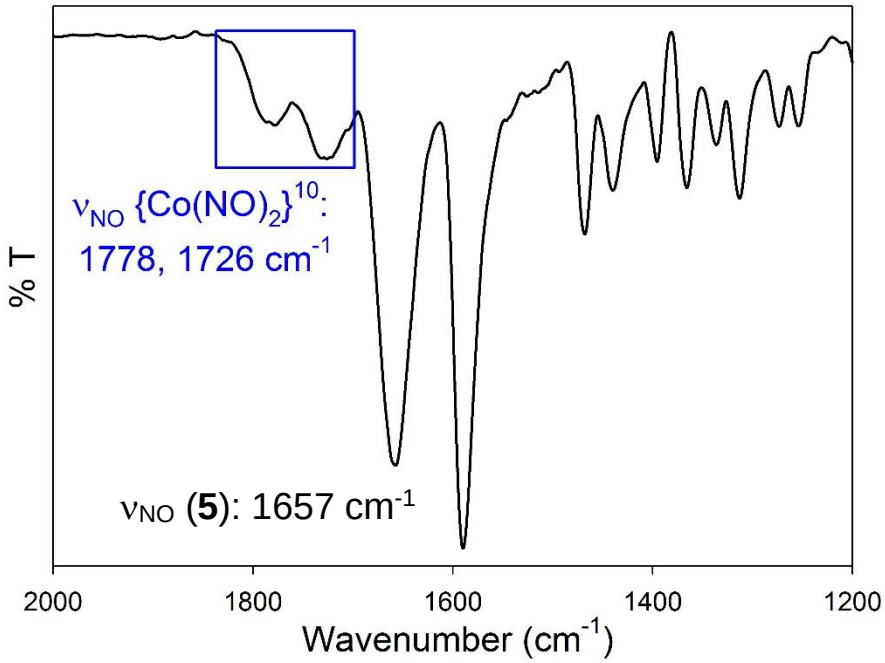

Figure 2.4. FTIR spectrum (KBr) of the bulk reaction of {CoNO}^{8} (**5**) with *p*-Cl-PhSH (1:1) showing ν_{NO} peaks for unreacted **5** and {Co(NO)$_2$}^{10} complex [Co(SPh-*p*-Cl)$_2$(NO)$_2$]$^-$ (anion of **6**).

Scheme 2.3. Equilibrium of **5** and *p*-Cl-PhSH (1:1) in MeCN or THF after 24 h, RT. Note: this schematic does not represent a balanced equation.

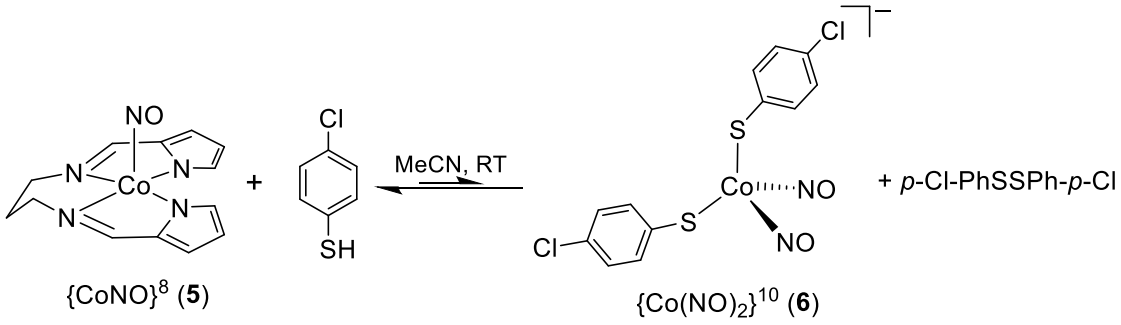

The oxidation states of the NO moiety and metal center are the key contributing factors that control the reactivity profiles of $\{FeNO\}^6$ complexes such as sodium nitroprusside (SNP)[54] and $\{MNO\}^8$ complexes such as **5** (see Chapter 1). This factor clearly explains why the NO of SNP, formally assigned as NO^+, is attacked by thiol/thiolate nucleophiles to form RSNO. In contrast, complex **5** and the analogous $\{FeNO\}^{7/8}$ complexes containing LN_4^{Pr} ($\{FeNO\}^7$ **8**, $\{FeNO\}^8$ **9**) undergo thiol-induced rearrangement/redox chemistry with no activation of the N-O bond. Perhaps the difference in reactivity amongst SNP and **5** originates from the multiple protonation sites available on the ligand frame in **5**. Indeed, pyrrole-NH groups ($pK_a = 23$[59]) are more basic than HNO ($pK_a = 11.6$[2]) or Fe-coordinated HNO (pK_a estimated to be > 11[60]) and explains the first site of protonation being the coordinated pyrrolide-N donors versus NO in the reactions of *p*-Cl-PhSH with **5**. However, pK_a alone does not explain the difference regarding the extent of the thiol reactions with the isoelectronic analogues $\{MNO\}^8$ **5** (Co) and **9** (Fe), which yields rRRE $[Fe_2(\mu\text{-SPh-}p\text{-Cl})_2(NO)_4]^-$ after reacting with *p*-Cl-PhSH. For reference, $\{FeNO\}^7$ complex **8** affords the RRE upon reacting with *p*-Cl-PhSH. $\{FeNO\}^8$ complex **9** has been described to be in resonance between low-spin Fe^{II}-$^1NO^-$ ↔ low-spin Fe^I-NO assignments ($S = 0$).[12] On the other hand, complex **5** and other $\{CoNO\}^8$ complexes with similar imine-pyrrole ligands have been assigned as low-spin Co^{III}-$^1NO^-$ ($S = 0$).[53] Thus, the kinetic inertness of Co^{III} controls the extent to which **3** reacts with thiols or even stronger acids such as HBF_4.[53] As a point of comparison, Lippard and coworkers have shown clear reactivity differences between M^{II}-coordinated tropocoronand complexes with NO such as [Co(TC-5,5)] and [Fe(TC-5,5)] (where TC-5,5 = macrocyclic N_4 tropocoronand ligand with a 5,5-polymethylene chain linker).[18,47] When in the presence of NO(g), the Fe^{II} complex promotes NO disproportionation ultimately forming N_2O and [Fe(TC-5,5-NO_2)(NO)], i.e., N-O and Fe-N(O) bond activation. The Co^{II} complex, on

the other hand, simply forms the $\{CoNO\}^8$ complex $[Co^{III}(TC\text{-}5,5)(NO)]$ as the only isolable species. Although $\{FeNO\}^8$ **9** and $\{CoNO\}^8$ **5** have the same Enemark-Feltham notation, the differences in metal oxidation state, i.e., the kinetic inertness of LS Co^{III}, govern the thiol reactivity of the reported metal nitrosyl complexes.

The area of {MNO} reaction chemistry with thiols and thiolates has seen considerable advances over the last five years. However, this statement should be taken with some caution as to not mistake it with the relatively abundant chemistry known on M-SR coordination complexes and their interactions with NO. For example, a plethora of thiol/thiolate chemistry has been published with SNP (see Chapter 1) and more is likely to appear on this simple inorganic coordination complex, which is used clinically as an $NO^{\bullet}$ donor. Indeed, the N-coordinated intermediates $(HS)_2N\text{-}OH$ arising from **I** and (HS)SN-OH generated from **II** (DFT-calculated intermediates) are proposed in the SNP reaction with H_2S/HS^- to lead to the reduced N products NH_3 and N_2O (basic, anaerobic conditions; Schemes 1.5, 1.6). In support of this observation, SNP was also shown to release HNO (via a transient SNP $\{FeHNO\}^8$ complex) when the same reaction was performed under physiological conditions. Overall, this would be a net change of one with regards to the N-O bond order in SNP (B.O. = 3) to B.O. = 2 in the coordinated HNO species at pH 7.4. Presumably, the basic pH and exclusion of O_2 leads to more reduced products such as **I** and ultimately NH_3. While the factors governing N-O bond activation in such transients is unknown, several N-substituted hydroxylamines have been prepared and shown to release HNO to yield N_2O.[61] In contrast to the bond activation chemistry observed with SNP, reactions of thiols/thiolates with other {MNO} complexes appear to result in NO displacement or ligand exchange/redox reactions at the {MNO} unit. This result becomes more evident in the thiol chemistry of the nonheme complexes **8** and **9** that react with aromatic thiols to give $\{Fe(NO)_2\}$ units that differ only by the

net electron count in the metal nitrosyl. The extent of the reaction with RSH trends with the EF notations (oxidation state assignment tentative except for Co), i.e., $\{FeNO\}^8$ (LS-Fe^{II}-$^1NO^-$) >> $\{FeNO\}^7$ (LS-Fe^{II}-$NO^\bullet$) >> $\{CoNO\}^8$ (Co^{III}-$^1NO^-$). It appears that the $\{M(NO)_2\}$ fragment is the thermodynamic sink in the chemistry of M(L)-NO complexes, especially Fe, in the presence of thiols/thiolates with no significant influence from the nature of L (tetradentate, diamine-dipyrrolide ligand in our case). Ultimately, a better understanding of these M-NO/RSH interactions will lead to new paths for NO generation/transfer and NO_x reduction.

2.5 Conclusions

In conclusion, we report the synthesis of $\{CoNO\}^8$ **1** and its reaction with H^+ to afford an HNO donating intermediate. In the absence of an HNO target, reaction of **1** and H^+ ultimately leads to the Co-dinitrosyl complex **3** (via intermediate **4**). To our knowledge the reaction of **1** and H^+ is the first example of a $\{CoNO\}^8$ complex that specifically behaves as an HNO donor to known HNO targets (Fe^{III}-heme and Ph_3P). Proton-induced formation of other signaling molecules such as H_2S has been observed with synthetic 2Fe-2S clusters and excess NO.[62] In contrast, **1** alone does not exhibit any reactivity from temperatures ranging 298-310 K, emphasizing the importance of HNO versus NO^- and the underexplored potential of metal nitrosyls as HNO donors. Furthermore, these results confirm that $\{CoNO\}^8$ complexes are not inert and function as sources of HNO under specific pH conditions, thereby opening up a new frontier in HNO donor research.

2.6 Materials and Methods

2.6.1 General Information

All reagents were purchased from commercial suppliers and used as received unless otherwise noted. Research grade nitric oxide gas (NO(g), UHP, 99.5%) was obtained from Matheson Tri-Gas. The NO(g) was purified by passage through an Ascarite II® (sodium hydroxide-coated silica, purchased from Aldrich) column and handled under anaerobic conditions. ^{15}NO(g) (^{15}N ≥ 98%) was procured from Cambridge Isotope Labs and used as received. Acetonitrile (MeCN), tetrahydrofuran (THF), dichloromethane (CH_2Cl_2), and diethyl ether (Et_2O) were purified by passage through activated alumina columns using an MBraun MB-SPS solvent purification system and stored over 3 Å molecular sieves under an N_2 atmosphere before use. Anhydrous 2-methyltetrahydrofuran (2-MeTHF) was obtained by storage over 3 Å molecular sieves for 48 h, decanting from the sieves, and storage under N_2. The Co^{II} salt $(Et_4N)_2[CoCl_4]$ was prepared according to the published procedure.[63] The N_4-ligand (*N*^{1}*E*,*N*^{2}*E*)-*N*^{1},*N*^{2}-bis((1H-pyrrol-2-yl)methylene)-4,5-dichlorobenzene-1,2-diamine (abbreviated as $LN_4H_2^{PhCl}$, where H = dissociable protons) was synthesized according to the published procedure.[13] The $\{Co(NO)_2\}^{10}$ synthon, $[Co_2(\mu\text{-}Cl)_2(NO)_4]$, was also synthesized according to the published procedure,[64] as was $\{CoNO\}^8$ complex $[Co(LN_4^{Pr})(NO)]$ (**5**).[12] All reactions were performed under an inert atmosphere of N_2 using standard Schlenk techniques or in an MBraun Unilab glovebox under an atmosphere of purified N_2. Reactions involving NO(g) and nitroxyl transfer were performed with minimal light exposure by wrapping the reaction flasks/vials with aluminum foil to avoid any photochemical reactions.

2.6.2 Physical Methods

FTIR spectra were collected with a ThermoNicolet 6700 spectrophotometer running the OMNIC software. Solid-state samples were prepared as KBr pellets, while solution-state spectra were obtained using a demountable airtight liquid IR cell from Graseby-Specac with CaF_2 windows and 0.1 mm PTFE spacers. All FTIR samples were prepared inside a glovebox under an inert atmosphere of purified N_2. The closed liquid cell was taken out of the box and spectra were acquired immediately. X-band (9.60 GHz) EPR spectra were obtained using a Bruker ESP 300E EPR spectrometer controlled with a Bruker microwave bridge at 10 K. The EPR was equipped with a continuous-flow liquid He cryostat and a temperature controller (ESR 9) made by Oxford Instruments Inc. Electronic absorption spectra were performed at 298 or 310 K using a Cary-50 UV-vis spectrophotometer containing a Quantum Northwest TC 125 temperature control unit. The UV-vis samples were prepared anaerobically in gas-tight Teflon-lined screw cap quartz cells with an optical pathlength of 1 cm. Electrochemistry measurements were performed with a PAR Model 273A potentiostat using a non-aqueous Ag/Ag^+ (0.01 M $AgNO_3$/0.1 M $^nBu_4NPF_6$ in CH_3CN) reference electrode, Pt-wire counter electrode, and a Glassy Carbon working milli-electrode (diameter = 2 mm) under an Ar atmosphere. Measurements were performed at ambient temperature using 1.0-10.0 mM analyte in THF containing 0.1 M $^nBu_4NPF_6$ as the supporting electrolyte. Ferrocene (Fc) was used as an internal standard and all potentials are reported relative to the Fc^+/Fc couple ($E_{½}$ = 0.258 V in THF versus the prepared Ag/Ag^+ reference electrode). ^1H, ^{15}N, and ^{31}P NMR spectra were recorded in the listed deuterated solvent with a 400 MHz Bruker BZH 400/52 NMR spectrometer or a Varian Unity Inova 500 MHz NMR spectrometer at 298 K with chemical shifts internally referenced to tetramethylsilane (TMS = $Si(CH_3)_4$), CH_3NO_2, 85% H_3PO_4 (external), respectively, or the residual protio signal of the deuterated solvent as previously

reported.[65] The identification of P-containing molecules was verified by comparison to commercially-available standards or literature values. Under our conditions, the ^{31}P chemical shift of Ph_3P and $Ph_3P{=}O$ is -6.0 and 26.3 ppm, respectively ($(CD_3)_2SO$ vs. external 85% H_3PO_4). The reported ^{31}P chemical shift for $Ph_3P{=}NH$ is 35.45 ppm in $(CD_3)_2SO$,[36,66] which was confirmed by an independent synthesis of this material. However, this value is for the protonated salt $Ph_3P{=}NH{\bullet}0.5H_2SO_4$. Attempts to generate the free base $Ph_3P{=}NH$ resulted in $Ph_3P{=}O$ due to the unstable nature of the ylide. The reported ^{31}P value for $Ph_3P{=}NH$ in the solid-state is 21.8 ppm, whereas the protonated salt $Ph_3P{=}NH{\bullet}HBr$ is 34.8 ppm.[67] The former value is consistent with our value of 20.6 ppm. This value also trends with those obtained by King for in situ formation of $Ph_3P{=}NH$ in D_2O.[36] Low resolution ESI-MS data were collected on a Bruker Esquire 3000 plus ion trap mass spectrometer. High resolution ESI-MS data were collected using an Orbitrap Elite system with CID for MS-MS with precision to the third decimal place. Elemental microanalyses for C, H, and N were performed by Columbia Analytical Services (Tucson, AZ) or QTI-Intertek (Whitehouse, NJ). HPLC was conducted for separation and analysis using a Waters 2487 HPLC with a Waters 600 Controller and dual λ absorbance detector monitoring at 212 nm and 228 nm. Separations were performed on a Phenomenex Luna® reverse phase C18 (250 × 4.6 mm/10 µm) column, 10 µm particle size, 200 µL loop volume with 150 µL loop injections (flow rate: 1 mL/min), and effected by means of an isocratic $MeCN/H_2O$ (65/35) gradient for separating Ph_3P and $Ph_3P{=}O$.[68]

2.6.3 Synthesis of compounds

$[Co(LN_4^{PhCl})(NO)]$, $\{CoNO\}^8$ (1). To a 2 mL MeCN slurry of red-brown $LN_4H_2^{PhCl}$ (300.0 mg, 0.9058 mmol) was added a 2 mL MeCN slurry of NaH (48.9 mg, 2.04 mmol) resulting in a

yellow-brown solution and H_2(g) evolution. This solution was stirred at RT for 30 min during which time an occasional vacuum was introduced to remove H_2(g). After this time, a 5 mL blue slurry of $(Et_4N)_2[CoCl_4]$ (417.8 mg, 0.9058 mmol) in MeCN was added causing an instantaneous color change to deep red-brown indicative of complex formation. A small amount of light gray solid was also observed in the reaction mixture (NaCl). The reaction mixture stirred at 60 °C with a H_2O bath for 3 h that resulted in no further change. The solution was then cooled to RT, filtered, and the NaCl solid washed with 2 mL of cold MeCN. The red-brown MeCN filtrate containing $(Et_4N)_2[Co(LN_4^{PhCl})Cl_2]$ was next purged with a stream of NO(g) for 1.5 min at 60 °C. Addition of NO(g) resulted in an immediate albeit slight color change; the solution became darker brown (red-tinted) and a dark microcrystalline precipitate was immediately observed. The reaction mixture stirred at 60 °C for 30 min under an NO atmosphere in the headspace of the flask. After this time, the solution was cooled to RT and excess NO(g) was removed by pulling vacuum and refilling with N_2. The reaction mixture was then placed in a -24 °C freezer for 2 h to induce further precipitation. The resulting microcrystalline solid was filtered, washed with 3 mL of MeCN, and dried under vacuum to afford 272.7 mg (0.6522 mmol, 72%) of product. FTIR (KBr matrix), ν_{max} (cm^{-1}): 3091 (w), 1667 (s, ν_{NO}), 1568 (s), 1541 (s), 1522 (s), 1501 (s), 1453 (m), 1435 (w), 1379 (s), 1328 (w), 1291 (s), 1271 (s), 1256 (s), 1195 (m), 1118 (m), 1037 (s), 984 (m), 913 (m), 882 (w), 855 (m), 827 (w), 810 (w), 753 (s), 680 (w), 663 (w), 602 (w), 529 (w), 472 (w), 432 (w). Solution FTIR (CaF_2 windows, 0.1 mm spacers, RT, cm^{-1}): ν_{NO} = 1670 (THF), 1679 (CH_2Cl_2). UV-vis (THF, 298 K), λ_{max}, nm (ε, M^{-1} cm^{-1}): 326 (14,000), 368 (18,000), 464 (9,300), 505 (sh 7,500). ^{1}H NMR (500 MHz, THF-d_8, δ from residual protio solvent): 8.14 (s, 1H), 7.78 (d, 1H, J = 2.0), 7.56 (s, 1H), 7.06 (br m, 1H), 6.37 (br m, 1H). Anal. Calcd. for $C_{16}H_{10}Cl_2CoN_5O$: C, 45.96; H, 2.41; N, 16.75. Found: C, 45.97; H, 2.68; N, 16.11.

[Co(LN$_4$^{PhCl})(^{15}NO)], {Co^{15}NO}^{8} (1-^{15}NO). The isotopically-labeled complex **1-^{15}NO** was prepared analogously to **1** except for using 200.0 mg (0.6039 mmol) of LN$_4$H$_2$^{PhCl}, 278.6 mg (0.6040 mmol) of (Et$_4$N)$_2$[CoCl$_4$], and 32.6 mg (1.36 mmol) of NaH to generate (Et$_4$N)$_2$[Co(LN$_4$H$_2$^{PhCl})Cl$_2$] *in situ* followed by purging of ^{15}NO(g). Yield: 135.1 mg (0.3223 mmol, 53%). FTIR, ν_{NO} (cm^{-1}): 1638 (KBr matrix, $\Delta\nu_{NO}$: 29 cm^{-1}); 1641 (THF, $\Delta\nu_{NO}$: 29 cm^{-1}), 1648 (CH$_2$Cl$_2$, $\Delta\nu_{NO}$: 31 cm^{-1}). ^{15}N NMR (50.7 MHz, THF-d_8, δ from CH$_3$NO$_2$): 688.

[Co(LN$_4$^{PhCl}H$_2$)(NO)$_2$]BF$_4$, {Co(NO)$_2$}^{10} (3). To a 2 mL THF solution of black [Co$_2$(μ-Cl)$_2$(NO)$_4$] (31.7 mg, 0.103 mmol) was added a 3 mL THF solution of yellow-tinted dark brown LN$_4$^{PhCl}H$_2$ (68.0 mg, 0.205 mmol). There was no significant color change upon mixing reactants; however, light brown insolubles formed within 1 min of stirring. After 2.5 h, the solution was filtered to afford the product as a brown solid (64.0 mg, 0.132 mmol, 64%, verified by IR: ν_{NO}: 1864, 1782 cm^{-1}, KBr). To corroborate results from reactivity studies, exchange of Cl$^-$ for BF$_4^-$ was performed. To a 3 mL MeOH solution containing Et$_4$NBF$_4$ (22.3 mg, 0.103 mmol), was added a 4 mL MeOH solution of dark brown **3-Cl** (25.0 mg, 0.0515 mmol). After the initial addition a slight darkening in color occurred. After 30 min mixing at RT, red-brown insolubles were noted. The solution was stirred further for 1.5 h and the mixture was filtered to afford deep red-brown insoluble product (14.2 mg) and a brown colored filtrate. The filtrate volume was reduced to ~2 mL and then placed at -20 °C overnight. Filtering this cooled solution led to an additional 7.9 mg of insoluble product (total: 22.1 mg; 0.0412 mmol, 80%). FTIR (KBr matrix), ν_{max} (selected peaks, cm^{-1}): 3328 (m, ν_{NH}), 1859 (s, ν_{NO}), 1793 (vs, ν_{NO}), 1052 (vs, ν_{BF}). ^{1}H NMR (400 MHz, CD$_3$OD, δ from residual protio solvent): 9.28 (s, 1H), 8.07 (s, 1H), 7.54 (s, 1H), 7.27 (s, 1H), 6.62 (s, 1H). HRMS-ESI (*m/z*): [M]$^+$ calcd for C$_{16}$H$_{12}$Cl$_2$CoN$_6$O$_2$ (relative abundance), 448.973 (100.0),

450.970 (63.9), 449.976 (17.3), 451.973 (11.1), 452.967 (10.2); found, 448.973 (100.0), 450.970 (64.1), 449.976 (16.8), 451.973 (10.9), 452.967 (9.8).

(Et_4N)[$Co(SPh\text{-}p\text{-}Cl)_2(NO)_2$], $\{Co(NO)_2\}^{10}$ (6^{Et4N}). To a 3 mL THF solution of black [$Co_2(\mu\text{-}Cl)_2(NO)_4$] (30.0 mg, 0.0972 mmol) was added a mostly clear 6 mL THF solution of (Et_4N)(SPh-*p*-Cl) (106.4 mg, 0.3886 mmol). The solution remained dark brown and the white insolubles were no longer apparent. After 1 min stirring, light colored insolubles began to form. After 2 h, the solution was filtered to afford a light blue powder (Et_4NCl, 38.4 mg, 0.232 mmol) and a dark brown filtrate. The filtrate was concentrated to dryness to afford a dark brown oily solid. The oily solid was redissolved in 2 mL of THF and was treated with 6 mL of pentane, then placed at -25 °C overnight. Following this period, the solution was decanted, yielding the product as a sticky solid (68.0 mg, 0.160 mmol, 86%). FTIR (KBr matrix, cm^{-1}): 2982 (w), 1891 (vw), 1774 (s, ν_{NO}), 1709 (s, ν_{NO}), 1586 (w), 1565 (m), 1481 (m), 1466 (vs), 1392 (m), 1303 (w), 1286 (w), 1249 (w), 1182 (m), 1171 (m), 1089 (vs), 1067 (m), 1031 (w) 1007 (s), 936 (w), 815 (vs), 785 (m), 696 (w), 669 (w), 629 (w), 542 (vs), 488 (s). ^1H NMR (400 MHz, CD_3OD, δ from residual protio solvent): 7.30 (d, 1H, J = 8.0 Hz), 6.98 (d, 1H, J = 8.0 Hz), 3.25 (q, 2H, J = 6.7 Hz), 1.24 (t, 3H, J = 6.0 Hz). ^1H NMR (400 MHz, CD_2Cl_2, δ from residual protio solvent): 7.30 (d, 1H, J = 8.0 Hz), 7.22 (s, 0.08H, unidentified), 6.97 (d, 1H, J = 8.0 Hz), 3.17 (d, 2H, J = 4.0 Hz), 1.26 (s, 3H). HRMS-ESI (*m/z*): $[M]^-$ calcd for $C_{12}H_8Cl_2CoN_2O_2S_2$ (relative abundance), 404.874 (100.0), 405.877 (13.0), 406.870 (64.8), 407.874 (8.3), 408.868 (10.2), 409.871 (1.4); found, 404.871 (100.0), 405.874 (9.3), 406.868 (71.9), 407.871 (6.6), 408.865 (11.9), 409.868 (1.3).

[Co(LN$_4^{Pr}$H$_2$)(NO)$_2$]Cl, {Co(NO)$_2$}^{10} (7). To a 2 mL Et_2O solution of black [$Co_2(\mu$-$Cl)_2(NO)_4$] (30.0 mg, 0.0972 mmol) was added a 6 mL Et_2O slurry of LN$_4^{pr}$H$_2$ (44.7 mg, 0.196 mmol). There was an immediate lightening of color with formation of brown insolubles. After 2 h, the solution was filtered to afford a light brown solid (35.0 mg, Et_4NCl) and a dark brown filtrate, which upon stripping to dryness yielded the product as a dark brown sticky solid (30.1 mg, 0.0787 mmol, 40%). FTIR (KBr matrix, cm^{-1}): 3090 (w, ν_{NH}), 2917 (w), 2849 (w), 1839 (vs, ν_{NO}), 1755 (vs, ν_{NO}), 1660 (m), 1582 (vs), 1442 (m), 1391 (m), 1367 (w), 1337 (w), 1313 (m), 1194 (w), 1117 (w), 1035 (s), 896 (w), 739 (m), 678 (w), 669 (m), 650 (w), 608 (w). ^{1}H NMR (400 MHz, CD_3OD, δ from residual protio solvent): 8.07 (s, 1H), 7.06 (s, 1H), 6.81 (s, 1H, *J* = 4.0 Hz), 6.27 (br m, 1H), 3.65 (t, 2H, *J* = 8.0 Hz), 1.85 (m, 1H, *J* = 8.0 Hz). ^{1}H NMR (400 MHz, CD_2Cl_2, δ from residual protio solvent): 7.91 (s, 1H), 7.63 (s, 0.5H), 7.30 (s, 0.5H), 7.10 (s, 1H), 6.84 (d, 1H, *J* = 4.0 Hz), 6.31 (d, 1H, *J* = 4.0 Hz), 6.26 (s, 1H, unidentified), 3.61 (t, 2H, *J* = 8.0 Hz), 1.84 (m, 1H, *J* = 8.0 Hz). HRMS-ESI (*m/z*): $[M]^+$ calcd for $C_{13}H_{16}CoN_6O_2$ (relative abundance), 347.067 (100.0), 348.064 (2.2), 348.070 (14.1), 349.073 (0.3); found, 347.065 (100.0), 348.063 (1.7), 348.069 (13.1), 349.072 (0.6).

2.6.4 Reactivity Studies

Reaction of 1 with HBF_4•Et_2O. To a red-tinted dark brown THF solution (1.5 mL) of **1** (15.0 mg, 0.0359 mmol) was added 6.35 μL (0.0463 mmol) of HBF_4•Et_2O in 1 mL of THF. The resulting solution remained homogeneous and dark brown but became yellow-tinted over time. The reaction mixture stirred at RT for 24 h. FTIR (KBr) was used to monitor the reaction, and a spectrum was obtained at t = 0.5, 2.5, 3.5, and 24 h (see Figures 2.S8 and 2.S9 for spectrum at 0.5 and 24 h, respectively; 2.5 and 3.5 h did not show any significant differences from the 0.5 h spectrum). After

24 h, the products were dried *in vacuo*, leaving a dark brown sticky residue. The products from this reaction were characterized by UV-vis and ESI-MS. An analogous smaller scale reaction (complex **1**: 6.0 mg, 0.014 mmol; HBF_4: 2.53 μL, 0.0186 mmol) was monitored *in situ* by ^{1}H NMR spectroscopy (298 K, 400 MHz) at t = 0.17, 1, 3, 5, 24, 48, 72, and 96 h (see Figures 2.S10-2.S12 for 0.17, 1, and 24 h).

Reaction of 1-^{15}NO with HBF_4•Et_2O. The reaction with the isotopically-labeled complex **1-^{15}NO** was performed analogously to **1** except for using **1-^{15}NO** (10.0 mg, 0.0239 mmol) and 4.23 μL (0.0308 mmol) of HBF_4•Et_2O; total THF reaction volume was 2 mL. The reaction was monitored by FTIR (KBr) at t = 0.5, 2.5, 3.5, and 24 h and by NMR at t = 0.17, 1, 3, 5, 24, 48, 72, and 96 h.

UV-vis monitor of the reaction of 1 with [Fe(TPP)Cl]. A 1 mM stock solution of [Fe(TPP)Cl] was prepared in THF. After a THF blank was recorded at 298 K, a 0.025 mL aliquot of the [Fe(TPP)Cl] stock solution was added to 3.000 mL of THF in a quartz cuvette, and the UV-vis spectrum was recorded, which matched the literature value.[69] No changes occurred in the UV-vis spectrum over 30 min. To this cuvette was then added a 0.025 mL aliquot of a 1 mM THF stock solution of the $\{CoNO\}^8$ (**1**), yielding a 1:1 stoichiometric ratio of [Fe(TPP)Cl]:**1** to initiate the reaction. The UV-vis was monitored for 24 h (intervals used: 2 min cycles in the first 2 h; 30 min cycles for the next 24 h, see Figure 2.S6 for 24 h trace – no changes after this time).

UV-vis monitor of the reaction of 1 with [Fe(TPP)Cl] in the presence of HBF_4•Et_2O. The above conditions were replicated and no reaction was noted within 24 h at T = 298 or 310 K.

A 1 mM stock solution of HBF_4•Et_2O in THF was prepared, and a 0.025 mL aliquot of this solution was added to the cuvette (1:1:1 stoichiometric ratio of **1**/ [Fe(TPP)Cl]/HBF_4•Et_2O). The UV-vis spectrum was monitored for 22 h (intervals used: 1 min cycles for the first 30 min; 2 min cycles for the next 1 h; 30 min cycles for t = 1.5 h – 22 h).

Bulk reaction of 1 with [Fe(TPP)Cl]. A solution of [Fe(TPP)Cl] (33.7 mg, 0.0479 mmol) was prepared in 1 mL of THF. To this solution was added a 3 mL THF solution containing **1** (20.0 mg, 0.0478 mmol) and the reaction was stirred under dark conditions at RT for 24 h. After this time an IR was taken, which revealed ***no reaction*** as evidenced by the strong ν_{NO} band of **1**. Then, a 0.5 mL THF solution containing HBF_4•Et_2O (6.51 μL, 0.0474 mmol) was added to the reaction mixture. This solution was allowed to mix at RT for 24 h, which indicated the presence of [Fe(TPP)NO] by FTIR (KBr matrix, ν_{NO} = 1698 cm^{-1}; disappearance of the ν_{NO} of **1** at 1667 cm^{-1}) and EPR spectroscopy (see Figure 2.S7). A similar spectrum was observed at t = 48 h. After this point, the THF was removed *in vacuo* to afford a dark brown purple residue. This residue was stirred in 3 mL of MeOH for 1 h and was then filtered to yield a deep purple solid identified to be [Fe(TPP)NO] (29.4 mg, 0.0421 mmol, 88%). The same result was obtained using **1-^{15}NO** (15.0 mg, 0.0358 mmol), [Fe(TPP)Cl] (25.2 mg, 0.0358 mmol), and HBF_4•Et_2O (4.87 μL, 0.0358 mmol) affording 22.5 mg of [Fe(TPP)^{15}NO] (0.0322 mmol, 90% yield) as confirmed by FTIR (KBr matrix, ν_{NO}: 1667 cm^{-1}, $\Delta\nu_{NO}$: 31 cm^{-1}) and EPR spectroscopy (see Figure 2.S7).

Bulk reaction of 1 with Ph_3P. This method was adapted based on a published procedure for O-atom transfer from Fe-coordinated nitrite to Ph_3P.[36-37] To a 2.000 mL THF:H_2O (10:1) solution of **1** (15.0 mg, 0.0359 mmol) was added a solution of Ph_3P (18.8 mg, 0.0717 mmol) in

1.500 mL THF:H_2O (10:1), and the reaction stirred at RT for 24 h under anaerobic conditions. After this time, the solution remained red-tinted dark brown with little to no insolubles noted. The reaction mixture was monitored by HPLC at t = 1 h, 3 h, 5 h, and 24 h, and a ^{31}P NMR spectrum was obtained at t = 24 h. Analysis indicated trace $Ph_3P{=}O$ (small peak at retention time (t_r): 4.7 min) in the HPLC chromatogram (Figure 2.S19). No P-containing peaks were observed in the ^{31}P NMR spectrum. At t = 24 h, a 0.500 mL THF:H_2O (10:1) solution containing $HBF_4{\bullet}Et_2O$ (6.35 μL, 0.0466 mmol) was added to the reaction mixture. After 1 h, the solution was yellow-tinted deep brown in color and by 24 h, the solution had lightened in color to a yellow-tinted transparent brown homogeneous solution. The reaction mixture was monitored by HPLC at t = 1 h, 3 h, 5 h, and 24 h after addition. At 24 h, the solvent was removed in vacuo, leaving a yellow-tinted brown residue. This residue was treated with Et_2O for 30 min (4 × 5 mL) and then filtered, yielding a yellow filtrate (17.2 mg after Et_2O removal) and a brown sticky solid (17.8 mg). A ^{31}P NMR spectrum was obtained for both the Et_2O soluble (unreacted Ph_3P) and Et_2O insoluble (unreacted Ph_3P, $Ph_3P{=}NH$, $Ph_3P{=}O$) fractions. Based on HPLC, a 20% yield of $Ph_3P{=}O$ (LRMS-ESI, $\{Ph_3P{=}O + H^+\}^+$, *m/z* 279.1; calcd: 279.1) was noted. Utilizing 10 equiv of PPh_3 afforded a 27% yield of PPh_3O. The modest yield of $Ph_3P{=}O$ may be due to coordination to Co. To quantify total $Ph_3P{=}O$, the reaction was performed in the same manner with the same quantities as stated above with the exception of adding excess $HBF_4{\bullet}Et_2O$ to remove any potential bound phosphine oxide. After 24 h mixing, a 500 μL THF:H_2O (10:1) solution containing $HBF_4{\bullet}Et_2O$ (122.0 μL, 0.8969 mmol, 25 equiv with respect to **1**) was added to the $\{CoNO\}^8$/2 Ph_3P/H^+ reaction mixture. This led to an immediate color change to deep yellow with no noted insolubles. No further changes occurred after stirring at RT for 2 h. This mixture was then analyzed by HPLC, which revealed a 33% yield of $Ph_3P{=}O$. Identical conditions were used for the acid digest of $\{CoNO\}^8$/10 PPh_3/H^+

except for using a 500 μL THF:H_2O (10:1) solution of HBF_4•Et_2O (488.5 μL, 3.590 mmol, 100 equiv with respect to **1**); yield = 37%.

Bulk Reaction of 1 with O_2(g). A solution of **1** (15.0 mg, 0.0359 mmol) was prepared in 3 mL of MeCN:THF (1:1) and then purged with a stream of O_2(g) for 1.5 min at RT. Addition of O_2(g) resulted in an immediate albeit slight color change; the solution became darker brown (red-tinted) and no insolubles were noted. The reaction was stirred at RT under O_2(g) atmosphere and aliquots of the reaction mixture were taken at 24 h and 72 h. The FTIR spectrum of each aliquot indicated disappearance of the ν_{NO} of **1** after 24 h. The reaction mixture was dried *in vacuo*, yielding a red-brown solid (total recovered: 15.4 mg) that was a mixture of [Co(LN_4^{PhCl})(MeCN)(η^1-ONO_2)] (**2**) and [Co(LN_4^{PhCl})(MeCN)(NO_2)]. Formation of **2** and the Co-nitrito complex upon oxidation of {CoNO}^{8} complex **1** is not an unprecedented phenomenon.[14,70] Product **2** was obtained in 63% yield based on NMR integration. IR stretching frequencies have been assigned based on known ranges reported for typical Co-η^1-ONO_2 and Co-NO_2 complexes.[71] FTIR of peaks assigned to complex **2** (KBr matrix), ν_{max} (cm^{-1}): 2302 (w, $\nu_{C\equiv N}$), 1509 (m, ν_{NO}), 1489 (m, ν_{NO}), 1270 (s, ν_{NO}), 1046 (s, ν_{NO}). ^{1}H NMR of peaks assigned to **2** (400 MHz, CD_3CN, δ from residual protio solvent: 8.26 (s, 1H), 8.01 (s, 1H), 7.77 (s, 1H), 7.17 (d, 1H), 6.51 (d, 1H).

Reaction of {CoNO}^{8} [Co(LN_4^{pr})(NO)] (5) with *p*-Cl-PhSH. To a dark brown MeCN solution (6 mL) of {CoNO}^{8} **5** (29.0 mg, 0.0920 mmol) was added a clear MeCN solution of *p*-Cl-PhSH (13.3 mg, 0.0920 mmol). The resulting solution remained dark brown and few insolubles were noted. The reaction mixture stirred at RT for 24 h, and more insolubles gradually formed over that time. After 24 h, the products were dried *in vacuo*, leaving a dark brown sticky residue.

Attempts to separate species remaining after 24 h were unsuccessful due to similar solubilities. Based on ^{1}H NMR integration using DMSO as an internal standard, disulfide (*p*-Cl-PhSSPh-*p*-Cl) and $[Co(SPh\text{-}p\text{-}Cl)_2(NO)_2]^-$ (anion of **6**) were obtained in 8% and 17% yields respectively, and 31% of $\{CoNO\}^8$ **5** and 45% of RSH remained in the mixture. The products from this reaction were characterized by FTIR (KBr), ESI-MS, and ^{1}H NMR spectroscopy (CD_2Cl_2). An analogous reaction was performed in THF and similarly characterized. Any spectroscopic change in the products formed was negligible, and the quantification of the products (*p*-Cl-PhSSPh-*p*-Cl (5%), $[Co(SPh\text{-}p\text{-}Cl)_2(NO)_2]^-$ (anion of **6**) (8%), unreacted $\{CoNO\}^8$ **5** (46%) and *p*-Cl-PhSH (41%)) was consistent with both reaction conditions, highlighting that the equilibrium favors the reactants in either solvent.

2.7 Supporting Information

*X-ray Crystallographic Data Collection and Structure Solution and Refinement***.**

Dark brown crystals of $[Co(LN_4^{PhCl})(NO)]$ (**1**) were grown under anaerobic conditions by slow diffusion of Et_2O into a 2-MeTHF solution of **1** at -20 °C. Red crystals of $[Co(LN_4^{PhCl})(\eta^1\text{-}ONO_2)]$ (**2**) were grown under pseudo-anaerobic conditions by slow diffusion of Et_2O into a THF:MeCN (1:1) solution of **1** at 8 °C, resulting in single crystals of nitrato complex **2** due to oxidation of the NO ligand in **1**. Suitable crystals were mounted on a glass fiber. The X-ray intensity data were measured at 100 K on a Bruker SMART APEX II X-ray diffractometer system with graphite-monochromated Mo Kα radiation (λ= 0.71073 Å) using ω-scan technique controlled by the SMART software package.[72] The data were collected in 1464 frames with 10 second exposure times. The data were corrected for Lorentz and polarization effects[73] and integrated with the manufacturer's SAINT software. Absorption corrections were applied with the program

SADABS.[74] Subsequent solution and refinement was performed using the SHELXTL 6.1 solution package operating on a Pentium computer.[75-76] The structure was solved by direct methods using the SHELXTL 6.1 software package.[77] Non-hydrogen atomic scattering factors were taken from the literature tabulations.[78] Selected data and metric parameters for complexes **1** and **2** are summarized in Table 2.S1. Selected bond distances and angles for **1** and **2** are given in Table 2.S2. Perspective views of the complexes were obtained using ORTEP.[79] The asymmetric unit of **1** contains one half of a discrete THF molecule, which was disordered residing on an inversion center with half occupancies of each atom.

Table 2.S1. Summary of crystal data and intensity collection and structure refinement parameters for [Co(LN_4^{PhCl})(NO)]•0.5THF (**1**•0.5THF) and [Co(LN_4^{PhCl})(MeCN)(η^1-ONO_2)] (**2**).

Parameters	**1**•0.5 THF	**2**
Formula	$C_{18}H_{14}Cl_2CoN_5O_{1.5}$	$C_{18}H_{13}Cl_2CoN_6O_3$
Formula weight	454.17	491.17
Crystal system	Triclinic	Orthorhombic
Space group	*P*-1	$P2_12_12_1$
Crystal color, habit	Dark brown	Red
a, Å	7.8436(9)	11.086(8)
b, Å	9.7124(11)	12.066(8)
c, Å	12.4551(13)	14.350(10)
α, deg	85.689(2)	90
β, deg	77.5370(10)	90
γ, deg	83.590(2)	90
V, Å^3	919.40(18)	1919(2)
Z	1	4
$\rho_{calcd,}$ g/cm^3	1.641	1.700
T, K	100(2)	100(2)
abs coeff, μ (Mo Kα), mm^{-1}	1.246	1.208
θ limits, deg	2.11-27.00	2.21-25.05
total no. of data	11541	18909
no. of unique data	3999	3405
no. of parameters	271	272
GOF of F^2	1.052	1.016
R_1,[a] %	4.94	7.53
wR_2,[b] %	13.18	11.95
max, min peaks, e/Å^3	1.108, -0.683	0.375, -0.465

[a]$R_1 = \Sigma| |F_O| - |F_c| | / \Sigma |F_O|$; [b]$wR_2 = \{\Sigma[w(F_o^2 - F_c^2)^2]/\Sigma[w(F_o^2)^2]\}^{1/2}$

Table 2.S2. Selected bond distances (Å) and bond angles (deg) for [Co(LN_4^{PhCl})(NO)]•0.5THF (**1**•0.5THF) and [Co(LN_4^{PhCl})(MeCN)(η^1-ONO_2)] (**2**).

1•0.5THF		**2**	
Co1-N1	1.927(3)	Co1-N1	1.936(7)
Co1-N2	1.897(3)	Co1-N2	1.901(7)
Co1-N3	1.892(3)	Co1-N3	1.884(7)
Co1-N4	1.911(3)	Co1-N4	1.915(7)
Co1-N5	1.798(3)	Co1-N5	1.907(8)
N5-O1	1.172(4)	Co1-O1	1.904(6)
		N6-O1	1.227(9)
		N6-O2	1.237(10)
		N6-O3	1.239(9)
O1-N5-Co1	124.4(3)	N1-Co1-N2	83.0(3)
N1-Co1-N2	83.06(12)	N1-Co1-N3	166.5(3)
N1-Co1-N3	162.15(13)	N1-Co1-N4	109.5(3)
N1-Co1-N4	106.63(13)	N1-Co1-N5	90.1(3)
N1-Co1-N5	96.97(13)	N1-Co1-O1	93.0(3)
N2-Co1-N3	82.74(12)	N2-Co1-N3	83.6(3)
N2-Co1-N4	157.59(13)	N2-Co1-N4	167.3(3)
N2-Co1-N5	101.93(13)	N2-Co1-N5	90.9(3)
N3-Co1-N4	83.25(13)	N2-Co1-O1	86.9(3)
N3-Co1-N5	96.50(13)	N3-Co1-N4	84.0(3)
N4-Co1-N5	96.97(13)	N3-Co1-N5	91.4(3)
		N4-Co1-N5	87.0(3)
		O1-Co1-N3	85.0(3)
		O1-Co1-N4	94.4(3)
		O1-Co1-N5	175.9(3)
		O1-N6-O2	124.3(8)
		O1-N6-O3	118.6(9)
		O2-N6-O3	117.0(10)

X-Ray Absorption Spectroscopy (XAS): Solid $\{CoNO\}^8$ **1** was prepared anaerobically at a 3:1 stoichiometric dilution with boron nitride, loaded into transmission cells wrapped with kapton tape and immediately frozen in liquid nitrogen. Two independent duplicates were prepared to ensure spectral reproducibility. XAS data were collected at the Stanford Synchrotron Radiation Light Source (SSRL), on beamline 7-3, and the National Synchrotron Light Source (NSLS), on beamline X3-A. Beamline 7-3 was equipped with a Si[220] double crystal monochromator and beamline X3-A was equipped with a Si[111] monochromator; both beamlines were equipped with harmonic rejection mirrors. During data collection, the sample at SSRL was maintained at 10 K using an Oxford Instruments continuous-flow liquid helium cryostat and the sample at NSLS was maintained at 24 K using a helium Displex cryostat. Transmission spectra, collected with a simultaneous Co foil spectrum for monochromator calibration, were measured at both locations using nitrogen gas ionization chamber detectors placed in series. The first inflection point of the Co foil spectrum was assigned to 7709.5 eV. At both facilities, XAS spectra were collected in 5 eV increments in the pre-edge region (7542-7702 eV), 0.25 eV increments in the edge region (7702-7780 eV) and 0.05 $Å^{-1}$ increments in the extended X-ray absorption fine structure (EXAFS) region. Data were collected to k = 14.0 $Å^{-1}$ and integrated from 1 to 25 seconds in a k^3-weighted manner for a total scan length of approximately 40 minutes. Spectra displayed in Figure 2.2 represent the average of two independent spectra.

XAS data were processed using the Macintosh OS X version of the EXAFSPAK program suite integrated with Feff v7.2 for theoretical model generation.[80] Data reduction utilized a polynomial function in the pre-edge region and a four point cubic spline throughout the EXAFS region for background signal removal. Data were converted to k space using a Cobalt E_0 value of 7725 eV. Normalized XANES data were subjected to pre-edge analysis. Edge inflection energies

were calculated as the maximum of the first derivative of the XANES spectra. Only spectra collected using the higher resolution Si[220] monochromator crystals were subjected to edge analysis. Pre- and post-edge splines were fit to the experimental spectra within the energy ranges of 7707-7718 eV. The extrapolated line was then subtracted from raw data to yield baseline corrected spectra. Pre-edge features were modeled using pseudo-Voigt line shapes (simple sums of Lorentzian & Gaussian functions) and the energy position measured at the peak height; the full width at half-maximum (fwhm) and the peak heights for each transition were varied. A fixed 50:50 ratio of Lorentzian to Gaussian function successfully reproduced the spectral features of the pre-edge transitions.[81] Peak transition areas were determined for all spectra over the energy range of 7707-7718 eV using the program Kaleidagraph.[82] Normalized areas are represented in units of 10^{-2} eV.[83]

EXAFS data were fit using single scattering theoretical model amplitudes and phase functions. The k^3- weighted EXAFS was truncated between 1.0 and 13 $Å^{-1}$ for filtering purposes and Fourier transformed for display. This *k* range corresponds to a spectral resolution of 0.13 Å for all Co-ligand interactions; therefore, only independent scattering environments at distances > 0.13 Å were considered resolvable in the EXAFS fitting analysis. A scale factor (Sc) of 0.98 and a threshold shift (ΔE_0) value of -11.3, calibrated by fitting crystallographically characterized cobalt complexes, were used in simulating the complex **1** sample. During the simulations, only the bond length and Debye-Waller disorder factor were allowed to vary, Sc and E_0 were held constant and the coordination number for the fit manually varied in 0.5 value increments. Criteria for judging the best-fit simulation utilized both the lowest mean-square deviation between data and fit (F′), corrected for the number of degrees of freedom, and a reasonable Debye-Waller factor ($\sigma^2 < 0.006$

Å^2).[84] The final fitting results listed in Table 2.S3 are from averaged values obtained from simulations of raw unfiltered data.

Table 2.S3. Summary of best-fit simulations to Co EXAFS.[a]

Data	Nearest Neighbor Ligand Environment[b]				Long Range Ligand Environment[b]								
	Atom[c]	**R(Å)**[d]	**CN**[e]	**σ^2** [f]	**Atom**[c]	**R(Å)**[d]	**CN**[e]	**σ^2** [f]	**Atom**[c]	**R(Å)**[d]	**CN**[e]	**σ^2** [f]	***F'***[g]
Complex **1**	N	1.88	4.5	4.64	C	2.76	4.5	1.90	C	3.92	4.5	3.16	1.12

[a] Data were fit over a *k* range of 1 to 13.0 Å^{-1}.

[b] Independent metal-ligand scattering environment.

[c] Scattering atoms: N (nitrogen) C (carbon).

[d] Average metal-ligand bond length from two transmission scans.

[e] Average metal-ligand coordination number from two transmission scans.

[f] Average Debye-Waller factor in Å^2 x 10^3 from two transmission scans.

[g] Number of degrees of freedom weighted mean square deviation between data and fit.

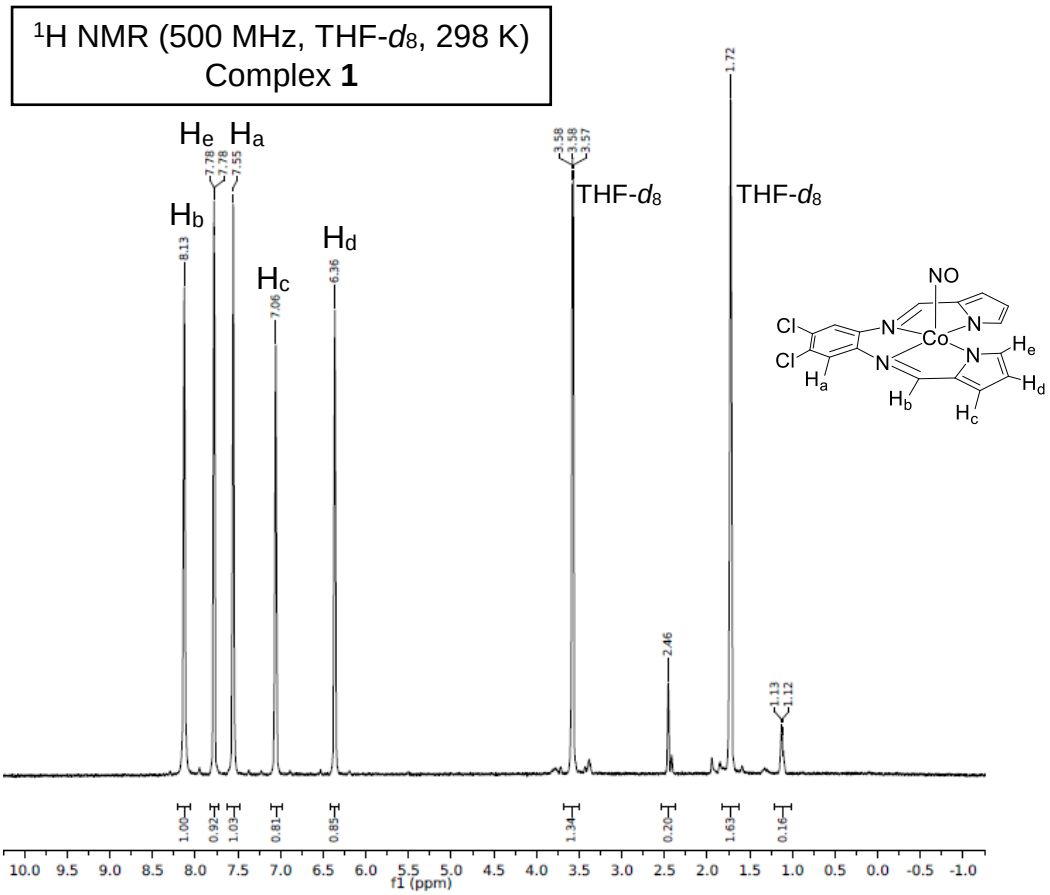

Figure 2.S1. ^{1}H NMR spectrum of [Co(LN$_4^{PhCl}$)(NO)] (**1**) in THF-d_8 at 298 K. The peaks at 3.58 and 1.72 ppm are from residual protio solvent. The peak at 2.46 ppm is from trace H_2O.

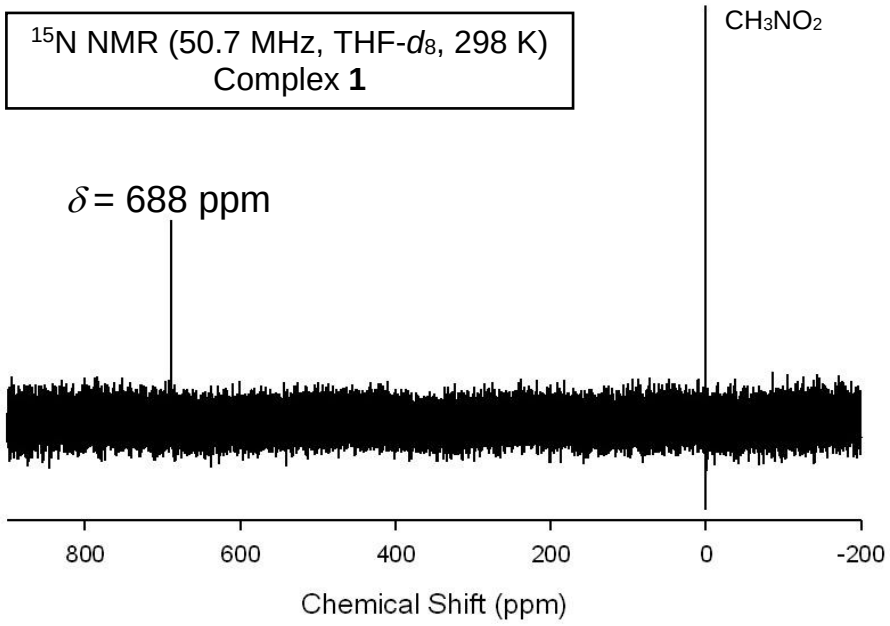

Figure 2.S2. ^{15}N NMR spectrum of [Co(LN_4^{PhCl})(^{15}NO)] (**1-^{15}NO**) in THF-d_8 at 298 K (vs. CH_3NO_2).

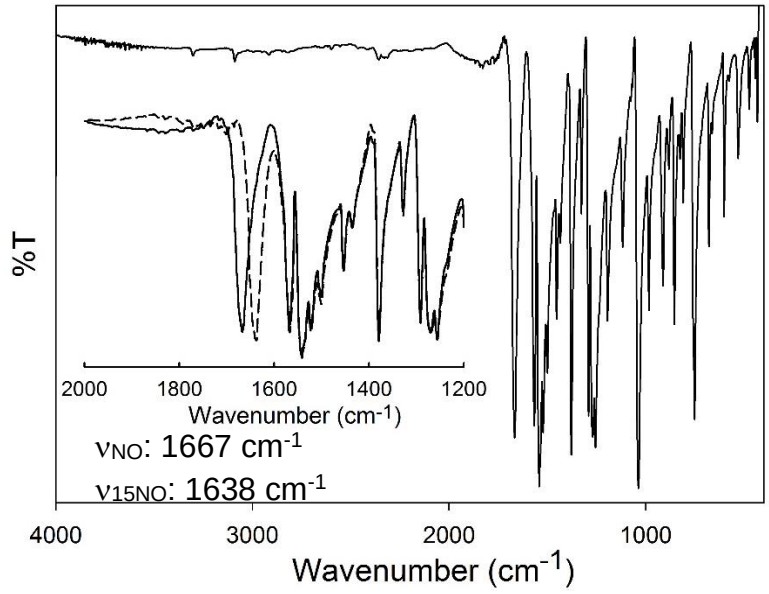

Figure 2.S3. FTIR spectra of [Co(LN_4^{PhCl})(NO)] (**1**) (solid line) and [Co(LN_4^{PhCl})(^{15}NO)] (**1-^{15}NO**) (dashed line; inset) in a KBr matrix.

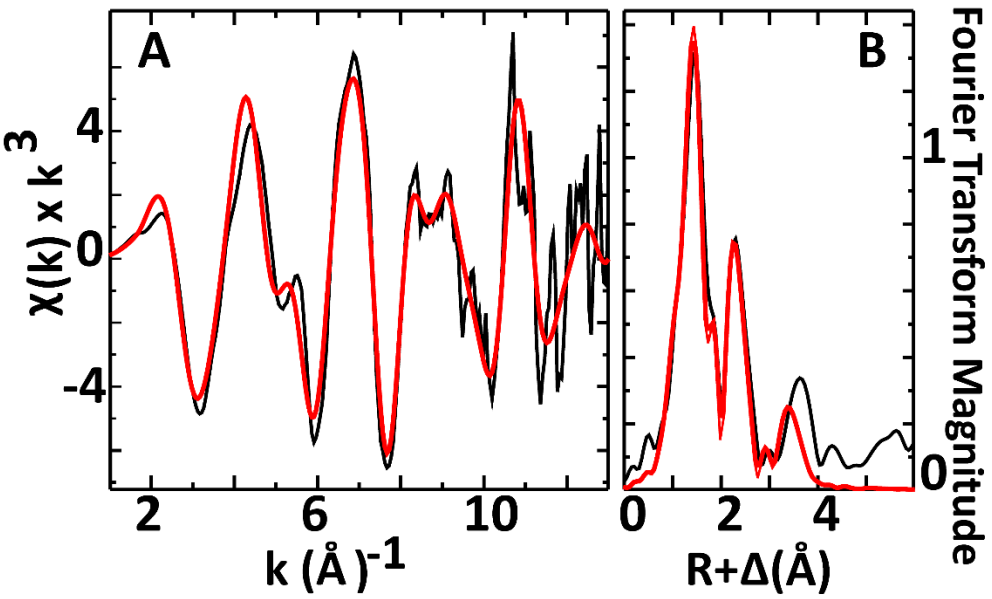

Figure 2.S4. EXAFS and Fourier transforms of EXAFS data for $\{CoNO\}^8$ **1**. (A): Raw EXAFS data displayed in black and best fits in red. (B): Corresponding Fourier transform plot of raw EXAFS data.

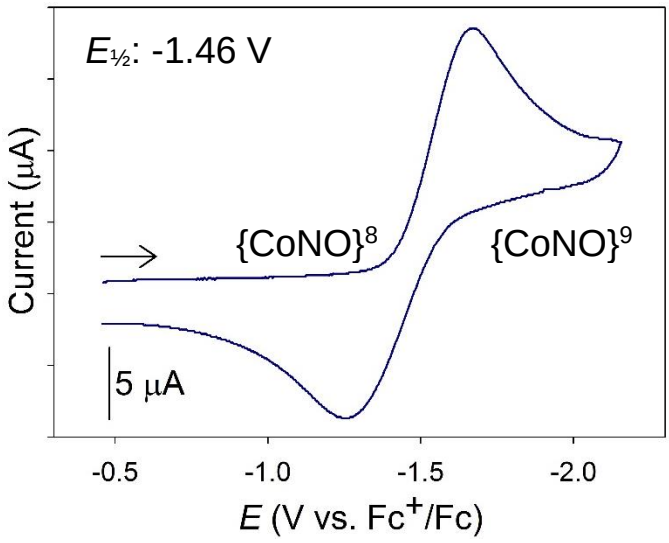

Figure 2.S5. Cyclic voltammogram of **1** (3 mM) in THF with 0.1 M ^{n}BuN$_4$PF$_6$ as supporting electrolyte. GC working electrode; scan rate: 100 mV•s^{-1}. Arrow shows direction of scan.

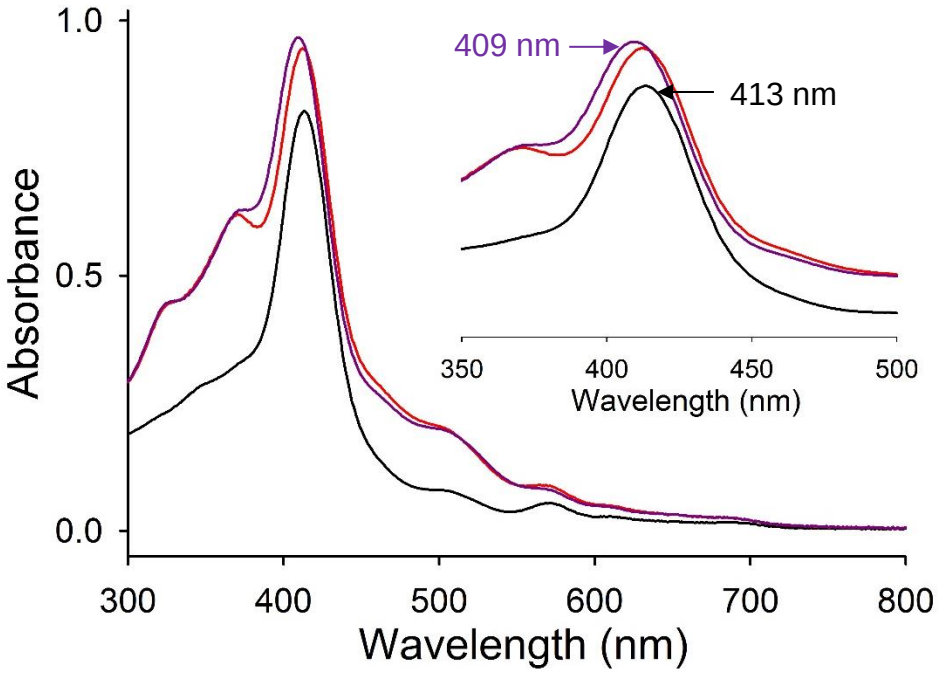

Figure 2.S6. UV-vis spectrum of 8.2 μM [Fe(TPP)Cl] (black), [Fe(TPP)Cl] + complex **1** (1:1) after 24 h mixing (red), and [Fe(TPP)Cl] + complex **1** + HBF_4•Et_2O (1:1:1) after 4 min mixing (violet). No significant changes after this time. Reaction performed in THF at 298 K. *Inset*: expansion of the Soret band of the reaction mixture (same coloring as in full spectrum). λ_{max} for black and red traces: 413 nm; λ_{max} for violet trace: 409 nm.

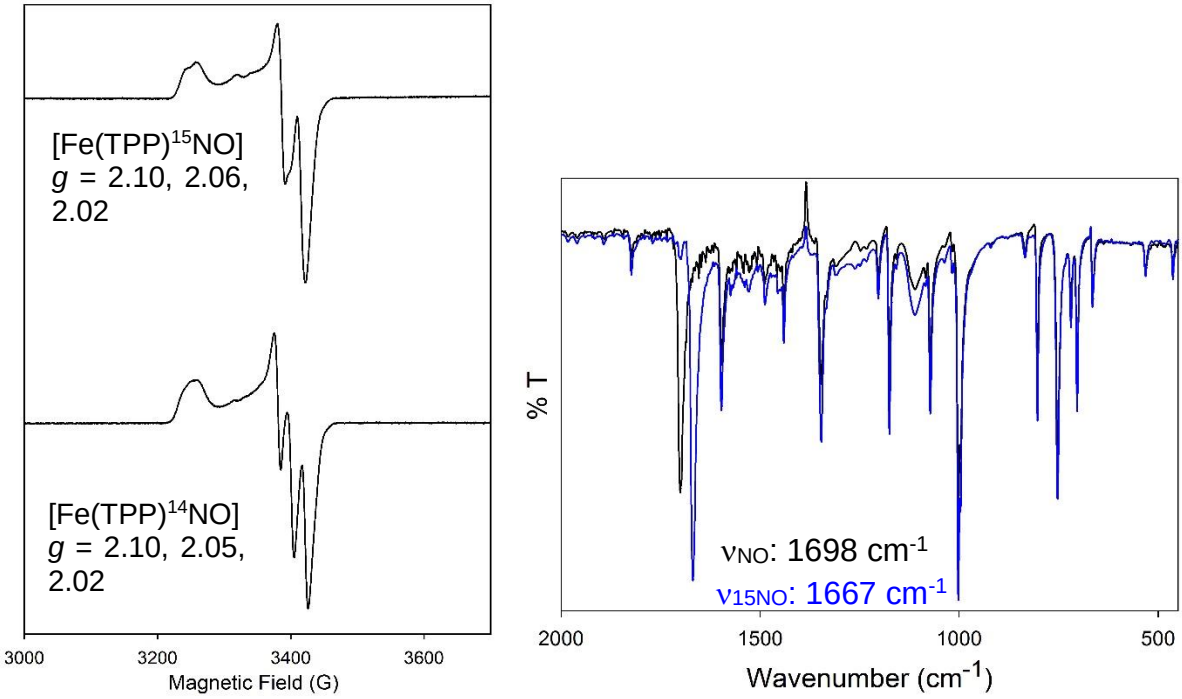

Figure 2.S7. *Left*: X-band EPR spectrum of the reaction of **1** (bottom) or **1-^{15}NO** (top) with [Fe(TPP)Cl] showing formation of the corresponding $\{FeNO\}^7$ complex [Fe(TPP)(NO)] (g_1 = 2.10, a_1(^{14}N) = 12 G; g_2 = 2.05, a_2(^{14}N) = 17 G; g_3 = 2.02, a_3(^{14}N) = 17 G) and $\{Fe^{15}NO\}^7$ complex [Fe(TPP)(^{15}NO)], respectively. *Right*: Solid-state (KBr) FTIR spectrum of the ν_{NO} region of the same reaction mixture using **1** (black) or **1-^{15}NO** (blue).

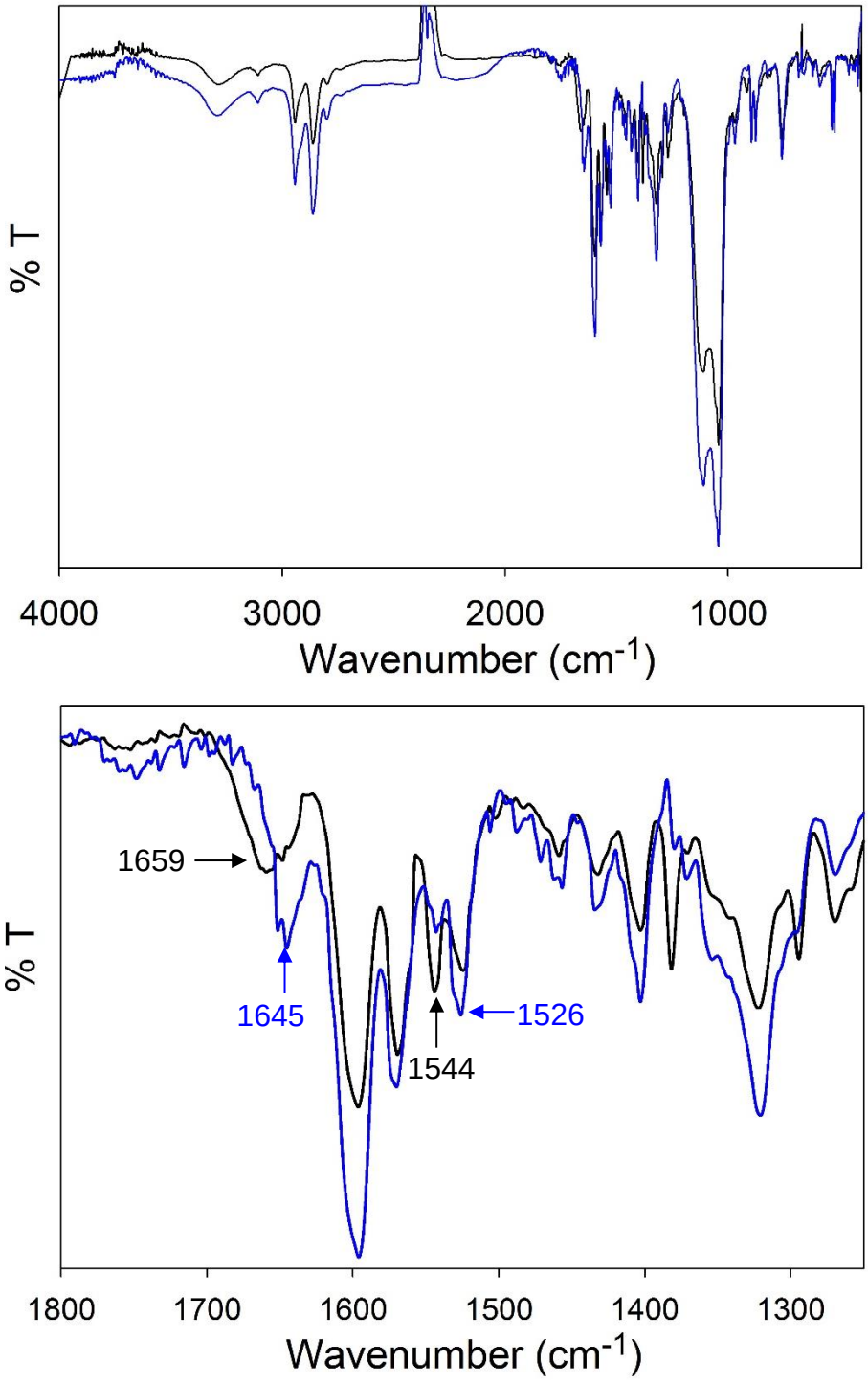

Figure 2.S8. Solid-state FTIR spectrum of **1** + HBF_4•Et_2O (1:1.3) (black trace) and **1-^{15}NO** + HBF_4•Et_2O (1:1.3) (blue trace) after 0.5 h. *Top*: Full spectrum. *Bottom*: Expansion of ν_{NO} region. Sample measured as a KBr pellet at RT. Isotope-sensitive ν_{NO} peaks are labeled in cm^{-1}.

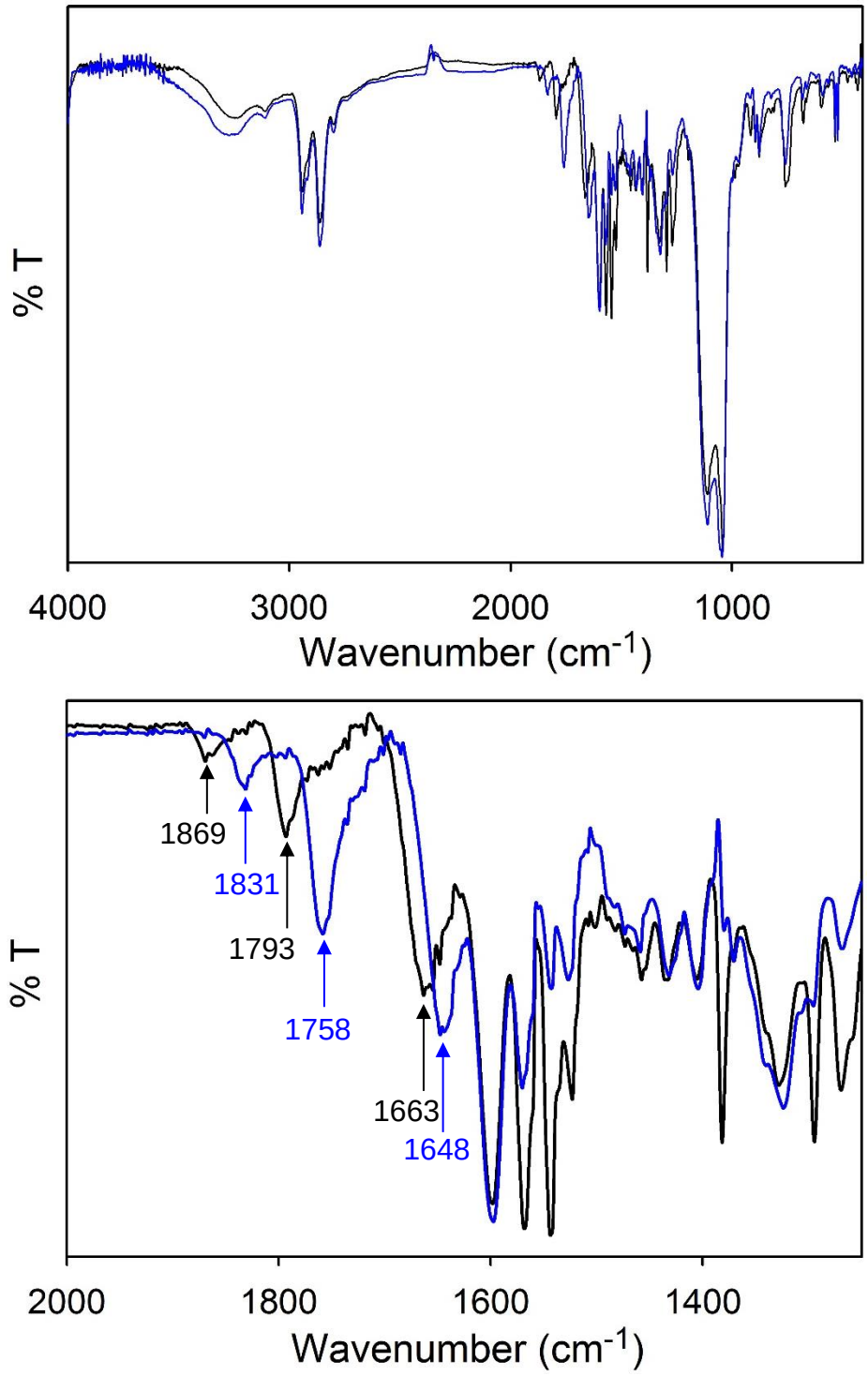

Figure 2.S9. Solid-state FTIR spectrum of **1** + HBF_4•Et_2O (1:1.3) (black trace) and **1-^{15}NO** + HBF_4•Et_2O (1:1.3) (blue trace) after 24 h. *Top*: Full spectrum. *Bottom*: Expansion of ν_{NO} region. Sample measured as a KBr pellet at RT. Isotope-sensitive ν_{NO} peaks are labeled in cm^{-1}.

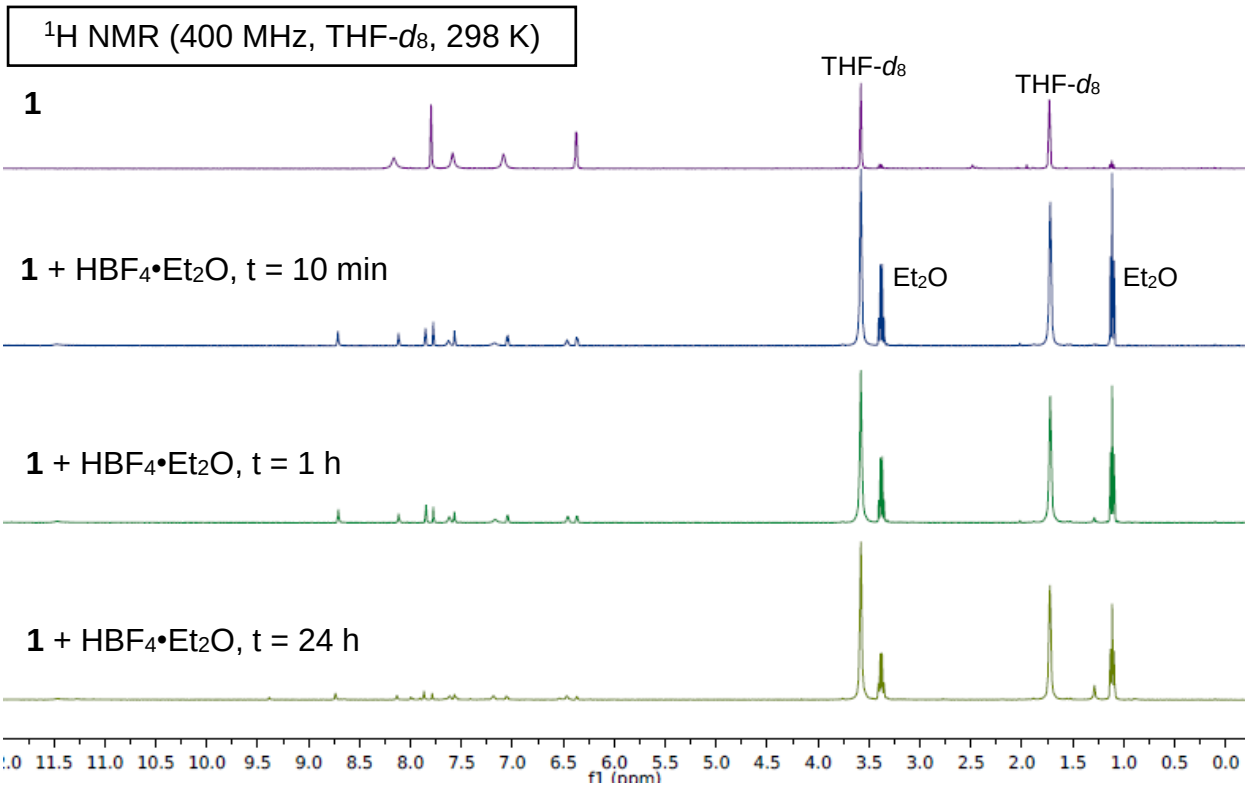

Figure 2.S10. ^{1}H NMR spectral monitoring of the reaction of **1** and HBF$_4$•Et$_2$O (1:1.3) in THF-d_8 at 298 K. Peaks at 3.58 and 1.72 ppm are from residual protio solvent. Peaks at 3.38 (q) and 1.12 (t) ppm are from the associated Et$_2$O of HBF$_4$•Et$_2$O. See Figure 2.S11 for expansion.

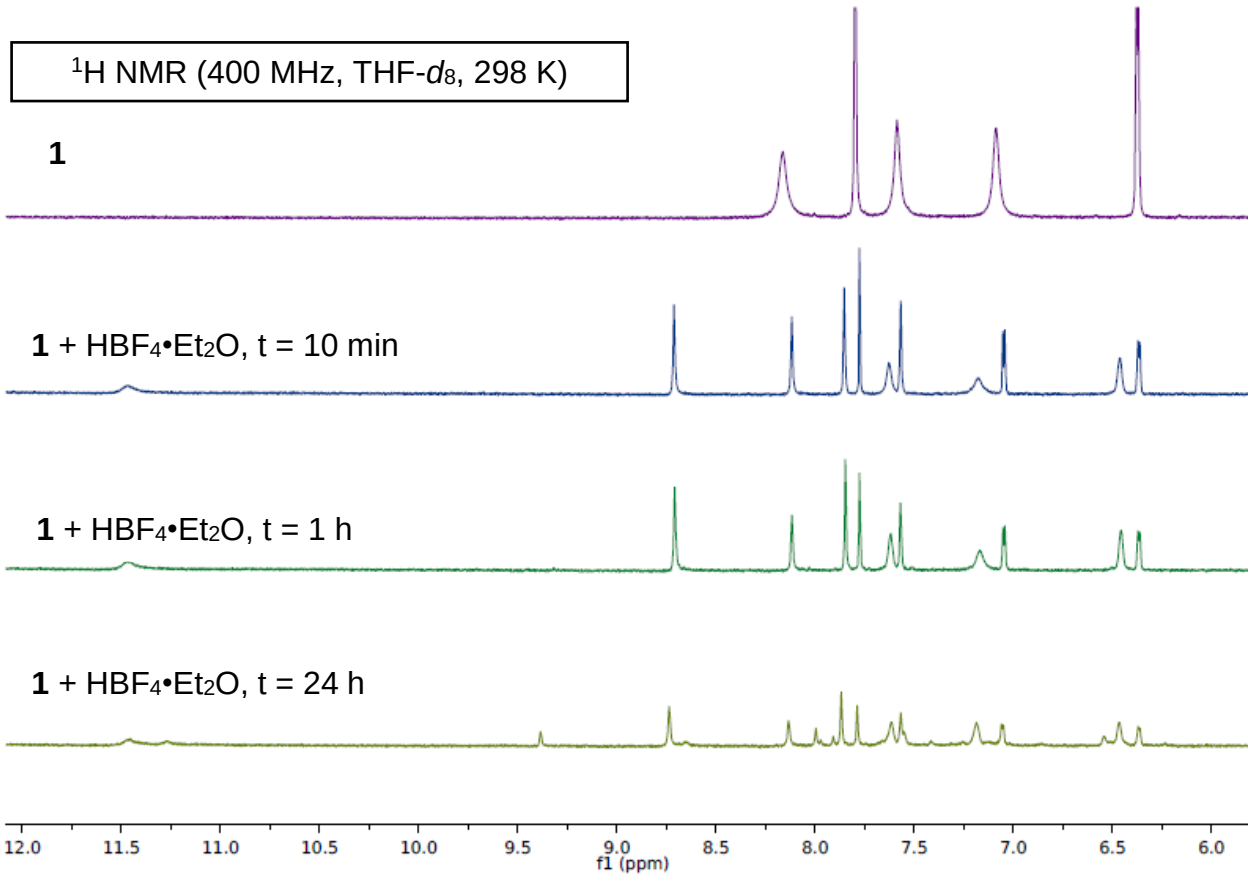

Figure 2.S11. Expansion of the aromatic region of the ^{1}H NMR spectra from Figure 2.S10.

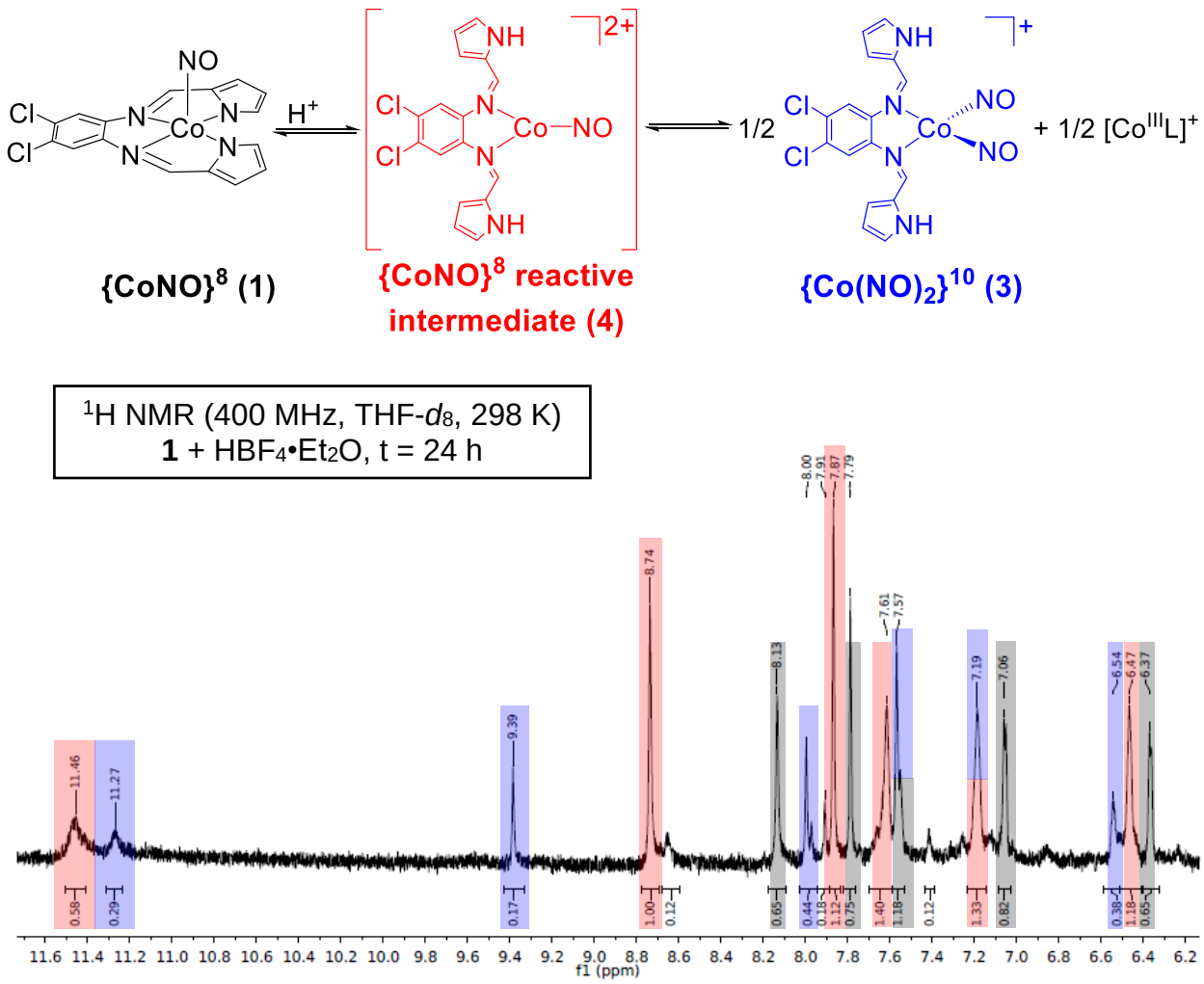

Figure 2.S12. *Top*: color-coded reaction scheme of **1** + H^+. *Bottom*: Zoom-in of 24 h spectrum from Figure 2.S11. Peaks are color-coded accordingly: $\{CoNO\}^8$ (**1**): gray, $\{Co(NO)_2\}^{10}$ (**3**): blue, three-coordinate $[Co(LN_4^{PhCl}H_2)(NO)](BF_4)_2$ (**4**): red based on comparison to authentic standards except for **4**.

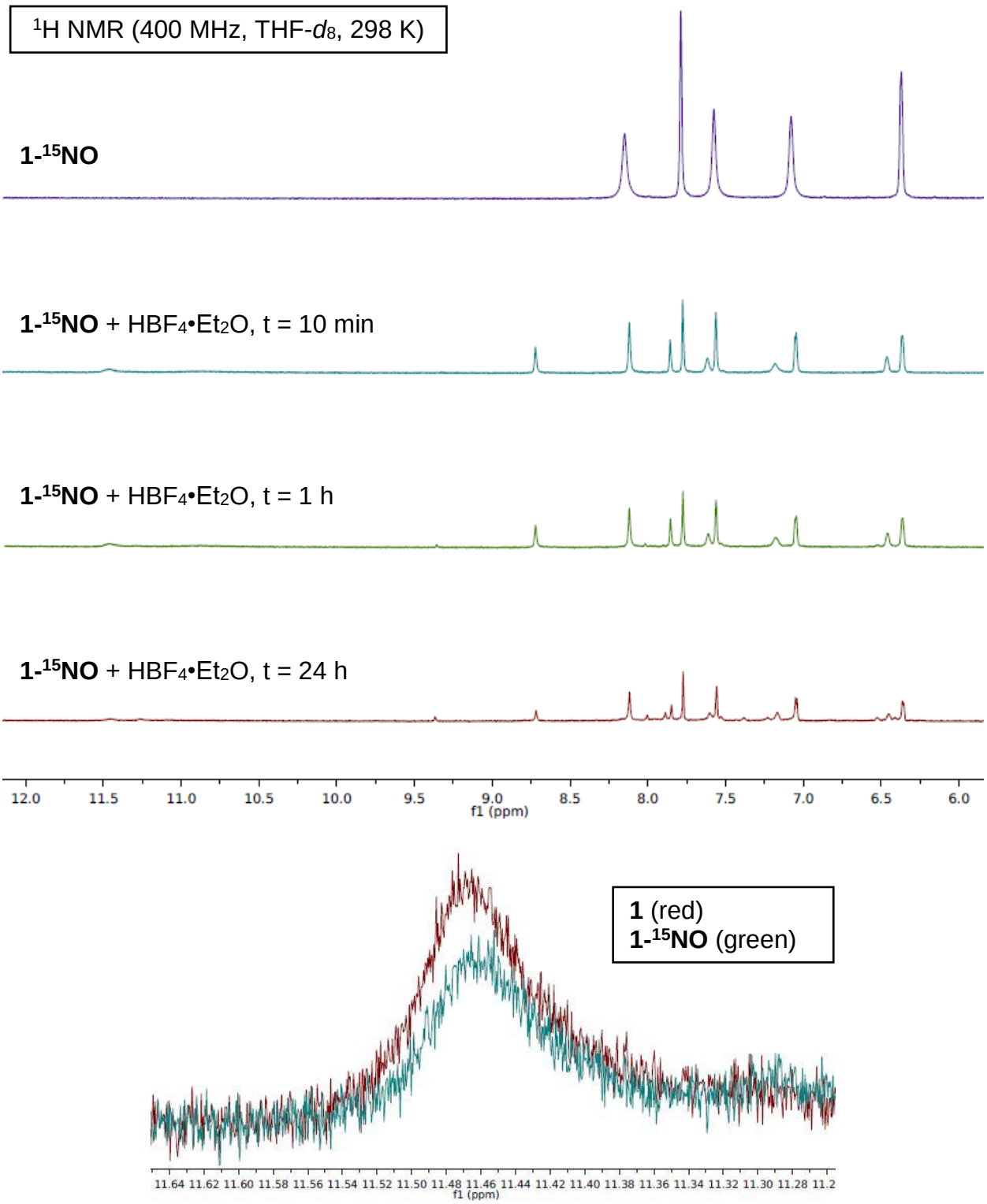

Figure 2.S13. Aromatic region of the ^{1}H NMR monitor of the reaction of **1-^{15}NO** and HBF_4•Et_2O (1:1.3) in THF-d_8 at 298 K. Bottom figure is a zoom-in of the 11.46 ppm peak after 1 h.

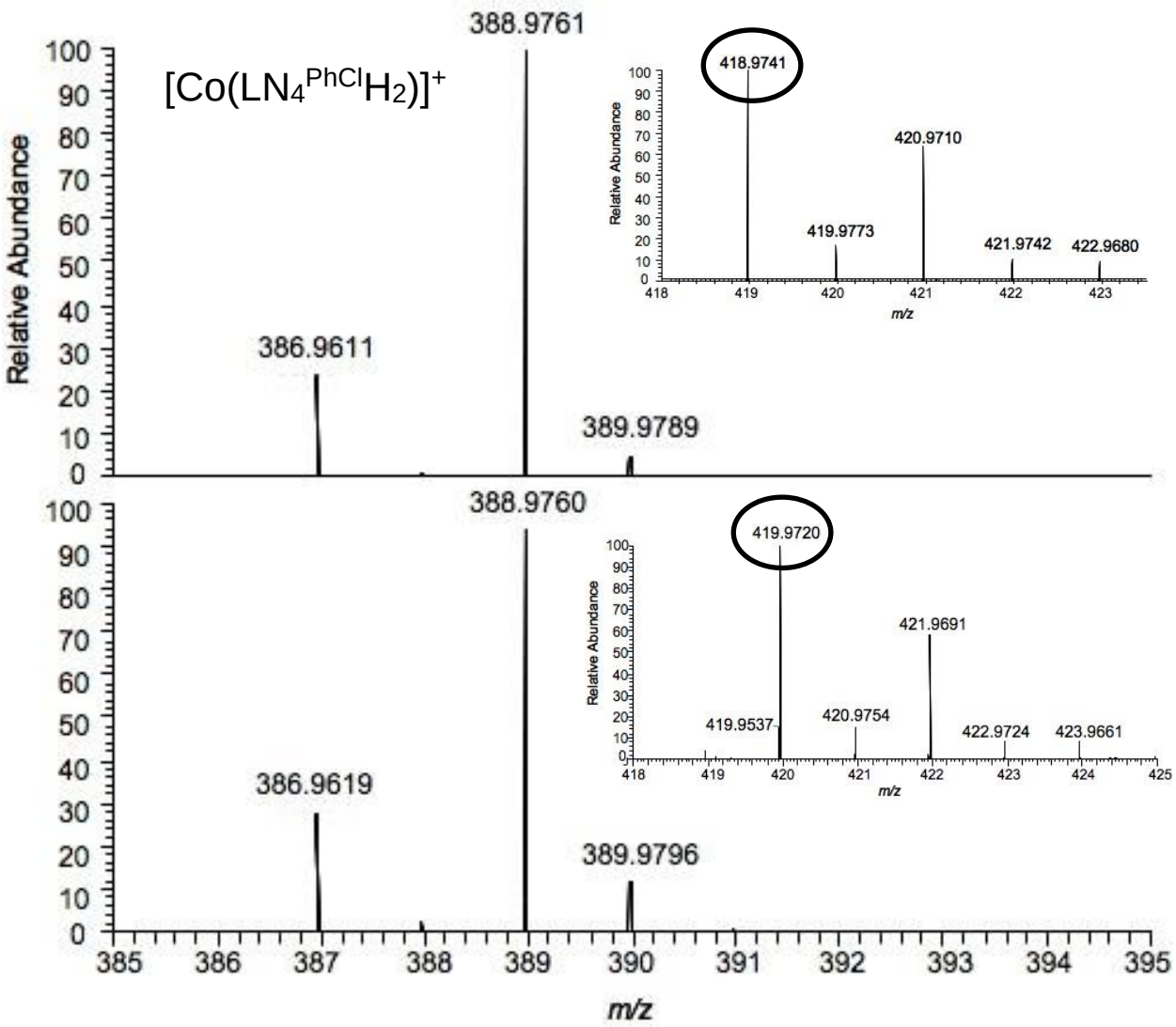

Figure 2.S14. *Top*: High-resolution ESI-MS-MS (positive mode) of peak at *m/z*: 418.9741 (see inset) from the reaction of **1** + HBF_4•Et_2O (1:1.3). *Bottom*: ESI-MS-MS (positive mode) of peak at *m/z*: 419.9720 (see inset) from the reaction of **1-^{15}NO** + HBF_4•Et_2O (1:1.3). Samples were run in THF with an isolation width of 1 amu. The peak at *m/z*: 388.976 in both MS-MS experiments corresponds to the complex $[Co(LN_4^{PhCl}H_2)]^+$ via loss of NO or ^{15}NO.

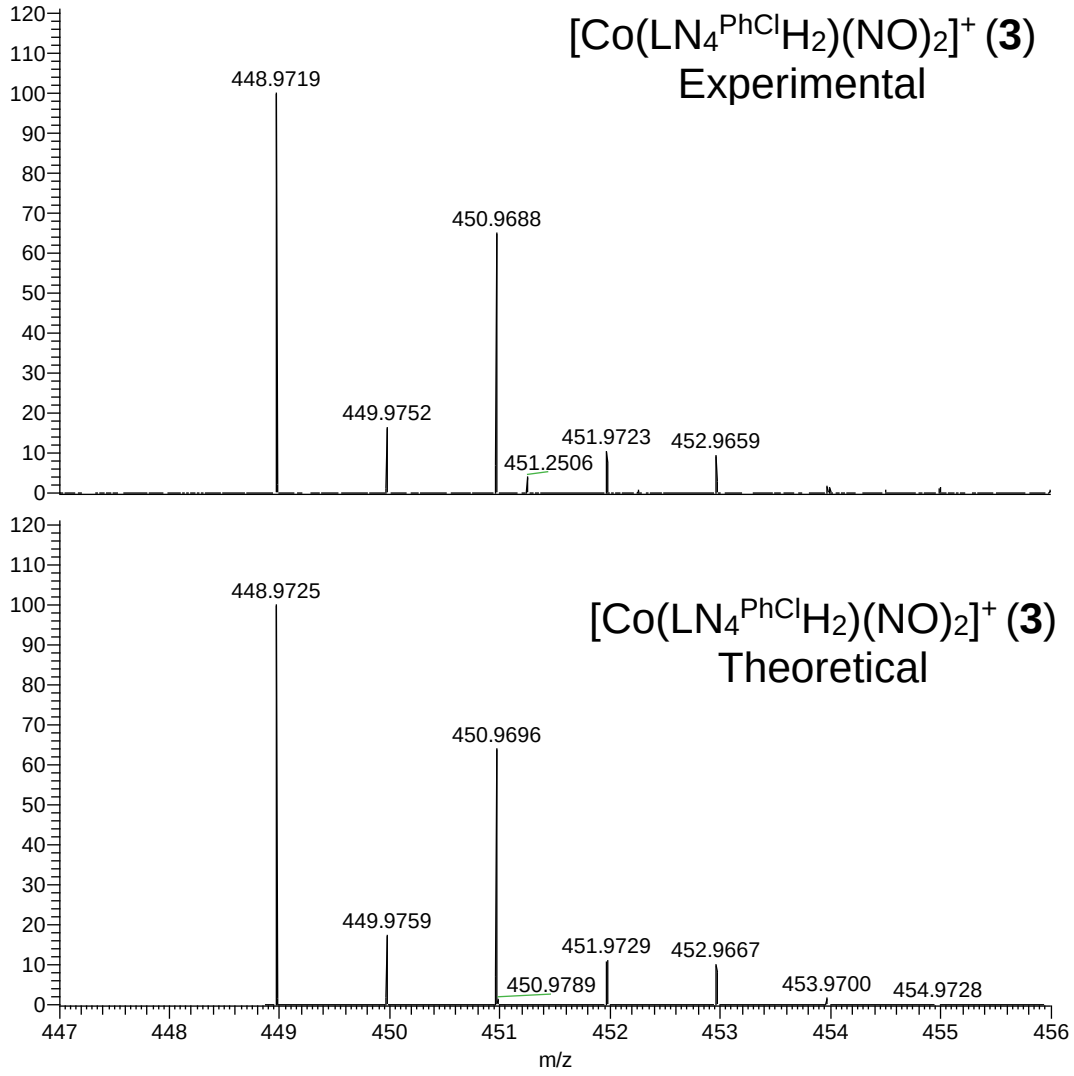

Figure 2.S15. *Top*: High-resolution ESI-MS (positive mode) of $[Co(LN_4^{PhCl}H_2)(NO)_2]BF_4$ (**3**) from the reaction of **1** + HBF_4•Et_2O (1:1.3) after 24 h. *Bottom*: Theoretical MS for complex **3**.

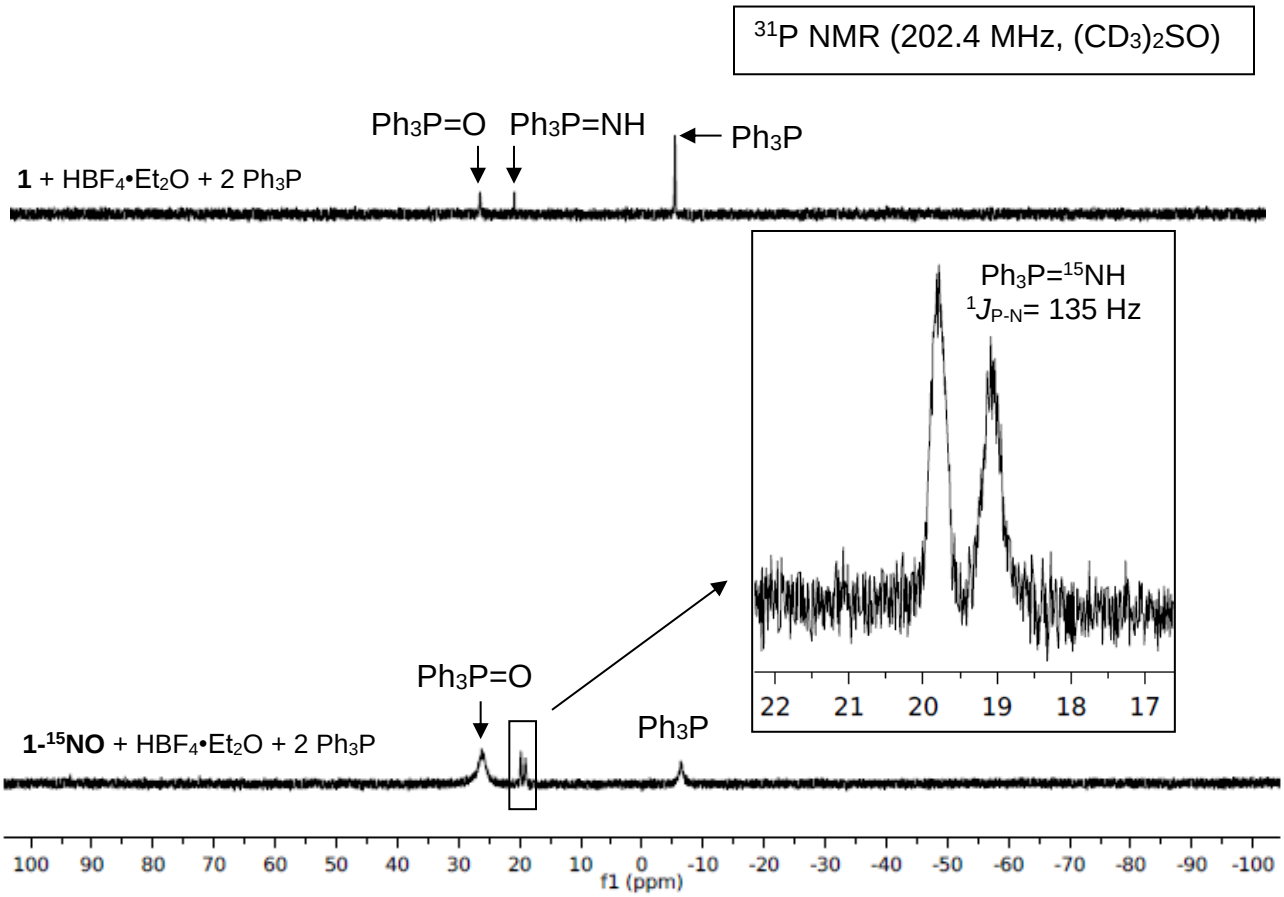

Figure 2.S16. ^{31}P NMR spectra of the reaction of **1** + 1.3 HBF_4•Et_2O + 2 Ph_3P (top), and **1-^{15}NO** + 1.3 HBF_4•Et_2O + 2Ph_3P (bottom) after 24 h reacting at RT. All spectra recorded $(CD_3)_2SO$ at 298 K, δ vs. external 85% H_3PO_4. *Inset for **1-^{15}NO** reaction*: expansion of the Ph_3P=^{15}NH peak showing the splitting due to the ^{15}N nucleus.

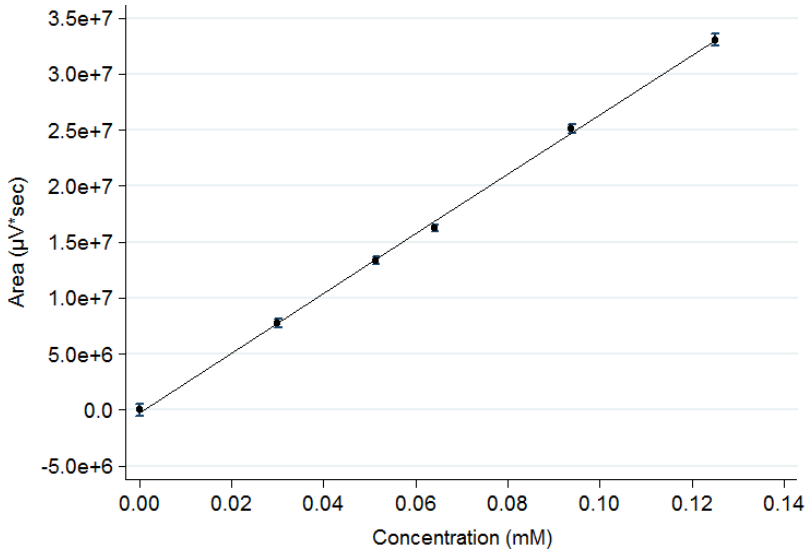

Figure 2.S17. HPLC-generated calibration curve for $Ph_3P=O$ in MeCN/H_2O (65/35). Each point represents the average of three trials.

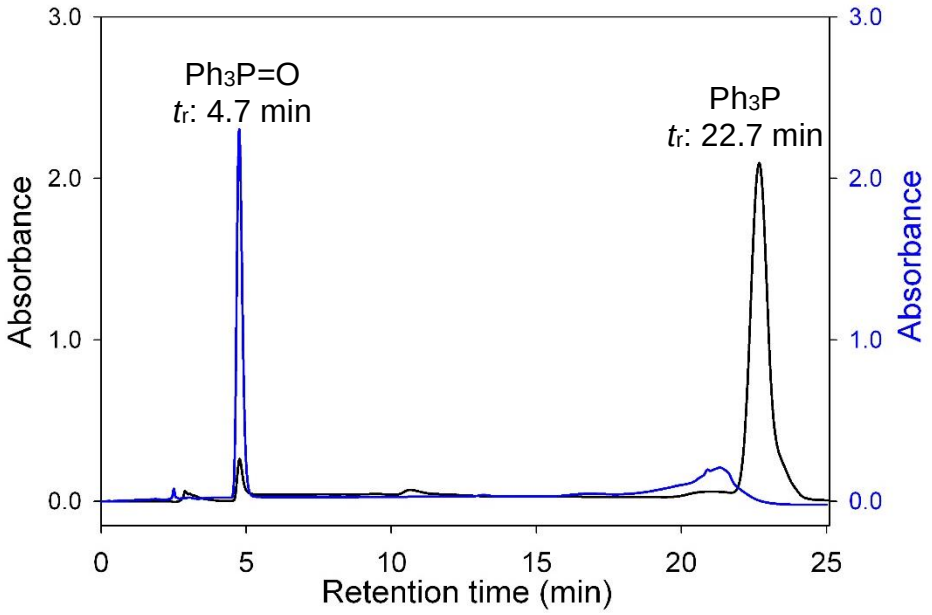

Figure 2.S18. HPLC chromatograms of Ph_3P (t_r: 22.7 min) and $Ph_3P=O$ (t_r: 4.7 min) controls in MeCN/H_2O (65/35).

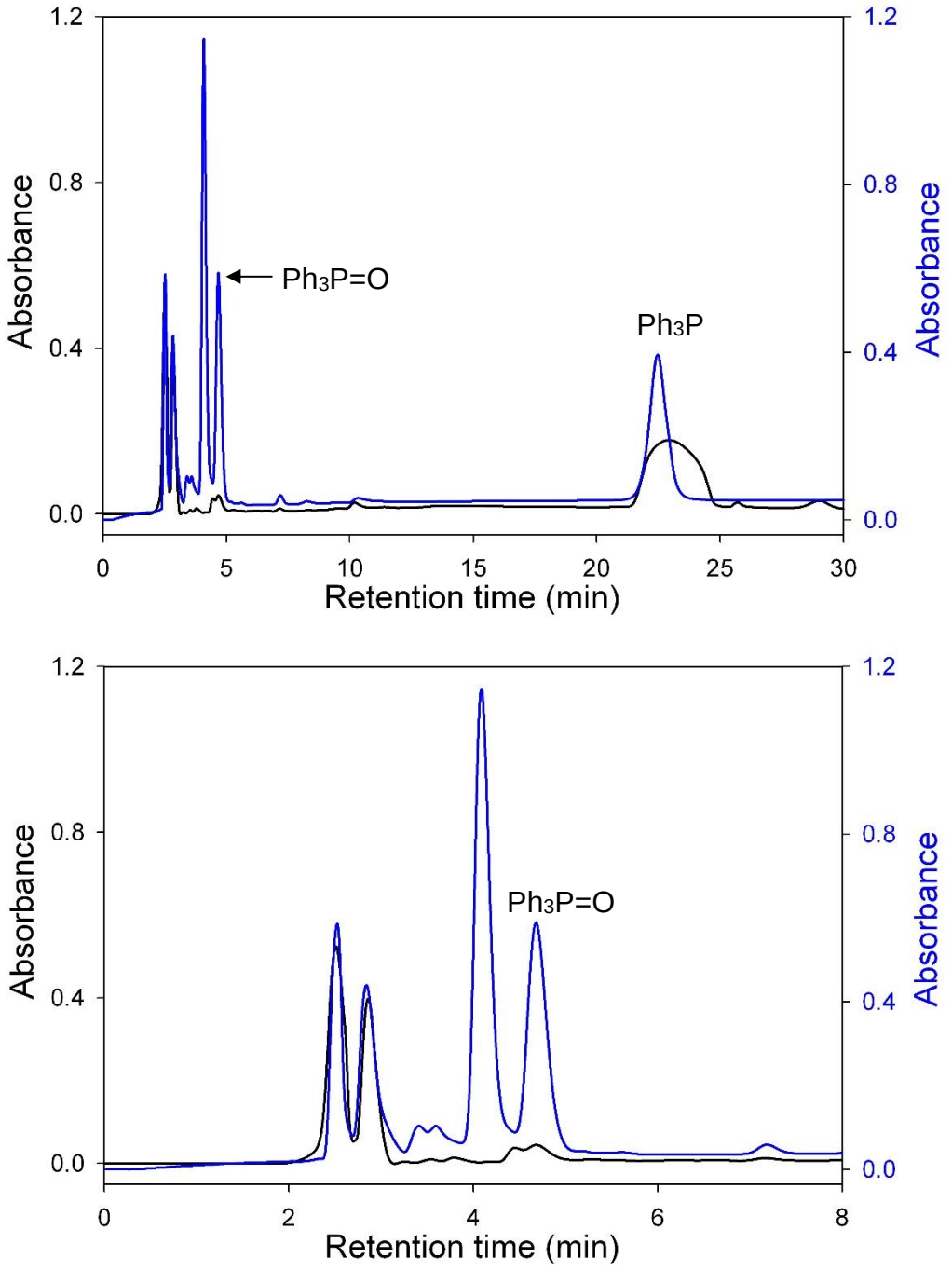

Figure 2.S19. HPLC chromatograms of the reaction of **1** + 2 Ph_3P (*black*) and **1** + 2 Ph_3P+ 1.3 HBF_4•Et_2O (blue) after 24 h mixing at RT in THF/H_2O (10/1). *Top*: full chromatogram. *Bottom*: zoom-in of area where Ph_3P=O elutes. Peaks at 2.5, 2.9, and 4.1 min are from **1**, $LN_4^{PhCl}H_2$, and an unidentified compound, respectively.

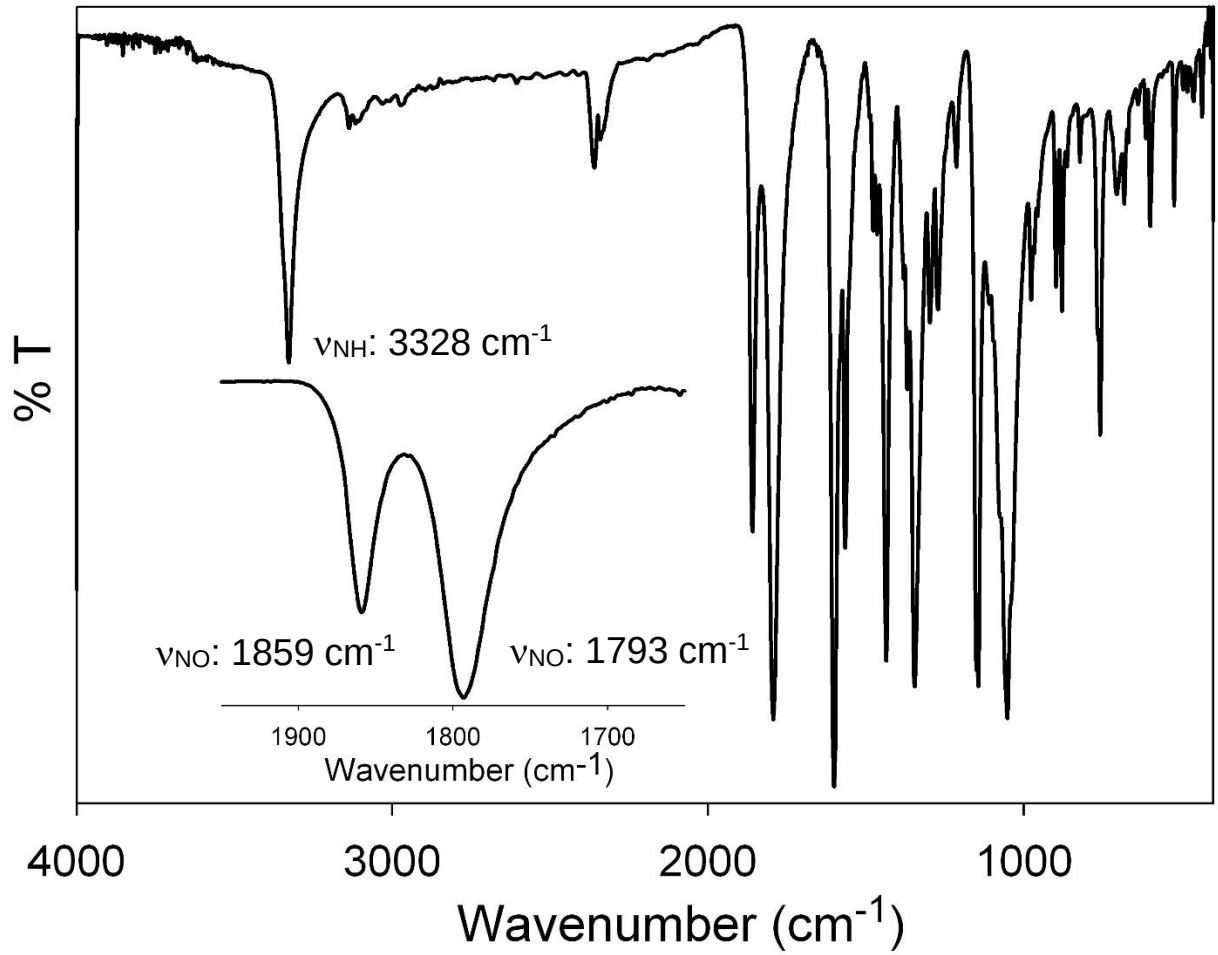

Figure 2.S20. FTIR spectrum of $[Co(LN_4^{PhCl}H_2)(NO)_2]BF_4$ (**3**) in a KBr matrix. *Inset*: expansion of the N-O stretching (ν_{NO}) region.

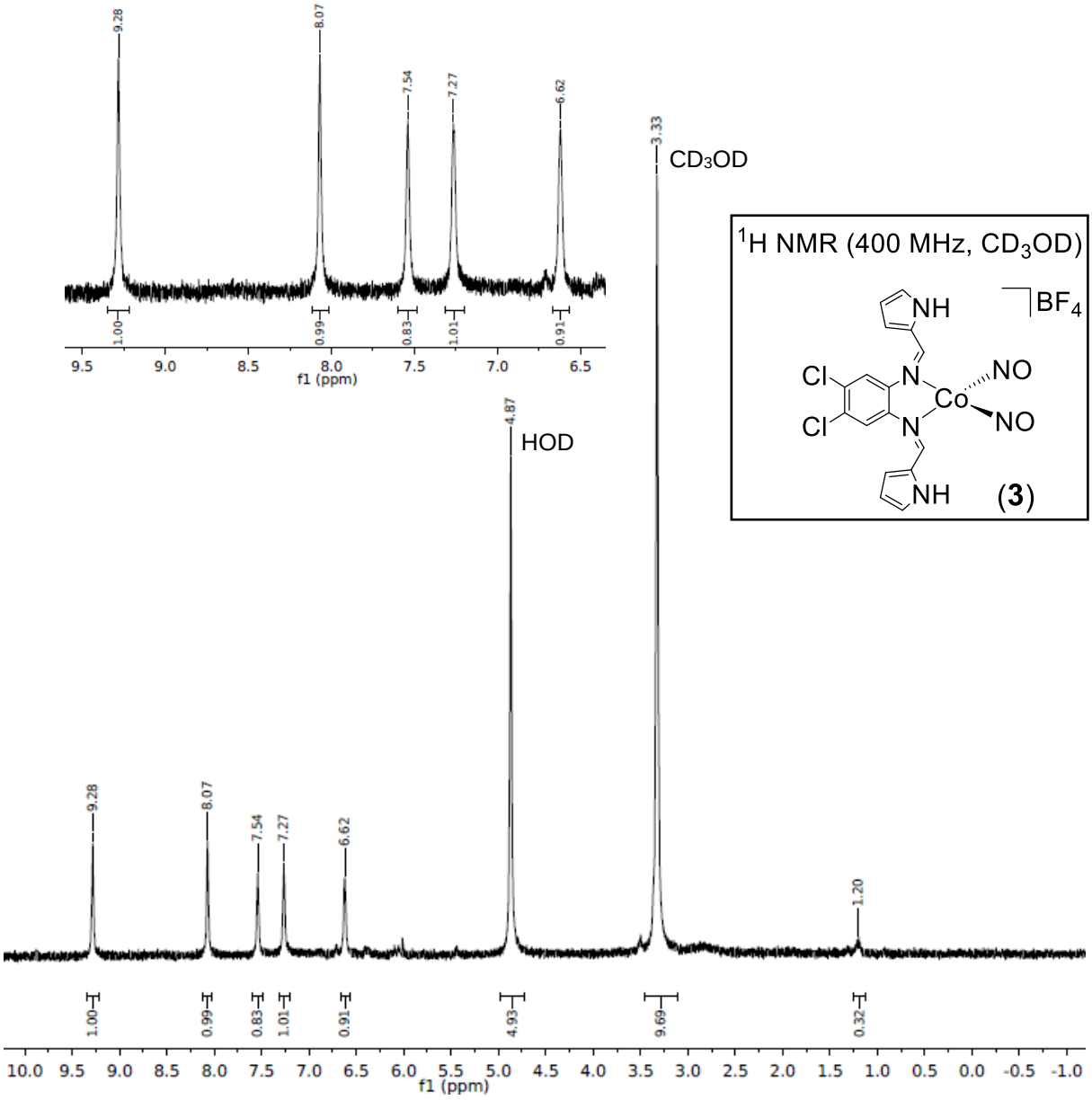

Figure 2.S21. ^{1}H NMR spectrum of [Co(LN$_4^{PhCl}$H$_2$)(NO)$_2$]BF$_4$ (**3**) in CD$_3$OD at 298 K. The peaks at 3.33 and 4.87 are from residual protio solvent and H$_2$O, respectively. *Inset*: expansion of the aromatic region of the spectrum.

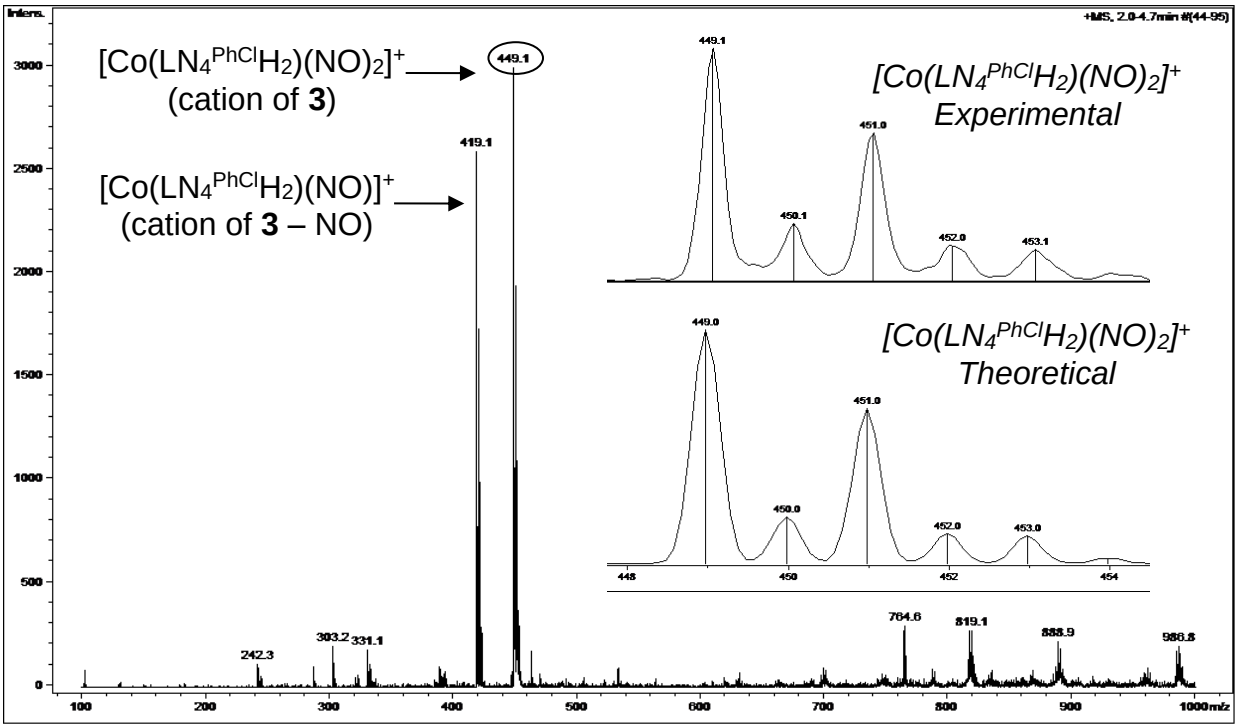

Figure 2.S22. LR-ESI-MS (positive mode) of $[Co(LN_4^{PhCl}H_2)(NO)_2]BF_4$ (**3**) in MeOH. *Inset*: expansion of the molecular ion peak at *m/z*: 449.1 (top) and the theoretical fit (bottom).

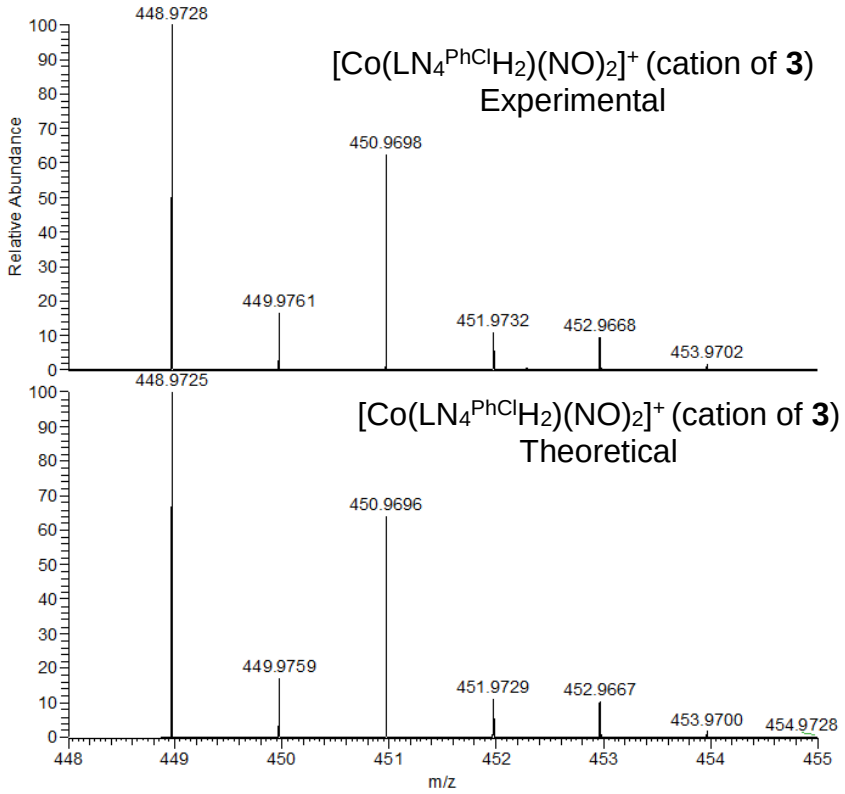

Figure 2.S23. *Top*: High-resolution ESI-MS (positive mode) of $[Co(LN_4^{PhCl}H_2)(NO)_2]BF_4$ (**3**) in MeOH. *Bottom*: Theoretical MS for **3**.

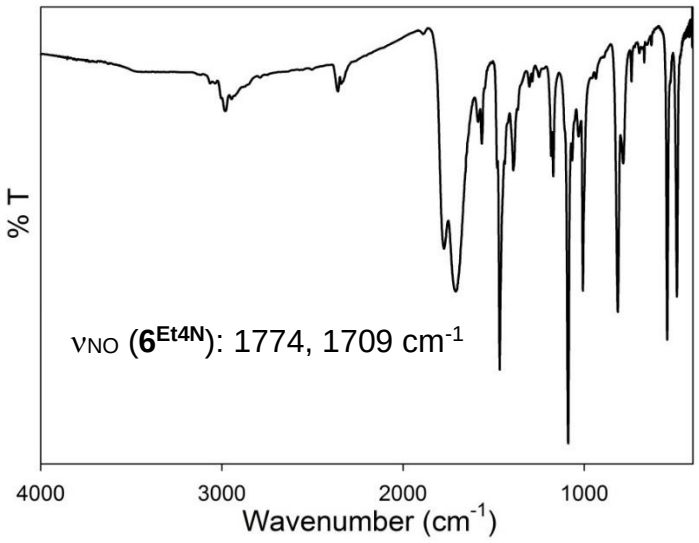

Figure 2.S24. Solid-state FTIR spectrum of $(Et_4N)[Co(SPh\text{-}p\text{-}Cl)_2(NO)_2]$ (**6**$^{\mathbf{Et4N}}$) (KBr).

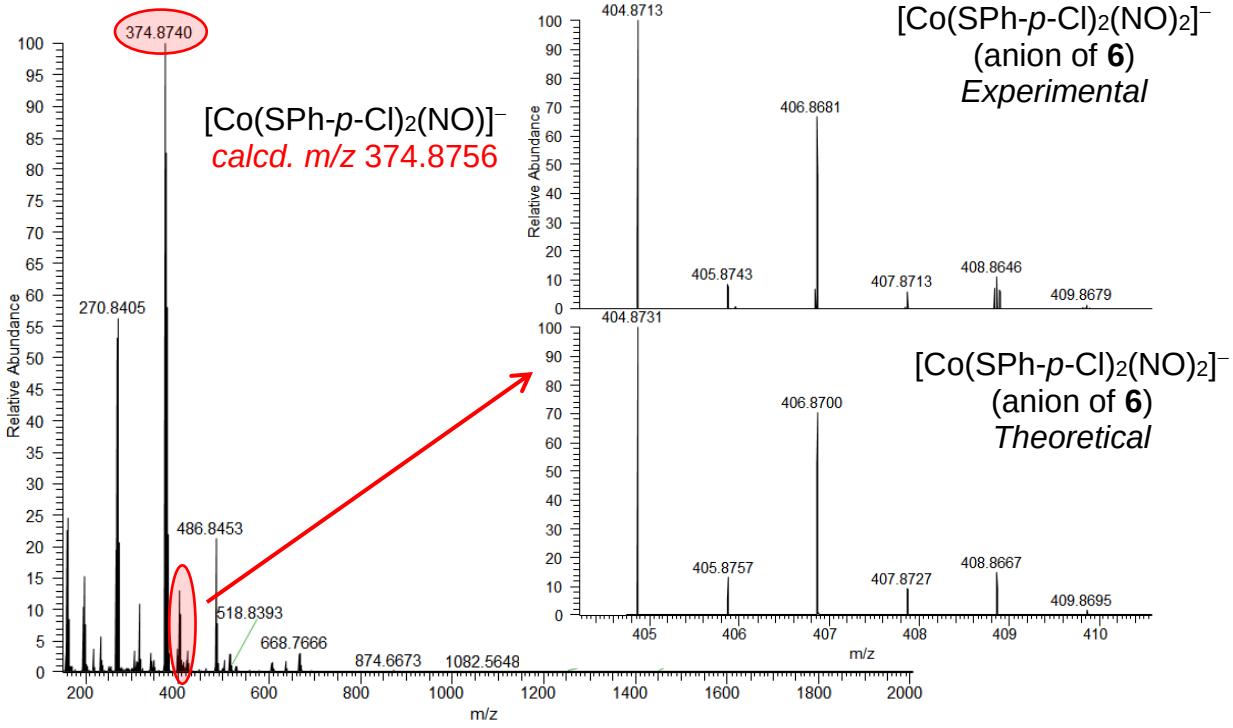

Figure 2.S25. High-resolution ESI-MS (negative mode, full spectrum) of $(Et_4N)[Co(SPh\text{-}p\text{-}Cl)_2(NO)_2]$ ($\mathbf{6}^{\mathbf{Et4N}}$) in THF. The major peak at *m/z* 374.8740 corresponds to loss of one NO moiety or $[Co(SPh\text{-}p\text{-}Cl)_2(NO)]^-$ $\{M - NO\}^-$ *m/z*: 374.8756 (theoretical). Inset is an expansion of the molecular ion peak $\{M\}^-$.

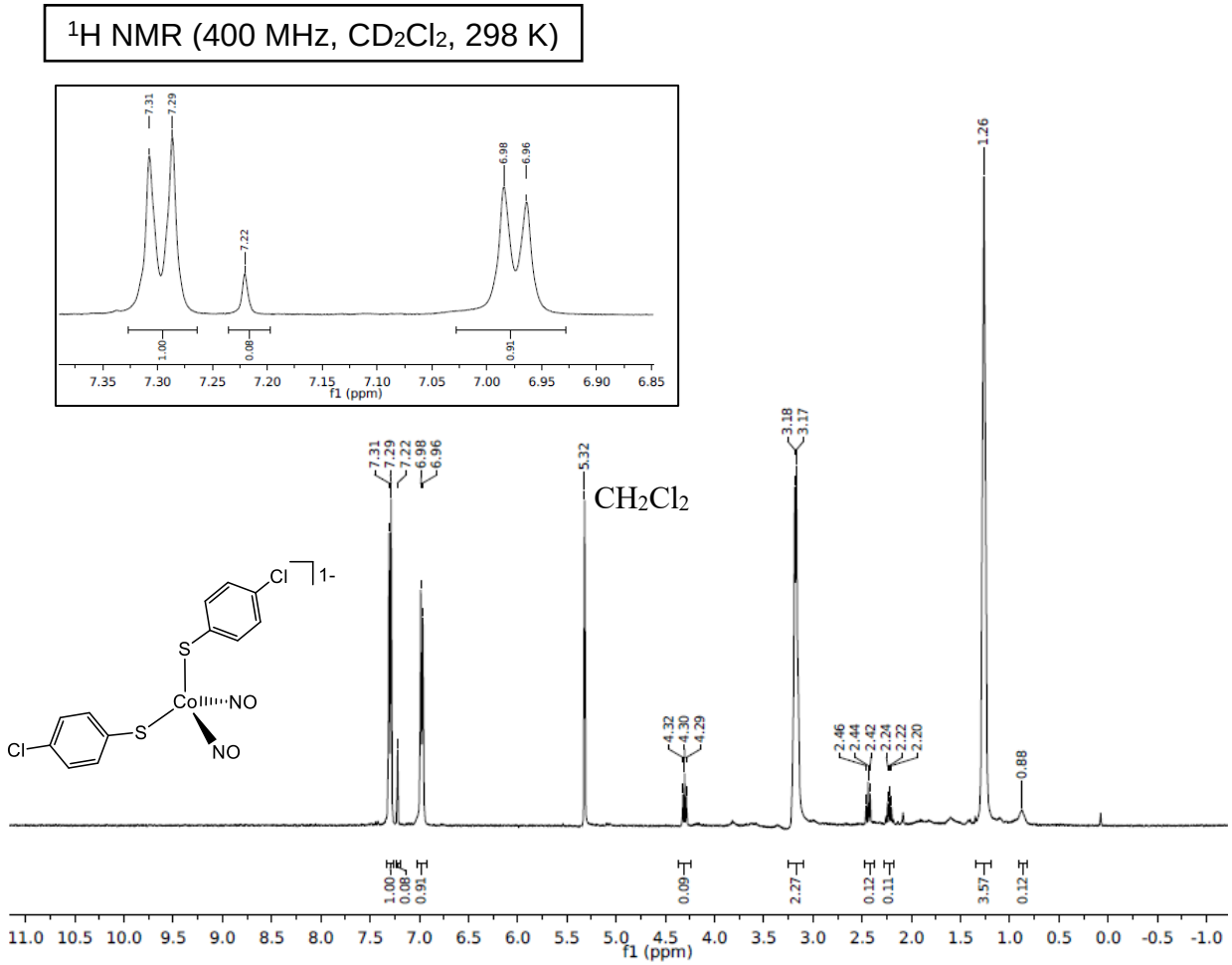

Figure 2.S26. ^{1}H NMR spectrum of $\{Co(NO)_2\}^{10}$ complex $(Et_4N)[Co(SPh\text{-}p\text{-}Cl)_2(NO)_2]$ (**6**$^{\mathbf{Et4N}}$) in CD_2Cl_2 at RT. *Inset*: expansion of aromatic region. Peak at 5.32 ppm is from residual protio solvent. Peaks at 7.22, 4.30, 2.44 and 2.24 ppm that integrate for ~0.1 H have not been identified.

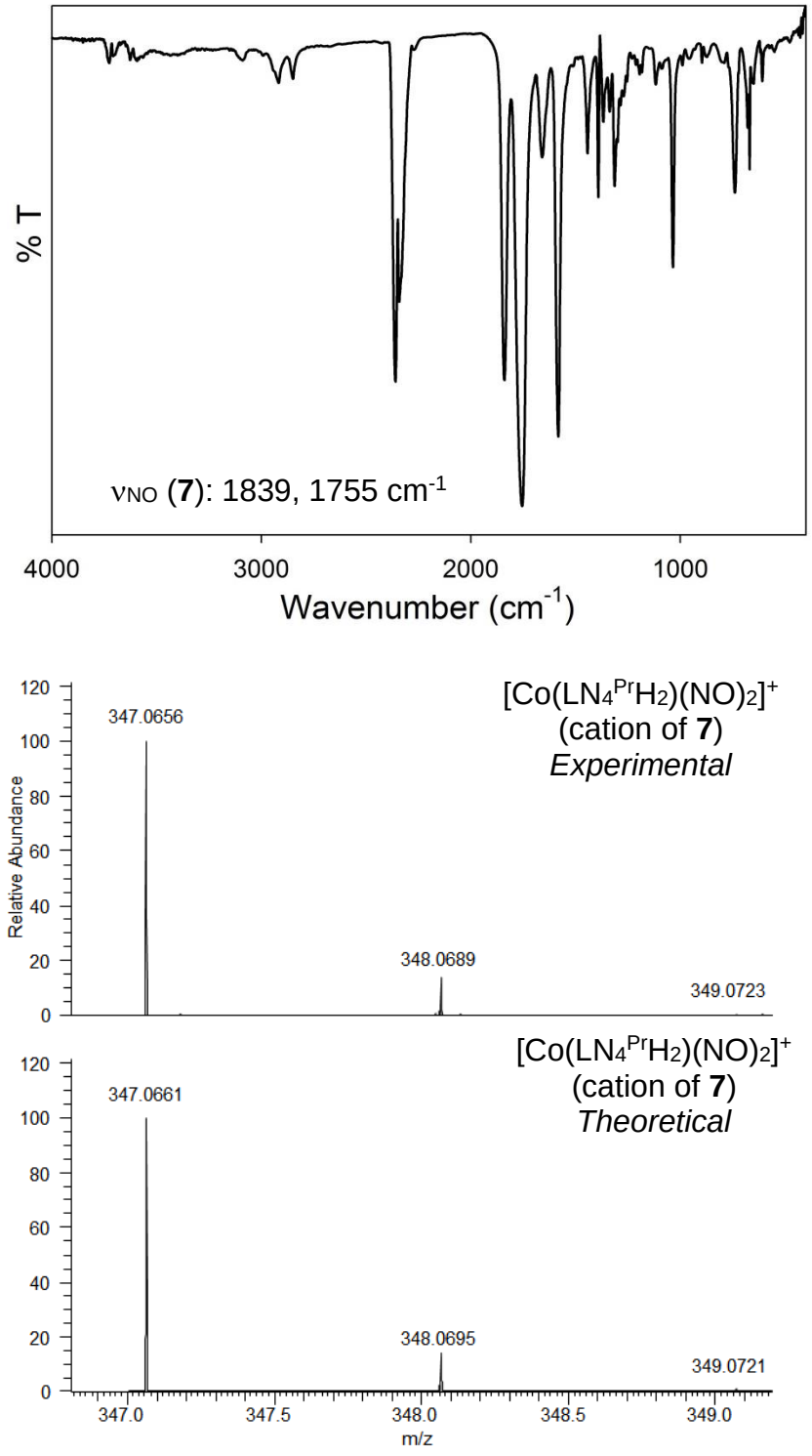

Figure 2.S27. (*Top*) Solid-state FTIR spectrum of $[Co(LN_4^{Pr}H_2)(NO)_2]Cl$ (**7**) (KBr). (*Bottom*) High-resolution ESI-MS(+) of $[Co(LN_4^{Pr}H_2)(NO)_2]Cl$ (**7**) in THF.

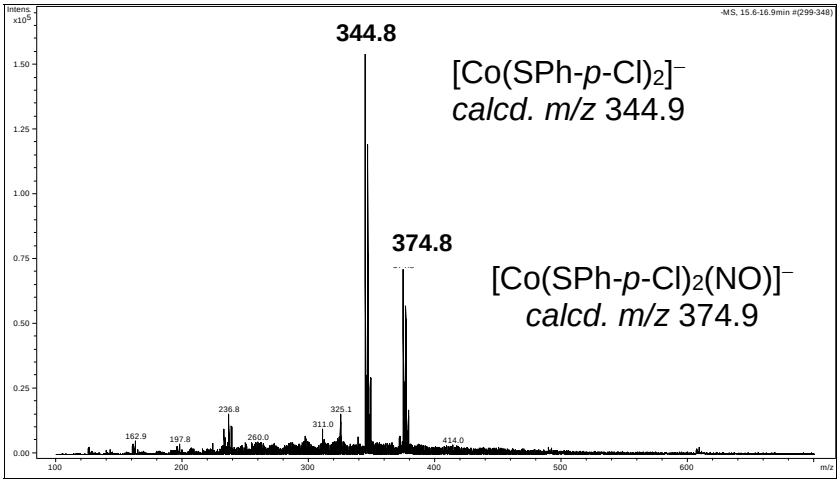

Figure 2.S28. LR-ESI-MS(–) of products from the reaction of {CoNO}^{8} [Co(LN$_4^{Pr}$)(NO)] (**5**) and *p*-Cl-PhSH at t = 24 h in THF at RT.

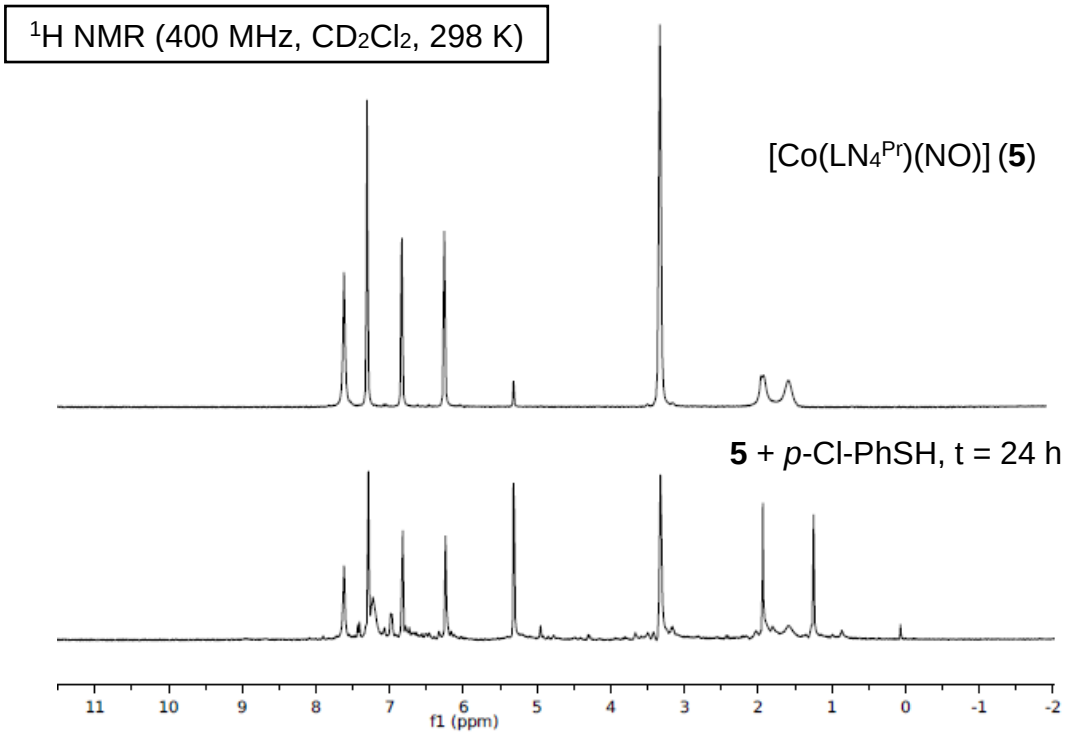

Figure 2.S29. (*Top*) ^{1}H NMR spectrum of {CoNO}^{8} [Co(LN$_4^{Pr}$)(NO)] (**5**) in CD_2Cl_2 at 298 K. (*Bottom*) ^{1}H NMR spectrum of the reaction of {CoNO}^{8} **5** with *p*-Cl-PhSH (1:1) after 24 h mixing (CD_2Cl_2, 298 K).

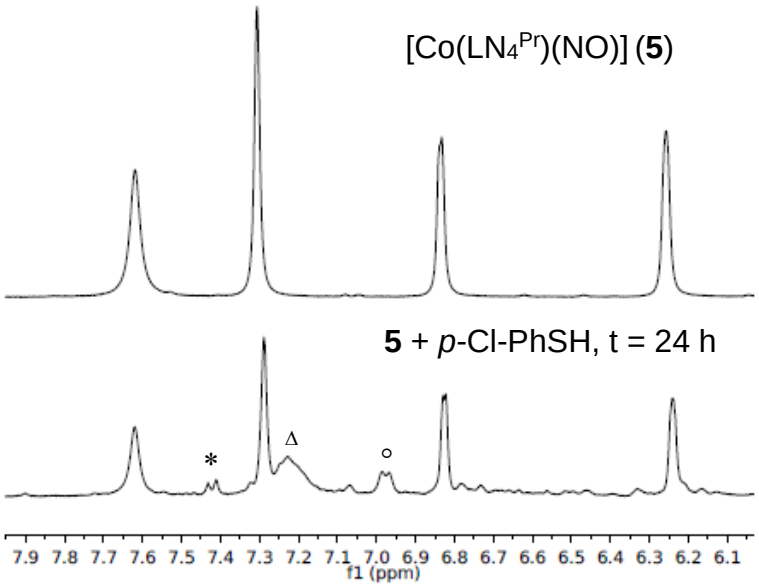

Figure 2.S30. (*Top*) Aromatic region of the ^{1}H NMR spectrum of {CoNO}^{8} (**5**) from Figure 2.S29-top (CD_2Cl_2, 298 K). (*Bottom*) Aromatic region of the ^{1}H NMR spectrum from Figure 2.S29-bottom of the reaction of {CoNO}^{8} **5** and *p*-Cl-PhSH (1:1) after 24 h mixing (CD_2Cl_2, 298 K). Peaks denoted with * = *p*-Cl-PhSSPh-*p*-Cl; Δ = unreacted *p*-Cl-PhSH; ° = $[Co(SPh\text{-}p\text{-}Cl)_2(NO)_2]^-$ (anion of **6**) based on authentic syntheses.

2.8 References

(1) Moncada, S.; Higgs, E. A. *Br. J. Pharmacol.* **2006**, *147*, S193.

(2) Bartberger, M. D.; Liu, W.; Ford, E.; Miranda, K. M.; Switzer, C.; Fukuto, J. M.; Farmer, P. J.; Wink, D. A.; Houk, K. N. *Proc. Natl. Acad. Sci. U.S.A.* **2002**, *99*, 10958.

(3) Shafirovich, V.; Lymar, S. V. *Proc. Natl. Acad. Sci. U.S.A.* **2002**, *99*, 7340.

(4) Irvine, J. C.; Ritchie, R. H.; Favaloro, J. L.; Andrews, K. L.; Widdop, R. E.; Kemp-Harper, B. K. *Trends Pharmacol. Sci.* **2008**, *29*, 601.

(5) Miranda, K. M. *Coord. Chem. Rev.* **2005**, *249*, 433.

(6) Paolocci, N.; Jackson, M. I.; Lopez, B. E.; Miranda, K.; Tocchetti, C. G.; Wink, D. A.; Hobbs, A. J.; Fukuto, J. M. *Pharmacol. Ther.* **2007**, *113*, 442.

(7) Angeli, A.; Angelico, F.; Scurti, F. *Chem. Zentralbl.* **1902**, *73*, 691.

(8) Bonner, F. T.; Ko, Y. *Inorg. Chem.* **1992**, *31*, 2514.

(9) Adak, S.; Wang, Q.; Stuehr, D. J. *J. Biol. Chem.* **2000**, *275*, 33554.

(10) Rusche, K. M.; Spiering, M. M.; Marletta, M. A. *Biochemistry* **1998**, *37*, 15503.

(11) Enemark, J. H.; Feltham, R. D. *Coord. Chem. Rev.* **1974**, *13*, 339. $\{MNO\}^n$ where n = number of metal d + NO π^* electrons.

(12) Patra, A. K.; Dube, K. S.; Sanders, B. C.; Papaefthymiou, G. C.; Conradie, J.; Ghosh, A.; Harrop, T. C. *Chem. Sci.* **2012**, *3*, 364.

(13) Sanders, B. C.; Patra, A. K.; Harrop, T. C. *J. Inorg. Biochem.* **2013**, *118*, 115.

(14) Trogler, W. C.; Marzilli, L. G. *Inorg. Chem.* **1974**, *13*, 1008.

(15) Addison, A. W.; Rao, T. N.; Reedijk, J.; van Rijn, J.; Verschoor, G. C. *J. Chem. Soc. Dalton Trans.* **1984**, 1349.

(16) Franz, K. J.; Doerrer, L. H.; Spingler, B.; Lippard, S. J. *Inorg. Chem.* **2001**, *40*, 3774.

(17) Hess, J. L.; Conder, H. L.; Green, K. N.; Darensbourg, M. Y. *Inorg. Chem.* **2008**, *47*, 2056.

(18) Kozhukh, J.; Lippard, S. J. *J. Am. Chem. Soc.* **2012**, *134*, 11120.

(19) McCleverty, J. A. *Chem. Rev.* **2004**, *104*, 403 and references therein.

(20) Mason, J.; Larkworthy, L. F.; Moore, E. A. *Chem. Rev.* **2002**, *102*, 913.

(21) Dalby, F. W. *Can. J. Phys.* **1958**, *36*, 1336.

(22) Wyllie, G. R. A.; Scheidt, W. R. *Chem. Rev.* **2002**, *102*, 1067 and references therein.

(23) Padden, K. M.; Krebs, J. F.; MacBeth, C. E.; Scarrow, R. C.; Borovik, A. S. *J. Am. Chem. Soc.* **2001**, *123*, 1072.

(24) Padden, K. M.; Krebs, J. F.; Trafford, K. T.; Yap, G. P. A.; Rheingold, A. H.; Borovik, A. S.; Scarrow, R. C. *Chem. Mater.* **2001**, *13*, 4305.

(25) McCleverty, J. A. *Chem. Rev.* **1979**, *79*, 53.

(26) Duffin, P. A.; Larkworthy, L. F.; Mason, J.; Stephens, A. N.; Thompson, R. M. *Inorg. Chem.* **1987**, *26*, 2034.

(27) Huheey, J. E.; Keiter, E. A.; Keiter, R. L., *Inorganic Chemistry: Principles of Structure and Reactivity, 4th edition.* HarperCollins College Publishers: New York, 1993.

(28) Bari, S. E.; Martí, M. A.; Amorebieta, V. T.; Estrin, D. A.; Doctorovich, F. *J. Am. Chem. Soc.* **2003**, *125*, 15272.

(29) Martí, M. A.; Bari, S. E.; Estrin, D. A.; Doctorovich, F. *J. Am. Chem. Soc.* **2005**, *127*, 4680.

(30) Bazylinski, D. A.; Goretski, J.; Hollocher, T. C. *J. Am. Chem. Soc.* **1985**, *107*, 7986.

(31) Bazylinski, D. A.; Hollocher, T. C. *J. Am. Chem. Soc.* **1985**, *107*, 7982.

(32) Doyle, M. P.; Mahapatro, S. N.; Broene, R. D.; Guy, J. K. *J. Am. Chem. Soc.* **1988**, *110*, 593.

(33) Miranda, K. M.; Nims, R. W.; Thomas, D. D.; Espey, M. G.; Citrin, D.; Bartberger, M. D.; Paolocci, N.; Fukuto, J. M.; Feelisch, M.; Wink, D. A. *J. Inorg. Biochem.* **2003**, *93*, 52.

(34) Bottomley, L. A.; Kadish, K. M. *Inorg. Chem.* **1981**, *20*, 1348.

(35) Chiang, C.-Y.; Darensbourg, M. Y. *J. Biol. Inorg. Chem.* **2006**, *11*, 359.

(36) Reisz, J. A.; Klorig, E. B.; Wright, M. W.; King, S. B. *Org. Lett.* **2009**, *11*, 2719.

(37) Reisz, J. A.; Zink, C. N.; King, S. B. *J. Am. Chem. Soc.* **2011**, *133*, 11675.

(38) Oxidation-reduction reactions have been previously shown to occur in coordination complexes when examined by ESI-MS.

(39) Henderson, W.; McIndoe, J. S., The ESI MS Behaviour of Coordination Complexes. In *Mass Spectrometry of Inorganic and Organometallic Compounds*, John Wiley & Sons Ltd: Chichester, 2005.

(40) Gwost, D.; Caulton, K. G. *Inorg. Chem.* **1973**, *12*, 2095.

(41) According to peak integrations, **3** makes up ~20% of the reaction mixture (Figure 2.S12). We attribute the low amount of **3** due to its poor solubility and the large amount of unreacted **1**.

(42) Berto, T. C.; Speelman, A. L.; Zheng, S.; Lehnert, N. *Coord. Chem. Rev.* **2013**, *257*, 244.

(43) Farmer, P. J.; Sulc, F. *J. Inorg. Biochem.* **2005**, *99*, 166.

(44) Pellegrino, J.; Bari, S. E.; Bikiel, D. E.; Doctorovich, F. *J. Am. Chem. Soc.* **2010**, *132*, 989.

(45) Sanders, B. C.; Rhine, M. A.; Harrop, T. C. *Struct. Bond.* **2014**, *160*, 57.

(46) Addition of NO(g) to MeOH solutions containing $LN_4^{PhCl}H_2$ and Co^{II} afford a mixture of species. A medium intensity peak at ~2200 cm^{-1} may be from a coordinated N_2O ligand, which is a known disproportionation product of coordinated NO: $3NO \rightarrow N_2O + NO_2$. See reference 47.

(47) Franz, K. J.; Lippard, S. J. *J. Am. Chem. Soc.* **1999**, *121*, 10504.

(48) Del Zotto, A.; Mezzetti, A.; Rigo, P. *Inorg. Chim. Acta* **1990**, *171*, 61.

(49) Armor, J. *Inorg. Chem.* **1973**, *12*, 1959.

(50) Doyle, M. P.; Pickering, R. A.; Dykstra, R. L.; Cook, B. R. *J. Am. Chem. Soc.* **1982**, *104*, 3392. The species responsible for release of the NO moiety may be a reduced cobalt nitrosyl given the presence of excess reductant.

(51) Doyle, M. P.; Van Doornik, F. J.; Funckes, C. L. *Inorg. Chim. Acta* **1980**, *46*, L111. $[Co(NH_3)_5(NO)]Cl_2$ reacts with both Fe^{III}- and Fe^{II}- heme proteins.

(52) Ungermann, C. B.; Caulton, K. G. *J. Am. Chem. Soc.* **1976**, *98*, 3862.

(53) Rhine, M. A.; Rodrigues, A. V.; Bieber Urbauer, R. J.; Urbauer, J. L.; Stemmler, T. L.; Harrop, T. C. *J. Am. Chem. Soc.* **2014**, *136*, 12560.

(54) Rhine, M. A.; Sanders, B. C.; Patra, A. K.; Harrop, T. C. *Inorg. Chem.* **2015**, *54*, 9351.

(55) Tennyson, A. G.; Dhar, S.; Lippard, S. J. *J. Am. Chem. Soc.* **2008**, *130*, 15087.

(56) Bitterwolf, T. E.; Pal, P. *Inorg. Chim. Acta* **2006**, *359*, 1501.

(57) Tsai, M.-L.; Tsou, C.-C.; Liaw, W.-F. *Acc. Chem. Res.* **2015**, *48*, 1184.

(58) Chen, Y.-J.; Ku, W.-C.; Feng, L.-T.; Tsai, M.-L.; Hsieh, C.-H.; Hsu, W.-H.; Liaw, W.-F.; Hung, C.-H.; Chen, Y.-J. *J. Am. Chem. Soc.* **2008**, *130*, 10929.

(59) Jones, R. A., ed., *Pyrroles. The Synthesis and the Physical and Chemical Aspects of the Pyrrole Ring*. John Wiley & Sons: New York, 1990.

(60) Gao, Y.; Toubaei, A.; Kong, X.; Wu, G. *Angew. Chem. Int. Ed.* **2014**, *53*, 11547.

(61) Guthrie, D. A.; Kim, N. Y.; Siegler, M. A.; Moore, C. D.; Toscano, J. P. *J. Am. Chem. Soc.* **2012**, *134*, 1962.

(62) Tran, C. T.; Kim, E. *Inorg. Chem.* **2012**, *51*, 10086.

(63) Gill, N. S.; Taylor, F. B. *Inorg. Synth.* **1967**, *9*, 136.

(64) Sacco, A.; Rossi, M.; Nobile, C. F. *Ann. Chim. (Rome)* **1967**, *57*, 499.

(65) Fulmer, G. R.; Miller, A. J. M.; Sherden, N. H.; Gottlieb, H. E.; Nudelman, A.; Stoltz, B. M.; Bercaw, J. E.; Goldberg, K. I. *Organometallics* **2010**, *29*, 2176.

(66) Armstrong, A.; Jones, L. H.; Knight, J. D.; Kelsey, R. D. *Org. Lett.* **2005**, *7*, 713.

(67) Cherryman, J. C.; Harris, R. K.; Davidson, M. G.; Price, R. D. *J. Braz. Chem. Soc.* **1999**, *10*, 287.

(68) Patra, A. K.; Afshar, R. K.; Rowland, J. M.; Olmstead, M. M.; Mascharak, P. K. *Angew. Chem. Int. Ed.* **2003**, *42*, 4517.

(69) Walker, F. A.; Lo, M.-W.; Ree, M. T. *J. Am. Chem. Soc.* **1976**, *98*, 5552.

(70) Clarkson, S. G.; Basolo, F. *Inorg. Chem.* **1973**, *12*, 1528.

(71) Nakamoto, K., *Infrared and Raman Spectra of Inorganic and Coordination Compounds*. John Wiley & Sons: New York, 1986.

(72) *SMART v5.626: Software for the CCD Detector System*. Bruker AXS: Madison, WI, 2000.

(73) Walker, N.; Stuart, D. *Acta Crystallogr. A* **1983**, *A39*, 158.

(74) Sheldrick, G. M. *SADABS, Area Detector Absorption Correction*, University of Göttingen: Göttingen, Germany, 2001.

(75) Sheldrick, G. M. *SHELX-97, Program for Refinement of Crystal Structures*, University of Göttingen: Göttingen, Germany, 1997.

(76) Sheldrick, G. M. *Acta Crystallogr. A* **2008**, *A64*, 112.

(77) Sheldrick, G. M. *SHELXTL 6.1, Crystallographic Computing System*, Siemens Analytical X-Ray Instruments: Madison, WI, 2000.

(78) Cromer, D. T.; Waber, J. T., *International Tables for X-Ray Crystallography, Vol. IV, Table 2.2B*. The Kynoch Press: Birmingham, England, 1974.

(79) Burnett, M. N.; Johnson, C. K. *ORTEP-III, Report ORNL-6895*, Oak Ridge National Laboratory: Oak Ridge, TN, 1996.

(80) George, G. N.; George, S. J.; Pickering, I. J., EXAFSPAK, Stanford Synchrotron Radiation Lightsource, Menlo Park, CA. http://www-ssrl.slac.stanford.edu/~george/exafspak/exafs.htm. 2001.

(81) Cook, J. D.; Kondapalli, K. C.; Rawat, S.; Childs, W. C.; Murugesan, Y.; Dancis, A.; Stemmler, T. L. *Biochemistry* **2010**, *49*, 8756.

(82) Synergy Software, KaleidaGraph 4.1.3: [data analysis-graphing application: for Macintosh and Windows operating systems] http://www.synergy.com. 2011.

(83) Randall, C. R.; Shu, L.; Chiou, Y.-M.; Hagen, K. S.; Ito, M.; Kitajima, N.; Lachicotte, R. J.; Zang, Y.; Que Jr., L. *Inorg. Chem.* **1995**, *34*, 1036.

(84) Riggs-Gelasco, P. J.; Stemmler, T. L.; Penner-Hahn, J. E. *Coord. Chem. Rev.* **1995**, *144*, 245.

CHAPTER 3

SYNTHESIS OF Co^{II}-NO^{-} COMPLEXES AND THEIR REACTIVITY AS A SOURCE OF NITROXYL[1]

[1] Walter, M. R.; Dzul, S. P.; Rodrigues, A. V.; Stemmler, T. L.; Telser, T.; Conradie, J.; Ghosh, A.; Harrop, T. C. Submitted to the *Journal of the American Chemical Society*, 06/08/2016.

3.1 Abstract

Metal-nitroxyl (M-HNO/M-NO^-) coordination units are found in denitrification enzymes of the global nitrogen cycle, and free HNO exhibits pharmacological properties related to cardiovascular physiology that are distinct from nitric oxide (NO). To elucidate the properties that control the binding and release of coordinated nitroxyl or its anion at these biological metal sites we synthesized $\{CoNO\}^8$ (**1**, **2**) and $\{CoNO\}^9$ (**3**, **4**) complexes that contain diimine-dipyrrolide supporting ligands. Experimental (NMR, IR, MS, EPR, XAS, XRD) and computational data (DFT) support an oxidation state assignment for **3** and **4** of high spin Co^{II} (S_{Co} = 3/2) coordinated to $^3NO^-$ (S_{NO} = 1) for S_{tot} = 1/2. As suggested by DFT, upon protonation, a spin transition occurs to generate a putative $\{CoHNO\}^9$ containing a low spin Co^{II}-^{1}HNO (S_{Co} = S_{tot} = 1/2); the Co-NO bond is ~0.2 Å longer, more labile, and facilitates the release of HNO. This property was confirmed experimentally through the detection and quantification of N_2O (~70% yield), a byproduct of the established HNO self-reaction ($2HNO \rightarrow N_2O + H_2O$). Additionally, **3** and **4** function as HNO donors in aqueous media at pH 7.4 and react with known HNO targets such as a water-soluble Mn^{III}-porphyrin ($[Mn^{III}(TPPS)]^{3-}$; TPPS = *meso*-tetrakis(4-sulfonatophenyl)porphyrinate) and ferric myoglobin (metMb) to quantitatively yield $[Mn(TPPS)(NO)]^{4-}$ and MbNO, respectively.

3.2 Introduction

Metal-nitroxyl (HNO/NO^-, $pK_a = 11.6$[1]) complexes represent critical intermediates in the global nitrogen cycle, and inhibited states of metalloenzymes that lead to a variety of disorders.[2-4] For example, Fe-HNO intermediates are generated in the reduction of nitric oxide (NO) to nitrous oxide (N_2O) as a detoxification path in fungal[5-7] and bacterial NO reductases.[8] Cytochrome *c* nitrite reductase (C*c*NiR)[9-10], responsible for the six-electron reduction of NO_2^- to NH_3, goes through two Fe-nitroxyl intermediates, designated as $\{FeNO\}^8$ in the notation by Enemark and Feltham.[11] The extent of the Fe-NO_x π-backbonding in C*c*NiR prevents the release of any NH_xO_y intermediates during catalysis.[10] HNO-bound myoglobin (MbHNO) has also been well documented, likely due to its uncommon stability.[12-13] In addition to Fe proteins, cobalamins (Cbl), which serve as cofactors for vitamin B_{12}-dependent enzymes such as methionine synthase and methylmalonyl CoA-mutase,[14] are known to react with NO and HNO to form the corresponding $\{CoNO\}^8$ complex NOCbl.[15-19] Indeed, inhibition and/or deficiency of Cbl, which results from interactions with NO amongst other reasons, has been shown to lead to megaloblastic anemia or neurological disorders.[20-21]

In addition to representing intermediates in NO_x reduction, the pharmacological roles of HNO are rapidly emerging.[22-24] Despite its structural similarity, nitroxyl has therapeutic advantages distinct from NO,[25-27] probably due to its preference for thiols and Fe^{III}-hemes. For example, HNO increases heart muscle strength (positive cardiac inotrope; increases myocardial contractility) and plasma levels of calcitonin gene-related peptide (CGRP), whose cardiovascular effects include vasodilation.[26-27] As a result, nitroxyl has been looked to as a promising cardiovascular therapeutic. While the endogenous formation of HNO has yet to be firmly established, possible candidates include NO synthase (in the absence of its cofactor),[28] thiol-

containing species such as H_2S[29-31] or $SSNO^-$,[32] and anti-oxidants such as tyrosine and ascorbate.[33] Unfortunately, the rapid self-reaction ($k = 10^6$ M^{-1} s^{-1})[34] of HNO to N_2O and H_2O makes its detection challenging. Moreover, the instability of HNO necessitates the use of donor molecules.[35-37]

Several classes of HNO donors, both organic and inorganic, have been employed in research and even clinically. For example, Angeli's Salt ($Na_2N_2O_3$), which generates HNO and NO_2^- at physiological pH, is the most studied and utilized donor.[23,35,38] Cyanamide (H_2N-C≡N) is a drug that is used as an anti-alcoholism agent;[39-40] it is oxidatively bioactivated by catalase and releases HNO and CN^- as a by-product. The mechanism of action is the inhibition of aldehyde dehydrogenase, an enzyme that is vital to metabolism of ethanol, resulting in elevated blood acetaldehyde levels. Although a number of such donors have been found effective, each is condition-dependent and has limitations that hinder its widespread utility, including concomitant release of undesirable by-products (e.g., NO_2^-, CN^-), short half-lives, or ineffective release of HNO under physiological conditions.[23,26] Thus, there is a clear need for more effective HNO delivery agents.[26,35]

Given that metal sites appear to be biological HNO targets and potential HNO sources, our lab has initiated a program aimed at elucidating the structural, electronic, and reactive properties of metal-coordinated nitroxyls, formally $\{MNO\}^8$, through the synthesis of coordination complexes that resemble biological active sites.[41-42] The objectives are two-fold: (i) to assess the ability of these systems to release HNO under physiological conditions; and (ii) to provide insight into the fundamental M-NO bonding properties in denitrifying enzymes that convert NO_x into reduced and bioavailable nitrogen compounds. We have previously communicated the five-coordinate (5C) $\{CoNO\}^8$ complex, [Co(LN_4^{PhCl})(NO)] (LN_4^{PhCl} = dianion of (N^1E,N^2E)-N^1,N^2-

bis((1H-pyrrol-2-yl)methylene)-4,5-dichlorobenzene-1,2-diamine, see Scheme 3.1), that exhibits H^+-induced release of nitroxyl in organic solvents.[43] To realize HNO-release in water, we have synthesized and characterized the one-electron reduced $\{CoNO\}^9$ complexes in the present account (Scheme 3.1). While numerous $\{CoNO\}^8$ complexes exist,[41,43-54] few[53,55-58] describe NO release prior to our work. Furthermore, the $\{CoNO\}^9$ state is rare, with the exception of a few isolated tetrahedral complexes containing ligated carbonyls,[59-60] tris-pyrazolyl borates,[61-62] tris(2-diphenylphosphinoethyl)amines,[63-64] and one complex bearing an *N*-confused porphyrin.[65] However, the reaction chemistry of $\{CoNO\}^{8/9}$ systems is underexplored. Herein we report the synthesis and properties of 5C $\{CoNO\}^9$ complexes via a combined experimental and theoretical approach. Our results point to a high spin (HS) Co^{II}-$^3NO^-$ assignment for $\{CoNO\}^9$, which changes to low spin (LS) Co^{II}-^{1}HNO upon protonation of the NO ligand. Most notably, the reported $\{CoNO\}^9$ complexes demonstrate the release of nitroxyl to Mn^{III}-P complexes (P = porphyrin) and Fe^{III}-myoglobin (metMb) in water at pH 7.4.

Scheme 3.1. Synthesis and Interconversion of $\{CoNO\}^8$ and $\{CoNO\}^9$ complexes. R = H for **1**, **3**; R = Cl for **2**, **4**.

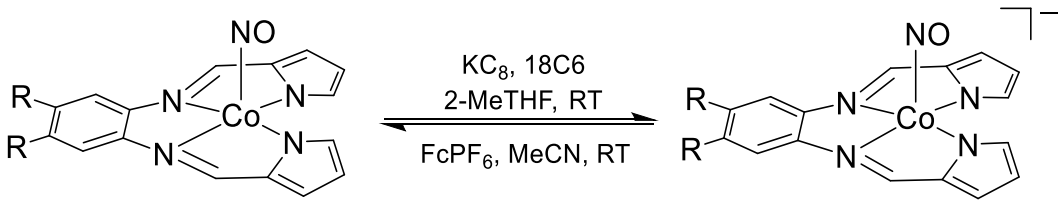

$\{CoNO\}^8$ (**1**, **2**)

$[Co(LN_4^{Ph})(NO)]$ (**1**)

$[Co(LN_4^{PhCl})(NO)]$ (**2**)

$\{CoNO\}^9$ (**3**, **4**)

$[K(18C6)][Co(LN_4^{Ph})(NO)]$ (**3**)

$[K(18C6)][Co(LN_4^{PhCl})(NO)]$ (**4**)

3.3 Synthesis and Spectroscopy of {CoNO}^{8} Complexes

The {CoNO}^{8} complexes [Co(LN_4^{Ph})(NO)] (**1**) (LN_4^{Ph} = dianion of (*N*^{1}*E*,*N*^{2}*E*)-*N*^{1},*N*^{2}-bis((1H-pyrrol-2-yl)methylene)-benzene-1,2-diamine) and [Co(LN_4^{PhCl})(NO)] (**2**)[43] were synthesized in ~80% yield by direct purge of NO(g) into MeCN solutions of the parent Co^{II}-LN_4^R complexes. Peripheral variations on the phenylene-diimine unit were made to explore ligand inductive effects on the redox properties of the Co-nitrosyls. Their structure and purity were confirmed by a variety of spectroscopic techniques as well as elemental analysis and X-ray crystallography (vide infra). For example, the FTIR spectrum of **1** displayed a strong double-humped ν_{NO} band at 1667 cm^{-1} and 1656 cm^{-1} (KBr) that shifted to 1641 cm^{-1} ($\Delta\nu_{NO}$: 26 cm^{-1}) and 1628 cm^{-1} ($\Delta\nu_{NO}$: 28 cm^{-1}) upon isotopic substitution with ^{15}NO(g) (see Figure 3.S1 in the supporting information = SI). The morphology of the ν_{NO} peak in **1** is attributed to a disordered nitrosyl, which is seen in the X-ray structure (Figure 3.S4). The ^{15}N NMR of the ^{15}N-labeled complex (**1-^{15}NO**) in THF-d_8 exhibited one ^{15}N peak at 675 ppm (vs. CH_3NO_2) and is consistent with a bent metal-nitrosyl, i.e., Co-N-O of ~125° (Figure 3.S3).[66] As noted with other 5C square-pyramidal {CoNO}^{8} complexes,[41,43-54] these properties suggest a general assignment of LS-Co^{III} (S_{Co} = 0) coordinated to singlet nitroxyl anion $^1NO^-$ (S_{NO} = 0) for an overall diamagnetic ground state. We note that the resonance structure LS-Co^{III}-$^1NO^-$ ↔ LS-Co^{II}-NO• has also been evoked for the {CoNO}^{8} unit in NOCbl.[15]

3.4 {CoNO}^{8} Structural Properties

Analogous to **2** and other 5C {CoNO}^{8} complexes,[41,43-54] the structure of **1** indicates a square-pyramidal (τ = 0.013[67]) Co with a mostly planar N_4 ligand and an axially bound NO (Figure 3.1, Tables 3.S1-3.S2). Co is displaced by 0.242 Å out of the plane of the N_4 ligand with Co-N(O)

(1.804 Å) and N-O (1.162 Å) bond lengths typical for this class of metal-nitrosyls. For comparison, the N-O bond distance in **1** and **2** (1.162, 1.172 Å, respectively) is in between NO• (1.15 Å) and ^{1}HNO (1.21 Å) and suggests some degree of delocalization in the Co-N-O bond.[44] It appears that the range of N-O bond lengths observed in the majority of 5C pyramidal $\{CoNO\}^{8}$ (1.15-1.20 Å) advocates for an NO^{-} oxidation state, which is reflected in the bent Co-N-O angle, 124.9°. The bent Co-N-O observed in the structure of **1** and other $\{CoNO\}^{8}$ complexes is consistent with sp^{2} hybridization of the nitrosyl nitrogen, which is also in-line with the solution-state ^{15}N NMR spectrum (vide supra).

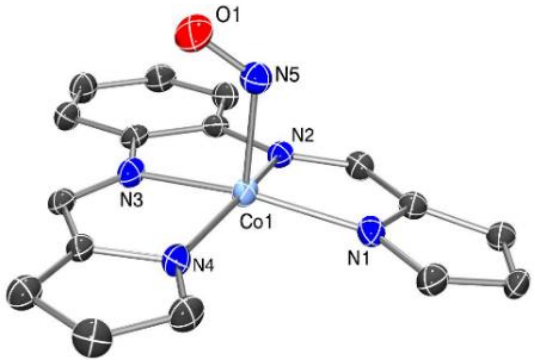

Figure 3.1. X-ray structure of [Co(LN_4^{Ph})(NO)] (**1**) at 50% thermal probability for all non-hydrogen atoms. Hydrogen atoms and second unique molecule in unit cell have been omitted for clarity.

3.5 Electrochemical Properties

The cyclic voltammogram (CV) of **1** was measured in MeCN and is reported versus the ferrocene/ferrocenium (Fc/Fc^{+}) couple. The CV of **1** displays a reversible $\{CoNO\}^{8}/\{CoNO\}^{9}$ couple at -1.39 V (Figures 3.S5-3.S7). Other irreversible peaks observed in the CV are attributed to ligand-based redox events (Figure 3.S5). Comparisons can be made with related Co-NO

complexes and with metal-nitrosyls that also contain dianionic planar ligands. For example, **1** exhibits an $E_{1/2}$ value that is shifted by -0.11 V from **2**, which contains a more electron-deficient N_4 ligand. This result is consistent with the shift in the $\{FeNO\}^7/\{FeNO\}^8$ couple observed in the Fe analogues reported previously by our lab.[42] Additionally, the $\{CoNO\}^8/\{CoNO\}^9$ couple is readily modulated by changes beyond the ligand periphery. Indeed, attachment of $W(CO)_4$ to the coordinated thiolates in a $Co(N_2S_2)(NO)$ complex results in a dramatic +0.49 V shift in $E_{1/2}$.[51] Overall, the reversible $\{CoNO\}^{8/9}$ couple of **1**, **2**, and other $\{CoNO\}^8$ complexes[41,43,51-52] highlight the potential for accessing one-electron reduced $\{CoNO\}^9$ complexes.

3.6 $\{CoNO\}^9$ Synthesis and Properties

$\{CoNO\}^9$ complexes were synthesized by adding stoichiometric KC_8 to a 2-MeTHF solution of **1** or **2** containing 18-crown-6 ether (18C6) (Scheme 3.1). Accordingly, the $\{CoNO\}^9$ complexes [K(18C6)][Co(LN_4^{Ph})(NO)] (**3**) and [K(18C6)][Co(LN_4^{PhCl})(NO)] (**4**) were obtained in analytically pure form in 70 and 82% yields, respectively. The isolated brown $\{CoNO\}^9$ complexes could also be converted back to the corresponding $\{CoNO\}^8$ complexes **1** and **2** by addition of oxidants such as Fc^+ (Scheme 3.1).

Spectroscopic analysis confirmed the $\{CoNO\}^9$ assignment for **3** and **4**. The FTIR spectrum of **3** exhibited a ν_{NO} band at 1609 cm^{-1} that shifted to ~1580 cm^{-1} in **3-^{15}NO** ($\Delta\nu_{NO}$ = 28 cm^{-1} from **3**; Figures 3.S8-3.S9) whereas **4** exhibited ν_{NO} at 1617 cm^{-1}. Values of ν_{NO} for **3** and **4** resemble those reported for other $\{CoNO\}^9$ complexes.[52,59-65] The ν_{NO} of **4-^{15}NO** overlaps significantly with ligand C=N stretches making a definitive assignment difficult (Figure 3.S10). Similar complications in identifying ν_{NO} have also been observed in an $\{FeNO\}^8$ porphyrin complex due to overlapping ligand vibrations.[68] Regardless, ν_{NO} peaks of **3** and **4** are ~50 cm^{-1}

red-shifted from the $\{CoNO\}^8$ analogs, a shift which is consistent with a Co-centered reduction. In comparison, reduction of coordinated NO generally results in a dramatic ν_{NO} red-shift (~100-200 cm^{-1}) as observed in the reduction of $\{FeNO\}^7$ complexes to $\{FeNO\}^8$.[2,4,69-70] Moreover, ligand-based redox events to generate pyrrolide radicals[71] can be eliminated based on EPR data (vide infra). High resolution mass spectrometry (HRMS) experiments provide additional evidence for the formation of **3** and **4**. For example, the molecular ion peak $[M]^-$ for **3** is observed at *m/z:* 349.037 (calcd. *m/z*: 349.037) with the appropriate isotopic distribution (Figure 3.S11). HRMS on the ^{15}N isotopologue **3-^{15}NO** (calcd. *m/z*: 350.034; obsvd. *m/z*: 350.035) further supports the predicted formulation (Figure 3.S12). HRMS also confirm formation of **4** and **4-^{15}NO** (Figures 3.S13-3.S14).

3.7 EPR of $\{CoNO\}^9$ Complexes

X-band (9.60 GHz) measurements of **3** and **4** reveal an asymmetric coordination environment with significant nuclear hyperfine coupling (hfc) from the ^{59}Co nucleus (I = 7/2) whereas the ^{14}N splitting is minimal (Figure 3.2; Figure 3.S15). The large ^{59}Co hfc differs from EPR of Co^{II}-O_2 complexes[72-73] and from typical LS-Co^{II} where the unpaired electron (upe) is in the d_{z2} orbital, leading to $g_\perp > g_\parallel \approx 2.0$, large $A_\parallel(^{59}Co)$, and small $A_\perp(^{59}Co)$.[74-76] For example, the spin Hamiltonian parameters of $[Co^{II}(OEP)L]$ complexes (where OEP = octaethylporphyrin; L is a wide range of N-donors, e.g., py, Im), in which the upe resides in the d_{z2} orbital, were reported with $g_\perp = 2.315 \pm 0.010$ with $A_\parallel(^{59}Co)$ = 225 - 240 MHz (~80 - 85 G) and $g_\parallel = 2.03 \pm 0.01$ where $A_\perp(^{59}Co)$ is small (< 10 MHz, 3 G) and unresolved.[74] Contrastingly, **3** and **4** exhibit $g_\parallel > g_\perp$ ($g_\parallel$ = 2.269, $g_\perp$ = 2.080(2); $g_\parallel$ = 2.278(2); $g_\perp$ = 2.078(2), respectively) and both $A_{\parallel,\perp}$ values are large (~350 MHz and ~200 MHz, respectively) (Figure 3.2). This result indicates the upe being

predominantly in the d_{x2-y2} orbital,[77] resembling what is commonly seen in square-planar/pyramidal Cu^{II} complexes.[78-79] Further support of a d_{x2-y2} upe is shown in the proposed frontier MOs (vide infra) and in comparison to other M-NO systems. In a cyclam-ligated $\{FeNO\}^6$ complex, calculations of frontier MOs using spin-restricted B3LYP suggest the NO-π^* orbital is lower in energy than the nearby d_{x2-y2} orbital.[80] In contrast to the $\{FeNO\}^6$ case, it is likely that the NO-π^* orbital in **3** and **4** is higher in energy than d_{x2-y2} due to stronger π-bonding in Co-N versus Fe-N. Due to the high covalency of the Co-N(O) bond, the effect of the equatorial N-ligands can be detected by inspection of EPR linewidths.[81] The X-band EPR of the isotopologues **3-^{15}NO** and **4-^{15}NO**, exhibit no significant effect from labeling on the ^{59}Co hfc, although there is an increase in the EPR linewidths, indicative of unresolved ^{14,15}N hfc.

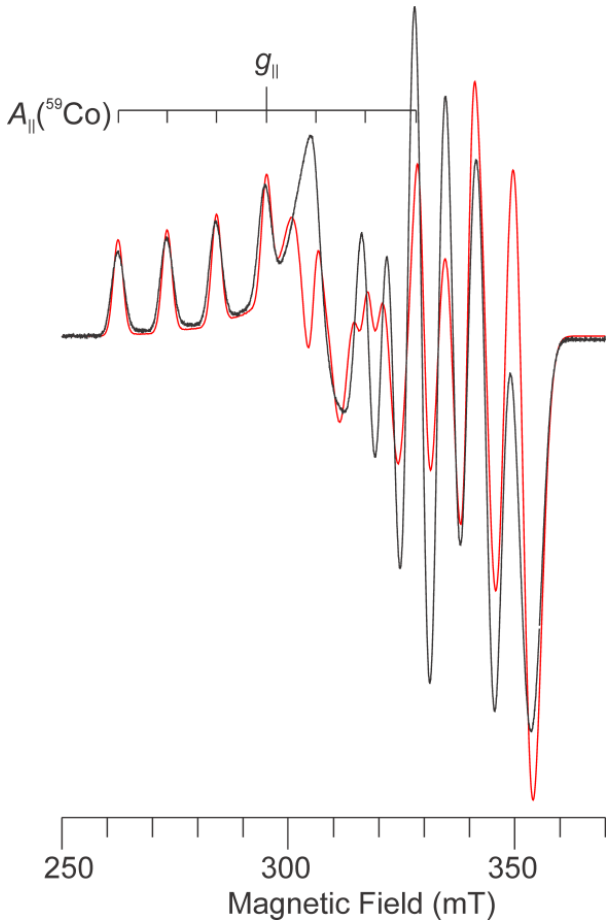

Figure 3.2. X-band EPR spectrum of **3** in 2-MeTHF at 10 K (black) with simulation (red). Spectrometer settings: microwave frequency, 9.582 GHz; microwave power, 1.0 mW; modulation frequency, 100 kHz; modulation amplitude, 6.48 G. Simulation parameters: S_{tot} = 1/2, $g_{\perp}$ = 2.080(2), $g_{||}$ = 2.269, $A_{\perp}(^{59}Co)$ = 200 MHz, $A_{||}(^{59}Co)$ = 355 MHz, single crystal Gaussian linewidths, $W_{\perp}$ = 80 MHz, $W_{||}$ = 40 MHz (half-width at half-maximum).

The X-band EPR is modelled as perfectly axial; as such, higher frequency EPR (Q-band; 35 GHz) was recorded in order to obtain better dispersion of the *g*-values (which are field-dependent). However, the field-independent hfc is more readily determined from lower frequencies (X-band, or even lower (S- or L-band)[82] EPR). This multifrequency approach has been

pervasive for Cu^{II} complexes,[83] but only recently applied to LS-Co^{II} species.[84] The Q-band EPR corroborates the X-band measurement (Figure 3.S16), and resolution of slight rhombic splitting is attainable with the higher frequency. The Q-band spectrum of **3** (200(10), 200(10), 345(5); W = 130 MHz) was simulated with the same $A(^{59}Co)$ values as in the X-band data (200(5), 200(5), 355, W_{xy} = 80 MHz), and the $g_{\perp}$ used in the X-band simulation (2.080(2)) is exactly the average of the Q-band $g_{x,y}$ values (2.06(1), 2.10(1)) (Figure 3.S16). It is important to note that even at Q-band, $\{CoNO\}^9$ complexes **3** and **4**, comprising the two different ligands LN_4^{Ph} and LN_4^{PhCl}, respectively, give identical EPR spectra.

3.8 X-ray Absorption Spectroscopy (XAS) of $\{CoNO\}^{8/9}$ Complexes

The XAS data confirm the crystallographic results of **1** (Figures 3.3 - 3.4). In the X-ray absorption near edge spectrum (XANES), the lowest energy pre-edge peak occurs at 7710.1 eV, which corresponds to a symmetry-forbidden 1s→3d transition. The relatively large area under this transition (0.44 eV) is consistent with an increased distortion in bond symmetry that permits mixing of 3*d* and 4*p* orbitals in the formation of a LS 5C Co complex.[85] The first inflection point of the XANES is shifted to higher energy relative to the Co^{II} control, which is indicative of reduced electron density on the metal and more consistent with a Co^{III} oxidation state in **1**. Simulations of the extended X-ray absorption fine structure (EXAFS) region show an average bond length in the nearest neighbor environment for **1** of 1.88 Å, constructed of five O/N ligands (spectral resolution: 0.12 Å) (Figure 3.4). This value compares well with the distances determined from X-ray crystallography (avg: 1.89 Å, Table 3.S2). The XAS of **2** is also comparable to **1**.[43]

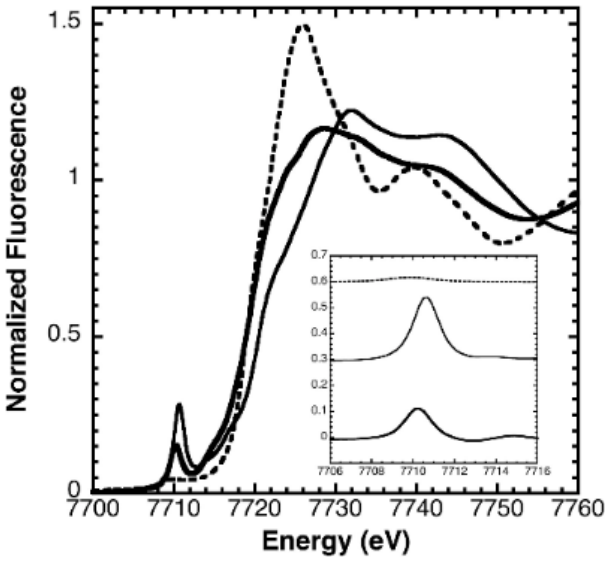

Figure 3.3. XANES for $\{CoNO\}^8$ **1** (normal), $\{CoNO\}^9$ **3** (bold), and $[Co^{II}(H_2O)_6](NO_3)_2$ (dotted). Inset: baseline subtracted expansion of 1s→3d pre-edge features for **1**, **3**, and Co^{II} control (coloring same as full XANES).

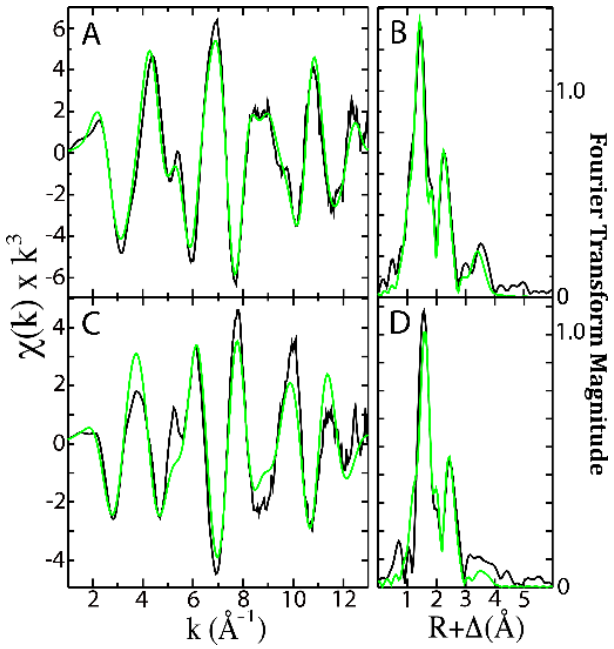

Figure 3.4. Raw (panels A, C) and Fourier transformed EXAFS (panels B, D) (black) of $\{CoNO\}^8$ **1** (top) and $\{CoNO\}^9$ **3** (bottom) with best fit simulation (green).

The XAS of **3** shows distinct features that correspond to a Co-centered reduction when going from $\{CoNO\}^8$ to $\{CoNO\}^9$. The XANES region of the spectrum displays a 1s→3d pre-edge feature at 7709.7 eV for **3** (shifted -0.4 eV from **1**) and is nearly identical in position to the pre-edge feature of the Co^{II} control (Figure 3.3), suggesting a Co^{II} center in **3**. The 1s→3d feature in this region has also been observed in a tetrahedral $\{CoNO\}^9$ complex[62] and other 5C/6C Co^{II} complexes.[85-86] The area under this transition is an indication of the symmetry about the Co center. In general, more centrosymmetric complexes exhibit weaker 1s→3d transitions. Indeed, the area of the pre-edge feature of **3** (0.18 eV) is less than in **1** (0.44 eV), which suggests a more symmetric coordination environment in **3** versus **1** (Figure 3.3). Either a change in coordination geometry (centrosymmetric, e.g., octahedral or square-planar) or spin-state could explain the weaker pre-edge intensity. However, EPR in combination with EXAFS (vide infra), eliminate a geometry change. For example, octahedral and planar Co^{II} complexes exhibit very weak 1s→3d peaks with areas ranging from 0.050-0.061 eV.[87] Additionally, the EPR is clearly consistent with an $S = ½$ species and spectra of the ^{15}NO-isotopologues show no significant change, suggesting the majority of the spin-density is on Co.[62] As the EXAFS and computational (vide infra) results confirm, a 5C coordination sphere is retained in **3** and **4**. Thus, the symmetry difference between **1** and **3** is likely associated with a change in the Co-N-O bond angle from bent (~125°) in $\{CoNO\}^8$ (**1**, **2**) to less bent but still not linear (140-150°) in $\{CoNO\}^9$ (**3**, **4**).

Simulations of the EXAFS region of **3** show an average bond length of 2.06 Å constructed of 4 ± 1 O/N ligands (Figure 3.4, Table 3.S3). Based on the large Debye-Waller factor ($\sigma^2 = 4.14 \times 10^3$ Å^2) in the nearest neighbor fit for **3**, there is a higher level of metal-ligand bond disorder for this system, which explains the abnormally low apparent metal-ligand coordination number. Furthermore, based on the chemical reversibility of the **3**-to-**1** conversion, a 5C Co is still expected

in **3**. This average distance compares well with distances determined from EXAFS analysis of other N-ligated Co^{II} complexes, such as Co-substituted ferric uptake regulatory protein[88] and Co^{II}-substituted alcohol dehydrogenase.[89] The EXAFS also indicate there is an increase in the Co-ligand distances between $\{CoNO\}^8$ **1** and $\{CoNO\}^9$ **3** of 0.18 Å, a shift which is again consistent with a metal-based reduction. Similar metric changes are also observed for **4** (see Table 3.S3).

3.9 Theoretical Modeling

Density functional theory (DFT) calculations provide a satisfactory theoretical framework for understanding many of the properties of the $\{CoNO\}^9$ state outlined above.[90-91] The assumption of C_s symmetry allowed us to investigate at least two different states. All-electron occupation 1 ($\alpha||\beta$: A′ 61||60, A″ 45||45) corresponds to a LS d^7 Co^{II} state with the 8th and 9th electrons (Enemark-Feltham count) added to a ligand (NO π* or other) orbital (Figure 3.S19).[92] Occupation 2 ($\alpha||\beta$: A′ 60||60, A′′ 46||45) is described as a HS Co^{II}–NO^- state with a singly occupied d_{x2-y2} orbital (Figure 3.5). All functionals tested (BP86, OLYP, B3LYP) indicate occupation 2 as the ground state, in agreement with the EPR data, albeit by different margins of energy, relative to occupation 1 (Figure 3.S19). Some of the key calculated properties of occupation 2 follow.

Single occupancy of the d_{x2-y2} orbital resulted in relatively long equatorial Co-N distances of about 2.1 Å, relative to occupation 1 and the $\{CoNO\}^8$ state (Co-N: 1.9 Å; see Figure 3.S20), in agreement with the EXAFS results. This orbital occupancy is also responsible for a substantial displacement of the metal (~0.7 Å) above the N_4 plane of the ligand, a structural effect that remains to be observed experimentally. The Co-N(O) bond length is 1.692 Å, essentially unchanged from the $\{CoNO\}^8$ state. Another significant structural change is the less bent nature of Co-N-O (144.9°) in $\{CoNO\}^9$, which explains the intensity change of the 1s→3d feature in the XAS.

The spin density profile for occupation 2 is characterized by a full unpaired electron in the d_{x2-y2} orbital, smaller amounts of positive spin density in the d_{xz} and d_{yz} orbitals, and a significant amount of negative spin density on the NO distributed in a cylindrically symmetric manner about the N-O axis (Figure 3.5). These spin populations are strongly indicative of HS Co^{II}, ($S_{Co} = 3/2$) with a $(d_{xy})^2(d_{z2})^2(d_{xz})^1(d_{yz})^1(d_{x2-y2})^1$ configuration, antiferromagnetically coupled to an NO^- diradical ($S_{NO} = 1$).

The spin-density profiles obtained with the three functionals differ somewhat. As noted before, the hybrid functional B3LYP resulted in the largest separation of α and β spin density, the classic pure functional BP86 resulted in the smallest such separation, and the comparatively newer OLYP functional separated the α and β spins to an intermediate degree. Despite the quantitative differences, the fact that all three functionals indicate occupation 2 as the ground state may be viewed as powerful evidence in support of our electronic structural description. As mentioned, this description is fully consistent with the conclusion from XAS and EPR.

DFT (OLYP) calculations on the Co-HNO complex indicate a low-spin d_{z2}^1 Co^{II} ground state axially coordinated to a closed shell HNO (Figure 3.5). The singly occupied molecular orbital (SOMO) represents a σ-antibonding interaction between the Co d_{z2} (43.4%) and NO p_z (17.7%). Such an electronic description is consistent with a longer Co-N(O) (1.891 Å) and N-O (1.229 Å), and shorter equatorial Co-N (avg: 1.937 Å), relative to the $\{CoNO\}^9$ state (Figures 3.5, 3.S21). The lengthening of Co-N(O) is important, as it primes the HNO for dissociation and further reactivity, and reflects the relatively weak π-acceptor ability of HNO (compared with NO) as well as the antibonding nature of the SOMO. The calculations did not reveal any other low-energy states for the Co-HNO complex; assumption of $M_S = 3/2$ led to a high-spin Co^{II} ~0.5 eV above the ground state.

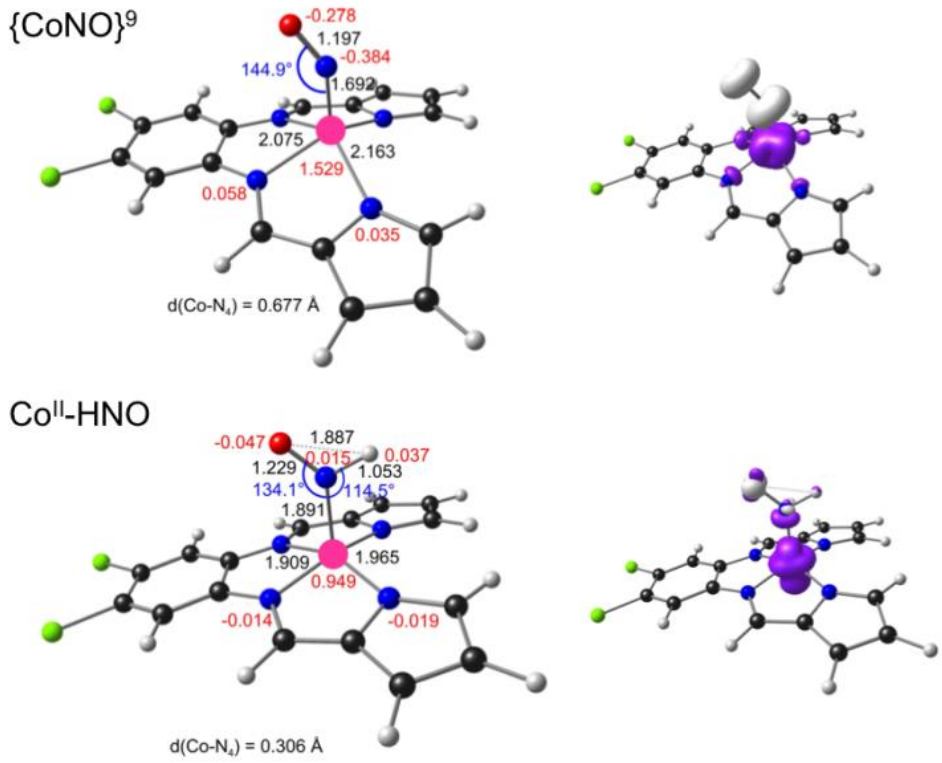

Figure 3.5. Selected OLYP/TZP results for the lowest-energy $\{CoNO\}^9$ (top) and Co^{II}-HNO (bottom) states: optimized structures on the left with distances (Å, black), angles (deg, blue), and Mulliken spin populations (red); spin density profiles on right.

3.10 Nitroxyl-Relevant Reactivity in Water

3.10.1 Reaction of $\{CoNO\}^9$ Complexes with H^+ and formation of HNO

Given the fast self-reaction of nitroxyl[34] to form N_2O and water (vide supra), N_2O serves as an indirect marker for HNO, and its presence provides evidence of the formation and liberation of HNO from the reported CoNO complexes.[93] After addition of HBF_4•Et_2O to $\{CoNO\}^9$ (**3**) in H_2O (10:1), the reaction headspace revealed IR bands consistent with the P- and R-branches of N_2O at 2236 and 2208 cm^{-1} that shift to 2167 and 2145 cm^{-1} when using the ^{15}NO isotopologue (Figure 3.6).[8,94-95] Indeed, the yield of N_2O from **3** was 63 ± 3%, quantified using a calibration

curve with N_2O produced from the HNO donor Piloty's Acid (Figure 3.S22).[96] *Thus, {CoNO}^{9} complexes produce HNO in water*. Notably, no other gaseous ^{15}N-containing species were observed in the IR (Figure 3.S23). Reaction of **3** with HBF_4•Et_2O (1:7) in THF, a solvent in which other products are readily identified, also produces N_2O. Additional species identified in the THF reaction were {CoNO}^{8} **1**, as well as the corresponding tetrahedral dinitrosyl cobalt complex $[Co(LN_4^{Ph}H_2)(NO)_2]BF_4$ (**5**, a {Co(NO)$_2$}^{10} complex; Figures 3.S24-3.S25) via protonation of the pyrrolide-N-donors of LN_4^{2-}.[97] Contrastingly, {CoNO}^{8} complexes (**1**, **2**) are not reactive, likely due to a lower HNO pK_a, and largely H_2O-insoluble, precluding **1** or **2** from effectively releasing HNO in water.[98]

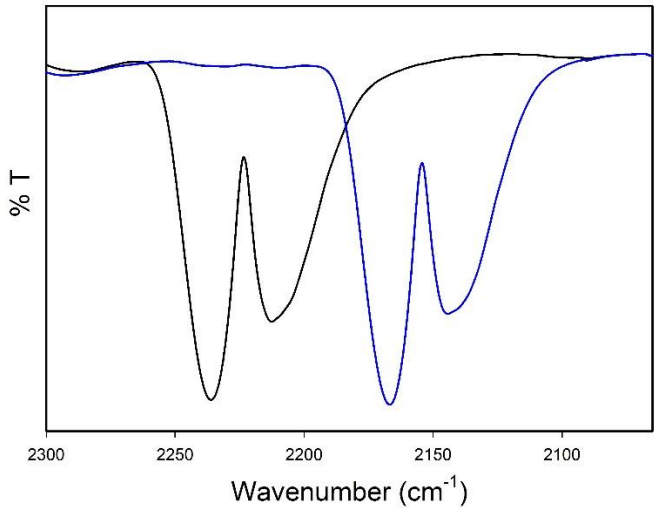

Figure 3.6. Headspace IR of the reaction of HBF_4•Et_2O with **3** (black) or **3-^{15}NO** (blue) (10:1) at t = 24 h. Conditions: DMSO/H_2O (1:9), RT. See Figure 3.S23 for full spectrum.

3.10.2 Reaction of {CoNO}$^{8/9}$ Complexes with a Nitroxyl Target (Mn^{III}-porphyrin)

Based on the high affinity and superior selectivity of HNO for Mn^{III}-P,[99] HNO donor reactions were investigated using water-soluble $[Mn^{III}(TPPS)]^{3-}$ (TPPS = *meso*-tetrakis(4-sulfonatophenyl)porphyrinate; λ_{max} = 467 nm) in phosphate-buffered saline (PBS; pH 7.4) at 298

K. Indeed, the reaction of **3** with $[Mn^{III}(TPPS)]^{3-}$ (5:1) afforded $[Mn(TPPS)(NO)]^{4-}$ (λ_{max} = 424 nm) in 6.5 h with a pseudo first-order rate constant (k_{obs}) of 9.00 ± 3.96 × 10^{-5} s^{-1} (Figure 3.7). In contrast, no reaction was observed between $\{CoNO\}^8$ **1** and $[Mn^{III}(TPPS)]^{3-}$ over a 24 h period under identical conditions (Figure 3.S26). As demonstrated by Doctorovich,[99] the reaction between $[Mn^{III}(TPPS)]^{3-}$ and a large excess of Angeli's Salt occurs with $k_{obs} \sim 10^{-2}$ s^{-1} ($t_{1/2}$: 117 min) at pH 7. Additionally, they demonstrate that $E_{1/2}(Mn^{III}/Mn^{II})$ of Mn-P influences the reaction mechanism with HNO donors, viz. an Mn-P with $E_{½} > 0$ accelerates decomposition of the donor through a donor/Mn-P bonding interaction, whereas an Mn-P with $E_{1/2} < 0$ reacts directly with free HNO after donor decomposition.[100-101] This mechanistic distinction may be facilitated by electrostatics, given the negative charge of HNO donors such as Angeli's Salt and Piloty's Acid. Indeed, when Mn^{III}-P and the HNO donor directly interact, $t_{1/2}$ is on the order of seconds. In contrast, $t_{1/2}$ is on the order of minutes-to-hours when donor decomposition/release of free HNO is the rate-limiting step. The latter occurs when the Mn^{III}-P $E_{½}$ is negative. Taken together, the clean reaction of **3** with $[Mn^{III}(TPPS)]^{3-}$ ($E_{1/2}$ = -0.16 V vs. NHE) to form the $\{MnNO\}^6$ complex over 6.5 h is consistent with production of free HNO from the $\{CoNO\}^9$ platform in **3**.

Given that one of the products of the $\{CoNO\}^9$ **3**/H^+ reaction in THF is the corresponding $\{Co(NO)_2\}^{10}$ complex **5**, we also probed the reaction between **5** and $[Mn^{III}(TPPS)]^{3-}$ (Figure 3.S27). Based on UV-vis spectral monitoring, the reaction of **5** with $[Mn^{III}(TPPS)]^{3-}$ (2.5/1) goes to completion in 21 h. Thus, **5** is capable of reductively nitrosylating Mn^{III}-P and is an alternative HNO donor. This result draws parallels to thiolate-ligated $\{Fe(NO)_2\}^9$ dinitrosyls that have been demonstrated to store and release NO equivalents in a proton-responsive manner.[102-104] However, it appears that $\{CoNO\}^9$ **3** reacts on a slightly faster timescale than its dinitrosyl analogue and is thus an unlikely HNO donor in the aforementioned reaction.

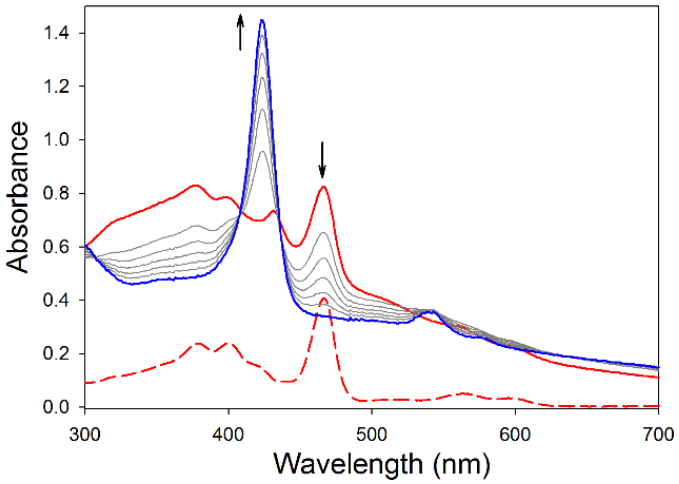

Figure 3.7. UV-vis spectral monitor of a 9.90 µM PBS solution (pH 7.4, 298 K) of $[Mn^{III}(TPPS)]^{3-}$ (red dash) and immediately after addition of **3** (red solid; 5 equiv). Final trace of $[Mn(TPPS)(NO)]^{4-}$ in blue (t = 6.5 h).

3.10.3 Reaction of {CoNO}$^{8/9}$ Complexes with a Biological Nitroxyl Target (metMb)

Biological HNO targets were pursued to assess whether HNO/NO^- coordination occurs with known proteins under aqueous conditions. As such, the reaction of the Co-nitrosyls with equine skeletal metMb was investigated in PBS (pH 7.4) at 310 K. The addition of $\{CoNO\}^9$ **3** to metMb (5:1) afforded nitrosylated myoglobin (MbNO) over 1.5 h based on shifts in the Soret (409 nm → 420 nm) and Q-bands (503 nm, 637 nm → 545 nm, 582 nm; Figure 3.8). Using the ε values of metMb[105-106] and MbNO,[107] formation of MbNO was found to be nearly quantitative (99%) with k_{obs} = 4.88 ± 0.72 × 10^{-4} s^{-1}. The $\{CoNO\}^9$/metMb reaction is slower than the immediate HNO/NO^- transfer that occurs with the analogous $\{FeNO\}^8$ system.[41] For reference, the reaction of Angeli's Salt with sperm whale metMb takes 15.5 min to go to completion,[108] and recently, a dinitrosyl iron complex (DNIC) was shown to form MbNO in 10 min (both at 25 °C).[109] The slower

HNO release of **3** is an advantageous kinetic control that we did not have with the Fe systems. In contrast, there was no reaction between **1** and metMb (Figure 3.S29).

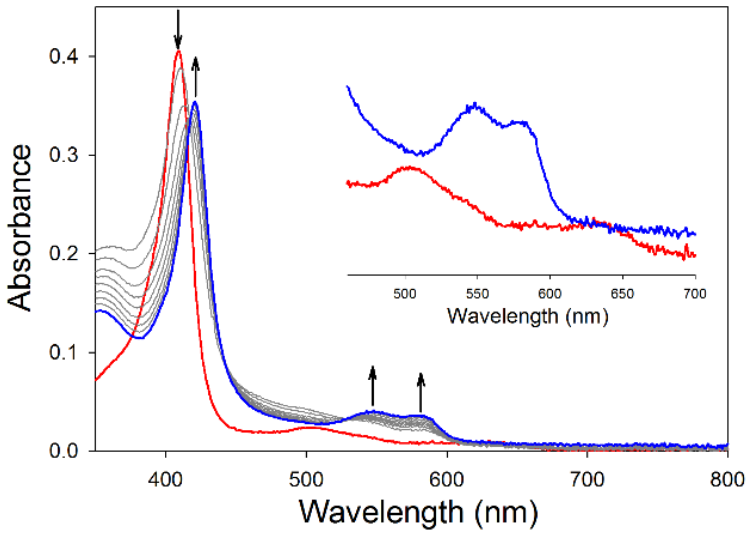

Figure 3.8. UV-vis spectrum of a 2.19 µM solution of equine skeletal muscle metMb before (red) and after 1.5 h (blue) reaction with **3** (5 equiv) at 310 K in PBS (pH 7.4; traces in grey represent 10 min intervals). Inset: expansion of the Q-band region for the initial and final spectrum.

Mechanistically, there is no evidence of a reduced Fe^{II}-Mb intermediate (Soret = 435 nm[105]), although the timescale with which such an intermediate is formed and then nitrosylated could be more rapid than the timescale with which the reaction was monitored (< 1 min). To eliminate the possibility that $\{CoNO\}^9$ reductively nitrosylates metMb by electron-transfer followed by NO• release from $\{CoNO\}^8$, we studied the reaction of $\{CoNO\}^8$ **1** with ferrous myoglobin (deoxyMb). Interestingly, complex **1** is capable of nitrosylating deoxyMb, to form MbNO (Figure 3.S31). However, this reaction is complete soon after mixing the two compounds. If metMb reduction by $\{CoNO\}^9$ occurred before nitrosylation, then the completion time would likely be faster than the observed 1.5 h. Therefore, these results, along with the Mn^{III}-P assay, suggest free HNO transfer from **3**. In contrast to its reaction with Mn^{III}-P, $\{Co(NO)_2\}^{10}$ **5** is not

capable of reductively nitrosylating metMb under identical conditions (24 h), likely a result of electrostatic repulsion between the positively charged metMb and the cationic dinitrosyl (Figure 3.S32).

3.11 Proposed Reaction Pathway

Spectroscopic evidence (^{1}H NMR, IR, MS) of the **3**/H^+ reaction points to free HNO via N_2O in addition to the presence of the Co-nitrosyl **1** and dinitrosyl **5** as major products. A smaller amount of $[Co^{III}L]^+$ and $[Co^{I}L]^-$ is also observed. Several paths that account for these compounds are depicted in Scheme 3.2. In the absence of an HNO target, three competing reactions occur. Reaction A produces free HNO which self-reacts to form N_2O and H_2O. An alternate reaction (B) produces one equiv of $\{CoNO\}^8$ **1** with concurrent evolution of 0.5 equiv of H_2. Reactions analogous to B have been reported[68,110-111] with an $\{FeNO\}^8$ complex to form H_2 and the corresponding $\{FeNO\}^7$. Two of the reactions (B and C) account for the observation of dinitrosyl **5**. We have previously demonstrated that $\{CoNO\}^8$ and H^+ are in equilibrium with $\{Co(NO)_2\}^{10}$ and $[Co^{III}L]^+$ (Scheme 3.2, bottom).[43] The $\{CoNO\}^8$/H^+ equilibrium favors the reactant side under stoichiometric conditions. The other possibility (C) generates **5** with the concomitant production of a $[Co^{I}L]^-$ monoanion. These three competing reactions explain the observed product speciation, diamagnetism, as well as the relative quantities based on NMR integration. Path A is favored with excess H^+ whereas B and C are favored under stoichiometric conditions. Assuming a pK_a of 11 for the Co-coordinated NO,[112] nearly all (99.8%) of the complex is Co-HNO at pH 7.4 and thus reaction A predominates under physiological conditions.

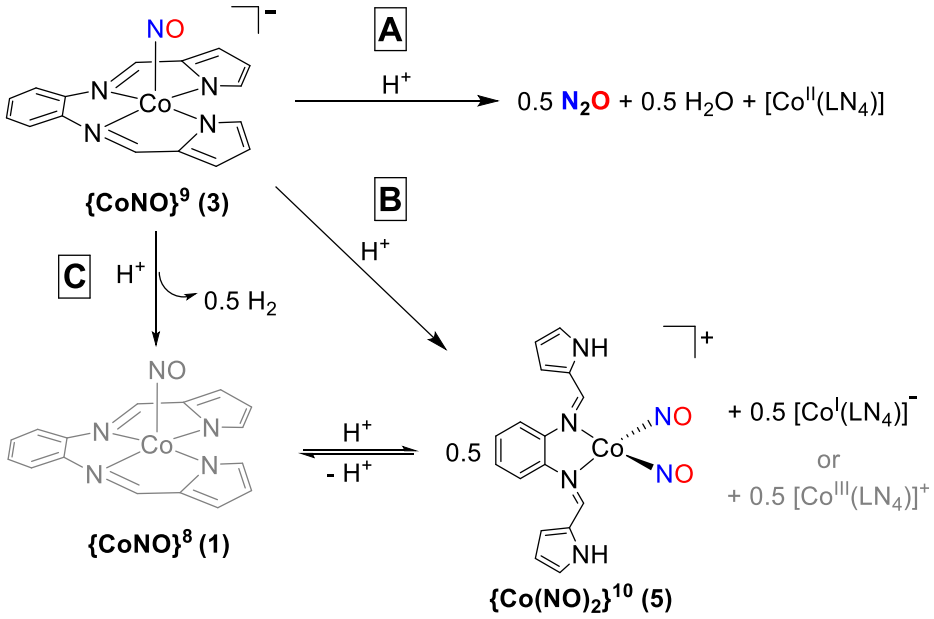

Scheme 3.2. Interconversions of Co nitrosyls upon protonation in the absence of an HNO target. Path A is favored with excess H^+.[97] Grey represents $\{CoNO\}^8/H^+$ path.[43]

The first step towards free HNO is protonation of **3** to form **3-HNO** which, as suggested by DFT, changes the Co from HS to LS, i.e., LS-Co^{II}-^{1}HNO (Scheme 3.3). Protonation leads to elongation of the Co-NO distance by 0.2 Å and labilizes this bond so that HNO can readily dissociate from the $[Co^{II}L]$ platform. HNO can then either (i) form N_2O and/or (ii) react with an HNO target, e.g., $[Mn^{III}(TPPS)]^{3-}$ or metMb. Indeed, in the presence of an HNO target, the free HNO produced from **3** is captured (see Figures 3.6-3.8). As there is no spectral evidence for any intermediates in the $\{CoNO\}^9$ reaction with metMb or Mn^{III}-P, and given the isosbestic behavior, it is likely that free HNO dissociates from Co and reacts with the M^{III}-P center directly.

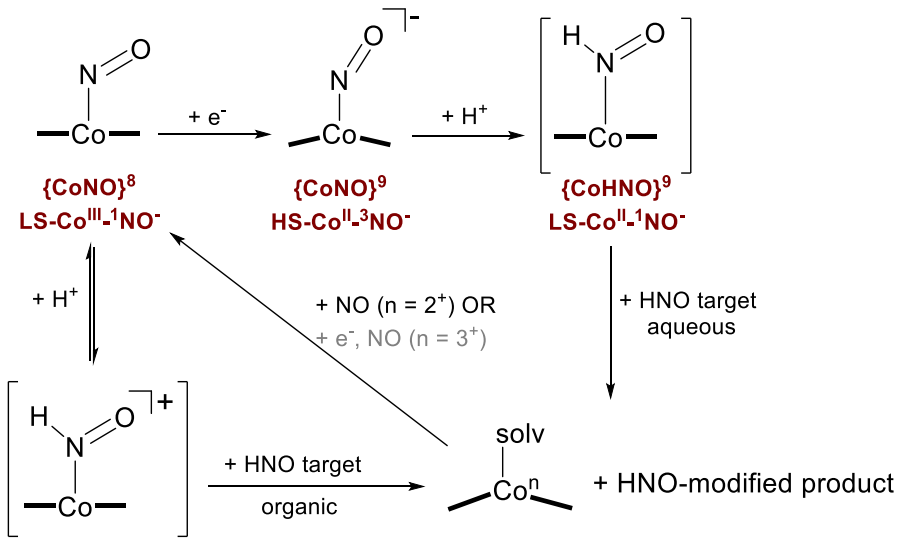

Scheme 3.3. Proposal of HNO-release. Compounds in brackets represent intermediates not isolated or observed spectroscopically in the reaction.

3.12 Conclusions

A combined structural (XAS), spectroscopic (FTIR, EPR, MS) and theoretical (DFT) effort has shown that 5C $\{CoNO\}^9$ species exhibit rare electronic structural properties that change upon the addition of H^+.[113-114] The isolated nitroxyl anion complexes (**3**, **4**) are assigned as HS-Co^{II} coordinated to $^3NO^-$, while a putative LS-Co^{II}-^{1}HNO intermediate exists after H^+ addition. These protonated $\{CoNO\}^9$ complexes liberate free HNO in water as demonstrated by the detection and quantification of N_2O via headspace gas IR. As a cautionary note, experiments performed under limiting H^+ conditions reveal that several competing paths exist that could prevent the release of HNO, one of which involves the formation of the corresponding dinitrosyl $\{Co(NO)_2\}^{10}$ complex **5** as a potential dead end. However, this limitation is somewhat muted by the fact that **5** may also generate HNO. Nitroxyl trapping experiments with Mn^{III}-P and metMb conducted under physiological conditions are consistent with free HNO being released from **3** and **4** with the $\{CoHNO\}^9$ intermediate being generated along the reaction path. The enhanced reactivity of **3** and

4 in water is in stark contrast to the relative inertness of $\{CoNO\}^8$ **1** and **2** and can be explained by the increased lability of the Co-NO bond resulting from the *primarily* Co-centered reduction in the $\{CoNO\}^9$ complexes. Numerous $\{CoNO\}^8$ complexes have been synthesized and the results presented here and elsewhere[43,55-56] suggest that many could be reasonable HNO donors. However, their one-electron reduced $\{CoNO\}^9$ analogues are even more promising, especially as HNO donors in aqueous media. Our findings further expand the useful roles of Co complexes, which include H_2 evolution,[115-120] NO_2^- reduction,[52] and the reductive activation of other small molecules of biological/industrial interest such as N_2[121-122] and CO_2.[123] Taken together, this work provides the first example of an extensively characterized set of $\{CoNO\}^{8/9}$ complexes and suggests that these types of molecules will likely play a role in the development of HNO donors.

3.13 Materials and Methods

3.13.1 General Information

Same as Chapter 2 with the following exceptions. 18-crown-6 ether (18C6) was obtained from Aldrich and used as received. Piloty's Acid (PA) was used as received from Cayman Chemical and stored at -20 °C. The Piloty's acid solution used for the N_2O calibration curve was prepared with milli-Q H_2O and adjusted with NaOH to pH 13.0. Anhydrous 2-methyltetrahydrofuran (2-MeTHF) and methanol (MeOH) were obtained by storage over 3 Å molecular sieves for 48 h, decanting from the sieves, and storage under N_2. LN_4 ligand (*N*[1]*E*,*N*[2]*E*)-*N*[1],*N*[2]-bis((1H-pyrrol-2-yl)methylene)-benzene-1,2-diamine ($LN_4H_2^{Ph}$, where H = dissociable protons)[42] and $\{CoNO\}^8$ complexes $[Co(LN_4^{PhCl})(NO)]$ (**2**) and $[Co(LN_4^{PhCl})(^{15}NO)]$ (**2-^{15}NO**) were synthesized according to the published procedures.[43]

3.13.2 Physical Methods

Same as Chapter 2 with the following exceptions. Gas-phase FTIR samples were run with a demountable airtight 50-mm Pike Technologies Pyrex cell with CaF_2 windows (38 mm × 6 mm). The closed gas cell was taken out of the glovebox and spectra were acquired immediately, using a vacuum background. X-band (9.60 GHz) EPR spectra were obtained on a Bruker ESP 300E EPR spectrometer controlled with a Bruker microwave bridge at 10 K. The EPR was equipped with a continuous-flow liquid He cryostat and a temperature controller (ESR 9) made by Oxford Instruments Inc. Continuous wave (CW) Q-band (35 GHz) EPR spectra were recorded at 2 K on a modified Varian spectrometer.[124] Under the experimental conditions employed here, which lead to "rapid-passage" effects,[125] 35 GHz EPR spectra are observed in the dispersion mode and appear as absorption lineshapes, rather than the standard absorption mode detection and first derivative presentation. Digital derivatives were taken to allow conventional presentation. EPR simulations were performed using the program QPOW,[126] as modified by J. Telser.

3.13.3 Computational Methods

DFT calculations were carried out with the ADF (Amsterdam Density Functional) 2013 program,[127] with three different exchange correlation functionals,[128] including the pure functionals BP86[129-131] and OLYP,[132-135] and the hybrid functional B3LYP.[136-137] All-electron STO-TZP basis sets were employed throughout, along with a fine mesh for numerical integration of matrix elements and tight criteria for both SCF and geometry optimizations.

3.13.4 Synthesis of Compounds and Reactivity

[Co(LN$_4$^{Ph})(NO)], {CoNO}^{8} (1). To a batch of yellow LN$_4$H$_2$^{Ph} (350.0 mg, 1.334 mmol) in 4 mL of MeCN, a 2 mL MeCN slurry of NaH (72.1 mg, 3.00 mmol) was added. A slightly heterogeneous dark yellow solution resulted from mixing the two reactants and H_2 gas was evolved. This solution stirred with quick vacuum for 30 min, following which a 5 mL blue MeCN slurry of (Et$_4$N)$_2$[CoCl$_4$] (615.4 mg, 1.334 mmol) was added. Upon mixing the Co^{II} salt and the deprotonated ligand, the solution immediately turned deep red-brown and a light grey solid slowly precipitated. The reaction mixture stirred at 60 °C with a water bath for 3 h. After cooling the reaction to RT, the solution was filtered to remove NaCl and washed with 3 mL of MeCN. The yellow-tinted dark brown MeCN filtrate containing (Et$_4$N)$_2$[Co(LN$_4$^{Ph})Cl$_2$] was then purged with purified NO(g) for 1.5 min at 60 °C. Addition of NO resulted in an immediate albeit slight color change; the solution became darker brown (red-tinted) and a microcrystalline precipitate was immediately observed. The reaction mixture stirred at 60 °C for 30 min under an NO atmosphere. The solution was then cooled to RT and excess NO(g) was removed by pulling vacuum and refilling with N_2. The reaction mixture was then placed in a -24 °C freezer overnight to induce further precipitation. The resulting microcrystalline solid was filtered, washed (3 × 1 mL) with MeCN and dried under vacuum to afford 391.3 mg (1.120 mmol, 84%) of product. ^{1}H NMR (500 MHz, THF, δ from residual protio solvent): 8.13 (s, 1H), 7.58 (br m, 1H), 7.51 (s, 1H), 7.08 (br m, 1H), 7.00 (s, 1H), 6.33 (s, 1H). ^{1}H NMR (500 MHz, CD$_3$CN, δ from residual protio solvent): 8.10 (s), 7.59 (m, 1H), 7.54 (s, 1H), 7.18 (m, 1H), 7.09 (d, 1H, J = 3.7 Hz), 6.41 (m, 1H). FTIR (KBr matrix), ν_{max} (cm^{-1}): 3293 (vw), 3059 (vw), 3010 (vw), 1667 (sh, vs, ν_{NO}), 1656 (vs, ν_{NO}), 1582 (m), 1552 (vs), 1507 (m), 1460 (m), 1446 (m), 1406 (w), 1380 (vs), 1326 (w), 1295 (vs), 1257 (s), 1196 (m), 1170 (w), 1154 (w), 1102 (w), 1076 (w), 1042 (s), 1033 (vs), 986 (m), 929 (w), 914 (w),

895 (m), 863 (w), 846 (w), 816 (w), 781 (w), 741 (vs), 729 (s), 677 (m), 648 (w), 627 (w), 603 (m), 532 (w), 480 (w). FTIR (solution, CaF_2 windows, 0.1 mm spacers, RT), ν_{NO} (cm^{-1}): 1668 (THF), 1670 (MeOH), 1668 (MeCN). UV-vis (THF, 298 K), λ_{max}, nm (ε, M^{-1} cm^{-1}): 318 (19,000), 364 (25,000), 453 (12,000), 497 (9,600). Anal. Calcd for $C_{16}H_{12}CoN_5O \bullet 0.5H_2O$: C, 53.64; H, 3.66; N, 19.55. Found: C, 53.75; H, 3.30; N, 19.23.

[Co(LN$_4^{Ph}$)(^{15}NO)], {Co^{15}NO}^{8} (1-^{15}NO). The isotopically-labeled complex **1-^{15}NO** was prepared analogously to **1** except for using 0.2000 g (0.7625 mmol) of $LN_4H_2^{Ph}$, 41.2 mg (1.72 mmol) of NaH, 351.7 g (0.7625 mmol) of $(Et_4N)_2[CoCl_4]$, and ^{15}NO(g). Yield: 0.1421 g (0.4057 mmol, 53%). FTIR (KBr matrix), ν_{NO} (cm^{-1}): 1641 ($\Delta\nu_{NO}$: 26 cm^{-1}), 1628 ($\Delta\nu_{NO}$: 28 cm^{-1}). ^{15}N NMR (50.7 MHz, THF-d_8, δ from CH_3NO_2): 675.

[K(18C6)][Co(LN$_4^{Ph}$)(NO)], {CoNO}^{9} (3). Solid KC_8 (31.0 mg, 0.229 mmol) was directly added to a 4 mL 2-MeTHF solution of **1** (50.0 mg, 0.143 mmol) containing 18C6 (75.6 mg, 0.286 mmol) and stirred for 1 h at RT. The color of the solution remained dark brown and the color of the insoluble KC_8 slowly changed from gold to silver flakes. The reaction was filtered, yielding insoluble silver flakes (graphite) and a dark brown filtrate, which was then dried *in vacuo* leaving a sticky residue. The sticky residue stirred in ~15 mL of Et_2O for 2 h in order to remove the excess 18C6 and was then filtered, affording 65.0 mg of **2** as a dark brown solid (0.0996 mmol, 70%). FTIR (KBr matrix), ν_{max} (cm^{-1}): 3078 (w), 2901 (m), 1609 (m, ν_{NO}), 1581 (s), 1557 (s), 1457 (m), 1382 (s), 1351 (m), 1285 (s), 1253 (m), 1213 (w), 1187 (m), 1105 (vs), 1025 (m), 961 (m), 920 (w), 867 (w), 836 (w), 784 (w), 759 (w), 736 (m), 687 (w), 610 (w), 592 (w), 583 (w), 525 (w), 477 (w), 450 (w), 419 (w). HRMS-ESI (*m/z*): $[M]^-$ calcd for $C_{16}H_{12}CoN_5O_1$ (relative abundance), 349.037 (100.0), 350.040 (17.3), 351.043 (1.2); found, 349.037 (100.0), 350.040 (14.4), 351.029 (0.8). UV-vis (THF, 298 K), λ_{max}, nm (ε, M^{-1} cm^{-1}): 317 (5,900), 365 (9,600), 451 (3,700), 498

(2,400). Anal. Calcd. for $C_{28}H_{36}CoKN_5O_7$: C, 51.53; H, 5.56; N, 10.73. Found: C, 51.05; H, 5.69; N, 10.21.

[K(18C6)][Co(LN$_4^{Ph}$)(^{15}NO)], {Co^{15}NO}^{9} (3-^{15}NO). The isotopically-labeled complex **3-^{15}NO** was prepared analogously to **3** except for using 50.0 mg (0.143 mmol) of **1-^{15}NO**, 30.9 mg (0.229 mmol) of KC_8, and 75.5 mg (0.286 mmol) of 18C6. Yield: 68.7 mg (0.105 mmol, 74% yield). FTIR (KBr matrix), ν_{NO} (cm^{-1}): ~1580; overlaps with broad imine stretches ($\nu_{C=N}$) in the same region. HRMS-ESI (*m/z*): $[M]^-$ calcd for $C_{16}H_{12}CoN_4{}^{15}N_1O_1$ (relative abundance), 350.034 (100.0), 351.037 (17.3), 352.040 (1.4); found, 350.035 (100.0), 351.038 (17.3), 352.037 (1.2).

[K(18C6)][Co(LN$_4^{PhCl}$)(NO)], {CoNO}^{9} (4). Solid KC_8 (25.9 mg, 0.191 mmol) was directly added to a 4 mL 2-MeTHF solution of **2** (50.0 mg, 0.120 mmol) containing 18C6 (63.2 mg, 0.239 mmol) and stirred for 1 h at RT. The color of the solution remained dark brown and the KC_8 slowly changed from gold to silver consistent with formation of graphite. The reaction mixture was filtered with a medium porosity glass frit to remove the insoluble silver graphite flakes. The resulting dark brown filtrate was then stripped to dryness in vacuo leaving a sticky residue. This residue was stirred in ~10 mL of Et_2O for 20 min in order to remove the excess 18C6, which afforded 70.4 mg (0.0976 mmol, 82%) of a dark brown solid after vacuum filtration and drying. FTIR (KBr matrix), ν_{max} (cm^{-1}): 3092 (w), 3079 (w), 2908 (m), 2892 (m), 2855 (m), 2823 (w), 2797 (w), 1617 (m, ν_{NO}), 1568 (vs), 1537 (s), 1455 (m), 1380 (s), 1350 (m), 1292 (s), 1270 (m), 1249 (w), 1191 (w), 1110 (vs), 1026 (m), 963 (m), 932 (w), 889 (w), 866 (w), 838 (w), 808 (w), 760 (w), 741 (w), 685 (w), 673 (w), 608 (w), 531 (w), 494 (w), 467 (w), 450 (w), 432 (w) 417 (w), 405 (w). HRMS-ESI (*m/z*): $[M]^-$ calcd for $C_{16}H_{10}Cl_2CoN_5O_1$ (relative abundance), 416.959 (100.0), 417.963 (17.3), 418.956 (64.8), 419.959 (11.2), 420.953 (10.5), 421.957 (1.8); found, 416.960 (100.0), 417.980 (23.5), 418.957 (65.9), 419.977 (15.0), 420.954 (10.0), 421.973 (1.9).

UV-vis (THF, 298 K), λ_{max}, nm (ε, M^{-1} cm^{-1}): 324 (5,000), 370 (8,400), 460 (3,700), 510 (2,300). Anal. Calcd. for $C_{28}H_{34}Cl_2CoKN_5O_7 \bullet H_2O$: C, 45.47; H, 4.91; N, 9.47. Found: C, 45.40; H, 4.45; N, 9.27.

[K(18C6)][Co(LN$_4^{PhCl}$)(^{15}NO)], {Co^{15}NO}^{9} (4-^{15}NO). The isotopically-labeled complex **4-^{15}NO** was prepared analogously to **4** except for using 50.1 mg (0.120 mmol) of **2-^{15}NO**, 25.9 mg (0.192 mmol) of KC_8, and 63.2 mg (0.239 mmol) of 18C6. Yield: 57.0 mg (0.0789 mmol, 66% yield). FTIR (KBr matrix), ν_{NO} (cm^{-1}): ~1585, unable to definitively identify ν_{15NO} due to broad imine stretches ($\nu_{C=N}$) in the same region. HRMS-ESI (*m/z*): $[M]^-$ calcd for $C_{16}H_{10}Cl_2CoN_4{}^{15}N_1O_1$ (relative abundance), 417.956 (100.0), 418.959 (17.3), 419.953 (63.9), 420.956 (11.1), 421.950 (10.2), 422.953 (1.8); found, 417.958 (100.0), 418.960 (17.8), 419.954 (67.8), 420.957 (11.3), 421.951 (10.9), 422.954 (1.7).

Oxidation of [K(18C6)][Co(LN$_4^{Ph}$)(NO)] (3) with FcPF$_6$ to establish {CoNO}^{9} ↔ {CoNO}^{8} interconversion. A dark blue 2 mL MeCN slurry of $FcPF_6$ (11.2 mg, 0.0338 mmol) was added to a 2 mL MeCN solution of **3** (20.0 mg, 0.0306 mmol) at RT. Upon mixing, the solution darkened in color as a result of the oxidation reaction and insoluble materials formed. The reaction mixture was stirred for 1 h at RT and then filtered to remove the dark brown insoluble solid. The product was dried in vacuo to yield 5.0 mg of {CoNO}^{8} complex **1** (0.014 mmol, 46%) as verified by FTIR. Additional complex **1** was also present in the MeCN filtrate. The less than stoichiometric yield is due to some loss of **1** in the filtrate detected by FTIR.

Oxidation of [K(18C6)][Co(LN$_4^{PhCl}$)(NO)] (4) with FcPF$_6$ to establish {CoNO}^{9} ↔ {CoNO}^{8} interconversion. A dark blue 2 mL MeCN slurry of $FcPF_6$ (7.6 mg, 0.023 mmol) was added to a 2 mL MeCN solution of **4** (15.0 mg, 0.0208 mmol) at RT. No significant color change was observed upon mixing reactants; however, more insolubles formed over time. The reaction

mixture was stirred for 1 h at RT and then filtered to remove the dark brown insoluble solid yielding 6.0 mg (0.014 mmol, 67%) of $\{CoNO\}^8$ complex **2** as verified by FTIR. The less than stoichiometric yield is due to some loss of **2** in the filtrate based on FTIR.

Bulk Reaction of $\{CoNO\}^9$ complexes 3 and 4 with HBF_4•Et_2O. Using **3** as the representative example: To a yellow-tinted dark brown THF solution (2.5 mL) of **3** (15.0 mg, 0.0230 mmol) was added 4.06 μL (0.0298 mmol) of HBF_4•Et_2O in 0.5 mL of THF. There was a slight lightening in color of the resulting solution. The reaction mixture stirred at RT for 24 h. After this time, the solvent was removed, affording a sticky brown residue (18.7 mg). This material was characterized by LR-ESI-MS (THF), FTIR (KBr), and ^{1}H NMR (CD_3CN). The collective characterization indicates $\{CoNO\}^8$ complex **1** (ν_{NO}: 1654 cm^{-1}) and a $\{Co(NO)_2\}^{10}$ species (ν_{NO}: 1869, 1792 cm^{-1}). LRMS-ESI (*m/z*): $[M]^+$ calcd for $C_{16}H_{14}CoN_6O_2$: 381.1, found, 381.3. The reaction of **4** (15.0 mg, 0.0208 mmol) with HBF_4•Et_2O (3.68 μL, 0.0270 mmol) afforded a total mass of 21.2 mg, which was mostly $\{CoNO\}^8$ complex **2** (ν_{NO}: 1661 cm^{-1}) and a $\{Co(NO)_2\}^{10}$ species (ν_{NO}: 1857, 1760 cm^{-1}).

Bulk Reaction of $\{CoNO\}^8$ (1, 2) and $\{CoNO\}^9$ (3, 4) with HBF_4•Et_2O for headspace analysis. Using **3** as the representative example: To a clear H_2O solution (1.800 mL) of HBF_4•Et_2O (20.9 μL, 0.153 mmol) was added a dark brown solution of **3** (10.0 mg, 0.0153 mmol) in 200 μL of DMSO. At t = 24 h, the headspace was collected in an airtight gas IR cell, and the resulting FTIR spectrum was analyzed for the presence of N_2O (ν: 2236, 2208 cm^{-1}; 63 ± 3% yield). Reaction conditions were repeated for $\{CoNO\}^8$ **1** in THF: To a red-tinted dark brown THF solution (1.500 mL) of **1** (10.0 mg, 0.0287 mmol) was added 5.07 μL (0.0372 mmol) of HBF_4•Et_2O in 0.500 mL of THF. An FTIR spectrum of the headspace was collected at 24 h. These reactions were repeated under identical conditions for $\{Co^{15}NO\}^8$ **1-^{15}NO** and $\{Co^{15}NO\}^9$ **3-^{15}NO**, leading

to formation of $^{15}N_2O$ (ν: 2167, 2145 cm^{-1}). Because $\{CoNO\}^8$ complex **1** immediately precipitates from H_2O, N_2O formation in the $\{CoNO\}^8/H^+$ reaction was monitored in THF.

UV-vis monitor of the reaction of $\{CoNO\}^8$ (1), $\{CoNO\}^9$ (3), and $\{Co(NO)_2\}^{10}$ complex 5 with $[Mn^{III}(TPPS)]$. A 1 mM stock solution of $[Mn^{III}(TPPS)]$ was prepared in 10 mM PBS (pH 7.4) and the UV-vis spectrum was recorded at 298 K, which was consistent with the literature.[99] No significant changes occurred in the spectrum over 30 min. To the cuvette was then added a 0.050 mL aliquot of a 3 mM MeCN stock solution of the $\{CoNO\}^{8/9}$ complexes, yielding a 1:5 ratio of $[Mn^{III}(TPPS)]/\{CoNO\}^{8/9}$ or a 1:2.5 ratio of $[Mn^{III}(TPPS)]/\{Co(NO)_2\}^{10}$. The UV-vis was monitored for 24 h at 298 K (intervals used: 10 min cycles in the first 3 h; 30 min cycles for the next 21 h).

General reaction of $\{CoNO\}^8$ complexes 1 and 2, $\{CoNO\}^9$ complexes 3 and 4, and $\{Co(NO)_2\}^{10}$ complex 5 with equine skeletal metmyoglobin (metMb). All reactions of metMb were monitored by UV-vis spectroscopy under anaerobic conditions in 10 mM phosphate buffered saline (PBS, pH 7.4) at 310 K. In general, $\{CoNO\}^{8/9}$ complexes were added as an MeCN aliquot (50-100 μL) to a quartz cuvette containing 3.100-3.200 mL of metMb in PBS. The UV-vis spectra were immediately collected after the addition of the complexes to the metMb solution and were monitored over a 24 h period.

Reaction of metMb and $\{CoNO\}^8$ (1 and 2). Using **1** as a general representative, a 100-μL MeCN aliquot (0.855 mM, 5 mol-equiv) was added to a cuvette containing metMb (5.35 μM, 3.200 mL) in PBS. The UV-vis spectrum was recorded immediately and monitored for 24 h. No significant changes in the Soret (409 nm) nor the Q-bands (503, 637 nm) were observed. Similar observations were noted for the reaction of **2** (0.42 mM, 5 mol-equiv) and metMb (2.6 μM, 3.150 mL) and **5** (1.08 mM, 2.5 mol-equiv) and metMb (6.42 μM, 3.150 mL) in PBS.

Reaction of metMb and {CoNO}^{9} (3 and 4). Using **3** as a general representative, a 50-μL MeCN aliquot (1.47 mM, 5-mol equiv) was added to a cuvette containing metMb (4.63 μM, 3.200 mL) in PBS. The UV-vis spectrum was recorded immediately and monitored for 24 h. The Soret band (409 nm) shifted to 420 nm over the first 2 h of the reaction. The Q-bands (503, 637 nm) diminished and the double-humped bands of MbNO (545, 582 nm) appeared and indicate quantitative formation of MbNO (Soret of MbNO: 421 nm, ε: 147 mM mM^{-1} cm^{-1})[105,107]. An A_{421} = 0.6729 corresponds to 4.58 μM of MbNO formed (99% yield). Similar results were obtained with complex **4** (50-μL aliquot, 0.963 mM, 5 mol-equiv) and metMb (6.0 μM, 3.200 mL) in PBS. An A_{421} = 1.015 corresponds to 6.91 μM of MbNO formed (114% yield). Competing absorbance from the Co species accounts for the yield.

3.14 Supporting Information

X-ray Crystallographic Data Collection and Structure Solution and Refinement. Dark red crystals of [Co(LN_4^{Ph})(NO)] (**1**) were grown under anaerobic conditions by slow diffusion of Et_2O into a 2-MeTHF solution of **1** at -20°C. Suitable crystals were mounted on a glass fiber. The X-ray intensity data were measured at 100 K on a Bruker SMART APEX II X-ray diffractometer system with graphite-monochromated Mo Kα radiation (λ = 0.71073 Å) using ω-scan technique controlled by the SMART software package.[138] The data were collected in 1464 frames with 10 s exposure times. The data were corrected for Lorentz and polarization effects[139] and integrated with the manufacturer's SAINT software. Absorption corrections were applied with the program SADABS.[140] Subsequent solution and refinement was performed using the SHELXTL 6.1 solution package operating on a Pentium computer.[141-142] The structure was solved by direct methods using the SHELXTL 6.1 software package.[143] Non-hydrogen atomic scattering factors were taken from

the literature tabulations.[144] Selected data and metric parameters for complex **1** are summarized in Table 3.S1. Selected bond distances and angles for **1** are given in Table 3.S2. Perspective views of the complexes were obtained using ORTEP.[145] The asymmetric unit of **1** contains two unique molecules, one of which was found to have disorder in the NO group, with two sets labeled as O(2) (one set) and O(2′) (second set). The first set containing O(2) has 82% occupancy while the second set containing O(2′) has 18% occupancy. The twinning features of the structure were detected and the reflections were indexed in two domains using the CELL-NOW program.

X-Ray Absorption Spectroscopy (XAS). Co samples were prepared anaerobically at a 3:1 stoichiometric dilution with boron nitride, loaded into transmission cells wrapped with Kapton® tape and immediately frozen in liquid nitrogen. Two independent duplicates were prepared to ensure spectral reproducibility. XAS data were collected at the Stanford Synchrotron Radiation Light Source (SSRL), on beamline 7-3, and the National Synchrotron Light Source (NSLS), on beamline X3-B. Beamline 7-3 was equipped with a Si[220] double crystal monochromator and beamline X3-B was equipped with a Si[111] monochromator; both beamlines were equipped with harmonic rejection mirrors. During data collection, the sample at SSRL was maintained at 10 K using an Oxford Instruments continuous-flow liquid helium cryostat and the sample at NSLS was maintained at 24 K using a helium Displex cryostat. Transmission spectra, collected with a simultaneous Co foil spectrum for monochromator calibration, were measured at both locations using nitrogen gas ionization chamber detectors placed in series. The first inflection point of the Co foil spectrum was assigned to 7709.5 eV. At both facilities, XAS spectra were collected in 5 eV increments in the pre-edge region (7542-7702 eV), 0.25 eV increments in the edge region (7702-7780 eV) and 0.05 $Å^{-1}$ increments in the extended X-ray absorption fine structure (EXAFS)

region. Data were collected to k = 14.0 Å^{-1} and integrated from 1 to 25 seconds in a k^3-weighted manner for a total scan length of approximately 40 minutes. Spectra displayed in Figure 3.4 represent the average of two independent spectra.

XAS data were processed using the Macintosh OS X version of the EXAFSPAK program suite integrated with Feff v7.2 for theoretical model generation.[146] Data reduction utilized a polynomial function in the pre-edge region and a four point cubic spline throughout the EXAFS region for background signal removal. Data were converted to k space using a Cobalt E_0 value of 7725 eV. Normalized XANES data were subjected to pre-edge analysis. Edge inflection energies were calculated as the maximum of the first derivative of the XANES spectra. Only spectra collected using the higher resolution Si[220] monochromator crystals were subjected to edge analysis. Pre- and post-edge splines were fit to the experimental spectra within the energy ranges of 7707-7718 eV. The extrapolated line was then subtracted from raw data to yield baseline corrected spectra. Pre-edge and edge features were processed and analyzed according to previously reported protocols.[43]

EXAFS data were fit using single scattering theoretical model amplitudes and phase functions. The k^3- weighted EXAFS was truncated between 1.0 and 13 Å^{-1} for filtering purposes and Fourier transformed for display. This k range corresponds to a spectral resolution of 0.13 Å for all Co-ligand interactions; therefore, only independent scattering environments at distances > 0.13 Å were considered resolvable in the EXAFS fitting analysis. A scale factor (Sc) of 0.98 and a threshold shift (ΔE_0) value of -11.3, calibrated by fitting crystallographically characterized cobalt complexes, were used in simulating the complex **1** sample. During the simulations, only the bond length and Debye-Waller disorder factor were allowed to vary, Sc and E_0 were held constant and the coordination number for the fit manually varied in 0.5 value increments. Criteria for judging

the best-fit simulation utilized both the lowest mean-square deviation between data and fit (F′), corrected for the number of degrees of freedom, and a reasonable Debye-Waller factor ($\sigma^2 < 0.006$ $Å^2$).[147]

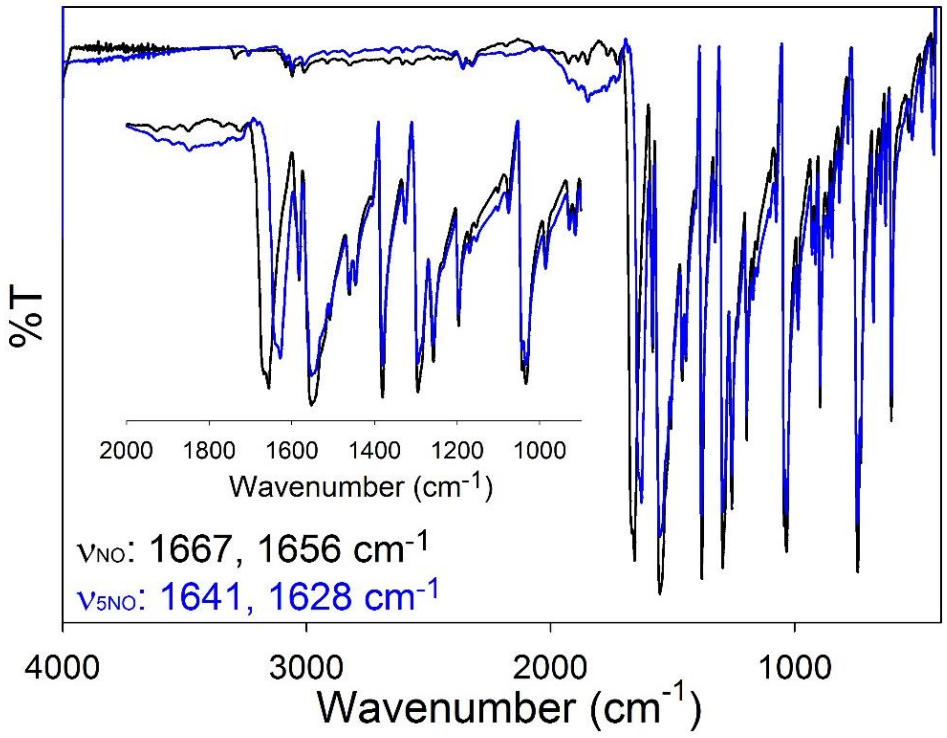

Figure 3.S1. Solid-state FTIR spectrum of $\{CoNO\}^8$ (**1**, black line) and $\{Co^{15}NO\}^8$ (**1-^{15}NO**, blue line) in a KBr matrix. *Inset:* Expansion of the N-O stretching region.

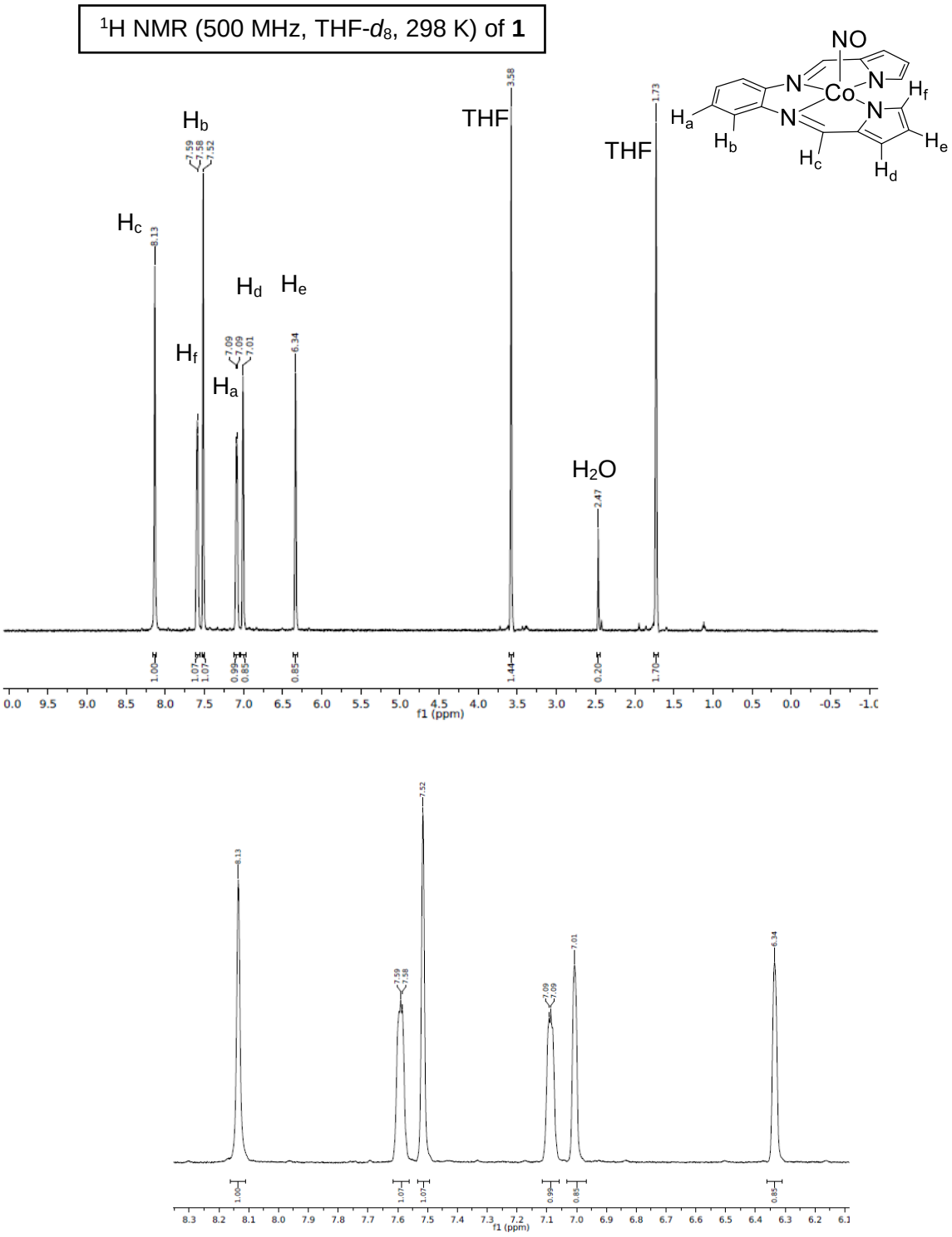

Figure 3.S2. *Top:* ^{1}H NMR spectrum of [Co(LN$_4^{Ph}$)(NO)] (**1**) in THF-d_8 at 298 K (δ vs. residual protio solvent signal). The peaks at 3.58 and 1.73 ppm are from residual protio solvent. The peak at 2.47 ppm is from trace H_2O. *Bottom:* Expansion of the aromatic region.

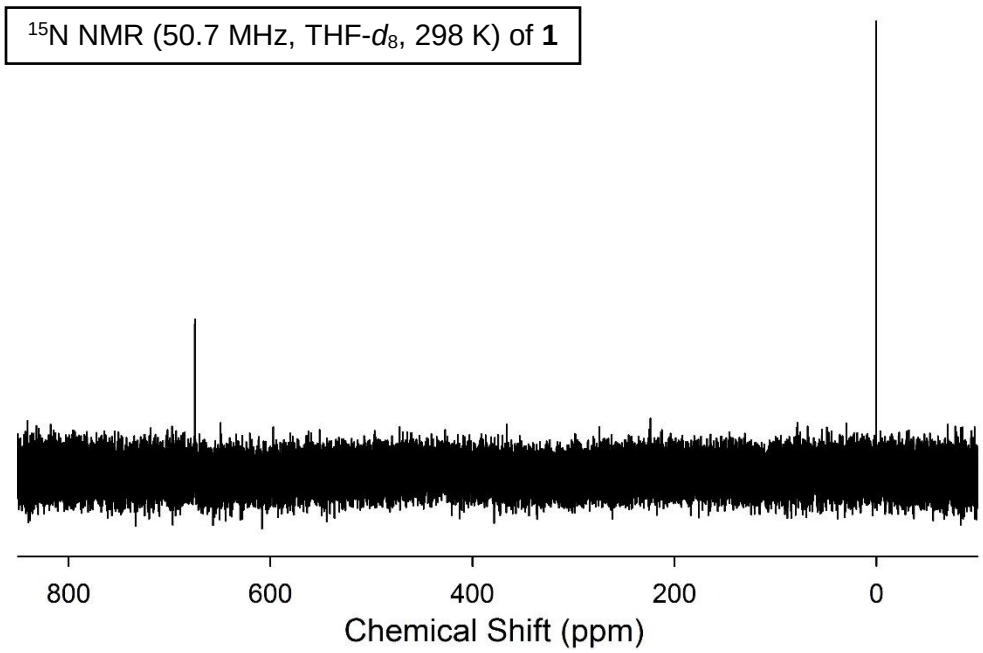

Figure 3.S3. ^{15}N NMR spectrum of [Co(LN_4^{Ph})(^{15}NO)] (**1-^{15}NO**) in THF-d_8 at 298 K (δ vs. CH_3NO_2). ^{15}N signal of ^{15}NO ligand = 675 ppm.

Table 3.S1. Summary of crystal data and intensity collection and structure refinement parameters for [Co(LN_4^{Ph})(NO)] (**1**).

Parameters	**1**
Formula	$C_{16}H_{12}CoN_5O_1$
Formula weight	349.24
Crystal system	Triclinic
Space group	*P*-1
Crystal color, habit	Dark red
a, Å	8.7573(7)
b, Å	9.2971(8)
c, Å	17.9518(15)
α, deg	96.3220(10)
β, deg	96.0850(10)
γ, deg	98.4760(10)
V, Å^3	1425.7(2)
Z	4
$\rho_{calcd,}$ g/cm^3	1.627
T, K	100(2)
abs coeff, μ (Mo Kα), mm^{-1}	1.215
θ limits, deg	2.23-27.00
total no. of data	6201
no. of parameters	425
GOF of F^2	1.086
R_1,[a] %	4.87
wR_2,[b] %	13.27
max, min peaks, e/Å^3	1.791, -1.006

[a]$R_1 = \Sigma| |F_o| - |F_c| | / \Sigma |F_o|$; [b]$wR_2 = \{\Sigma[w(F_o^2 - F_c^2)^2]/\Sigma[w(F_o^2)^2]\}^{1/2}$

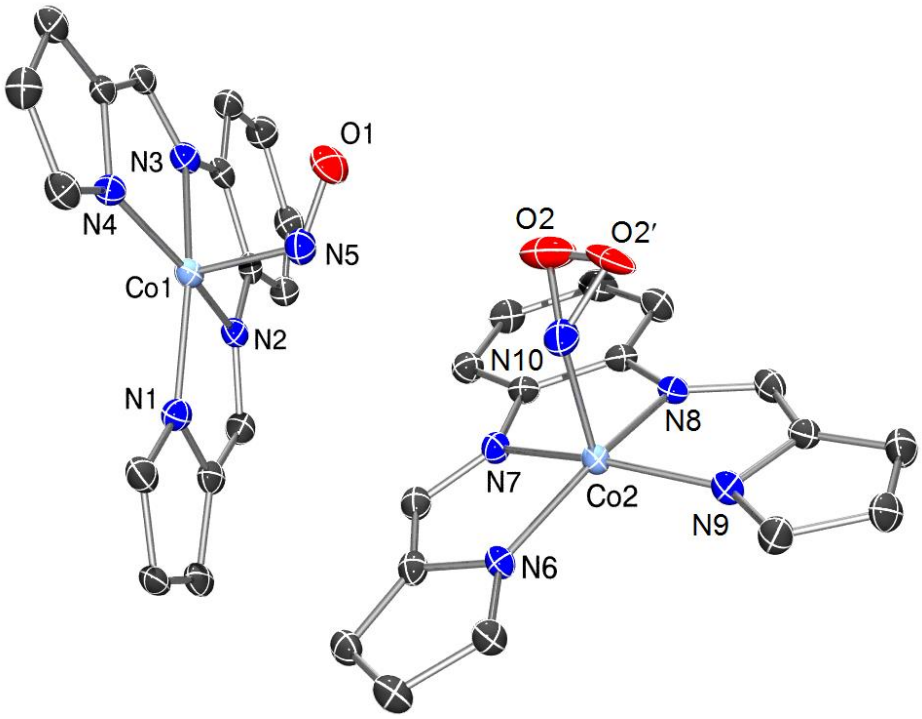

Figure 3.S4. ORTEP views of the two independent molecules in the asymmetric unit of [Co(LN_4^{Ph})(NO)] (**1**) at 50% thermal probability for all non-hydrogen atoms. Hydrogen atoms omitted for clarity.

Table 3.S2. Selected bond distances (Å) and bond angles (deg) for [Co(LN_4^{Ph})(NO)] (**1**).

Atoms	**Bond distance**	**Atoms**	**Bond distance**
Co1-N1	1.948(3)	Co2-N6	1.932(3)
Co1-N2	1.892(3)	Co2-N7	1.898(3)
Co1-N3	1.895(3)	Co2-N8	1.893(3)
Co1-N4	1.927(3)	Co2-N9	1.930(3)
Co1-N5	1.804(4)	Co2-N10	1.799(3)
N5-O1	1.162(5)	N10-O2	1.164(6)
		N10-O2′	1.149(14)
Atoms	**Angle**	**Atoms**	**Angle**
		O2-N10-Co1	125.1(4)
O1-N5-Co1	124.9(3)	O2′-N10-Co1	127.7(10)
N1-Co1-N2	83.05(14)	N6-Co1-N7	83.07(14)
N1-Co1-N3	161.62(15)	N6-Co1-N8	160.21(14)
N1-Co1-N4	106.87(14)	N6-Co1-N9	105.91(14)
N1-Co1-N5	96.46(15)	N6-Co1-N10	99.36(15)
N2-Co1-N3	83.39(14)	N7-Co1-N8	83.19(14)
N2-Co1-N4	160.82(14)	N7-Co1-N9	160.67(15)
N2-Co1-N5	100.60(15)	N7-Co1-N10	97.47(15)
N3-Co1-N4	82.97(14)	N8-Co1-N9	83.45(14)
N3-Co1-N5	98.18(15)	N8-Co1-N10	96.48(15)
N4-Co1-N5	94.64(15)	N9-Co1-N10	97.86(15)

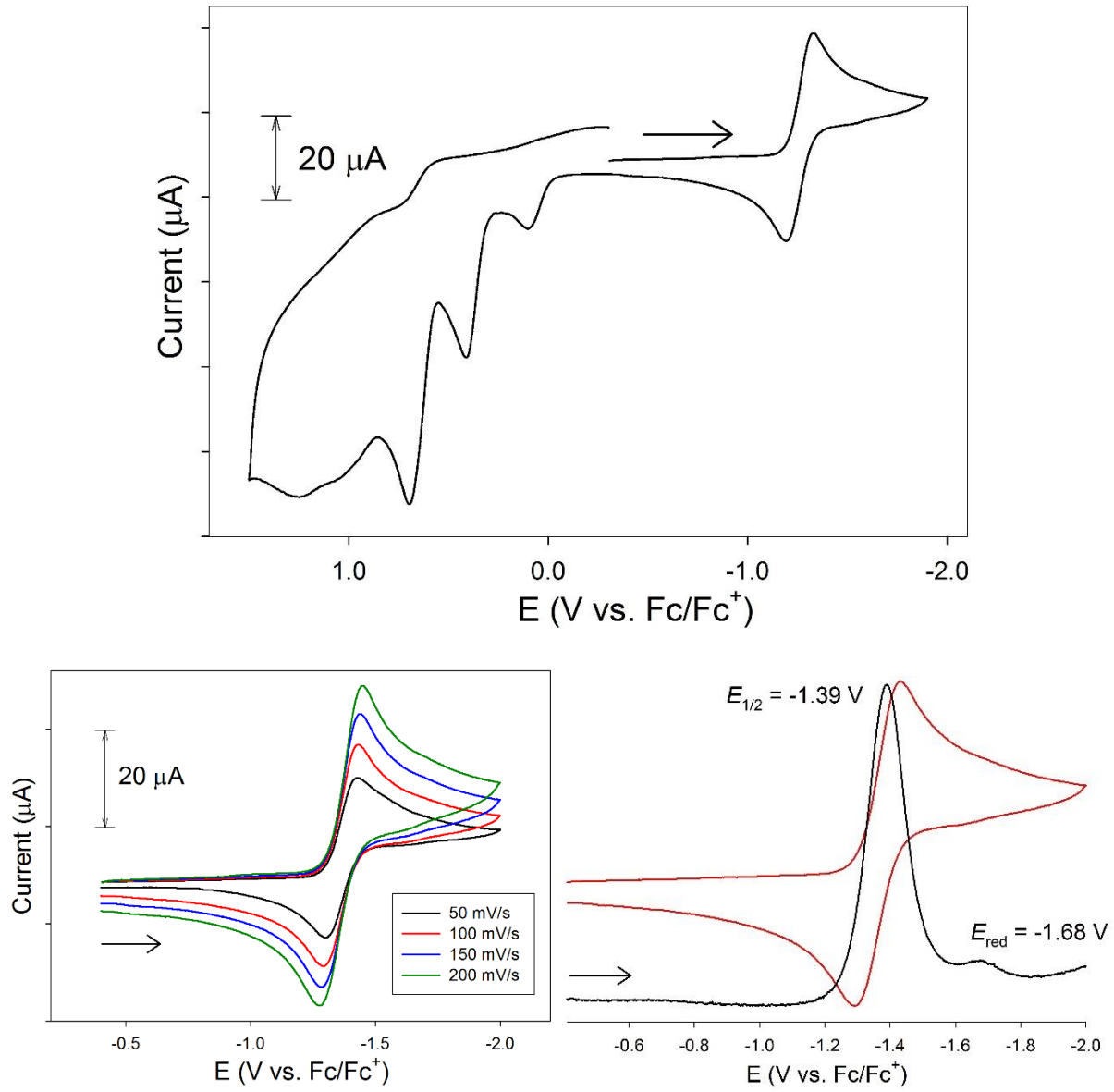

Figure 3.S5. (*Top*) Full CV of a 5 mM MeCN solution of [Co(LN_4^{Ph})(NO)] (**1**). (*Bottom, left*) Portion of the CV of **1** at different scan rates. (*Bottom, right*) Portion of CV (red) superimposed with its differential pulse voltammogram (DPV, black). DPV and CV were scaled to match. The DPV measurement reveals a minor (>1%) peak at -1.68 V that we attribute to **1** with a weakly-bound MeCN ligand, [Co(LN_4^{Ph})(MeCN)(NO)]. This peak is not observed in weak donor solvents such as THF. Conditions: 0.1 M $^{n}Bu_4NPF_6$ supporting electrolyte, glassy carbon working electrode, Pt-wire counter electrode, 100 mV/s scan rate, RT. Arrow displays direction of scan.

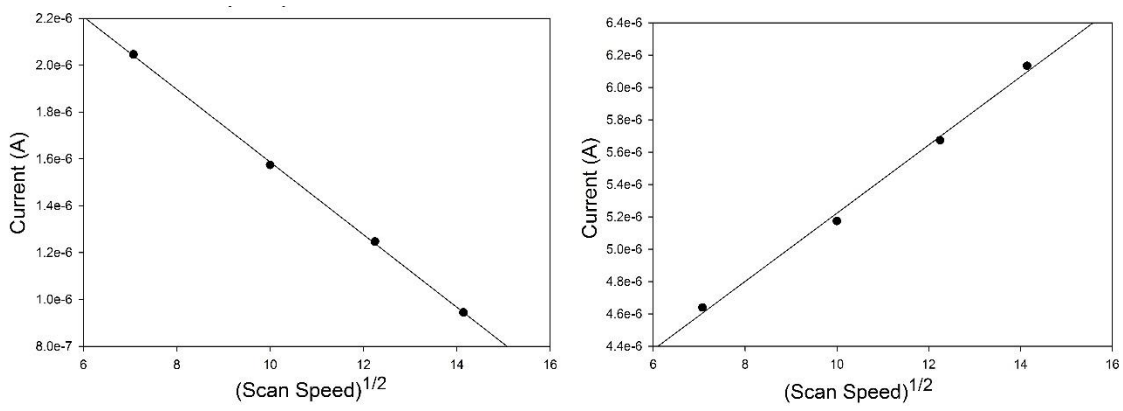

Figure 3.S6. Plots of the anodic, i_{pa}, (left, R^2 = 0.9996) and cathodic, i_{pc}, (right, R^2 = 0.9956) peak current versus square root of scan speed for the {CoNO}$^{8/9}$ redox couple for complex **1**.

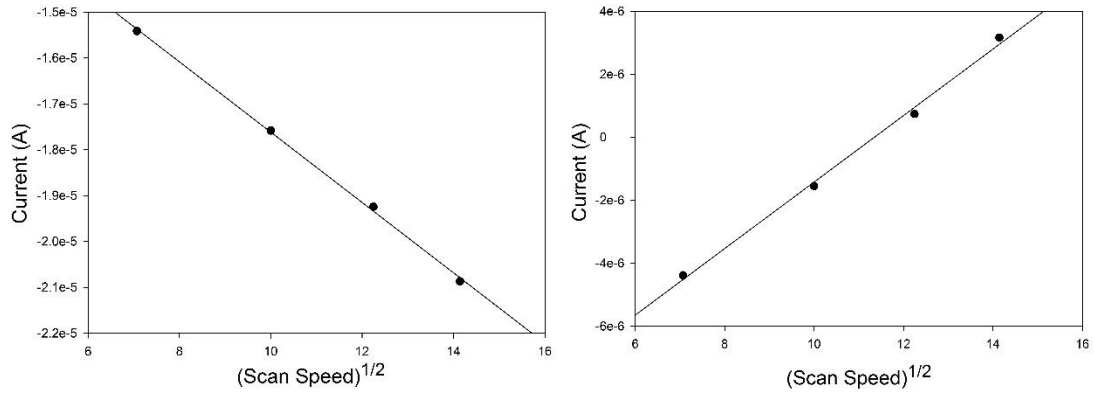

Figure 3.S7. Plots of the anodic, i_{pa}, (left, R^2 = 0.9989) and cathodic, i_{pc}, (right, R^2 = 0.9961) peak current versus square root of scan speed for the {CoNO}$^{8/9}$ redox couple for complex **2**.

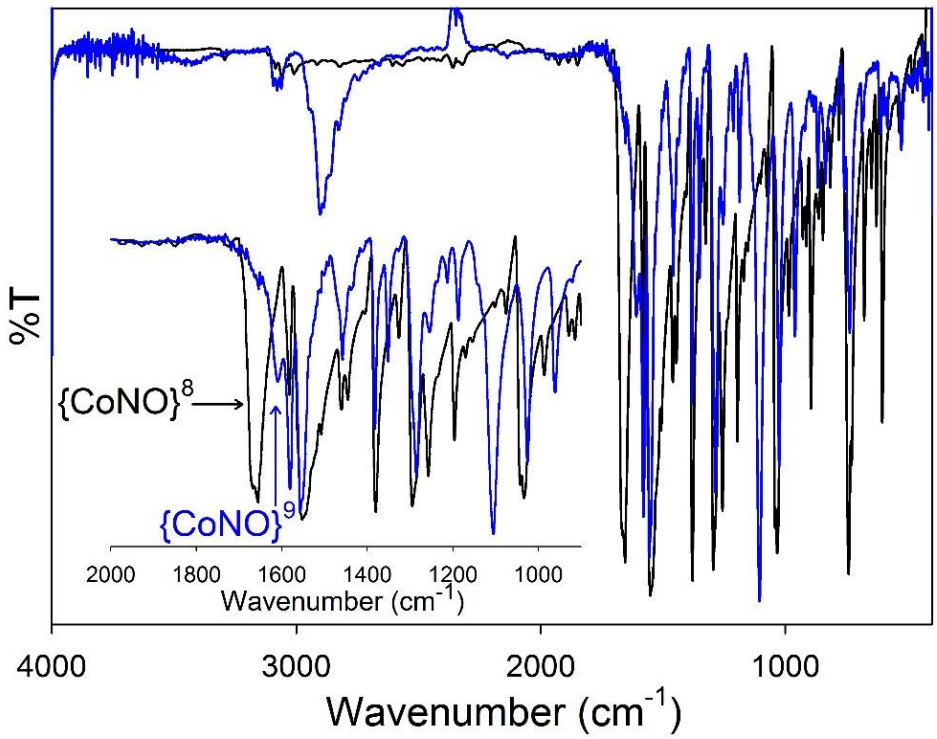

Figure 3.S8. Solid-state FTIR spectrum of $\{CoNO\}^8$ complex (**1**, black line) and $\{CoNO\}^9$ (**3**, blue line) in a KBr matrix. *Inset:* Expansion of N-O stretching region.

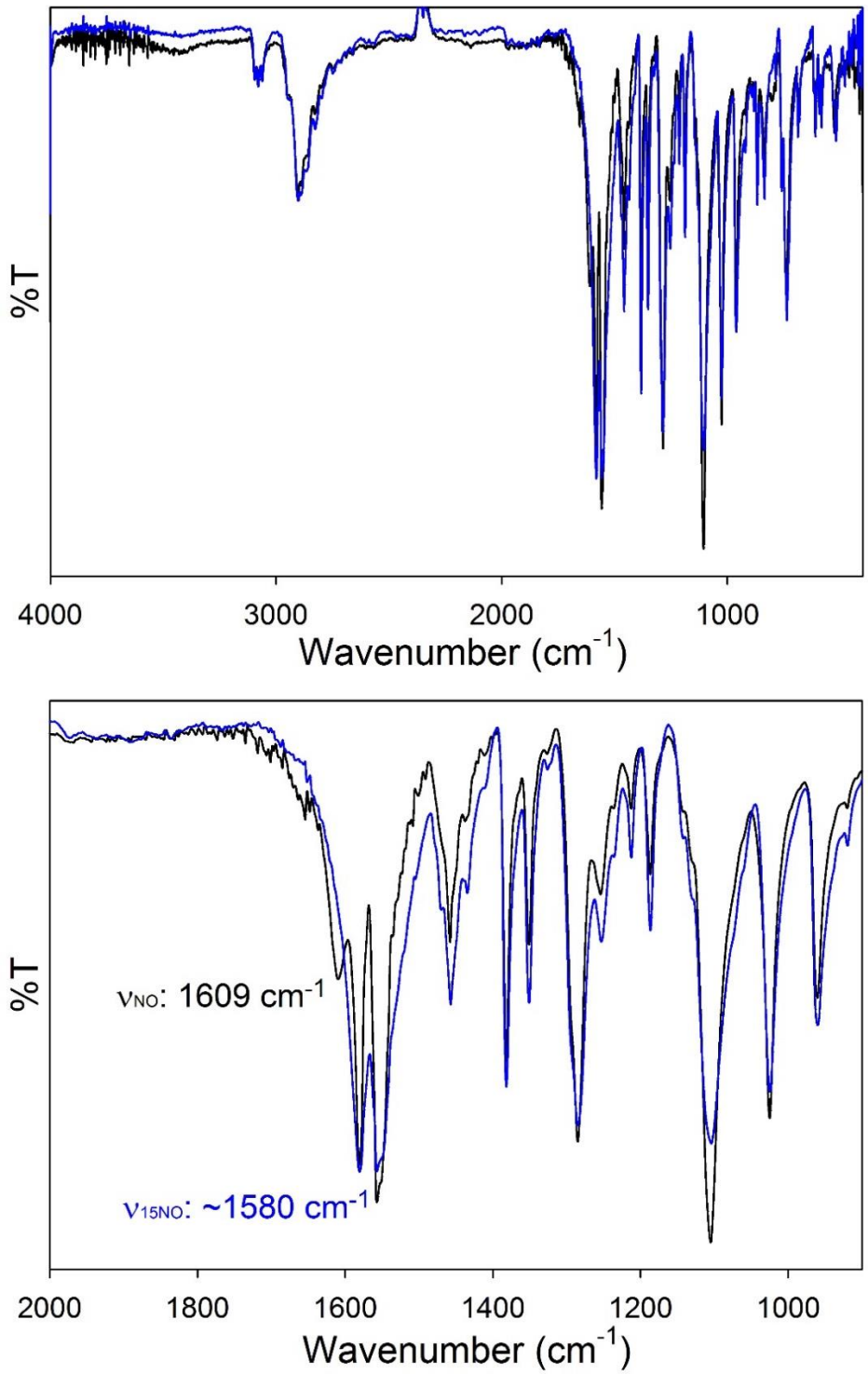

Figure 3.S9. Solid-state FTIR spectrum of $\{CoNO\}^9$ (**3**, black line) and $\{Co^{15}NO\}^9$ complex (**3-^{15}NO**, blue line) in a KBr matrix. *Bottom:* Expansion of N-O stretching region.

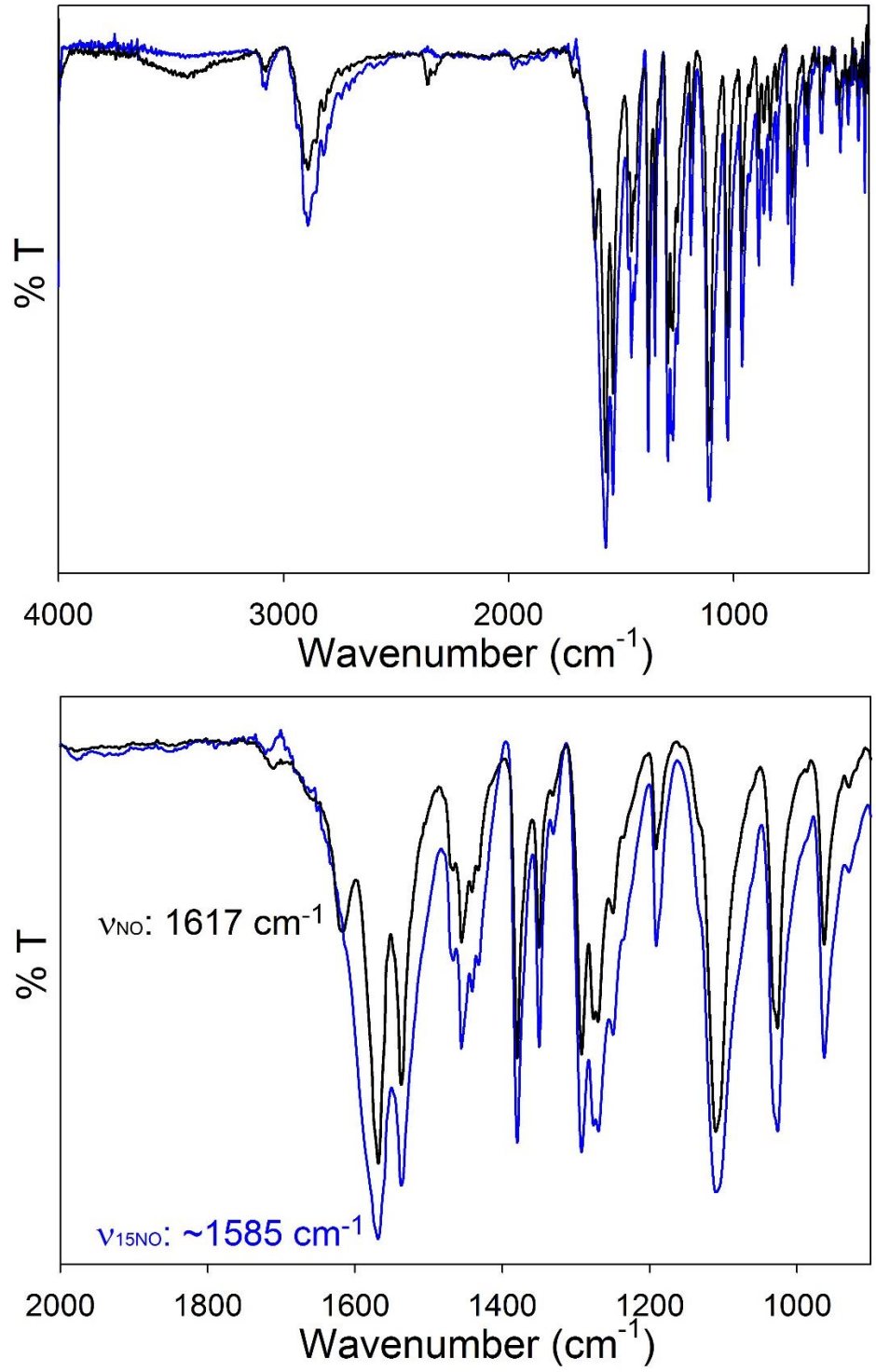

Figure 3.S10. Solid-state FTIR spectrum of $\{CoNO\}^9$ (**4**, black line) and $\{Co^{15}NO\}^9$ (**4-^{15}NO**, blue line) in a KBr matrix. *Bottom:* Expansion of N-O stretching region.

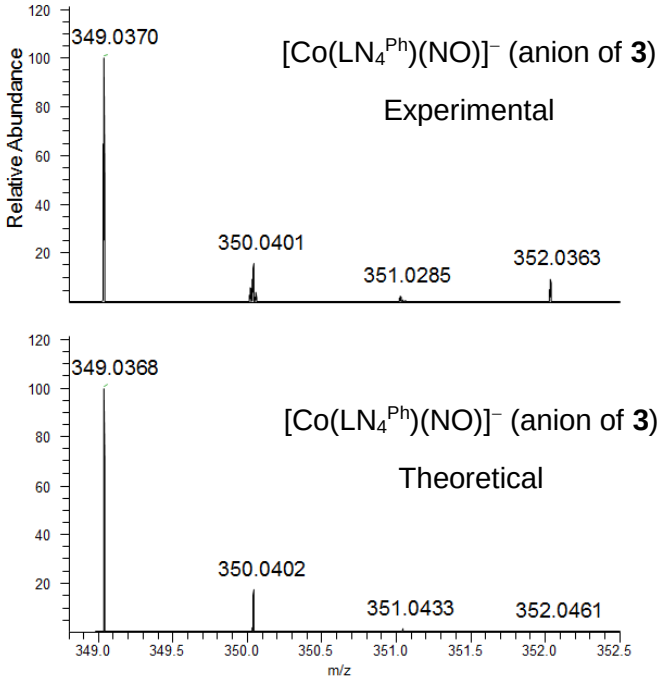

Figure 3.S11. *Top*: High-resolution ESI-MS (negative mode) of the anion of **3**. *Bottom*: Theoretical isotopic distribution.

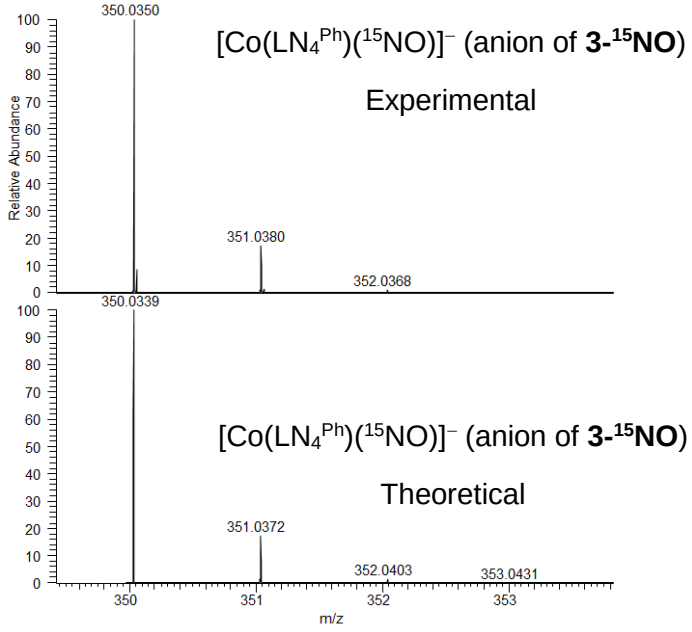

Figure 3.S12. *Top*: High-resolution ESI-MS (negative mode) of the anion of **3-^{15}NO**. *Bottom*: Theoretical isotopic distribution.

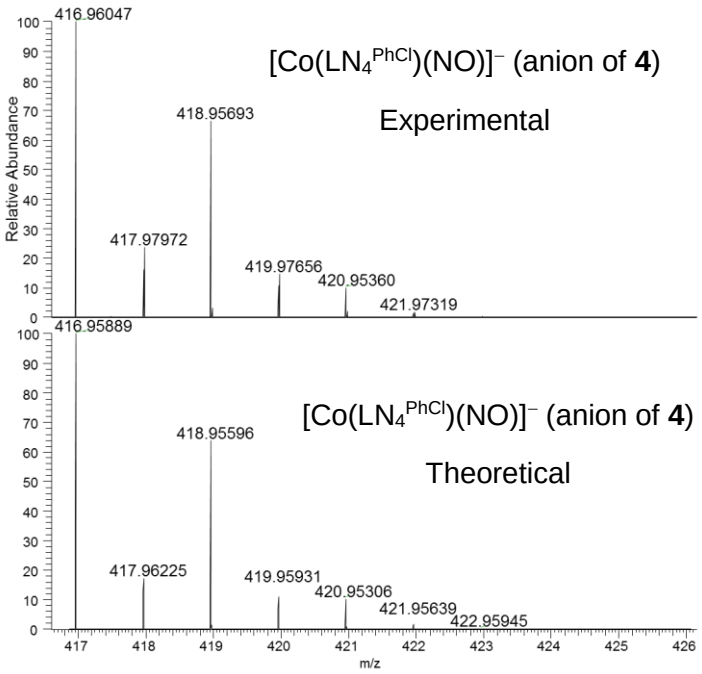

Figure 3.S13. *Top*: High-resolution ESI-MS (negative mode) of the anion of **4**. *Bottom*: Theoretical isotopic distribution.

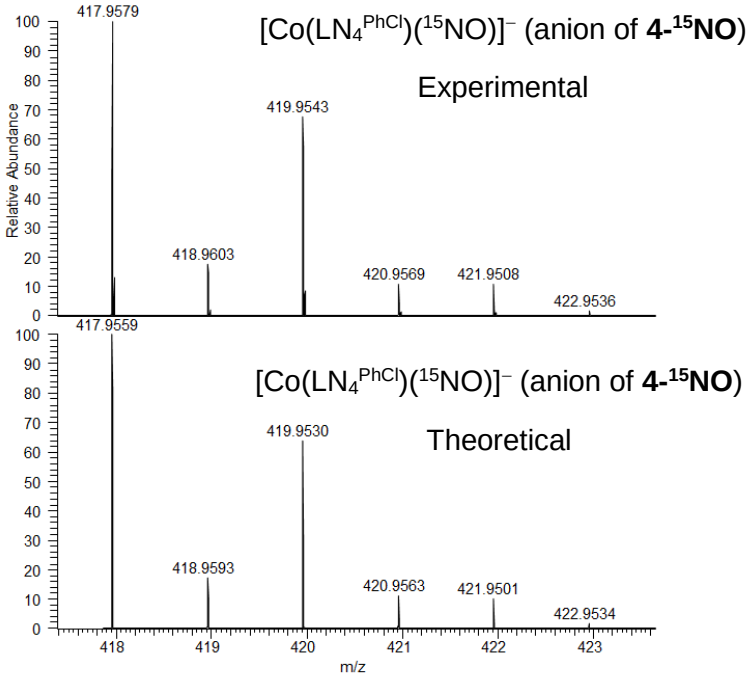

Figure 3.S14. *Top*: High-resolution ESI-MS (negative mode) of the anion of **4-^{15}NO**. *Bottom*: Theoretical isotopic distribution.

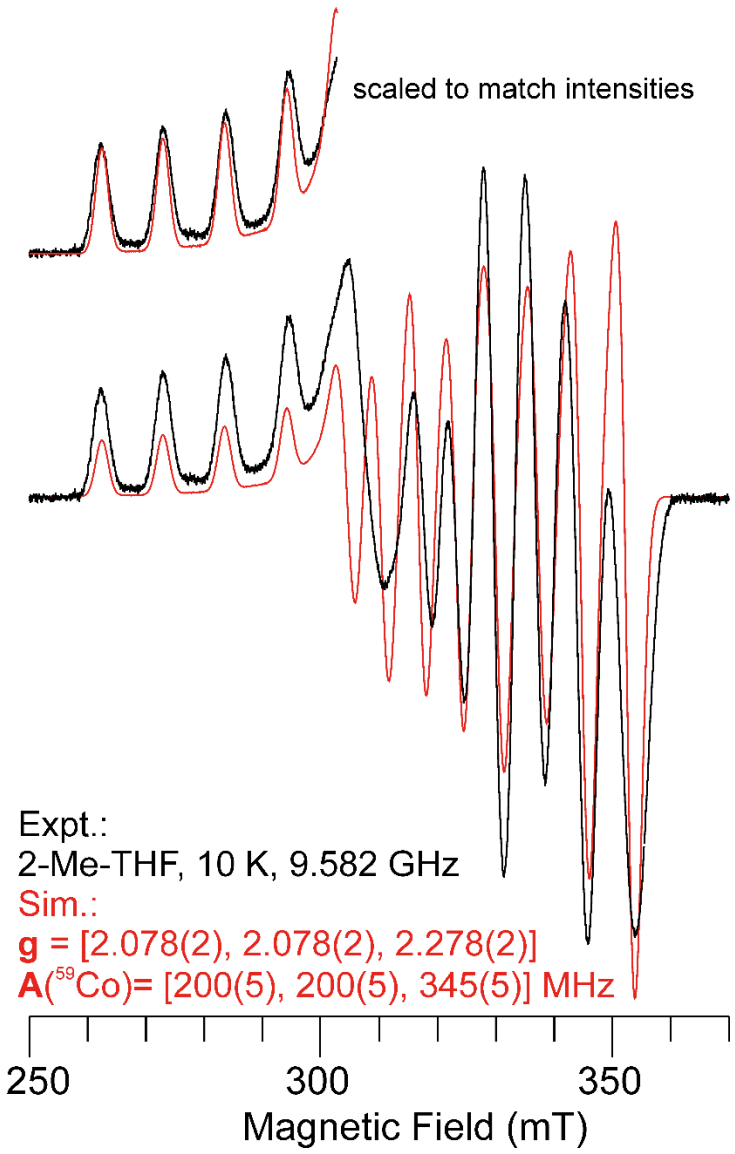

Figure 3.S15. X-band EPR spectrum of **4** in 2-MeTHF at 10 K (black trace) with simulation (red trace). Spectrometer settings: microwave frequency, 9.582 GHz; microwave power, 1.0 mW; modulation frequency, 100 kHz; modulation amplitude, 6.48 G. Simulation parameters: S_{tot} = 1/2, $g_{\perp}$ = 2.078(2), $g_{\parallel}$ = 2.278(2), $A_{\perp}(^{59}Co)$ = 200(5) MHz, $A_{\parallel}(^{59}Co)$ = 345(5) MHz.

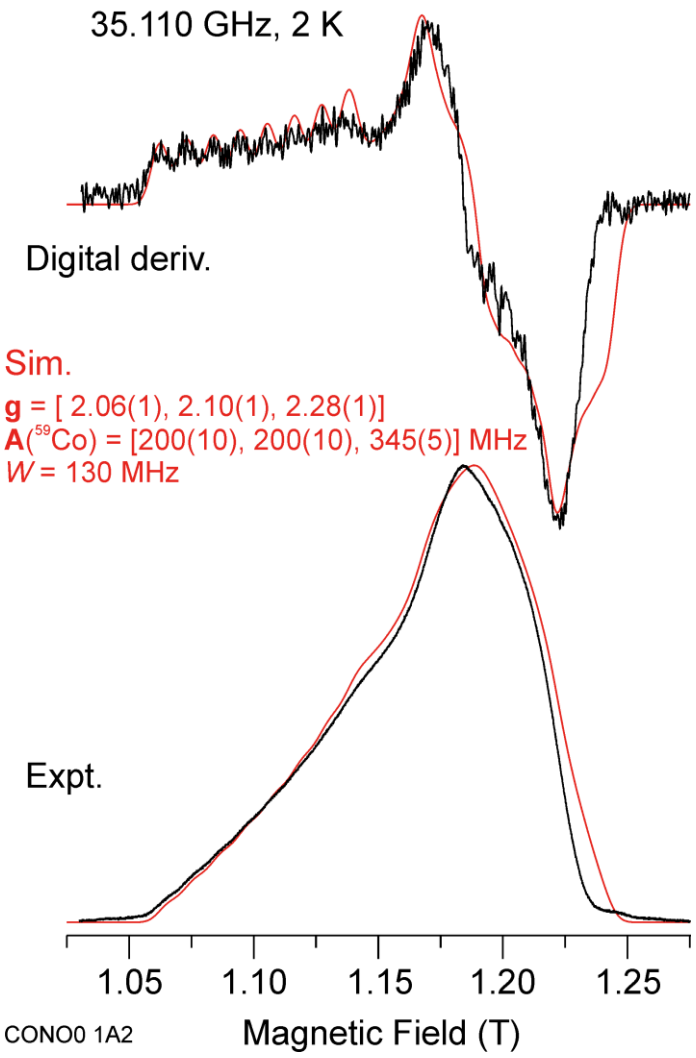

Figure 3.S16. 35 GHz (Q-band) EPR spectrum of [K(18C6)][Co(LN_4^{Ph})(NO)] (**3**) in 2-MeTHF. Experimental spectrum (black trace): temperature, 2 K; microwave frequency, 35.110 GHz; microwave power, 1 mW (20 dBm); 100 kHz field modulation amplitude, 0.1 mT; time constant, 32 ms; scan time, 4 min. Simulated spectrum (red trace): S = 1/2, **g** = [2.06, 2.10, 2.28], **A**(^{59}Co)= [200, 200, 345] MHz; isotropic single crystal Gaussian linewidths, W = 130 MHz (half-width at half-maximum). The lower pair of traces present the absorption lineshape, as experimentally observed under "rapid passage" conditions; the upper pair of traces are digital first derivatives to provide a more familiar EPR presentation. {CoNO}^{9} complexes **3** and **4** give identical Q-band spectra.

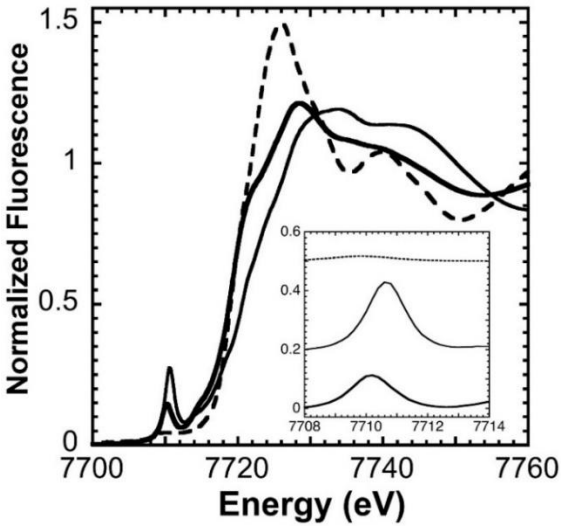

Figure 3.S17. XANES spectra of {CoNO}^{8} complex **2** (thin line) and {CoNO}^{9} complex **4** (thick line). The spectrum of Co^{II} nitrate is displayed as a dashed black line; spectra collected at 10 K. The XANES of {CoNO}^{8} **2** was previously published[43] and is presented here for comparison to {CoNO}^{9} **4**.

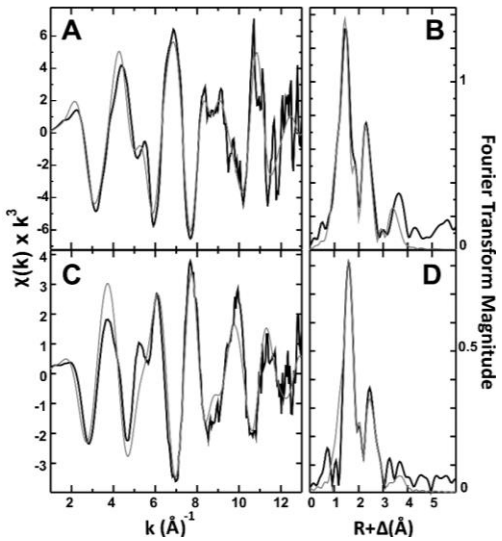

Figure 3.S18. EXAFS and Fourier transforms of the EXAFS data for {CoNO}^{8} (**2**) and {CoNO}^{9} (**4**). Raw EXAFS/Fourier transform data (black) and best fits (grey) for {CoNO}^{8} **2** (Panels A/B) and {CoNO}^{9} **4** (panels C/D). The EXAFS for {CoNO}^{8} **2** (panels A/B) was previously published[43] and is presented here for comparison to {CoNO}^{9} **4**.

Table 3.S3. Summary of best fit simulations to Co EXAFS[a] for $\{CoNO\}^8$ (**1**, **2**) and $\{CoNO\}^9$ (**3**, **4**).

Complex	Nearest Neighbor Ligand Environment[b]				Long Range Ligand Environment[b]								*F'*[g]
	Atom[c]	R(A)[d]	CN[e]	σ^2 [f]	Atom[c]	R(A)[d]	CN[e]	σ^2 [f]	Atom[c]	R(A)[d]	CN[e]	σ^2 [f]	
1	N	1.88	4.0	4.03	C	2.75	5.5	3.73	C	3.92	5	4.61	0.37
2	N	1.88	4.5	4.64	C	2.76	4.5	1.90	C	3.92	4.5	3.16	1.12
3	N	2.06	3.5	4.14	C	2.93	3.5	2.95	C	4.06	1.5	5.16	0.51
4	N	2.07	3.75	5.83	C	2.94	3.5	4.98	C	4.06	1.5	1.66	0.42
					C	3.33	1.0	3.43					

[a] Data were fit over a *k* range of 1 to 13.0 $Å^{-1}$.

[b] Independent metal-ligand scattering environment.

[c] Scattering atoms: N (nitrogen), C (carbon).

[d] Average metal-ligand bond length from two scans.

[e] Average metal-ligand coordination number from two scans.

[f] Average Debye-Waller factor in $Å^2 \times 10^3$ from two scans.

[g] Number of degrees of freedom weighted mean square deviation between data and fit.

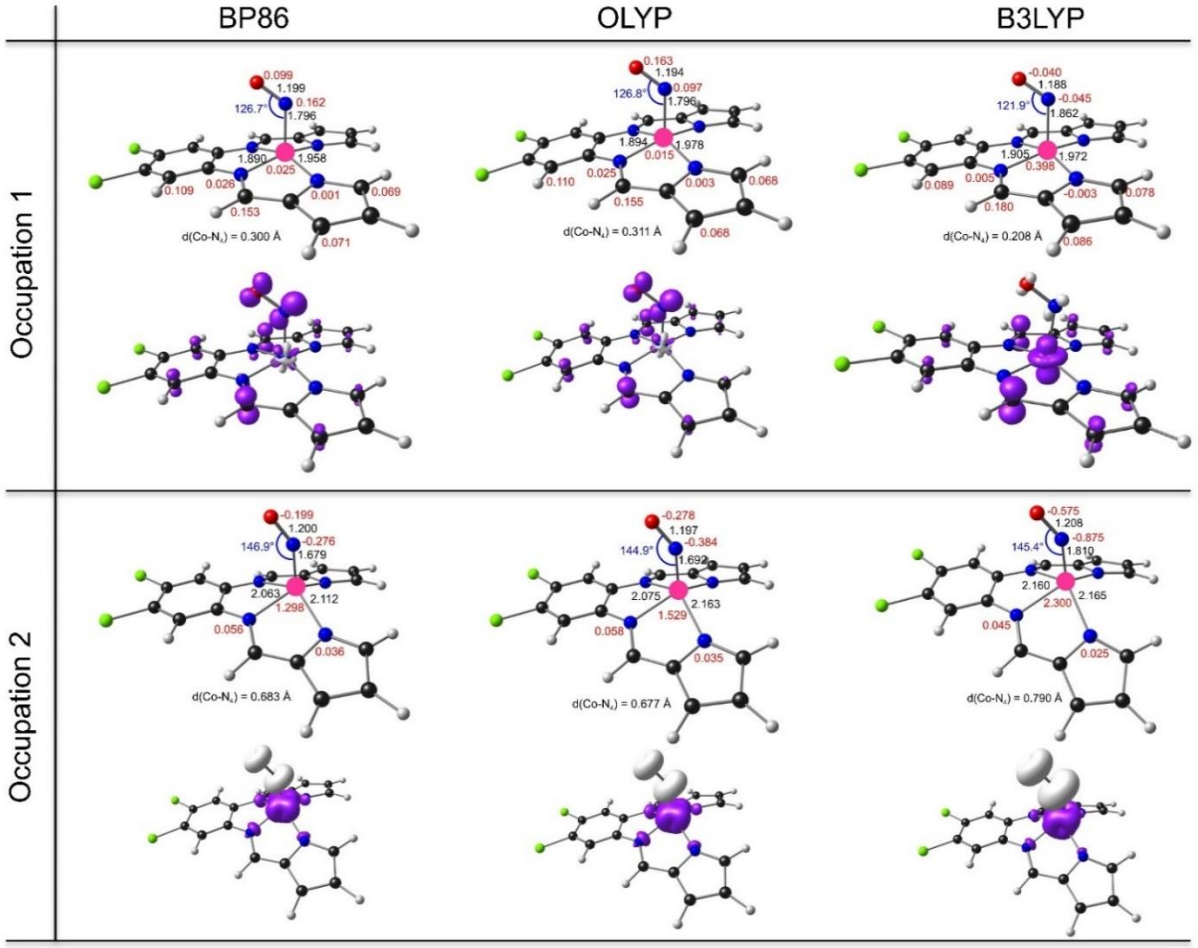

Figure 3.S19. Selected optimized distances (Å, black) and angles (deg, blue), and Mulliken spin populations (red) for the two $\{CoNO\}^9$ electronic states investigated (orbital occupations are defined in the main text). The displacement of Co from the N_4 equatorial plane is also given.

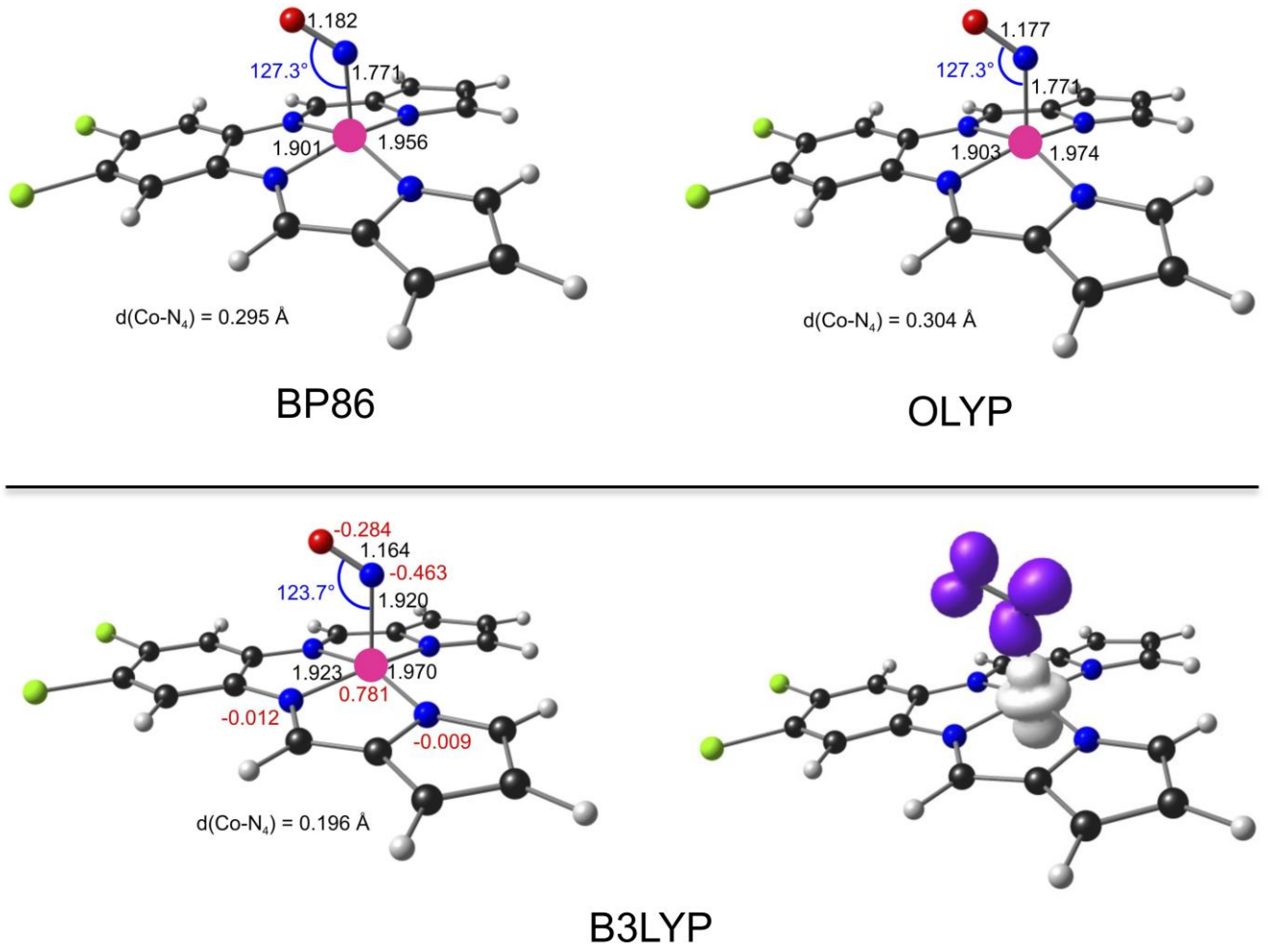

Figure 3.S20. Selected optimized distances (Å, black) and angles (deg, blue), and Mulliken spin populations (red) for the $\{CoNO\}^8$ state. The displacement of Co from the N_4 equatorial plane is also given.

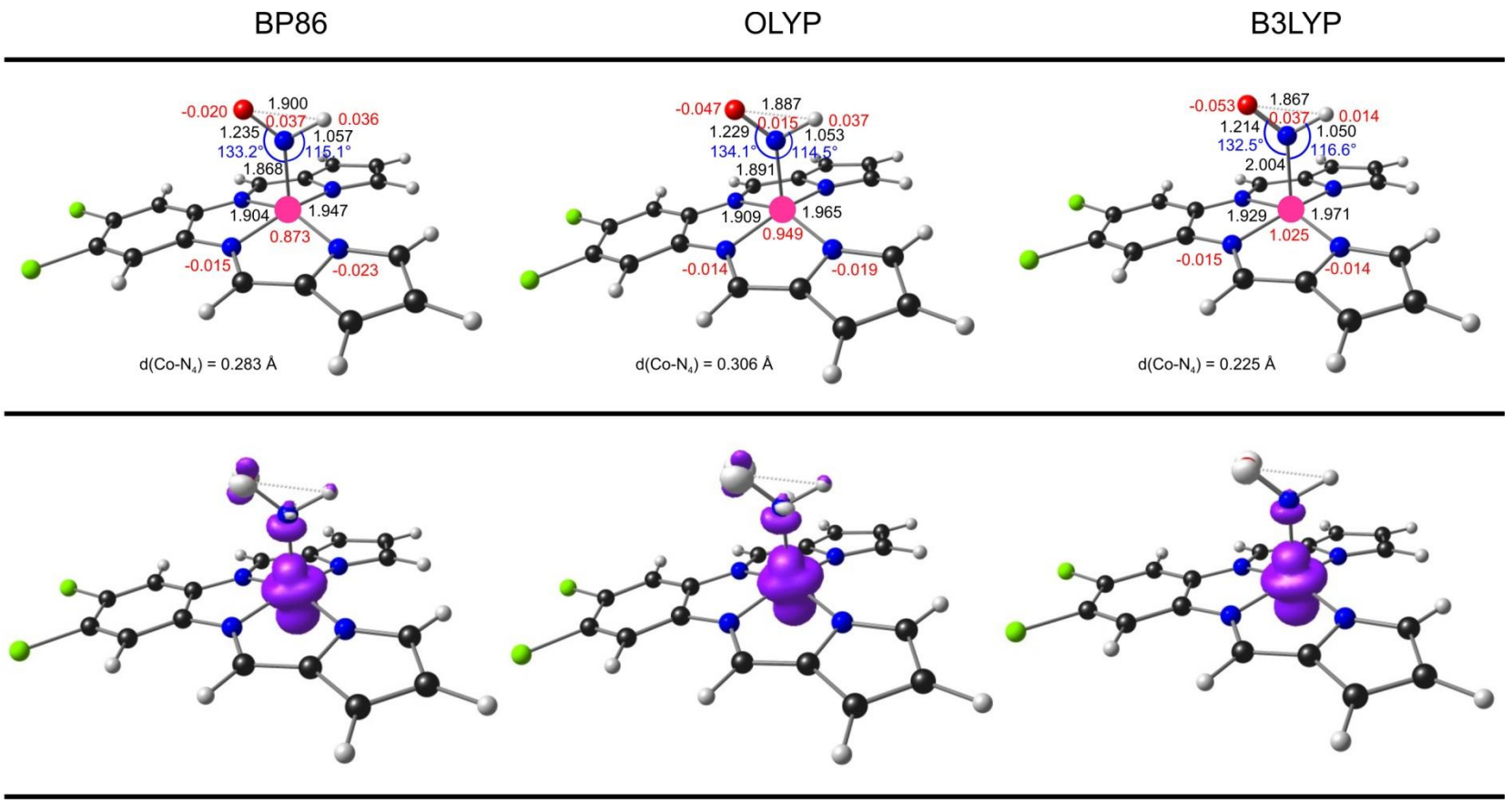

Figure 3.S21. Selected optimized distances (Å, black) and angles (deg, blue), and Mulliken spin populations (red) for the $\{CoHNO\}^9$ complex. The displacement of Co from the N_4 equatorial plane is also given.

Table 3.S4. Optimized BP86/TZP Cartesian coordinates for the $\{CoNO\}^8$ state, C_S, $S = 0$.

Co	0.141086000	-1.458680000	0.000000000
Cl	-0.128936000	5.142365000	1.607193000
Cl	-0.128936000	5.142365000	-1.607193000
C	-0.101918000	1.226794000	0.710412000
C	-0.101918000	1.226794000	-0.710412000
C	-0.110807000	2.438703000	1.406618000
C	-0.110807000	2.438703000	-1.406618000
C	-0.124476000	3.644947000	0.703724000
C	-0.124476000	3.644947000	-0.703724000
C	-0.239418000	-3.880939000	1.941526000
C	-0.239418000	-3.880939000	-1.941526000
C	-0.312449000	-0.431297000	2.516198000
C	-0.312449000	-0.431297000	-2.516198000
C	-0.342701000	-1.819678000	2.720131000
C	-0.342701000	-1.819678000	-2.720131000
C	-0.423679000	-3.979258000	3.343898000
C	-0.423679000	-3.979258000	-3.343898000
C	-0.491894000	-2.674499000	3.839589000
C	-0.491894000	-2.674499000	-3.839589000
H	-0.098908000	2.463504000	2.494276000
H	-0.098908000	2.463504000	-2.494276000
H	-0.143052000	-4.688956000	1.222319000
H	-0.143052000	-4.688956000	-1.222319000
H	-0.472443000	0.292163000	3.317980000
H	-0.472443000	0.292163000	-3.317980000
H	-0.504638000	-4.902275000	3.910724000
H	-0.504638000	-4.902275000	-3.910724000
H	-0.629255000	-2.365518000	4.871797000
H	-0.629255000	-2.365518000	-4.871797000
N	1.911861000	-1.455163000	0.000000000
N	-0.101608000	-0.055976000	1.259953000
N	-0.101608000	-0.055976000	-1.259953000
N	-0.196732000	-2.591280000	1.559141000
N	-0.196732000	-2.591280000	-1.559141000
O	2.626197000	-0.514037000	0.000000000

Table 3.S5. Optimized BP86/TZP Cartesian coordinates for the $\{CoNO\}^9$ state, C_S, S = 1/2, occupation 1.

Co	0.120676000	-1.450282000	0.000000000
Cl	-0.158231000	5.158967000	1.616896000
Cl	-0.158231000	5.158967000	-1.616896000
C	-0.096149000	1.226643000	0.711691000
C	-0.096149000	1.226643000	-0.711691000
C	-0.105901000	2.439966000	1.412586000
C	-0.105901000	2.439966000	-1.412586000
C	-0.126435000	3.651931000	0.697250000
C	-0.126435000	3.651931000	-0.697250000
C	-0.254364000	-0.411305000	2.534400000
C	-0.254364000	-0.411305000	-2.534400000
C	-0.278302000	-3.871779000	1.941774000
C	-0.278302000	-3.871779000	-1.941774000
C	-0.314511000	-1.805635000	2.735132000
C	-0.314511000	-1.805635000	-2.735132000
C	-0.407285000	-3.975063000	3.346669000
C	-0.407285000	-3.975063000	-3.346669000
C	-0.431153000	-2.665604000	3.855950000
C	-0.431153000	-2.665604000	-3.855950000
H	-0.102866000	2.464257000	2.499828000
H	-0.102866000	2.464257000	-2.499828000
H	-0.223832000	-4.672262000	1.209459000
H	-0.223832000	-4.672262000	-1.209459000
H	-0.336655000	0.321389000	3.338508000
H	-0.336655000	0.321389000	-3.338508000
H	-0.484849000	-4.900188000	3.914079000
H	-0.484849000	-4.900188000	-3.914079000
H	-0.516753000	-2.361182000	4.896213000
H	-0.516753000	-2.361182000	-4.896213000
N	1.912420000	-1.569374000	0.000000000
N	-0.114597000	-0.053044000	1.250799000
N	-0.114597000	-0.053044000	-1.250799000
N	-0.232196000	-2.573270000	1.564397000
N	-0.232196000	-2.573270000	-1.564397000
O	2.690812000	-0.657543000	0.000000000

Table 3.S6. Optimized BP86/TZP Cartesian coordinates for the $\{CoNO\}^9$ state, C_S, S = 1/2, occupation 2.

Co	0.526662000	-1.553802000	0.000000000
Cl	-0.214834000	5.161968000	1.616571000
Cl	-0.214834000	5.161968000	-1.616571000
C	-0.095061000	1.225360000	0.717553000
C	-0.095061000	1.225360000	-0.717553000
C	-0.127336000	2.446390000	1.404062000
C	-0.127336000	2.446390000	-1.404062000
C	-0.168715000	3.653632000	0.701534000
C	-0.168715000	3.653632000	-0.701534000
C	-0.318967000	-3.886317000	2.136102000
C	-0.318967000	-3.886317000	-2.136102000
C	-0.496933000	-0.400035000	2.463858000
C	-0.496933000	-0.400035000	-2.463858000
C	-0.529063000	-1.786470000	2.722297000
C	-0.529063000	-1.786470000	-2.722297000
C	-0.696498000	-3.889690000	3.505883000
C	-0.696498000	-3.889690000	-3.505883000
C	-0.840189000	-2.548272000	3.879945000
C	-0.840189000	-2.548272000	-3.879945000
H	-0.114741000	2.469122000	2.492976000
H	-0.114741000	2.469122000	-2.492976000
H	-0.145084000	-4.745628000	1.491636000
H	-0.145084000	-4.745628000	-1.491636000
H	-0.859631000	-4.768059000	4.128084000
H	-0.859631000	-4.768059000	-4.128084000
H	-0.871255000	0.323683000	3.199839000
H	-0.871255000	0.323683000	-3.199839000
H	-1.113180000	-2.156160000	4.857522000
H	-1.113180000	-2.156160000	-4.857522000
N	2.201502000	-1.430556000	0.000000000
N	-0.066115000	-0.039930000	1.269365000
N	-0.066115000	-0.039930000	-1.269365000
N	-0.221859000	-2.632019000	1.655159000
N	-0.221859000	-2.632019000	-1.655159000
O	3.156303000	-0.703292000	0.000000000

Table 3.S7. Optimized OLYP/TZP Cartesian coordinates for the $\{CoNO\}^8$ state, C_S, $S = 0$.

Co	0.169270000	-1.453515000	0.000000000
Cl	-0.159513000	5.138089000	1.618907000
Cl	-0.159513000	5.138089000	-1.618907000
C	-0.083862000	1.233320000	0.709284000
C	-0.083862000	1.233320000	-0.709284000
C	-0.106194000	2.446831000	1.400644000
C	-0.106194000	2.446831000	-1.400644000
C	-0.134513000	3.655125000	0.703513000
C	-0.134513000	3.655125000	-0.703513000
C	-0.248384000	-3.872061000	1.970124000
C	-0.248384000	-3.872061000	-1.970124000
C	-0.310930000	-0.426261000	2.506622000
C	-0.310930000	-0.426261000	-2.506622000
C	-0.347949000	-1.811324000	2.717369000
C	-0.347949000	-1.811324000	-2.717369000
C	-0.462557000	-3.954769000	3.367266000
C	-0.462557000	-3.954769000	-3.367266000
C	-0.528797000	-2.647149000	3.844487000
C	-0.528797000	-2.647149000	-3.844487000
H	-0.095351000	2.473619000	2.483909000
H	-0.095351000	2.473619000	-2.483909000
H	-0.146010000	-4.689411000	1.267110000
H	-0.146010000	-4.689411000	-1.267110000
H	-0.490760000	0.290067000	3.305976000
H	-0.490760000	0.290067000	-3.305976000
H	-0.564149000	-4.869125000	3.939684000
H	-0.564149000	-4.869125000	-3.939684000
H	-0.685242000	-2.323346000	4.866521000
H	-0.685242000	-2.323346000	-4.866521000
N	1.938756000	-1.529058000	0.000000000
N	-0.072733000	-0.046813000	1.259330000
N	-0.072733000	-0.046813000	-1.259330000
N	-0.184750000	-2.591604000	1.573850000
N	-0.184750000	-2.591604000	-1.573850000
O	2.691556000	-0.624056000	0.000000000

Table 3.S8. Optimized OLYP/TZP Cartesian coordinates for the $\{CoNO\}^9$ state, C_S, S = 1/2, occupation 1.

Co	0.146594000	-1.446495000	0.000000000
Cl	-0.198163000	5.156100000	1.627347000
Cl	-0.198163000	5.156100000	-1.627347000
C	-0.069875000	1.234641000	0.710603000
C	-0.069875000	1.234641000	-0.710603000
C	-0.097586000	2.449911000	1.406533000
C	-0.097586000	2.449911000	-1.406533000
C	-0.136752000	3.663797000	0.696914000
C	-0.136752000	3.663797000	-0.696914000
C	-0.238440000	-0.402607000	2.528173000
C	-0.238440000	-0.402607000	-2.528173000
C	-0.298724000	-3.860054000	1.976796000
C	-0.298724000	-3.860054000	-1.976796000
C	-0.314208000	-1.793065000	2.736649000
C	-0.314208000	-1.793065000	-2.736649000
C	-0.440095000	-3.945068000	3.379304000
C	-0.440095000	-3.945068000	-3.379304000
C	-0.450988000	-2.631785000	3.868779000
C	-0.450988000	-2.631785000	-3.868779000
H	-0.098422000	2.477210000	2.489046000
H	-0.098422000	2.477210000	-2.489046000
H	-0.250580000	-4.671422000	1.260696000
H	-0.250580000	-4.671422000	-1.260696000
H	-0.328307000	0.323249000	3.332990000
H	-0.328307000	0.323249000	-3.332990000
H	-0.535240000	-4.860122000	3.955305000
H	-0.535240000	-4.860122000	-3.955305000
H	-0.540915000	-2.310874000	4.900957000
H	-0.540915000	-2.310874000	-4.900957000
N	1.929172000	-1.664221000	0.000000000
N	-0.078298000	-0.042364000	1.250686000
N	-0.078298000	-0.042364000	-1.250686000
N	-0.233590000	-2.571202000	1.582445000
N	-0.233590000	-2.571202000	-1.582445000
O	2.754153000	-0.801589000	0.000000000

Table 3.S9. Optimized OLYP/TZP Cartesian coordinates for the $\{CoNO\}^9$ state, C_S, S = 1/2, occupation 2.

Co	0.513801000	-1.560829000	0.000000000
Cl	-0.215006000	5.152511000	1.628049000
Cl	-0.215006000	5.152511000	-1.628049000
C	-0.114170000	1.224284000	0.717050000
C	-0.114170000	1.224284000	-0.717050000
C	-0.141064000	2.448296000	1.396965000
C	-0.141064000	2.448296000	-1.396965000
C	-0.177393000	3.658177000	0.700903000
C	-0.177393000	3.658177000	-0.700903000
C	-0.309659000	-3.880721000	2.241712000
C	-0.309659000	-3.880721000	-2.241712000
C	-0.493633000	-0.393022000	2.473504000
C	-0.493633000	-0.393022000	-2.473504000
C	-0.517988000	-1.774550000	2.758112000
C	-0.517988000	-1.774550000	-2.758112000
C	-0.667186000	-3.845444000	3.614013000
C	-0.667186000	-3.845444000	-3.614013000
C	-0.810442000	-2.495826000	3.944184000
C	-0.810442000	-2.495826000	-3.944184000
H	-0.124374000	2.473167000	2.480994000
H	-0.124374000	2.473167000	-2.480994000
H	-0.140016000	-4.758411000	1.624481000
H	-0.140016000	-4.758411000	-1.624481000
H	-0.815361000	-4.702170000	4.264695000
H	-0.815361000	-4.702170000	-4.264695000
H	-0.856848000	0.328377000	3.212311000
H	-0.856848000	0.328377000	-3.212311000
H	-1.070031000	-2.072586000	4.909437000
H	-1.070031000	-2.072586000	-4.909437000
N	2.204615000	-1.495060000	0.000000000
N	-0.081291000	-0.036227000	1.274788000
N	-0.081291000	-0.036227000	-1.274788000
N	-0.223006000	-2.646965000	1.719448000
N	-0.223006000	-2.646965000	-1.719448000
O	3.156182000	-0.768175000	0.000000000

Table 3.S10. Optimized B3LYP/TZP Cartesian coordinates for the $\{CoNO\}^8$ state, C_S, $M_S = 0$ (broken-symmetry).

Co	0.022537000	-1.474201000	0.000000000
Cl	-0.085514000	5.152029000	1.627012000
Cl	-0.085514000	5.152029000	-1.627012000
C	-0.132052000	3.655683000	0.702908000
C	-0.132052000	3.655683000	-0.702908000
C	-0.154749000	2.445627000	1.400159000
C	-0.154749000	2.445627000	-1.400159000
C	-0.170207000	-3.887484000	2.001010000
C	-0.170207000	-3.887484000	-2.001010000
C	-0.178869000	1.230536000	0.712658000
C	-0.178869000	1.230536000	-0.712658000
C	-0.298767000	-1.823479000	2.741488000
C	-0.298767000	-1.823479000	-2.741488000
C	-0.306239000	-3.968729000	3.411733000
C	-0.306239000	-3.968729000	-3.411733000
C	-0.318057000	-0.433283000	2.526916000
C	-0.318057000	-0.433283000	-2.526916000
C	-0.389539000	-2.659145000	3.882710000
C	-0.389539000	-2.659145000	-3.882710000
H	-0.075846000	-4.704222000	1.298190000
H	-0.075846000	-4.704222000	-1.298190000
H	-0.136756000	2.467433000	2.482758000
H	-0.136756000	2.467433000	-2.482758000
H	-0.340258000	-4.878334000	3.993786000
H	-0.340258000	-4.878334000	-3.993786000
H	-0.449405000	0.274266000	3.342878000
H	-0.449405000	0.274266000	-3.342878000
H	-0.500270000	-2.335895000	4.908087000
H	-0.500270000	-2.335895000	-4.908087000
N	1.942924000	-1.478303000	0.000000000
N	-0.166931000	-2.613481000	1.595867000
N	-0.166931000	-2.613481000	-1.595867000
N	-0.180689000	-0.047098000	1.273429000
N	-0.180689000	-0.047098000	-1.273429000
O	2.590256000	-0.511035000	0.000000000

Table 3.S11. Optimized B3LYP/TZP Cartesian coordinates for the $\{CoNO\}^9$ state, C_S, S = 1/2, occupation 1.

Co	-0.021306000	-1.459481000	0.000000000
Cl	-0.053853000	5.158194000	1.633977000
Cl	-0.053853000	5.158194000	-1.633977000
C	-0.113999000	3.652929000	0.696356000
C	-0.113999000	3.652929000	-0.696356000
C	-0.153477000	2.437049000	1.405284000
C	-0.153477000	2.437049000	-1.405284000
C	-0.179110000	-3.882931000	1.994762000
C	-0.179110000	-3.882931000	-1.994762000
C	-0.206031000	1.222205000	0.714790000
C	-0.206031000	1.222205000	-0.714790000
C	-0.221819000	-3.971840000	3.406211000
C	-0.221819000	-3.971840000	-3.406211000
C	-0.275753000	-1.816022000	2.752998000
C	-0.275753000	-1.816022000	-2.752998000
C	-0.282555000	-0.418298000	2.541739000
C	-0.282555000	-0.418298000	-2.541739000
C	-0.284137000	-2.657981000	3.893574000
C	-0.284137000	-2.657981000	-3.893574000
H	-0.121444000	-4.690924000	1.277764000
H	-0.121444000	-4.690924000	-1.277764000
H	-0.135592000	2.458401000	2.487440000
H	-0.135592000	2.458401000	-2.487440000
H	-0.212432000	-4.884942000	3.986458000
H	-0.212432000	-4.884942000	-3.986458000
H	-0.322662000	-2.341552000	4.927182000
H	-0.322662000	-2.341552000	-4.927182000
H	-0.322729000	0.300386000	3.356184000
H	-0.322729000	0.300386000	-3.356184000
N	1.839172000	-1.543686000	0.000000000
N	-0.220140000	-2.598623000	1.597683000
N	-0.220140000	-2.598623000	-1.597683000
N	-0.243450000	-0.051073000	1.263328000
N	-0.243450000	-0.051073000	-1.263328000
O	2.510885000	-0.564408000	0.000000000

Table 3.S12. Optimized B3LYP/TZP Cartesian coordinates for the $\{CoNO\}^9$ state, C_S, S = 1/2, occupation 2.

Co	0.687807000	-1.593454000	0.000000000
Cl	-0.215916000	5.177815000	1.633674000
Cl	-0.215916000	5.177815000	-1.633674000
C	-0.112150000	1.238271000	0.717667000
C	-0.112150000	1.238271000	-0.717667000
C	-0.148037000	2.459049000	1.398474000
C	-0.148037000	2.459049000	-1.398474000
C	-0.187627000	3.670356000	0.699965000
C	-0.187627000	3.670356000	-0.699965000
C	-0.313690000	-3.914925000	2.156143000
C	-0.313690000	-3.914925000	-2.156143000
C	-0.607018000	-0.425414000	2.393567000
C	-0.607018000	-0.425414000	-2.393567000
C	-0.614341000	-1.816539000	2.665427000
C	-0.614341000	-1.816539000	-2.665427000
C	-0.915571000	-3.904713000	3.442669000
C	-0.915571000	-3.904713000	-3.442669000
C	-1.114559000	-2.558979000	3.765468000
C	-1.114559000	-2.558979000	-3.765468000
H	-0.035431000	-4.780770000	1.567726000
H	-0.035431000	-4.780770000	-1.567726000
H	-0.122523000	2.476414000	2.481670000
H	-0.122523000	2.476414000	-2.481670000
H	-1.115941000	0.262814000	3.076048000
H	-1.115941000	0.262814000	-3.076048000
H	-1.178399000	-4.769969000	4.036812000
H	-1.178399000	-4.769969000	-4.036812000
H	-1.556734000	-2.154881000	4.666833000
H	-1.556734000	-2.154881000	-4.666833000
N	2.482065000	-1.351532000	0.000000000
N	-0.058867000	-0.022847000	1.281180000
N	-0.058867000	-0.022847000	-1.281180000
N	-0.131691000	-2.674678000	1.687085000
N	-0.131691000	-2.674678000	-1.687085000
O	3.375864000	-0.538360000	0.000000000

Table 3.S13. Optimized BP86/TZP Cartesian coordinates for the Co^{II}-HNO state, C_S, S = 1/2.

Co	0.108452000	-1.449595000	0.000000000
Cl	-0.143447000	5.154145000	1.607112000
Cl	-0.143447000	5.154145000	-1.607112000
C	-0.123562000	1.238852000	0.710622000
C	-0.123562000	1.238852000	-0.710622000
C	-0.130001000	2.451006000	1.406645000
C	-0.130001000	2.451006000	-1.406645000
C	-0.140238000	3.657147000	0.704095000
C	-0.140238000	3.657147000	-0.704095000
C	-0.265013000	-3.875766000	1.928840000
C	-0.265013000	-3.875766000	-1.928840000
C	-0.295907000	-0.423178000	2.522337000
C	-0.295907000	-0.423178000	-2.522337000
C	-0.324610000	-1.814714000	2.719148000
C	-0.324610000	-1.814714000	-2.719148000
C	-0.424142000	-3.977760000	3.333368000
C	-0.424142000	-3.977760000	-3.333368000
C	-0.464564000	-2.674260000	3.836092000
C	-0.464564000	-2.674260000	-3.836092000
H	2.382610000	-2.500667000	0.000000000
H	-0.120710000	2.475457000	2.494450000
H	-0.120710000	2.475457000	-2.494450000
H	-0.207066000	-4.681888000	1.203153000
H	-0.207066000	-4.681888000	-1.203153000
H	-0.419010000	0.294088000	3.336469000
H	-0.419010000	0.294088000	-3.336469000
H	-0.513550000	-4.902221000	3.896780000
H	-0.513550000	-4.902221000	-3.896780000
H	-0.583673000	-2.368966000	4.871775000
H	-0.583673000	-2.368966000	-4.871775000
N	1.974422000	-1.525876000	0.000000000
N	-0.131212000	-0.043259000	1.261328000
N	-0.131212000	-0.043259000	-1.261328000
N	-0.209275000	-2.582885000	1.551005000
N	-0.209275000	-2.582885000	-1.551005000
O	2.855282000	-0.660756000	0.000000000

Table 3.S14. Optimized OLYP/TZP Cartesian coordinates for the Co^{II}-HNO state or $\{CoHNO\}^9$, C_S, $S = 1/2$.

Co	0.158972000	-1.447364000	0.000000000
Cl	-0.168334000	5.146565000	1.618544000
Cl	-0.168334000	5.146565000	-1.618544000
C	-0.107511000	1.241874000	0.709515000
C	-0.107511000	1.241874000	-0.709515000
C	-0.126650000	2.455460000	1.400681000
C	-0.126650000	2.455460000	-1.400681000
C	-0.150382000	3.663633000	0.703699000
C	-0.150382000	3.663633000	-0.703699000
C	-0.269501000	-3.871923000	1.951771000
C	-0.269501000	-3.871923000	-1.951771000
C	-0.318086000	-0.423389000	2.508277000
C	-0.318086000	-0.423389000	-2.508277000
C	-0.348288000	-1.812056000	2.710424000
C	-0.348288000	-1.812056000	-2.710424000
C	-0.497084000	-3.959424000	3.345368000
C	-0.497084000	-3.959424000	-3.345368000
C	-0.550021000	-2.653198000	3.829433000
C	-0.550021000	-2.653198000	-3.829433000
H	2.432109000	-2.527738000	0.000000000
H	-0.115670000	2.481383000	2.483990000
H	-0.115670000	2.481383000	-2.483990000
H	-0.183787000	-4.686862000	1.243792000
H	-0.183787000	-4.686862000	-1.243792000
H	-0.487501000	0.285200000	3.317122000
H	-0.487501000	0.285200000	-3.317122000
H	-0.620877000	-4.875464000	3.910673000
H	-0.620877000	-4.875464000	-3.910673000
H	-0.718058000	-2.333835000	4.851014000
H	-0.718058000	-2.333835000	-4.851014000
N	2.047228000	-1.548012000	0.000000000
N	-0.102318000	-0.037509000	1.260500000
N	-0.102318000	-0.037509000	-1.260500000
N	-0.182664000	-2.587904000	1.563062000
N	-0.182664000	-2.587904000	-1.563062000
O	2.948764000	-0.712332000	0.000000000

Table 3.S15. Optimized B3LYP/TZP Cartesian coordinates for the Co^{II}-HNO state or $\{CoHNO\}^9$, C_S, $S = 1/2$.

Co	0.059597000	-1.469693000	0.000000000
Cl	-0.120670000	5.161926000	1.627529000
Cl	-0.120670000	5.161926000	-1.627529000
C	-0.144994000	3.664413000	0.702715000
C	-0.144994000	3.664413000	-0.702715000
C	-0.151725000	2.454457000	1.400366000
C	-0.151725000	2.454457000	-1.400366000
C	-0.159568000	1.239455000	0.712790000
C	-0.159568000	1.239455000	-0.712790000
C	-0.234038000	-3.885674000	1.992206000
C	-0.234038000	-3.885674000	-1.992206000
C	-0.316693000	-1.818771000	2.734423000
C	-0.316693000	-1.818771000	-2.734423000
C	-0.318268000	-0.425010000	2.522714000
C	-0.318268000	-0.425010000	-2.522714000
C	-0.418083000	-3.964999000	3.396163000
C	-0.418083000	-3.964999000	-3.396163000
C	-0.472178000	-2.653076000	3.868274000
C	-0.472178000	-2.653076000	-3.868274000
H	2.511501000	-2.467013000	0.000000000
H	-0.136100000	2.476492000	2.482989000
H	-0.136100000	2.476492000	-2.482989000
H	-0.158360000	-4.703654000	1.288211000
H	-0.158360000	-4.703654000	-1.288211000
H	-0.462146000	0.280647000	3.338533000
H	-0.462146000	0.280647000	-3.338533000
H	-0.507007000	-4.873604000	3.974064000
H	-0.507007000	-4.873604000	-3.974064000
H	-0.610178000	-2.328790000	4.890025000
H	-0.610178000	-2.328790000	-4.890025000
N	2.063178000	-1.517063000	0.000000000
N	-0.158016000	-0.038014000	1.274615000
N	-0.158016000	-0.038014000	-1.274615000
N	-0.171004000	-2.609484000	1.590914000
N	-0.171004000	-2.609484000	-1.590914000
O	2.904841000	-0.641748000	0.000000000

N_2O (mmol)	Avg. Area
0	0
0.1364	26.581
0.06813	15.346
0.01135	4.031
0.001137	0.552
0.0001137	0.04843

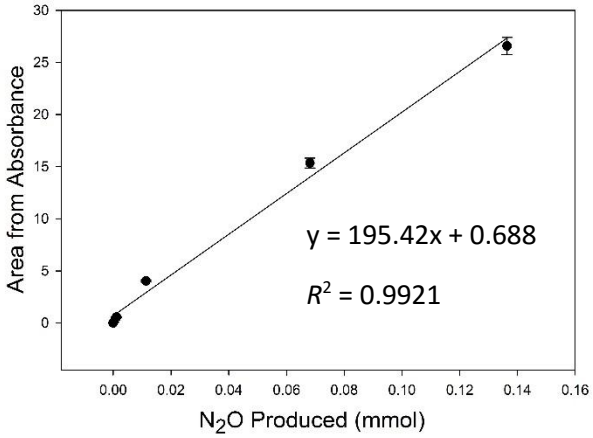

Figure 3.S22. (*Left*) Table presenting integrated area data in the N_2O IR spectrum (P and R branches combined) based on the concentration of Piloty's acid. (*Right*) Calibration curve of the IR spectral area derived from the decomposition of Piloty's acid in H_2O at pH > 12.0. Each point was recorded after reacting for 2 h by an FTIR headspace analysis of the N_2O produced. Each point represents the average of three trials.

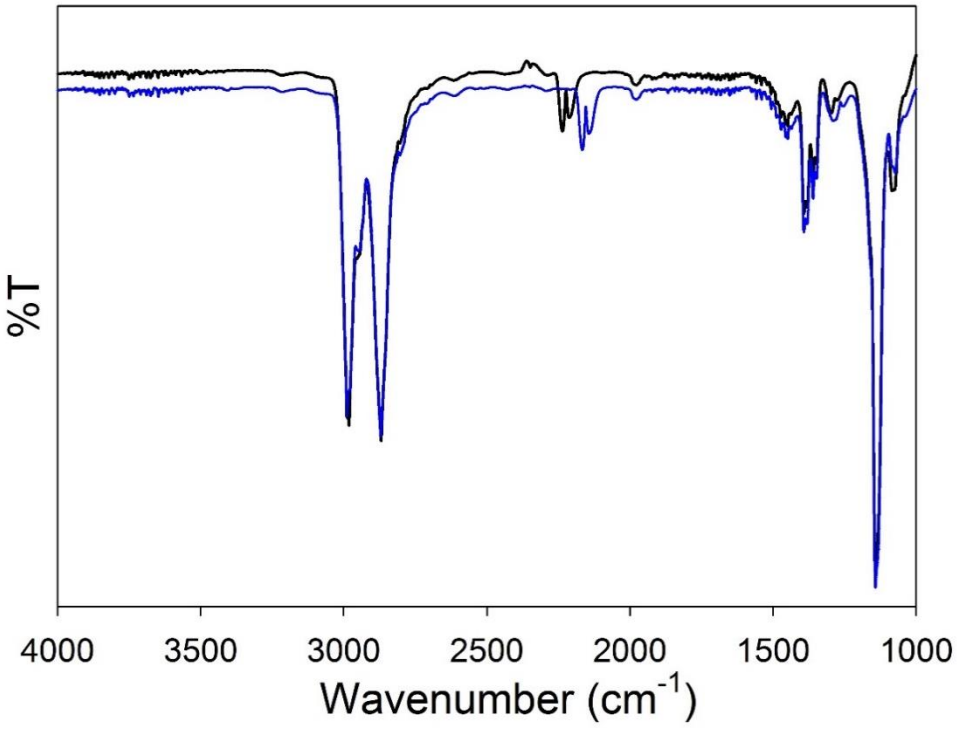

Figure 3.S23. Headspace FTIR spectrum of the reaction of 10 mol-equiv of HBF_4•Et_2O with **3** (black) or **3-^{15}NO** (blue) at t = 24 h (CaF_2 windows). Conditions: DMSO:H_2O (1:9), RT. Figure 3.7 highlights the N_2O bands at ~ 2200 cm^{-1}.

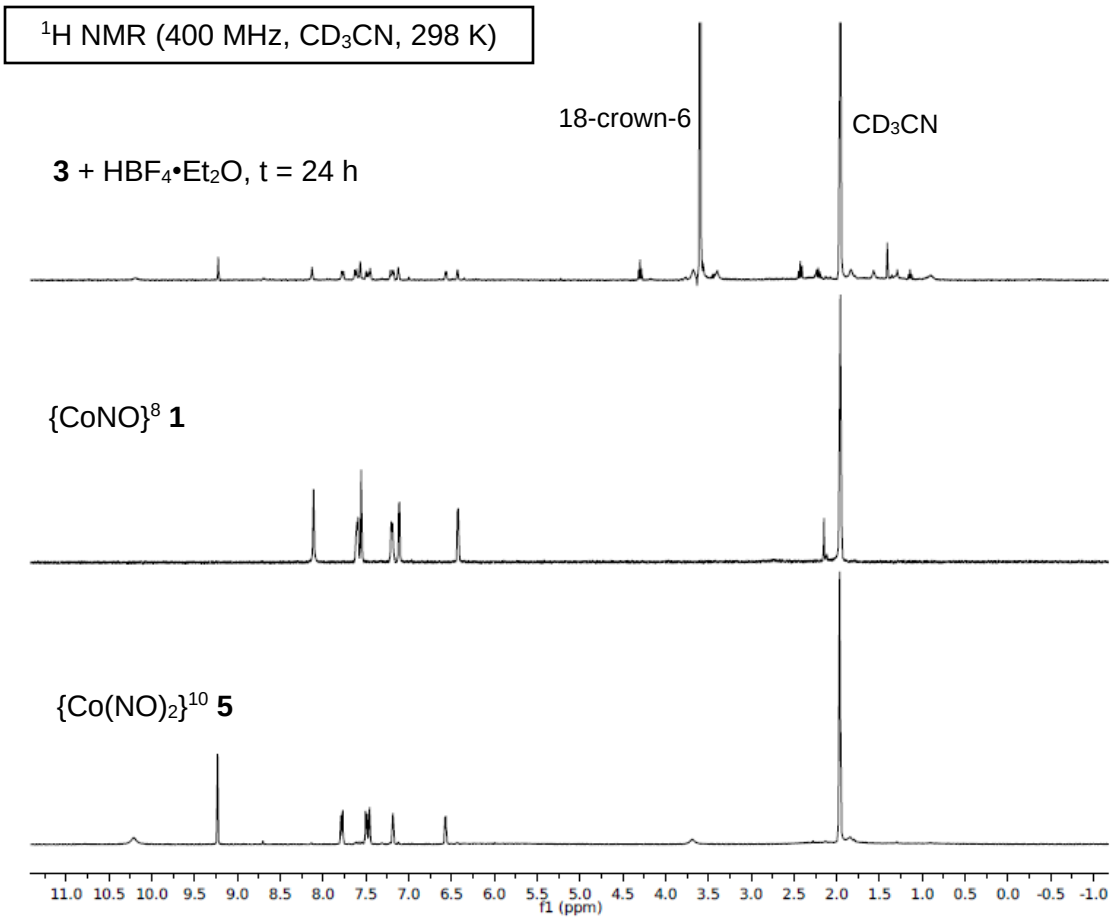

Figure 3.S24. ^{1}H NMR of the reaction of **3** and HBF_4•Et_2O (1/1.3; t = 24 h) in MeCN (*top*), independently synthesized {CoNO}^{8} **1** (*middle*), and independently synthesized {Co(NO)$_2$}^{10} **5** (*bottom*) (δ vs. residual protio solvent signal in CD_3CN). Peaks at 3.51 and 1.94 are from 18C6 and residual protio solvent, respectively. See Figure 3.S25 for expansion. 18C6 and CH_3CN peaks in the {CoNO}^{9} **3**/H^+ spectrum (*top*) were truncated for clarity.

^{1}H NMR (400 MHz, CD_3CN, 298 K)

3 + HBF_4•Et_2O, t = 24 h

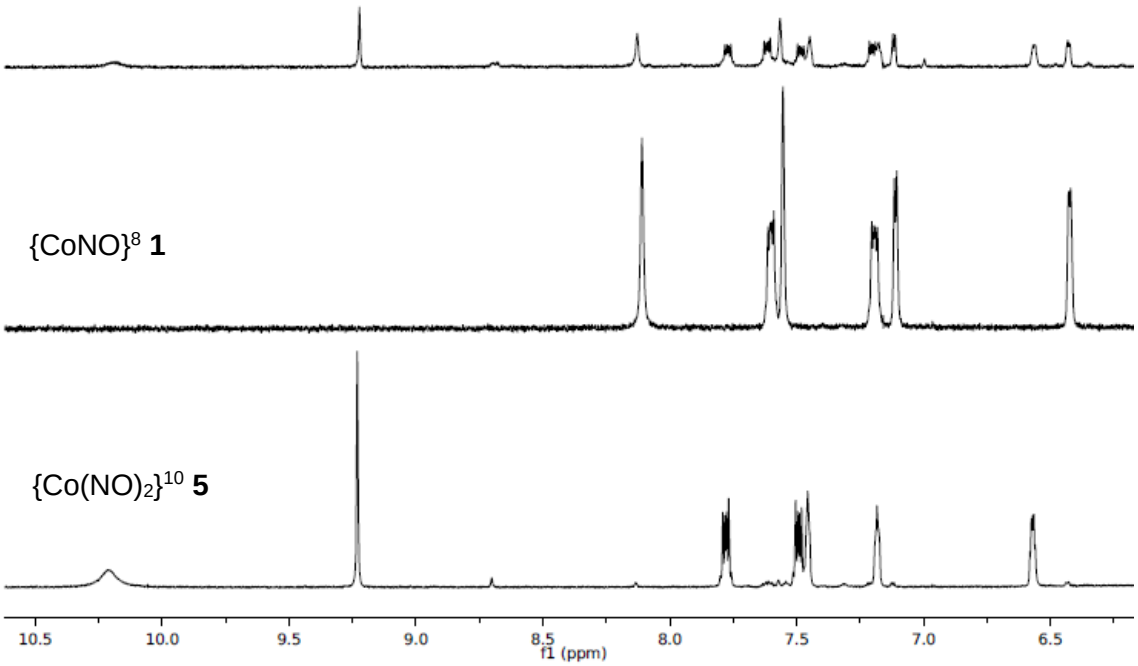

Figure 3.S25. Expansion of the aromatic region from Figure 3.S24. ^{1}H NMR of the reaction of **3** and HBF_4•Et_2O (1:1.3; t = 24 h) in MeCN (*top*), independently synthesized $\{CoNO\}^8$ **1** (*middle*), and independently synthesized $\{Co(NO)_2\}^{10}$ **5** (*bottom*) (δ vs. residual protio solvent signal in CD_3CN).

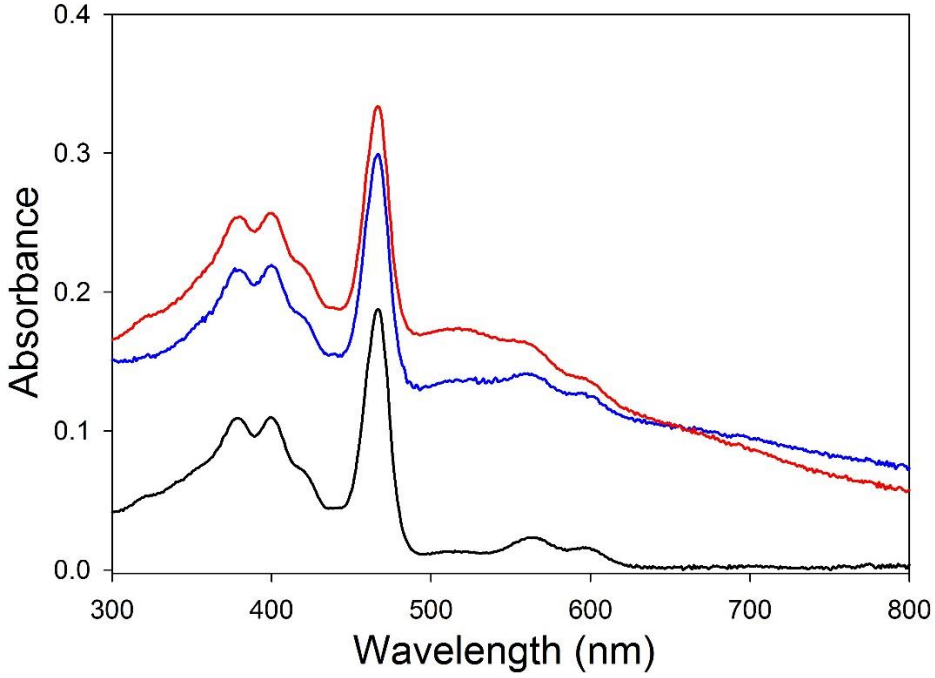

Figure 3.S26. UV-vis spectrum of a 4.35 μM buffer solution of $[Mn(TPPS)]^{3-}$ before (black line) and after (red line, t = 1 min; blue line, t = 24 h) reaction with $\{CoNO\}^{8}$ complex **1** (5 equiv) at 298 K in 10 mM PBS (pH 7.4).

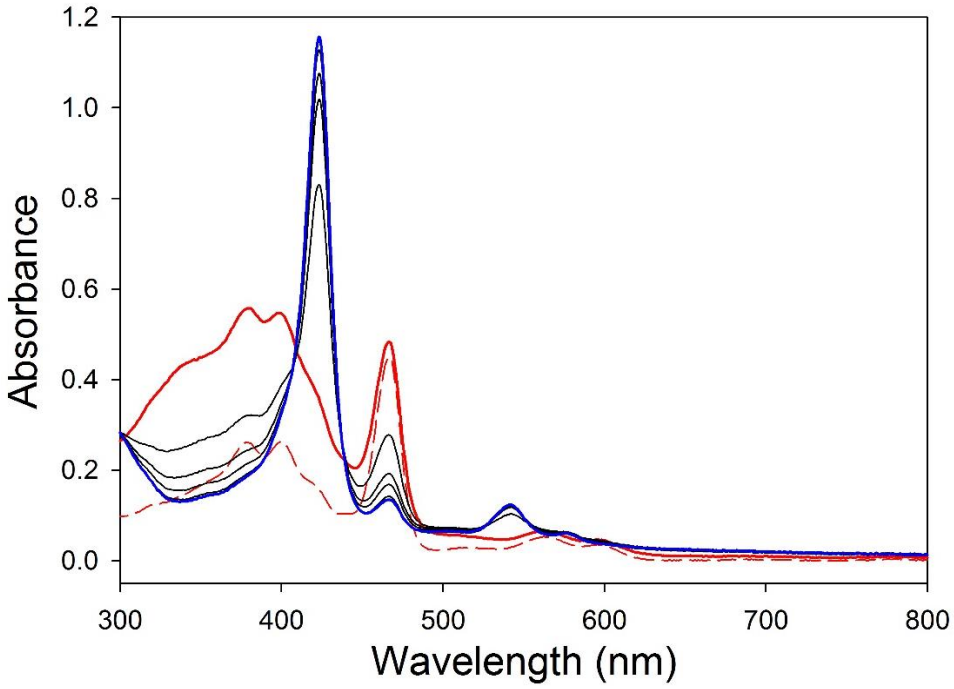

Figure 3.S27. UV-vis spectrum of a 9.90 μM buffer solution of $[Mn(TPPS)]^{3-}$ before (red dash) and immediately after addition of $\{Co(NO)_2\}^{10}$ complex **5** (red solid; 2.5 equiv) (10 mM PBS, pH 7.4, 298 K). Black traces represent 4 h intervals after the addition of **5**. Final trace of $[Mn(TPPS)(NO)]^{4-}$ in blue (t = 19 h).

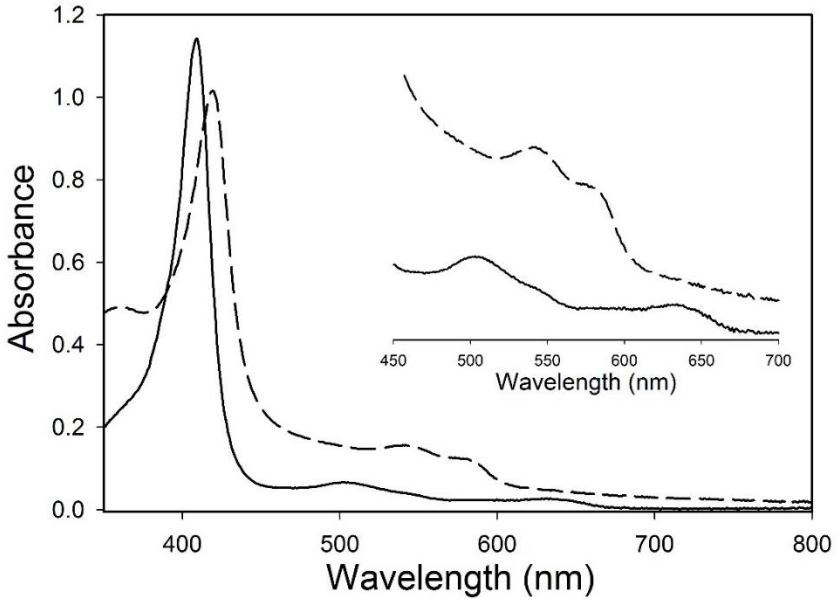

Figure 3.S28. UV-vis spectrum of a 6.02 µM solution of metMb before (black line) and after (t = 3.5 h; black dashed line) reaction with {CoNO}^{9} complex **4** (5 equiv) at 310 K in 10 mM PBS (pH 7.4). *Inset*: expansion of the Q-band region.

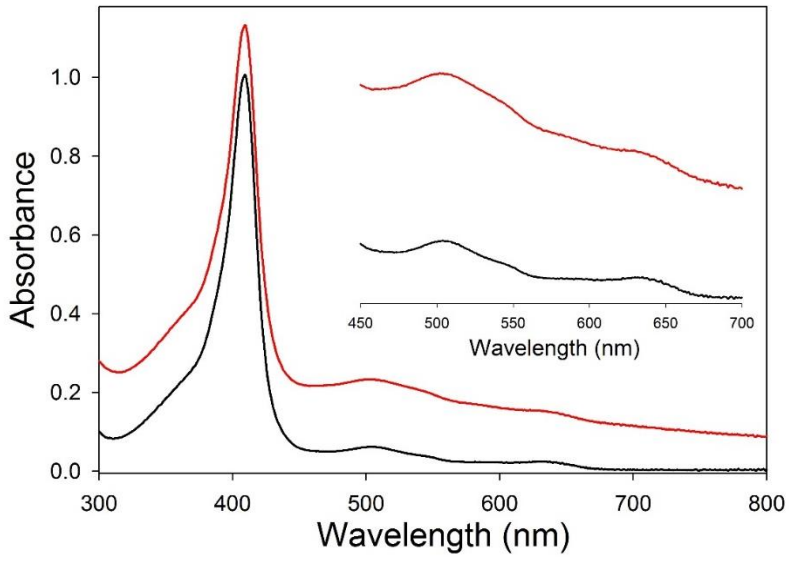

Figure 3.S29. UV-vis spectrum of a 5.35 µM solution of metMb before (black line) and after (t = 2 h; red line) reaction with {CoNO}^{8} complex **1** (5 equiv) at 310 K in 10 mM PBS (pH 7.4). *Inset*: expansion of the Q-band region.

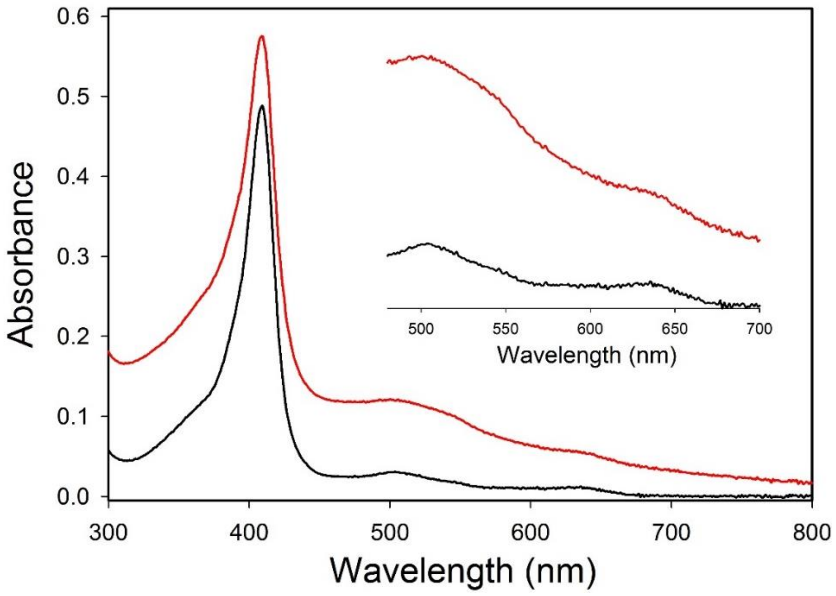

Figure 3.S30. UV-vis spectrum of a 2.64 μM solution of metMb before (black line) and after (t = 2 h; red line) reaction with $\{CoNO\}^8$ complex **2** (5 equiv) at 310 K in 10 mM PBS (pH 7.4). *Inset*: expansion of the Q-band region.

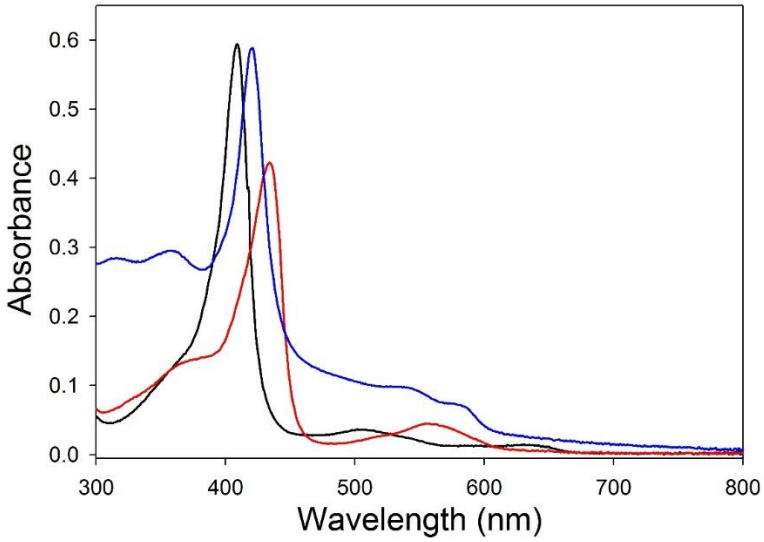

Figure 3.S31. UV-vis spectrum of a 3.16 μM buffer solution of metMb before (black), after the addition of 1 equiv of sodium dithionite (t = 1 min; red), and after the addition of 5 equiv of $\{CoNO\}^8$ complex **1** (blue trace: t = 5 min) (10 mM PBS, pH 7.4, 310 K).

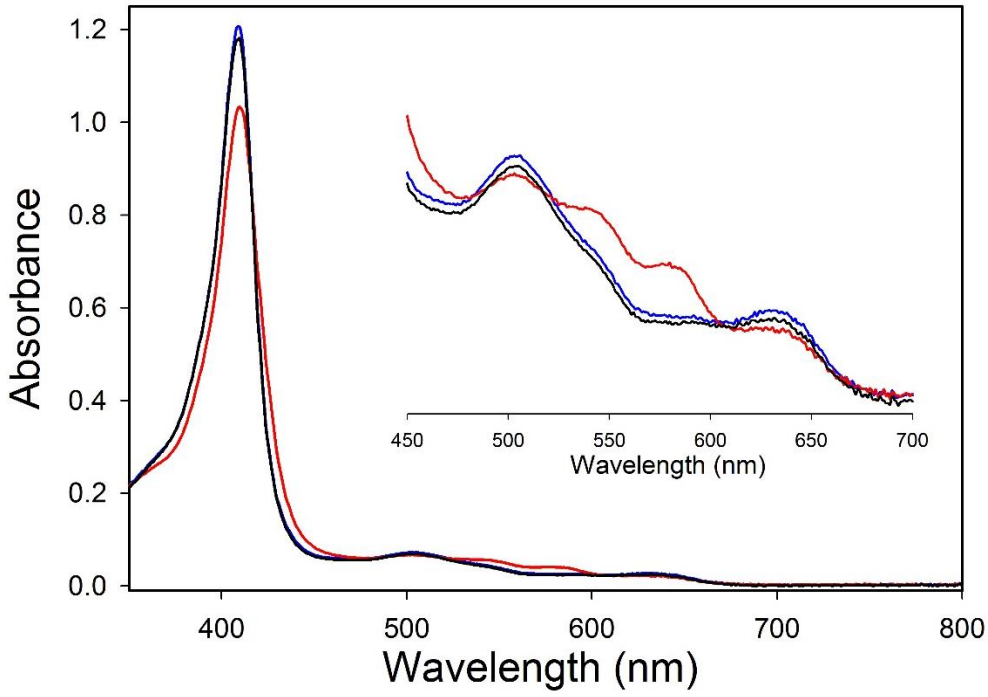

Figure 3.S32. UV-vis spectrum of a 6.42 µM buffer solution of metMb before (blue) and after the addition of 2.5 equiv $\{Co(NO)_2\}^{10}$ complex **5** at t = 4 h (red trace) and t = 24 h (black trace) (10 mM PBS, pH 7.4, 310 K).

3.15 References

(1) Bartberger, M. D.; Liu, W.; Ford, E.; Miranda, K. M.; Switzer, C.; Fukuto, J. M.; Farmer, P. J.; Wink, D. A.; Houk, K. N. *Proc. Natl. Acad. Sci. U.S.A.* **2002**, *99*, 10958.

(2) Speelman, A. L.; Lehnert, N. *Acc. Chem. Res.* **2014**, *47*, 1106.

(3) Kumar, M. R.; Fukuto, J. M.; Miranda, K. M.; Farmer, P. J. *Inorg. Chem.* **2010**, *49*, 6283.

(4) Lehnert, N.; Scheidt, W. R.; Wolf, M. W. *Struct. Bond.* **2014**, *154*, 155.

(5) Shiro, Y.; Fujii, M.; Iizuka, T.; Adachi, S.-i.; Tsukamoto, K.; Nakahara, K.; Shoun, H. *J. Biol. Chem.* **1995**, *270*, 1617.

(6) Daiber, A.; Nauser, T.; Takaya, N.; Kudo, T.; Weber, P.; Hultschig, C.; Shoun, H.; Ullrich, V. *J. Inorg. Biochem.* **2002**, *88*, 343.

(7) Obayashi, E.; Takahashi, S.; Shiro, Y. *J. Am. Chem. Soc.* **1998**, *120*, 12964.

(8) Zheng, S.; Berto, T. C.; Dahl, E. W.; Hoffman, M. B.; Speelman, A. L.; Lehnert, N. *J. Am. Chem. Soc.* **2013**, *135*, 4902.

(9) Maia, L. B.; Moura, J. J. G. *Chem. Rev.* **2014**, *114*, 5273.

(10) Bykov, D.; Neese, F. *Inorg. Chem.* **2015**, *54*, 9303.

(11) Enemark, J. H.; Feltham, R. D. *Coord. Chem. Rev.* **1974**, *13*, 339. $\{MNO\}^n$ where n = number of metal d + NO π^* electrons.

(12) Lin, R.; Farmer, P. J. *J. Am. Chem. Soc.* **2000**, *122*, 2393.

(13) Sulc, F.; Immoos, C. E.; Pervitsky, D.; Farmer, P. J. *J. Am. Chem. Soc.* **2004**, *126*, 1096.

(14) Brown, K. L. *Chem. Rev.* **2005**, *105*, 2075.

(15) Pallares, I. G.; Brunold, T. C. *Inorg. Chem.* **2014**, *53*, 7676.

(16) Brouwer, M.; Chamulitrat, W.; Ferruzzi, G.; Sauls, D. L.; Weinberg, J. B. *Blood* **1996**, *88*, 1857.

(17) Subedi, H.; Hassanin, H. A.; Brasch, N. E. *Inorg. Chem.* **2014**, *53*, 1570.

(18) Subedi, H.; Brasch, N. E. *Eur. J. Inorg. Chem.* **2015**, *2015*, 3825.

(19) Subedi, H.; Brasch, N. E. *Dalton Trans.* **2016**, *45*, 352.

(20) Carmel, R.; Jacobsen, D. W., *Homocysteine in Health and Disease*. Cambridge University Press: Cambridge, U.K., 2001.

(21) Qureshi, G. A.; Memon, S. A.; Collin, C.; Parvez, S. H. *Biogenic Amines* **2004**, *18*, 117.

(22) Fukuto, J. M.; Carrington, S. J. *Antioxid. Redox Sign.* **2011**, *14*, 1649.

(23) Paolocci, N.; Jackson, M. I.; Lopez, B. E.; Miranda, K.; Tocchetti, C. G.; Wink, D. A.; Hobbs, A. J.; Fukuto, J. M. *Pharmacol. Ther.* **2007**, *113*, 442.

(24) Flores-Santana, W.; Salmon, D. J.; Donzelli, S.; Switzer, C. H.; Basudhar, D.; Ridnour, L.; Cheng, R.; Glynn, S. A.; Paolocci, N.; Fukuto, J. M.; Miranda, K. M.; Wink, D. A. *Antioxid. Redox Sign.* **2011**, *14*, 1659.

(25) Moncada, S.; Higgs, E. A. *Br. J. Pharmacol.* **2006**, *147*, S193.

(26) Irvine, J. C.; Ritchie, R. H.; Favaloro, J. L.; Andrews, K. L.; Widdop, R. E.; Kemp-Harper, B. K. *Trends Pharmacol. Sci.* **2008**, *29*, 601.

(27) Paolocci, N.; Saavedra, W. F.; Miranda, K. M.; Martignani, C.; Isoda, T.; Hare, J. M.; Espey, M. G.; Fukuto, J. M.; Feelisch, M.; Wink, D. A.; Kass, D. A. *Proc. Natl. Acad. Sci. U.S.A.* **2001**, *98*, 10463.

(28) Rosen, G. M.; Tsai, P.; Pou, S. *Chem. Rev.* **2002**, *102*, 1191.

(29) Eberhardt, M.; Dux, M.; Namer, B.; Miljkovic, J.; Cordasic, N.; Will, C.; Kichko, T. I.; de la Roche, J.; Fischer, M.; Suárez, S. A.; Bikiel, D.; Dorsch, K.; Leffler, A.; Babes, A.; Lampert, A.; Lennerz, J. K.; Jacobi, J.; Martí, M. A.; Doctorovich, F.; Högestätt, E. D.; Zygmunt, P. M.;

Ivanović-Burmazović, I.; Messlinger, K.; Reeh, P.; Filipovic, M. R. *Nature Commun.* **2014**, *5*, 4381.

(30) Miljkovic, J. L.; Kenkel, I.; Ivanović-Burmazović, I.; Filipovic, M. R. *Angew. Chem. Int. Ed.* **2013**, *52*, 12061

(31) Filipovic, M. R.; Eberhardt, M.; Prokopovic, V.; Mijuskovic, A.; Orescanin-Dusic, Z.; Reeh, P.; Ivanović-Burmazović, I. *J. Med. Chem.* **2013**, *56*, 1499.

(32) Wedmann, R.; Zahl, A.; Shubina, T. E.; Dürr, M.; Heinemann, F. W.; Bugenhagen, B. E. C.; Burger, P.; Ivanović-Burmazović, I.; Filipovic, M. R. *Inorg. Chem.* **2015**, *54*, 9367.

(33) Suarez, S. A.; Neuman, N. I.; Muñoz, M.; Álvarez, L.; Bikiel, D. E.; Brondino, C. D.; Ivanović-Burmazović, I.; Miljkovic, J. L.; Filipovic, M. R.; Martí, M. A.; Doctorovich, F. *J. Am. Chem. Soc.* **2015**, *137*, 4720.

(34) Shafirovich, V.; Lymar, S. V. *Proc. Natl. Acad. Sci. U.S.A.* **2002**, *99*, 7340.

(35) Miranda, K. M. *Coord. Chem. Rev.* **2005**, *249*, 433.

(36) Kohout, F. C.; Lampe, F. W. *J. Am. Chem. Soc.* **1965**, *87*, 5795.

(37) Smith, P. A. S.; Hein, G. E. *J. Am. Chem. Soc.* **1960**, *82*, 5731.

(38) Angeli, A.; Angelico, F.; Scurti, F. *Chem. Zentralbl.* **1902**, *73*, 691.

(39) DeMaster, E. G.; Redfern, B.; Nagasawa, H. T. *Biochem. Pharmacol.* **1998**, *55*, 2007.

(40) Nagasawa, H. T.; DeMaster, E. G.; Redfern, B.; Shirota, F. N.; Goon, D. J. W. *J. Med. Chem.* **1990**, *33*, 3120.

(41) Patra, A. K.; Dube, K. S.; Sanders, B. C.; Papaefthymiou, G. C.; Conradie, J.; Ghosh, A.; Harrop, T. C. *Chem. Sci.* **2012**, *3*, 364.

(42) Sanders, B. C.; Patra, A. K.; Harrop, T. C. *J. Inorg. Biochem.* **2013**, *118*, 115.

(43) Rhine, M. A.; Rodrigues, A. V.; Bieber Urbauer, R. J.; Urbauer, J. L.; Stemmler, T. L.; Harrop, T. C. *J. Am. Chem. Soc.* **2014**, *136*, 12560.

(44) McCleverty, J. A. *Chem. Rev.* **2004**, *104*, 403 and references therein.

(45) Wyllie, G. R. A.; Scheidt, W. R. *Chem. Rev.* **2002**, *102*, 1067 and references therein.

(46) Wright, A. M.; Hayton, T. W. *Comment Inorg. Chem.* **2012**, *33*, 207 and references therein.

(47) Ellison, M. K.; Scheidt, W. R. *Inorg. Chem.* **1998**, *37*, 382.

(48) Fujita, E.; Chang, C. K.; Fajer, J. *J. Am. Chem. Soc.* **1985**, *107*, 7665.

(49) Franz, K. J.; Doerrer, L. H.; Spingler, B.; Lippard, S. J. *Inorg. Chem.* **2001**, *40*, 3774.

(50) Kozhukh, J.; Lippard, S. J. *J. Am. Chem. Soc.* **2012**, *134*, 11120.

(51) Hess, J. L.; Conder, H. L.; Green, K. N.; Darensbourg, M. Y. *Inorg. Chem.* **2008**, *47*, 2056.

(52) Uyeda, C.; Peters, J. C. *J. Am. Chem. Soc.* **2013**, *135*, 12023.

(53) Kumar, P.; Lee, Y.-M.; Hu, L.; Chen, J.; Park, Y. J.; Yao, J.; Chen, H.; Karlin, K. D.; Nam, W. *J. Am. Chem. Soc.* **2016**, *138*, 7753.

(54) Kumar, P.; Lee, Y.-M.; Park, Y. J.; Siegler, M. A.; Karlin, K. D.; Nam, W. *J. Am. Chem. Soc.* **2015**, *137*, 4284.

(55) Doyle, M. P.; Pickering, R. A.; Dykstra, R. L.; Cook, B. R. *J. Am. Chem. Soc.* **1982**, *104*, 3392. The species responsible for release of the NO moiety may be a reduced cobalt nitrosyl given the presence of excess reductant.

(56) Doyle, M. P.; Van Doornik, F. J.; Funckes, C. L. *Inorg. Chim. Acta* **1980**, *46*, L111. $[Co(NH_3)_5(NO)]Cl_2$ reacts with both Fe^{III}- and Fe^{II}-heme proteins.

(57) Ungermann, C. B.; Caulton, K. G. *J. Am. Chem. Soc.* **1976**, *98*, 3862.

(58) Caulton, K. G. *J. Am. Chem. Soc.* **1973**, *95*, 4076.

(59) Blanchard, A. A.; Rafter, J. R.; Adams, W. B., Jr. *J. Am. Chem. Soc.* **1934**, *56*, 16.

(60) Coleman, G. W.; Blanchard, A. A. *J. Am. Chem. Soc.* **1936**, *58*, 2160.

(61) Thyagarajan, S.; Incarvito, C. D.; Rheingold, A. L.; Theopold, K. H. *Inorg. Chim. Acta* **2003**, *345*, 333.

(62) Tomson, N. C.; Crimmin, M. R.; Petrenko, T.; Rosebrugh, L. E.; Sproules, S.; Boyd, W. C.; Bergman, R. G.; DeBeer, S.; Toste, F. D.; Wieghardt, K. *J. Am. Chem. Soc.* **2011**, *133*, 18785.

(63) Sacconi, L.; Ghilardi, C. A.; Mealli, C.; Zanobini, F. *Inorg. Chem.* **1975**, *14*, 1380.

(64) Di Vaira, M.; Ghilardi, C. A.; Sacconi, L. *Inorg. Chem.* **1976**, *15*, 1555.

(65) Chuang, C.-H.; Liaw, W.-F.; Hung, C.-H. *Angew. Chem. Int. Ed.* **2016**, *55*, 5190.

(66) Mason, J.; Larkworthy, L. F.; Moore, E. A. *Chem. Rev.* **2002**, *102*, 913.

(67) Addison, A. W.; Rao, T. N.; Reedijk, J.; van Rijn, J.; Verschoor, G. C. *J. Chem. Soc. Dalton Trans.* **1984**, 1349.

(68) Pellegrino, J.; Bari, S. E.; Bikiel, D. E.; Doctorovich, F. *J. Am. Chem. Soc.* **2010**, *132*, 989.

(69) Sanders, B. C.; Rhine, M. A.; Harrop, T. C. *Struct. Bond.* **2014**, *160*, 57.

(70) Harrop, T. C. *Adv. Inorg. Chem.* **2015**, *67*, 243.

(71) Gautam, R.; Loughrey, J. J.; Astashkin, A. V.; Shearer, J.; Tomat, E. *Angew. Chem. Int. Ed.* **2015**, *54*, 14894.

(72) Ramdhanie, B.; Telser, J.; Caneschi, A.; Zakharov, L. N.; Rheingold, A. L.; Goldberg, D. P. *J. Am. Chem. Soc.* **2004**, *126*, 2515.

(73) Fujii, H.; Dou, Y.; Zhou, H.; Yoshida, T.; Ikeda-Saito, M. *J. Am. Chem. Soc.* **1998**, *120*, 8251.

(74) Little, R. G.; Hoffman, B. M.; Ibers, J. A. *Bioinorg. Chem.* **1974**, *3*, 207.

(75) Wayland, B. B.; Minkiewicz, J. V.; Abd-Elmageed, M. E. *J. Am. Chem. Soc.* **1974**, *96*, 2795.

(76) Wayland, B. B.; Abd-Elmageed, M. E. *J. Am. Chem. Soc.* **1974**, *96*, 4809.

(77) McGarvey, B. R. *Can. J. Chem.* **1975**, *53*, 2498.

(78) Solomon, E. I.; Heppner, D. E.; Johnston, E. M.; Ginsbach, J. W.; Cirera, J.; Qayyum, M.; Kieber-Emmons, M. T.; Kjaergaard, C. H.; Hadt, R. G.; Tian, L. *Chem. Rev.* **2014**, *114*, 3659.

(79) Garribba, E.; Micera, G. *J. Chem. Ed.* **2006**, *83*, 1229.

(80) García Serres, R.; Grapperhaus, C. A.; Bothe, E.; Bill, E.; Weyhermüller, T.; Neese, F.; Wieghardt, K. *J. Am. Chem. Soc.* **2004**, *126*, 5138.

(81) Brown, T. G.; Hoffman, B. M. *Mol. Phys.* **1980**, *39*, 1073.

(82) Hori, H.; Ikeda-Saito, M.; Froncisz, W.; Yonetani, T. *J. Biol. Chem.* **1983**, *258*, 12368.

(83) Hyde, J. S.; Froncisz, W. *Annu. Rev. Biophys. Bioeng.* **1982**, *11*, 391.

(84) Liptak, M. D.; Fleischhacker, A. S.; Matthews, R. G.; Telser, J.; Brunold, T. C. *J. Phys. Chem. B.* **2009**, *113*, 5245.

(85) Padden, K. M.; Krebs, J. F.; MacBeth, C. E.; Scarrow, R. C.; Borovik, A. S. *J. Am. Chem. Soc.* **2001**, *123*, 1072.

(86) Wirt, M. D.; Sagi, I.; Chen, E.; Frisbie, S. M.; Lee, R.; Chance, M. R. *J. Am. Chem. Soc.* **1991**, *113*, 5299.

(87) Padden, K. M.; Krebs, J. F.; Trafford, K. T.; Yap, G. P. A.; Rheingold, A. H.; Borovik, A. S.; Scarrow, R. C. *Chem. Mater.* **2001**, *13*, 4305.

(88) Adrait, A.; Jacquamet, L.; Le Pape, L.; Gonzalez de Peredo, A.; Aberdam, D.; Hazemann, J.-L.; Latour, J.-M.; Michaud-Soret, I. *Biochemistry* **1999**, *38*, 6248.

(89) Kleifeld, O.; Rulíšek, L.; Bogin, O.; Frenkel, A.; Havlas, Z.; Burstein, Y.; Sagi, I. *Biochemistry* **2004**, *43*, 7151.

(90) Reviews on quantum chemical studies on nitrosyls: (a) Ghosh, A. *Acc. Chem. Res*. **2005**, *38*, 943. (b) Ghosh, A.; Hopmann, K. H.; Conradie, *J. in Computational Inorganic and Bioinorganic Chemistry*, eds. Solomon, E. I.; Scott, R. A.; King, R. B., John Wiley & Sons Ltd: Chichester, UK,

2009, pp. 389− 410. (c) Goodrich, L. E.; Paulat, F.; Praneeth, V. K. K.; Lehnert, N. *Inorg. Chem.* **2010**, *49*, 6293.

(91) DFT calculation on CoNO complexes: (a) Jaworska, M. *Chem. Phys.* **2007**, *332*, 203. (b) Hopmann, K. H.; Conradie, J.; Tangen, E.; Tonzetich, Z. J.; Lippard, S. J.; Ghosh, A. *Inorg. Chem.* **2015**, *54*, 7362.

(92) The notation A´ 61||60 means that there are 61 *a* or spin-up electrons and 60 *b* or spin-down electrons in the irreducible representation A´ (C_s point group symmetry).

(93) The $\{CoNO\}^9$ porphyrin in reference 65 functions as an NO reductase model and liberates N_2O in THF mixtures with a protic solvent (H_2O, MeOH, EtOH) via a putative N_2O_2-bridging intermediate.

(94) Heinecke, J. L.; Khin, C.; Pereira, J. C. M.; Suárez, S. A.; Iretskii, A. V.; Doctorovich, F.; Ford, P. C. *J. Am. Chem. Soc.* **2013**, *135*, 4007.

(95) Łapiński, A.; Spanget-Larsen, J.; Waluk, J.; Radziszewski, J. G. *J. Chem. Phys.* **2001**, *115*, 1757.

(96) Hughes, M. N.; Cammack, R. *Methods Enzymol.* **1999**, *301*, 279.

(97) $[Co^{III}(LN_4^{Ph})]^+$ and $[Co^{I}(LN_4^{Ph})]^-$ may be the products of $[Co^{II}(LN_4^{Ph})]$ disproportionation.

(98) Reactions of **1** and **2** with HBF_4•Et_2O (1:1.3) in THF reveal the presence of trace N_2O by IR.

(99) Martí, M. A.; Bari, S. E.; Estrin, D. A.; Doctorovich, F. *J. Am. Chem. Soc.* **2005**, *127*, 4680.

(100) Álvarez, L.; Suarez, S. A.; Bikiel, D. E.; Reboucas, J. S.; Batinić-Haberle, I.; Martí, M. A.; Doctorovich, F. *Inorg. Chem.* **2014**, *53*, 7351.

(101) Doctorovich, F.; Bikiel, D. E.; Pellegrino, J.; Suárez, S. A.; Martí, M. A. *Acc. Chem. Res.* **2014**, *47*, 2907.

(102) Pereira, J. C. M.; Iretskii, A. V.; Han, R.-M.; Ford, P. C. *J. Am. Chem. Soc.* **2015**, *137*, 328.

(103) Fitzpatrick, J.; Kim, E. *Acc. Chem. Res.* **2015**, *48*, 2453.

(104) Tran, C. T.; Kim, E. *Inorg. Chem.* **2012**, *51*, 10086.

(105) Romberg, R. W.; Kassner, R. J. *Biochemistry* **1979**, *18*, 5387.

(106) Antonini, E.; Brunori, M., *Hemoglobin and Myoglobin in their Reactions with Ligands*. North-Holland Publishing Company: Amsterdam, 1971.

(107) Andrei, D.; Salmon, D. J.; Donzelli, S.; Wahab, A.; Klose, J. R.; Citro, M. L.; Saavedra, J. E.; Wink, D. A.; Miranda, K. M.; Keefer, L. K. *J. Am. Chem. Soc.* **2010**, *132*, 16526.

(108) Bazylinski, D. A.; Hollocher, T. C. *J. Am. Chem. Soc.* **1985**, *107*, 7982.

(109) Tseng, Y.-T.; Chen, C.-H.; Lin, J.-Y.; Li, B.-H.; Lu, Y.-H.; Lin, C.-H.; Chen, H.-T.; Weng, T.-C.; Sokaras, D.; Chen, H.-Y.; Soo, Y.-L.; Lu, T.-T. *Chem. Eur. J.* **2015**, *21*, 17570.

(110) Goodrich, L. E.; Roy, S.; Alp, E. E.; Zhao, J.; Hu, M. Y.; Lehnert, N. *Inorg. Chem.* **2013**, *52*, 7766.

(111) Choi, I.-K.; Liu, Y.; Feng, D.; Paeng, K.-J.; Ryan, M. D. *Inorg. Chem.* **1991**, *30*, 1832.

(112) Gao, Y.; Toubaei, A.; Kong, X.; Wu, G. *Angew. Chem. Int. Ed.* **2014**, *53*, 11547.

(113) Lehnert, N.; Praneeth, V. K. K.; Paulat, F. *J. Comput. Chem.* **2006**, *27*, 1338.

(114) A similar trend has been observed upon protonation of a 6C $\{FeNO\}^8$ complex with ~0.05 Å increases in Fe-N(O) and N-O. However, there is no spin-state change. See reference 113.

(115) McCrory, C. C. L.; Uyeda, C.; Peters, J. C. *J. Am. Chem. Soc.* **2012**, *134*, 3164.

(116) Stubbert, B. D.; Peters, J. C.; Gray, H. B. *J. Am. Chem. Soc.* **2011**, *133*, 18070.

(117) Valdez, C. N.; Dempsey, J. L.; Brunschwig, B. S.; Winkler, J. R.; Gray, H. B. *Proc. Natl. Acad. Sci. U.S.A.* **2012**, *109*, 15589.

(118) Zee, D. Z.; Chantarojsiri, T.; Long, J. R.; Chang, C. J. *Acc. Chem. Res.* **2015**, *48*, 2027 and references therein.

(119) Kelley, P.; Day, M. W.; Agapie, T. *Eur. J. Inorg. Chem.* **2013**, *2013*, 3840.

(120) Basu, D.; Mazumder, S.; Niklas, J.; Baydoun, H.; Wanniarachchi, D.; Shi, X.; Staples, R. J.; Poluektov, O.; Schlegel, H. B.; Verani, C. N. *Chem. Sci.* **2016**, *7*, 3264.

(121) Ding, K.; Brennessel, W. W.; Holland, P. L. *J. Am. Chem. Soc.* **2009**, *131*, 10804.

(122) Betley, T. A.; Peters, J. C. *J. Am. Chem. Soc.* **2003**, *125*, 10782.

(123) Chapovetsky, A.; Do, T. H.; Haiges, R.; Takase, M. K.; Marinescu, S. C. *J. Am. Chem. Soc.* **2016**, *138*, 5765.

(124) Werst, M. M.; Davoust, C. E.; Hoffman, B. M. *J. Am. Chem. Soc.* **1991**, *113*, 1533.

(125) Mailer, C.; Taylor, C. P. S. *Biochim. Biophys. Acta* **1973**, *322*, 195.

(126) Belford, R. L.; Nilges, M. J., In *EPR Symposium, 21st Rocky Mountain Conference*, Denver, Colorado. August, 1979.

(127) Te Velde, G.; Bickelhaupt, F. M.; Baerends, E. J.; Fenseca Guerra, C.; Van Gisbergen, S. J. A.; Snijders, J. G.; Ziegler, T. *J. Comput. Chem.* **2001**, *22*, 931.

(128) For a comparison of different exchange-correlation functionals for transition metal systems, see, e.g.: (a) M. Reiher; Salomon, O.; Hess, B. A. *Theor. Chem. Acc*. **2001**, *107*, 48. (b) Ghosh, A.; Taylor, P. R. *Curr. Opin. Chem. Biol*. **2003**, *7*, 113. (c) Conradie, J.; Swarts, J. C.; Ghosh, A. *J. Phys. Chem. B* **2004**, *108*, 452. (d) Swart, M.; Ehlers, A. W.; Lammertsma, K. *Mol. Phys*. **2004**, *102*, 2647. (e) Conradie, J.; Ghosh, A. *J. Phys. Chem. B* **2007**, *111*, 12621; (f) Hopmann, K. H.; Conradie J.; Ghosh, A. *J. Phys. Chem. B* **2009**, *113*, 10540; (g) Conradie, M. M.; Conradie, J.; Ghosh, A. *J. Inorg. Biochem*. **2011**, *105*, 84.

(129) Becke, A. D. *Phys. Rev. A* **1988**, *38*, 3098.

(130) Perdew, J. P. *Phys. Rev. B* **1986**, *33*, 8822.

(131) Erratum.; Perdew, J. P. *Phys. Rev. B* **1986**, *34*, 7406.

(132) Handy, N. C.; Cohen, A. J. *Mol. Phys.* **2001**, *99*, 403.

(133) Lee, C. H.; Yang, W.; Parr, R. G. *Phys. Rev. B* **1988**, *37*, 785.

(134) Johnson, B. G.; Gill, P. M. W.; Pople, J. A. *J. Chem. Phys.* **1993**, *98*, 5612.

(135) Russo, T. V.; Martin, R. L.; Hay, P. J. *J. Chem. Phys.* **1994**, *101*, 7729.

(136) Becke, A. D. *J. Chem. Phys.* **1993**, *98*, 5648.

(137) Stephens, P. J.; Devlin, F. J.; Chabalowski, C. F.; Frisch, M. J. *J. Phys. Chem.* **1994**, *98*, 11623.

(138) *SMART v5.626: Software for the CCD Detector System*. Bruker AXS: Madison, WI, 2000.

(139) Walker, N.; Stuart, D. *Acta Crystallogr. A* **1983**, *A39*, 158.

(140) Sheldrick, G. M. *SADABS, Area Detector Absorption Correction*, University of Göttingen: Göttingen, Germany, 2001.

(141) Sheldrick, G. M. *SHELX-97, Program for Refinement of Crystal Structures*, University of Göttingen: Göttingen, Germany, 1997.

(142) Sheldrick, G. M. *Acta Crystallogr. A* **2008**, *A64*, 112.

(143) Sheldrick, G. M. *SHELXTL 6.1, Crystallographic Computing System*, Siemens Analytical X-Ray Instruments: Madison, WI, 2000.

(144) Cromer, D. T.; Waber, J. T., *International Tables for X-Ray Crystallography, Vol. IV, Table 2.2B*. The Kynoch Press: Birmingham, England, 1974.

(145) Burnett, M. N.; Johnson, C. K. *ORTEP-III, Report ORNL-6895*, Oak Ridge National Laboratory: Oak Ridge, TN, 1996.

(146) George, G. N.; George, S. J.; Pickering, I. J., EXAFSPAK, Stanford Synchrotron Radiation Lightsource, Menlo Park, CA. http://www-ssrl.slac.stanford.edu/~george/exafspak/exafs.htm. 2001.

(147) Riggs-Gelasco, P. J.; Stemmler, T. L.; Penner-Hahn, J. E. *Coord. Chem. Rev.* **1995**, *144*, 245.

CHAPTER 4

HS^--INDUCED RELEASE OF HNO FROM A WATER-SOLUBLE $\{CoNO\}^8$ COMPLEX

4.1 Abstract

The integrated biochemistry of small molecule signaling agents has been realized as vital to the regulation of numerous physiological processes. Nitroxyl (HNO/NO^-) is known for its pharmacological implications that are distinct from its redox sibling nitric oxide ($NO^\bullet$), particularly as they relate to cardiovascular physiology. Although the crosstalk of these species has been studied, the fate of coordinated HNO/NO^- with such small molecules ($NO^\bullet$, H_2S/HS^-, etc.) has yet to be investigated. Herein, we report the synthesis and characterization of H_2O-soluble Co complexes used to study such interactions, namely $[Co(LN_4^{PrIm})(MeCN)_2](BF_4)_2$ (**1**), $[Co(LN_4^{PrIm})(LN_4^{PrIm}\text{-}\kappa^2\text{-}C,N)]_2(BPh_4)_2$ (**2**), and $\{CoNO\}^8$ complex $[Co(LN_4^{PrIm})(S)(NO)](BF_4)_2$ (**3**) (where S = solvent). We observe two crosstalk pathways using this Co platform: (i) oxidation of a coordinated NO by free $NO^\bullet$ to form the corresponding nitro species $[Co(LN_4^{PrIm})(MeCN)(\eta^1\text{-}NO_2)](BF_4)_2$ (**4**); and (ii) H_2S/HS^--induced release of free HNO from an otherwise unreactive Co-coordinated nitrosyl (**3**). HNO release was monitored by the reductive nitrosylation of $[Mn^{III}(TPPS)]^{3-}$ to form $[Mn(TPPS)(NO)]^{4-}$ (pH 7.4, 298 K), likely through an HSNO intermediate.

4.2 Introduction

The integrated chemistry amongst small molecule signaling agents ($NO^{\bullet}$, CO, H_2S) involves an intricate network of downstream signaling cascades.[1] Independent of each other, these small molecules are critical to mammalian physiology,[2] but studies in the past few years have shown that the downstream effects of the crosstalk between these species can play a significant role in the physiological implications and fundamental chemistry of each small molecule. For example, hydrogen sulfide (H_2S, $pK_{a1} = 7.02$; $pK_{a2} > 12$ at 25°C)[3-4] has only recently emerged as a gaseous signaling molecule with physiological implications similar to those of $NO^{\bullet}$.[5] H_2S/HS^- serves as a neuroprotectant, modulates neurotransmission, and shows therapeutic potential for many neurodegenerative diseases, such as Alzheimer's disease and Parkinson's disease.[6] These signaling agents may have some inter-dependence for their biological effects and physiological implications resulting from their reactive interconnectivity. H_2S and $NO^{\bullet}$ cooperatively interact in order to stabilize the level of vasorelaxant cyclic GMP[7] and to regulate vascular tone, which occurs through production of HNO, thus activating the HNO-TRPA1-CGRP pathway.[8] Furthermore, H_2S reacts with *S*-nitrosothiols to form thionitrous acid (HSNO), and at the cellular level, HSNO can afford NO^+, $NO^{\bullet}$, and NO^-, all of which have distinct physiological intimations.[9] This integrated network of small molecule reactions and the implications of the subsequent by-products underscores the importance of understanding such reactions.

Small molecules, many of which are reactive nitrogen, oxygen, or sulfur species (RNS, ROS, RSS) share biochemical targets, which often employ metal centers to facilitate their signaling cascade. This places such highly reactive species in close proximity to engage in additional chemistry. To date, the best and only thoroughly characterized example of M-NO/H_2S reactivity involves the interactions of H_2S with sodium nitroprusside $Na_2[Fe(CN)_5(NO)]$ (SNP), a clinically

used Fe-based NO• donor; this results in an Fe-coordinated HSNO intermediate that ultimately releases HNO.[10] There have been a few studies on the reactivity of $Co^{III/II}$ cobalamins (Cbls)[11-13] and related model complexes[14-16] with H_2S/HS^-, all of which typically lead to the formation of polysulfido- and $Co^{II}L$ species. NO• is known to interact with Cbl, a Co-centered cofactor in mammalian vitamin B_{12}-dependent enzymes such as methionine synthase (MetH) and methylmalonyl CoA mutase (MMCM).[17-18] The resulting nitrosylcobalamin (NOCbl)[19] is a $\{CoNO\}^8$ complex, by the Enemark-Feltham (EF) notation.[20] Small molecule $\{CoNO\}^8$ complexes are well studied and generally characterized as LS Co^{III}-NO^-.[21-33] However, there remain few reports of their reactivity[32,34-37] and one-electron reduced $\{CoNO\}^9$ analogs,[38-44] possibly due to the kinetic inertness of LS Co^{III}. Similarly, there is no report of the reaction and fate of H_2S/HS^- with a $\{CoNO\}^8$ complex. Given the implications of such crosstalk[1] and the presence of metal nitrosyls in biology,[45-46] it is critical to explore the fate of coordinated $NO^{\bullet/-}$ when in the presence of small molecule signaling agents such as NO• and H_2S/HS^-. Therefore, we have synthesized a series of water-soluble $Co^{II/I}$ and $\{CoNO\}^8$ complexes and investigated their reactions with NO• and NaSH, respectively (Chart 4.1). The latter reaction leads to the formation of HNO, identified by trapping with HNO-specific target $[Mn^{III}(TPPS)]^{3-}$ to form $[Mn(TPPS)(NO)]^{4-}$. These results highlight that metal-coordinated nitroxyls react with H_2S/HS^- to form HNO.

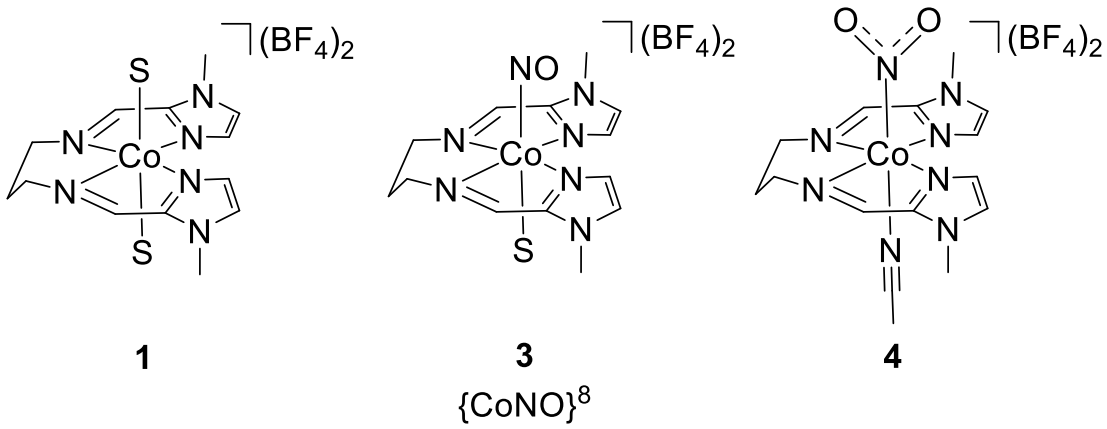

Chart 4.1. Structurally characterized Co complexes **1**, **3** and **4** reported in this work. S = solvent.

4.3 Synthesis and Spectroscopic Properties of Complexes 1 - 4.

The LN_4^{PrIm} ligand (where LN_4^{PrIm} = (*1E*,*1'E*)-*N*,*N'*-(propane-1,3-diyl)bis(1-(1-methyl-1H-imidazol-2-yl)methanimine)) was carefully constructed based on the data from the diimine/dipyrrolide ligands found in earlier chapters of this dissertation. The diminished Lewis basicity (pK_a(imidazole): 6.9; pK_a(pyrrole): 23.0) of the neutral diimine/diimidazole-based ligands was expected to positively shift the redox potential ($E_{1/2}$) from pyrrole-based LN_4^{2-} systems (~1.3 V vs. Fc^+/Fc in MeCN)[24,31] in Chapters 2 and 3 and lead to greater accessibility of certain NO_x transformations and EF notations. This increase in positive charge of the corresponding {CoNO}^{8} complex was expected to lead to a more facile reduction to the corresponding {CoNO}^{9} species, enhance the water solubility, and bring the redox couple of Co-NO_x species using this ligand scaffold closer to the biological redox window. Given these advantageous properties, we anticipated these imine-/imidazole-based complexes would be even effective than their pyrrole-based counterparts in biological (aqueous) conditions as HNO/NO^- donors as well as scavengers of NO_x in environmental denitrification.

$[Co(LN_4^{PrIm})(MeCN)_2](BF_4)_2$ (**1**) was synthesized via metalation of LN_4^{PrIm} with $[Co(H_2O)_6](BF_4)_2$ in an MeCN solution. The resulting orange microcrystalline product was precipitated with Et_2O and isolated as analytically pure material in 94% yield (see Supporting Information = SI; Figure 4.S1). Evidence of two axial MeCN ligands to complete an N6 donor set for Co^{II} is found in both FTIR (Figure 4.S2) and the X-ray crystal structure (vide infra). Solution-state magnetic susceptibility measurements (μ_{eff} = 3.90 BM; calcd μ_{eff} for 3 unpaired electrons: 3.87 BM) align with the EPR features (g = [5.71, 2.28], Figure 4.S3), which suggest a high-spin (S = 3/2) Co^{II}. The EPR spectrum of **1** is consistent with other S = 3/2 N/O-ligated 6C Co systems.[47-48] The UV-vis spectrum of **1** exhibits a strong band at 284 nm, a weak band at 466 nm, and a shoulder at 425 nm (Figure 4.S4). This further supports the S = 3/2 assignment and 6C geometry, as HS octahedral complexes typically exhibit *d-d* transitions at higher energies (530 ± 100 nm) relative to the lower energy transitions for 4C or 5C systems.[49] The strong feature 284 nm is attributed to ligand field bands resulting from the $\pi \rightarrow \pi^*$ transition.

The Co^{I} analog of **1** was also synthesized as it is another relevant oxidation state for Cbls.[50] Metalation of LN_4^{PrIm} with $[Co(PPh_3)_3Cl]$ in THF and subsequent salt metathesis using $NaBPh_4$ in MeOH afforded $[Co(LN_4^{PrIm})(LN_4^{PrIm}\text{-}\kappa^2\text{-}C,N)]_2(BPh_4)_2$ (**2**; 85%). The crystal structure of **2** revealed the dimeric nature of **2** in which each there are two distorted octahedral N_5C-ligated Co centers (vide infra). In contrast to **1**, there is no evidence in the FTIR or structure of ligating MeCN molecules for the Co^{I} species. The broad, paramagnetically shifted ^1H NMR spectrum of **2** is consistent with a high-spin d^8 system and aligns with other Co^{I} systems.[51] The UV-vis spectrum of **2** exhibits a strong band at ~270 nm and broad features at 440 and 536 nm (Figures 4.S4 and 4.S5), which are in line with other isolated Co^{I} species bearing tetragonal ligand scaffolds.[51-52] The

latter band is likely a result of a metal-to-ligand charge transfer (MLCT) due to the low-valent Co in **2**.

Complex **1** afforded a facile nitrosylation to form the corresponding $\{CoNO\}^8$ complex $[Co(LN_4^{PrIm})(MeOH)(NO)](BF_4)_2$ (**3**) via an NO(g) purge in MeOH (82%; Scheme 4.1). The metric parameters (vide infra) and diamagnetism of **3** are consistent with other $\{CoNO\}^8$ complexes, which are generally assigned as Co^{III}-NO^- (S_{tot} = 0; Figure 4.S6).[53] The ^{15}N NMR spectrum supports a bent Co-N-O in solution, as it exhibits a single peak that is significantly shifted downfield (804 ppm vs. CH_3NO_2 in CD_3OD; Figure 4.S7.)[54] The N-O stretching frequency (ν_{NO}) is 1748 cm^{-1} and shifts to 1717 cm^{-1} for **3-^{15}NO** ($\Delta\nu_{NO}$: 31 cm^{-1}; Figure 4.S8). This is ~40–100 cm^{-1} higher than other known $\{CoNO\}^8$ complexes (Table 1.3), which suggests more of a hybrid resonance structure between low-spin Co^{III}-NO^- ↔ low-spin Co^{II}-$NO^\bullet$ rather than exclusively Co^{III}-NO^-. Notably, nitrosylcobalamin (NOCbl), which forms in vivo, also evokes a resonance structure between Co^{III}-NO^- and Co^{II}-$NO^\bullet$.[19,55] The UV-vis profile of **3** in MeCN exhibits a strong band at 288 nm and a shoulder at 377 nm, the latter of which can serve as a spectroscopic marker for **3** in MeCN since **1** and **2** exhibit no shoulder (**1**) or broad features that are lower energy (**2**, at 440 and 536 nm; Figure 4.S4).

Although $\{CoNO\}^8$ **3** is isolable, modifying synthetic conditions to an NO(g) purge in a dilute heated MeCN solution, conditions used for the nitrosylation of the analogous pyrrole systems,[24] led to the formation of the corresponding nitro species $[Co(LN_4^{PrIm})(\eta^1\text{-}NO_2)](BF_4)_2$ (**4**) (Scheme 4.1; Figures 4.S9 and 4.S10). Oxidation of the coordinated NO by free NO(g) is an uncommon but not unprecedented phenomenon.[53,56-60] The reaction of $3NO^\bullet \rightarrow NO_2 + N_2O$ catalyzed by a Co nitrosyl was first observed by Caulton and coworkers in 1974 with $[Co(en)_2(NO)]Cl$ and $[Co(DMGH)_2(NO)]\cdot CH_3OH$ in the presence of pyridine, both of which

exclusively form NO_2 and N_2O (where en = ethylenediamine; DMGH = monoanion of dimethylglyoxime).[56] An earlier study reported similar behavior with $[Co(PPh_3)_3(NO)]$, although multiple mononitrosyl and dinitrosyl complexes were also produced.[61] Given the clean transformation of **3** to **4** sans additional concurrent oxidations, the pathway proposed involving a hyponitrito ($N_2O_2^{2-}$) intermediate in Scheme 4.S1 is most likely.[53,60] A second equivalent of **3** can then coordinate the intermediate through a bridging nitrosyl, ultimately leading to formation of one equivalent of **4** and presumably liberation of free N_2O(g). Similar reactivity has also been observed in Co complexes with tropocoronand ligands.[28]

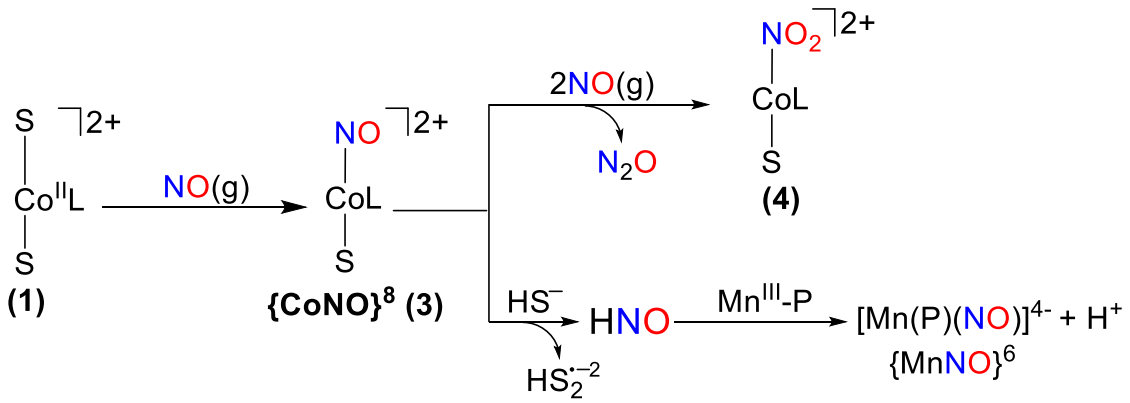

Scheme 4.1. Reported synthesis and reactivity of complex **3**. S = solvent molecule. P = a water-soluble porphyrin.

4.4 Structural Properties of Complexes 1 – 4.

X-ray quality crystals of complexes **1 - 4** have been successfully grown from Et_2O diffusion into MeCN at low temperatures (-20 to -25 °C). The structure of the bis-solvated Co^{II} center of **1** revealed an octahedral geometry with the diimine-diimidazole ligand providing an N_4 donor set in the basal plane (Figure 4.S11). The Co-N_{imine} (avg: 1.972 Å) and Co-$N_{imidazole}$ (avg: 1.983 Å) bond

distances are consistent with a HS Co^{II} (S = 3/2) center and are comparable to Co-N bonds in other non-macrocyclic Co^{II} complexes with neutral ligands.[62-63] The two axially ligated MeCN molecules reveal longer Co-N distances due to antibonding interactions of the d_{z2} and p_z orbitals. There is a significantly longer Co-N bond in the second axial site that is likely a result of a trans influence (Co-N(CMe): 2.162 and 2.385 Å, respectively). This longer bond coincides with a highly bent Co-N8-C(Me) bond angle of 130.78°, a far departure from the more typical Co-N7-C(Me) bond angle of 170.66°. The labile nature of this bond makes reactivity more likely at the second MeCN ligand. The structure of $[Co(LN_4^{PrIm})(LN_4^{PrIm}\text{-}\kappa^2\text{-}C,N)]_2(BPh_4)_2$ (**2**) revealed a dimer in which each distorted octahedral Co center is coordinated by the neutral N_4 donor set of LN_4^{PrIm}, and the remaining two ligands originate from the imine carbon and nitrogen of the second LN_4^{PrIm} present (Figure 4.S12). Whereas the imine bond distances in **1** are 1.284 and 1.282 Å, the imine bond distances of **2** are 1.296 Å (C5-N3) and an elongated 1.425 Å (C9-N4), which is closer to the length of a single C-N bond distance for an amine (1.469 Å).[64] The "imine" carbon acts more like a carbene forming a dative bond with Co. Co^I centers have been shown to facilitate a similar charge localization and dative bonding in a β-diketiminate ligand,[65] and they are known to activate C-H[66] and C-F bonds.[65] Bond distances in the primary coordination sphere of the distorted octahedron of **2** are slightly contracted by ~0.02 Å relative to **1** (Co1-N_{imine} avg: 1.949 Å and Co1-$N_{imidazole}$ avg: 1.966 Å), and the remaining two donor atoms from C9 and N4 complete the six-coordinate (6C) geometry with bond distances of 2.011 Å (Co1-C9) and 1.918 Å (Co1-N4). This slight contraction is an expected trend based on the greater extent of metal-to-ligand π-backbonding for lower valent Co and is in line with structural data of other N_4- or N_5-ligated Co complexes that utilize the same ligand for Co^{II} and Co^I.[51-52]

Following nitrosylation of **1**, compound **3** also proved amenable to structure determination via single-crystal X-ray diffraction (Figures 4.S13 and 4.S14). There is extreme planarity in the LN_4^{PrIm} basal plane with slight displacement of Co from the N_4 plane (0.017 Å), which deviates little from **1** (0.059 Å). The axial MeCN molecule exhibits a Co-N_{MeCN} bond distance (2.156 Å) comparable to one of the axial ligands in **1** (2.162 Å); however, the more labile axial MeCN moiety of **1** is displaced by NO•, which affords an apical NO moiety with a Co-N-O bond angle of 130.87° and a Co-N(O) bond distance of 1.850 Å.[67] This indicates that the NO is potentially more labile than the NO moiety in the analogous $\{CoNO\}^8$ complex bearing the diimine/dipyrrolide ligand that has a Co-N(O) distance of 1.766 Å.[31] The equatorial Co-N_{imine} (avg: 1.957 Å) and Co-$N_{imidazole}$ (avg: 1.969 Å) bond distances are consistent with a LS Co^{III} (S = 0) center and are comparable to Co-N bonds in other $\{CoNO\}^8$ complexes.[22] An N-O bond distance of 1.140 Å is slightly shorter than the distance reported for both ^{1}HNO (1.21 Å)[68] and NO• (1.15 Å),[21] and is consistent with the proposed hybrid resonance structure and ν_{NO} value of **3**. The structural properties of **3** fall in-line with other structurally characterized $\{CoNO\}^8$ complexes (Table 1.3). NO disproportionation at **3** and subsequent recrystallization led to isolation of $[Co(LN_4^{PrIm})(\eta^1\text{-}NO_2)](BF_4)_2$ (**4**), which reveals a slight contraction of the primary coordination sphere of the Co^{III} center, a likely result of the π-accepting ability of an N-bound NO_2^- ligand (Co-N_{imine}: 1.940 Å (avg); Co-$N_{imidazole}$: 1.938 Å (avg); Co-N_{MeCN}: 1.991 Å; Co-N(O_2): 1.903 Å; Figure 4.S15). Along with these distances, the O-N-O bond angle of 123.7° and the N-O bond distances (N8-O1: 1.203 Å; N8-O2: 1.211 Å) compare well with industrially used oxo-transfer catalyst [Co(TPP)(py)(NO_2)] and its nitro derivatives (TPP = tetraphenylporphyrin) where Co-N(O_2): ~ 1.9 Å, O-N-O: ~120°, and N-O: ~1.2 Å.[69]

4.5 Electrochemical Properties of {CoNO}^{8} 3 and Isolation Attempts of {CoNO}^{9} 5.

The cyclic voltammogram of **3** was measured in MeCN and displays a reversible {CoNO}^{8}/{CoNO}^{9} redox couple at -0.55 V vs. Fc/Fc$^+$ (Figures 4.S16 and 4.S17). The presence of a reversible electrochemical event at -0.55 V is comparable to the heterobimetallic {CoNO}^{8} complex [(NO)(Cl)Co(^{Me}doen)Mg(Me$_3$TACN)(H$_2$O)](BPh$_4$) whose $E_{1/2}$ is -0.65 V vs. Fc$^+$/Fc (^{Me}doen = a diimine dioxime ligand; Me$_3$TACN = 1,4,7-trimethyl-1,4,7-triazacyclononane).[30] This complex has been utilized in the nitrite reduction pathway, ultimately forming a transient {CoNO}^{9} intermediate prior to release of ½ equiv of N$_2$O. The analogous {CoNO}^{9} species has not yet been cleanly isolated. The $E_{1/2}$ of **3** is shifted by +0.85 V relative to the analogous diimine-dipyrrolide {CoNO}^{8} complex that bears a dianionic ligand ($E_{1/2}$ = -1.40 V vs. Fc/Fc$^+$).[31] This demonstrates the significant influence of the primary coordination sphere on the $E_{1/2}$ of the {CoNO}^{8}/{CoNO}^{9} reduction potential. Similar influence on the $E_{1/2}$ of an MNO unit by a peripheral ligand is observed in the redox potentials of [Co(N$_2$S$_2$)(NO)] and [Co(N$_2$S$_2$)(NO)](W(CO)$_4$] (where [W(CO)$_4$] coordinates W to the two S atoms).[29] The $E_{1/2}$ values are -1.08 V and -0.59 V, respectively. These dramatic shifts of +0.49 V for [Co(N$_2$S$_2$)(NO)](W(CO)$_4$][29] and +0.85 V for **3** highlight the keen ability to tune the electronic nature of Co-NO. Not only does the charged nature of **3** afford enhanced water solubility, but the $E_{1/2}$ indicates that the {CoNO}^{9} state is more easily accessed.

Complex **1** exhibits distinctly different features in the CV, notably the absence of a reversible wave ~ 0.5 V (Figure 4.S18). Complex **1** displays irreversible redox processes at ~ +1.2 V (E_{pa}) and ~ –0.3 V (E_{pc}) in MeCN vs. Fc$^+$/Fc. The former, more positive redox event may be a combination of ligand oxidation and the Co$^{III/II}$ redox couple. The event at ~ –0.3 V can be assigned to the Co$^{II/I}$ redox couple. The irreversible nature of these couples is a result of the loss of axial solvent ligand(s) because the reduction is taking place in the antibonding d_{z2} orbital. There is a

quasi-reversible redox event at ~ −1.3 V, which highlights that the $Co^{I/0}$ couple does not involve the same loss of axial ligands that is observed for the $Co^{II/I}$ couple. This is consistent with the crystal structure of **2** in that there are no weakly bound solvent molecules serving as axial ligands (vide supra). The electrochemistry of a series of Co^{III}-Schiff base complexes $[Co(acacen)(X)_2]^{2+}$ (acacen = dianion of bis-(acetylacetone) ethylenediamine) exhibit similar trends for the $Co^{III/II}$ and $Co^{II/I}$ redox couples at ~ -0.35 V and ~ -1.2 V in MeCN vs. Fc^+/Fc.[70] The shift by ~ +1 V is the result of Co bearing the neutral LN_4^{PrIm} of **1** and **2** versus a dianionic acacen ligand.

$\{CoNO\}^9$ complex **5** was pursued via three methods (Scheme 4.S2). Route 1 employed chemical reduction of **3** with $[CoCp_2]$, while routes 2 and 3 involved nitrosylation of the Co^I center of **2** with Ph_3CSNO or NO(g) respectively (Scheme 4.S2). All three synthetic methods afforded a mixture containing **5**, yet its clean isolation remains elusive. The FTIR of **5** exhibits new peaks at 1668 and 2248 cm^{-1}, attributed to an axially coordinated nitrosyl (ν_{NO}) and MeCN molecule (ν_{CN}) respectively (Figures 4.S20 and 4.S21). The molecular ion peak $[M]^+$ in the LR-ESI-MS is observed at *m/z* 347.1 (calcd. *m/z* 347.1) with the appropriate isotope distribution. The ^1H NMR exhibits paramagnetic broadening, consistent with a Co^{II} center, and the UV-vis has features at ~270 nm and 431 nm in MeCN (RT). Other Co^{II} complexes also display an electronic spectral band ~430 nm, such as complex **1** and Co^{II} complexes supported by diglyoxime ligands.[52] X-band EPR (9.60 GHz) measurements reveal an asymmetric coordination environment with *g* values of 5.3 and 2.14 (Figure 4.S22). The significant nuclear hyperfine coupling (hfc) is a result of the unpaired electron being on the ^{59}Co nucleus, which has a nuclear spin of 7/2. The EPR features of **5** strongly resemble analogous $\{CoNO\}^9$ complexes coordinated with a diimine-dipyrrolide N4 donor set.[71] The high-spin *g* values present at 5.3 and 3.3 are likely a HS Co^{II} impurity present due to the instability of **5**. Despite the presence of **5** in each synthetic method, none of the implemented

synthetic protocols led to clean isolation. Isotope labeling in route 3 with $^{15}NO(g)$ highlights many isotope-sensitive bands in the FTIR spectrum (Figure 4.S23). Based on the assigned N-O bands observed in **4** (ν: 1414, 1322; δ 821 cm^{-1}), route 3 affords $\{CoNO\}^9$ **5** as well as Co-NO_2 **4** (1375, 1301, 817 cm^{-1}) and possibly a $\{Co(NO)_2\}^{10}$ complex as a minor product (ν_{NO}: 1766, 1699 cm^{-1}). Other N-ligated $\{Co(NO)_2\}^{10}$ complexes exhibit slightly higher ν_{NO} values at ~1800 cm^{-1} and 1720 cm^{-1} for their symmetric and asymmetric stretches respectively.[28,72-76] The difficulty in isolating **5** with these methods shows that while accessible, other methods need to be pursued in order to isolate and investigate the reactivity of **5**.

4.6 HS^- Reactivity of $\{CoNO\}^8$ 3

In spite of the biological implications of the integrated biochemistry of free $H_2S/NO^{\bullet}$,[7-8] the fate of coordinated $NO^{\bullet/-}$ when in the presence of H_2S/HS^- has yet to be investigated. As such, the reaction of $\{CoNO\}^8$ **3** and H_2S/HS^- was pursued. HNO is the product of free $H_2S/NO^{\bullet}$, but due to the difficulty of directly detecting HNO, indirect methods are often employed. Mn^{III}-porphyrins are often used as targets due to their high affinity and excellent selectivity of HNO.[77] As such, HNO donor reactions were investigated utilizing $[Mn^{III}(TPPS)]^{3-}$, a water-soluble Mn^{III}-porphyrin where TPPS = *meso*-tetrakis(4-sulfonatophenyl)porphyrinate; λ_{max} = 467 nm), in phosphate-buffered saline (PBS; pH 7.4, 298 K; Scheme 4.1). Over a 20-h period, no reaction occurred between $\{CoNO\}^8$ **3** and $[Mn^{III}(TPPS)]^{3-}$ (5:1) (Figure 4.S24). However, upon the addition of 5 equivs of NaSH, the band at λ_{max} = 467 nm, which is attributed to the Soret of $[Mn^{III}(TPPS)]^{3-}$, disappeared with the concomitant appearance of a feature at λ_{max} = 424 nm, which is assigned to $[Mn(TPPS)(NO)]^{4-}$ (Figure 4.1). These changes are in-line with reductive nitrosylation of the Mn^{III}-center and *release of HNO* from the **3**/HS^- reaction. Increasing the equivs

of NaSH increased the relative kinetics of the reaction from 3.5 h for 5 equiv (Figure 4.S25) to 2 h for 10 equiv (Figure 4.1). However, in both cases, the reaction formed ~80% of $[Mn(TPPS)(NO)]^{4-}$ then started shifting back to the $[Mn^{III}(TPPS)]^{3-}$ starting material (Figure 4.1), indicative of an equilibrium that was reached over time. This could be a result of further reactivity of $[Mn(TPPS)(NO)]^{4-}$ with HS^- leading to a weakened Mn-N(O) bond and subsequent re-formation of $[Mn^{III}(TPPS)]^{3-}$. Doctorovich has previously shown that the $Mn^{III/II}$ couple of an Mn-P (P = porphyrin) influences the reaction mechanism with HNO/HNO donors. An Mn-P with $E_{1/2} > 0$ will accelerate HNO donor decomposition through a direct Mn-P/donor interaction, but an Mn-P with $E_{1/2} < 0$ reacts with free HNO without Mn-P/donor bonding.[78-79] Based on the $E_{1/2}$ of $[Mn^{III}(TPPS)]^{3-}$ of -0.160 V vs. SHE, the reaction of $[Mn^{III}(TPPS)]^{3-}$/$\{CoNO\}^8$ **3**/HS^- is strong evidence for the production of free HNO. Concurrent with the formation of $[Mn(TPPS)(NO)]^{4-}$, a band at 294 nm blue-shifts to 288 nm and increases in intensity, which also occurs from the decomposition of $\{CoNO\}^8$ **3** in PBS (pH 7.4) over time (Figure 4.S26). A low-energy band at 542 nm concomitantly increases in intensity as λ_{max} = 424 nm increases and is also assigned to $[Mn(TPPS)(NO)]^{4-}$.[77] Although further studies are needed to identify all products of this reaction (bulk studies, FTIR headspace analysis of N_2O, etc.), this reactivity highlights that HNO can form from the $\{CoNO\}^8$/HS^- reaction.

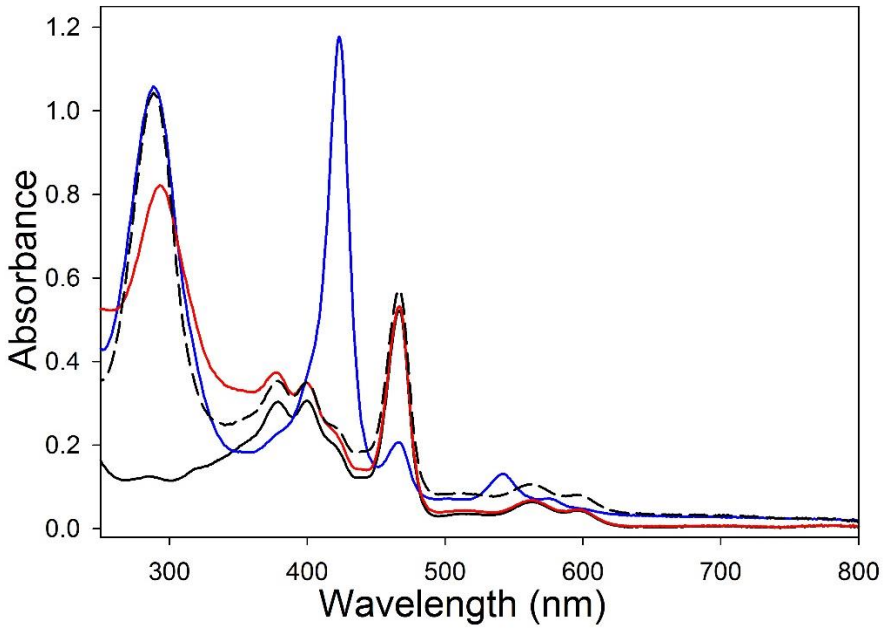

Figure 4.1. UV-vis spectrum of a 5.82 μM solution of $[Mn^{III}(TPPS)]^{3-}$ (black solid line) after the addition of $\{CoNO\}^8$ **3** (5 equiv; red line) and after the addition of NaSH (10 equiv; t = 2 h: blue line; t = 20 h: black dashed line) at 298 K in 10 mM PBS (pH 7.4).

Although there is a dearth of MNO/H_2S chemistry, there is precedent for the reactivity of $\{FeNO\}^6$ SNP, formally LS Fe^{II}-NO^+, with H_2S at pH 7.4. This reaction affords a $[(CN)_5FeN(O)SH]^{3-}$ intermediate, which reacts with a second equiv of HS^- to form $[(CN)_5Fe(HNO)]^{3-}$ and disulfide.[10] The HNO subsequently can labilize and form N_2O through its well-documented dehydrative self-dimerization.[80] A similar pathway is proposed here (Scheme 4.2, pathway 1). The $[(CN)_5FeN(O)SH]^{3-}$ intermediate exhibits a λ_{max} of 535 nm, characteristic of Fe^{II}-coordinated RSNOs,[10,79-81] and it rapidly forms and then reacts further on a timescale of 2.6 s.[10] If a Co-HSNO intermediate is indeed forming, there is no direct evidence in the UV-vis spectral monitoring. However, the timescale with which such an intermediate is formed then reacts is likely faster than the timescale with which the reaction was monitored (< 1 min). Additionally, insolubles

were observed in the reaction, which could be due to di- or polysulfide formation. It is unlikely that HS^- reduction of **3** to $\{CoNO\}^9$ complex **5** is the predominant pathway, based on known redox potentials. The $E_{1/2}$ of **3** is -0.15 V in MeCN whereas the redox potential of HS^- is +0.17 V at pH 7.0 (both vs. SHE)[81-82] The latter is a significantly weaker reductant than biologically abundant thiols such as glutathione and cysteine ($E° \sim$ -0.25 V vs. SHE).[83] If $\{CoNO\}^9$ **5** is indeed produced, **5** could serve as an effective HNO donor (Scheme 4.2, pathway 2),[71] and it can not be eliminated as a possible pathway until further experiments are conducted (aqueous electrochemistry of **3**, isolation of **5**, and reactivity of **5** with Mn^{III}-P). Contrastingly, given the SNP/H_2S precedent, it is reasonable to propose the presence of an HSNO intermediate as a result of the presence of insolubles and formation of $[Mn(TPPS)(NO)]^{4-}$, the latter of which is distinct evidence for the presence of free HNO. This is the first example of HS^--induced release of HNO from a $\{CoNO\}^8$ complex.

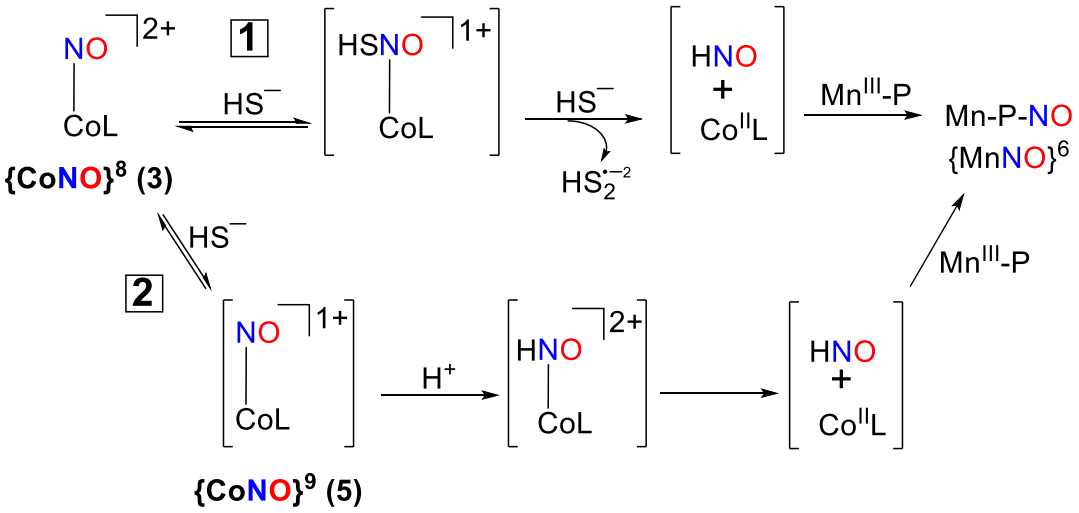

Scheme 4.2. Two possible mechanisms of HS^--induced HNO release from $\{CoNO\}^8$ complex **3**. Based on experimental and electrochemical studies to date, pathway 1 is more likely although neither pathway can be eliminated until further studies take place.

4.7 Conclusions and Outlook

In conclusion, a new family of Co complexes with neutral N-donors has been synthesized, and LN_4^{PrIm} provides a suitable platform to access multiple oxidation states of Co as well as $\{CoNO\}^8$ complex **3**. Complex **3** was shown to react with free $NO^{\bullet}$ to form the corresponding $[Co(L^{PrIm})(MeCN)(\eta^1\text{-}NO_2)](BF_4)_2$ (**4**), likely through a hyponitrito intermediate. **3** was shown to be unreactive toward water-soluble HNO target $[Mn^{III}(TPPS)]^{3-}$. However, in the presence of H_2S/HS^-, **3** releases HNO which subsequently reacts with $[Mn^{III}(TPPS)]^{3-}$ to form $[Mn(TPPS)(NO)]^{4-}$. This may occur via an HSNO-intermediate. This reactivity sheds insights into the fate of M-bound $NO^{\bullet/-}$ when in the vicinity of H_2S/HS^- and can serve as a benchmark for the implications of such crosstalk occurring at a metal center. Future studies will include further analysis and identification of all species formed in the $\{CoNO\}^8/H_2S$ reaction, isolation of $\{CoNO\}^9$ **5**, and investigation of the fate of H_2S/HS^- with $Co^{II/I}$ and $\{CoNO\}^9$ complexes.

4.8 Materials and Methods

4.8.1 General Information

Same as Chapter 2 with some exceptions. NaSH was used as received from Strem Chemicals. $[Mn^{III}(TPPS)]^{3-}$ was used as received in dark conditions from Frontier Scientific and compared with literature values.[77] LN_4^{PrIm} was prepared according to the published procedure,[84] as was Ph_3CSNO.[85]

4.8.2 Physical Methods

Same as Chapter 2 with some exceptions. EPR spectrometer and conditions were identical to those described in Chapter 3, Physical Methods section.

4.8.3 Synthesis of Compounds

$[Co(LN_4^{PrIm})(MeCN)_2](BF_4)_2$ (1). To a deep pink 3 mL MeCN solution of $[Co(H_2O)_6](BF_4)_2$ (379.9 mg, 1.115 mmol) was added a yellow/amber 3 mL MeCN solution of LN_4^{PrIm} (288.1 mg, 1.115 mmol) while stirring. The color of the reaction mixture remained deep pink and no insolubles were noted. The reaction mixture stirred for 2 h, became orange in color, and was dried until ~1 mL of MeCN remained. Complex **1** was then precipitated with ~4 mL of Et_2O. This heterogeneous mixture was placed in the glovebox freezer overnight. After this time, the reaction mixture was filtered, affording an orange crystalline solid (479.9 mg, 0.8390 mmol) that was washed with Et_2O (RT, 3 × 2 mL). The filtrate was stripped until minimal MeCN remained and then the precipitation/filtration process was repeated once, yielding an additional 120.0 mg (0.2098 mmol, 94% total yield). FTIR (KBr matrix), ν_{max} (cm^{-1}): 3469 (m), 3374 (m), 3163 (m), 3133 (m), 3117 (m), 3090 (w), 3008 (m), 2943 (m), 2858 (w), 2305 (m), 2278 (m, ν_{CN}), 2266 (m, ν_{CN}), 2252 (w, ν_{CN}), 1651 (m), 1634 (s), 1605 (m), 1541 (m), 1492 (s), 1458 (s), 1428 (s), 1379 (s), 1354 (w), 1326 (vw), 1294 (s), 1274 (m), 1195 (m), 1180 (s), 1117 (vs), 1054 (vs, ν_{BF}), 1035 (vs), 1035 (vs), 957 (s), 946 (s), 878 (m), 859 (m), 783 (s), 710 (m), 664 (m), 629 (w), 577 (vw), 555 (vw), 521 (s), 498 (vw), 483 (w), 437 (m), 406 (w). EPR (MeCN:toluene (1:2), 10 K, 9.582 GHz, 3.99 mW, 6.477 G): g = [5.71, 2.28]. LR-ESI-MS (*m/z*): $[M - 2BF_4 – 2MeCN]^{2+}$ calcd for $C_{13}H_{18}CoN_6$, 158.5 (100), 159.0 (14.1); found, 158.6 (100), 159.1 (11.0). $[M + BF_4 – 2MeCN]^–$ calcd for $C_{13}H_{18}CoN_6B_3F_{12}$, 576.1 (18.5), 577.1 (74.5), 578.1 (100), 579.1 (15.5); found, 576.1 (18.0), 577.0 (68.9), 578.0 (100), 579.0 (14.5). Anal. Calcd. for $C_{17}H_{28}B_2CoF_8N_8 \bullet 2H_2O$: C, 33.53; H, 4.63; N, 18.40. Found: C, 33.94; H, 4.06; N, 18.50. μ_{eff} (solution, 298 K): 3.90 BM in CD_3CN. UV-vis (MeCN, 298 K), λ_{max}, nm: 284, 425, 466.

[Co(LN$_4^{PrIm}$)(LN$_4^{PrIm}$-κ^2-*C*,*N*)]$_2$(BPh$_4$)$_2$ (2). To a dark green 9 mL THF slurry of [Co(PPh$_3$)$_3$Cl] (345.6 mg, 0.3922 mmol) was added a yellow 2 mL MeCN solution of LN$_4^{PrIm}$ (101.3 mg, 0.3922 mmol) while stirring. The color of the reaction mixture turned dark purple and dark purple insolubles were observed after 1 min of stirring. The reaction mixture stirred for 30 min and was then filtered, affording a dark purple thick solid and a dark purple filtrate. The solid was dissolved in 3 mL of MeOH affording a dark purple solution. A beige 1 mL MeOH solution of NaBPh$_4$ (268.4 mg, 0.7844 mmol) was added to the dark purple solution, which led to the immediate precipitation of purple insolubles. After 40 min, the reaction mixture was filtered, yielding a very thick dark purple solid as the product (212.0 mg, 0.1665 mmol, 85%) and pale purple mother liquor. FTIR (KBr matrix), ν_{max} (cm^{-1}): 3444 (w), 3119 (w), 3053 (s), 3033 (m), 2999 (m), 2982 (m), 2921 (m), 2856 (w), 1947 (w), 1882 (w), 1819 (w), 1761 (w), 1708 (w), 1693 (w), 1578 (s), 1569 (s), 1544 (m), 1479 (m), 1451 (m), 1425 (s), 1362 (m), 1335 (vw), 1292 (m), 1262 (w), 1248 (w), 1222 (w), 1203 (vw), 1166 (m), 1112 (m), 1088 (m), 1063 (m), 1032 (m), 927 (w), 899 (w), 846 (w), 807 (w), 743 (s), 733 (m), 706 (vs), 665 (m), 612 (s), 496 (w), 463 (w),439 (w), 430 (w), 417 (vw). LR-ESI-MS (*m/z*): [M]$^+$ calcd for $C_{13}H_{18}CoN_6$, 317.1 (100), 318.1 (16.3); found, 317.1 (100), 318.0 (21.9). [M]$^+$ calcd for $C_{50}H_{56}BCo_2N_{12}$, 952.4 (21.5), 953.4 (100.0), 954.4 (55.4), 955.4 (15.7), 956.4 (2.9); found, 952.4 (21.2), 953.2 (100.0), 954.1 (53.9), 955.1 (16.5), 956.1 (3.6). UV-vis (MeCN, RT), λ_{max}, nm: 267, 274, 290, 440 (sh), 536 (br).

[Co(LN$_4^{PrIm}$)(MeOH)(NO)](BF$_4$)$_2$ (3). Excess NO(g) was purged into a pale orange 1.5 mL MeOH solution of **1** (100.0 mg, 0.1745 mmol) for 90 s at RT. An immediate color change from pale orange to orange-tinted dark brown was noted. After stirring for 5 min while remaining under NO(g) headspace, the reaction product precipitated as a brown solid. The reaction mixture

was placed in the freezer for 1.5 h. The NO(g) headspace was then removed in vacuo and refilled with N_2. After being placed in the glovebox freezer for an additional 30 min, the reaction mixture was filtered, yielding a brown semi-crystalline solid (79.0 mg, 0.143 mmol, 82%) and a pale brown filtrate. FTIR (KBr matrix), ν_{max} (cm^{-1}): 3463 (br, w), 3164 (w), 3135 (m), 3049 (w), 2922 (w), 1748 (vs, ν_{NO}), 1701 (m), 1654 (w), 1648 (vw), 1624 (m), 1554 (m), 1499 (s), 1459 (vs), 1424 (s), 1418 (s), 1378 (m), 1292 (s), 1273 (m), 1197 (m), 1185 (m), 1103 (vs), 1065 (vs, ν_{BF}), 1043 (vs), 1032 (vs), 1005 (vs), 970 (m), 941 (m), 926 (m), 896 (w), 884 (m), 809 (w), 792 (s), 765 (w), 710 (w), 666 (m), 581 (vw), 520 (m), 491 (w), 471 (vw), 424 (m). ^{1}H NMR (400 MHz, CD_3OD, δ from residual protio solvent): 8.70 (s, 1H), 7.61 (s, 1H), 6.32 (s, 2H), 4.13 (s, 3H), 3.87 (s, 2H), 2.18 (d, 1H). LR-ESI-MS (*m/z*): $[M - 2BF_4 - MeCN + MeOH]^+$ calcd for $C_{14}H_{22}CoN_7O_2$, 379.1 (100.0), 380.1 (17.7); found, 379.0 (100.0), 380.0 (15.6). UV-vis (MeCN, 298 K), λ_{max}, nm: 288, 377 (sh). Anal. Calcd. for $C_{13}H_{18}B_2CoF_8N_7O$: C, 29.98; H, 3.48; N, 18.82. Found: C, 29.97; H, 3.65; N, 18.44.

$[Co(LN_4^{PrIm})(MeOH)(^{15}NO)](BF_4)_2$ (3-^{15}NO). The isotopically-labeled complex **3-^{15}NO** was prepared analogously to **3** using 100.0 mg (0.1745 mmol) except for using ^{15}NO(g). Yield: 86.8 mg (0.157 mmol, 90%). FTIR (KBr matrix), ν_{NO} (cm^{-1}): 1717 ($\Delta\nu_{NO}$: 31 cm^{-1}). ^{15}N NMR (50.7 MHz, CD_3OD, δ from CH_3NO_2): 804 ppm.

$[Co(LN_4^{PrIm})(MeCN)(NO_2)](BF_4)_2$ (4). Excess NO(g) was purged into an orange 1.5 mL MeCN solution of **1** (45.0 mg, 0.07854 mmol) for 1.5 min at 50°C. There was an immediate color change from orange to dark brown. The Schlenk flask remained under NO(g) headspace while heated at 50°C for 30 min. Upon removing the flask from the heat, the color of the solution began

to change to a lighter brown. After the flask cooled to RT, the product was precipitated with 4 mL of Et_2O via syringe while under NO(g) headspace. The pressure was occasionally released through the stopcock. This yielded orange insolubles, much lighter than the solution of the reaction mixture immediately following the NO(g) purge. The flask was then placed in the freezer for 3 h remaining under NO(g) headspace; following this time, the NO(g) was removed and the reaction mixture was filtered, yielding an orange powder (42.9 mg, 0.0742 mmol, 94%). FTIR (KBr matrix), ν_{max} (cm^{-1}): 3417 (br, w), 3181 (m), 3147 (m), 2942 (m), 2949 (vw), 2638 (vw), 2328 (m, ν_{CN}), 2301 (m, ν_{CN}), 2252 (w), 1624 (s), 1563 (m), 1537 (vw), 1501 (s), 1457 (vs), 1436 (s), 1428 (s), 1414 (s, ν_{NO2}), 1379 (s), 1322 (vs, ν_{NO2}), 1297 (s), 1277 (m), 1238 (w), 1192 (m), 1081 (vs, ν_{BF}), 1054 (vs, ν_{BF}), 1037 (vs, ν_{BF}), 987 (s), 947 (m), 923 (m), 895 (m), 867 (m), 821 (s, δ_{NO2}), 806 (m), 772 (s), 709 (w), 668 (m), 622 (w), 521 (m), 507 (m), 496 (m), 463 (m), 408 (vw). ^1H NMR (400 MHz, CD_3CN, δ from residual protio solvent): 8.53 (br s, 1H), 7.84 (s, 1H), 7.59 (s, 1H), 4.21 (t, 1H), 4.03 (s, 4H), 2.15 (m, 1H). LR-ESI-MS (*m/z*): $[M - 2BF_4 - MeCN]^+$ calcd for $C_{13}H_{18}CoN_7O_2$, 363.1 (100.0), 364.1 (17.0), 365.1 (1.7); found, 363.2 (100.0), 364.2 (18.9), 365.2 (1.9). Anal. Calcd. for $C_{15}H_{21}B_2CoF_8N_8O_2$: C, 31.17; H, 3.66; N, 19.39. Found: C, 31.07; H, 3.32; N, 19.28.

4.8.4 Reactivity

Attempted syntheses of [Co(LN_4^{PrIm})(NO)](BPh_4) (5) (Methods 1-3).

Method 1: Reduction of 3 with [$CoCp_2$]. To a 1.5 mL brown MeCN solution of **3** (40.0 mg, 0.0712 mmol) was added a 2 mL black MeCN solution of [$CoCp_2$] (13.5 mg, 0.0712 mmol) while stirring, which immediately resulted in a red-tinted brown solution. The homogenous reaction mixture stirred at RT for 1 h and was then dried in vacuo. Stirring the crude mixture in THF (3 × 3 mL) and filtering afforded a dark brown solid (35.2 mg) and brown filtrate (total mass

recovered: 49.3 mg). FTIR, ESI-MS, and ^{1}H NMR data indicate the formation of **5^{BF4}**, although it was unsuccessfully isolated from the [$CoCp_2$](BF_4) by-product.

Method 2: Reaction of 2 with Ph_3CSNO. To a dark purple 3 mL MeCN solution of [Co(LN_4^{PrIm})(LN_4^{PrIm}-κ^2-*C*,*N*)]$_2$(BPh_4)$_2$ (**2**) (65.4 mg, 0.0514 mmol) was added a green 2 mL MeCN slurry of Ph_3CSNO (37.6 mg, 0.123 mmol) while stirring. The solution color had a red hue immediately following the addition of Ph_3CSNO, and after stirring for 5 min, the color of the reaction mixture turned from dark purple to dark red. No insolubles were noted. After 50 min of stirring at RT, the solvent was removed in vacuo until a yellow-tinted brown solid remained. The crude mixture stirred in Et_2O (3 × 5 mL) for 5 min. Scraping the Et_2O insoluble product and filtering afforded a yellow-brown, semicrystalline solid (68.2 mg), which contained [Co(LN_4^{PrIm})(NO)](BPh_4) (**5^{BPh4}**). Multiple peaks in the ν_{NO} region (2000-1300 cm^{-1}) appeared following the nitrosylation, potentially in-line with formation of other Co-NO species. EPR data indicates a mixture of Co^{II} species.

Method 3: Reaction of 2 with NO(g). Addition of NO(g) to a dark purple 1.5 mL MeCN slurry of **2** (60.0 mg, 0.0471 mmol) for 90 s resulted in a slight color change; the solution became brown-tinted but remained dark purple with insolubles. The reaction mixture stirred at RT for 30 min under an NO(g) atmosphere and over time, the solution became brown in color and homogeneous. After this time, excess NO(g) was removed by pulling vacuum and refilling with N_2. The reaction mixture was dried in vacuo. Trituration with Et_2O (3 × 5 mL) afforded a yellow-brown solid (56.1 mg), that contained **5^{BPh4}**. Repeating this method with ^{15}NO(g) (**2**, 60.0 mg,

0.0471 mmol) afforded a yellow-brown solid (58.9 mg) with isotope-sensitive bands indicating the formation of **5^{BPh4}-^{15}NO** and the Co^{III}-NO_2 complex **4**.

Spectroscopic characterization of 5. This evidence was consistent across methods 1 - 3: FTIR (KBr matrix), ν_{max} (cm^{-1}): 2248 (ν_{CN}, w), 1668 (ν_{NO}, m). LRMS-ESI (*m/z*): $[M]^+$ calcd for $C_{13}H_{18}CoN_7O_1$, 347.1 (100), 348.1 (14.1); found, 347.1 (100), 348.1 (25.0). UV-vis (MeCN, RT), λ_{max}, nm: 267, 274, 290, 431. EPR (MeCN:toluene (1:1), 10 K, 9.582 GHz, 1.00 mW, 6.477 G): *g* = [2.14].

UV-vis monitor of the reaction of {CoNO}^{8} (3) with [Mn^{III}(TPPS)]$^{3-}$. A 1.1 mM stock solution of $[Mn^{III}(TPPS)]^{3-}$ was prepared in 10 mM PBS (pH 7.4) and the UV-vis spectrum was recorded at 298 K, which was consistent with the literature.[77] No significant changes occurred in the spectrum over 30 min. To the cuvette was then added a 0.020 mL aliquot of a 5.3 mM MeCN stock solution of the $\{CoNO\}^{8/9}$ complexes, yielding a 1:5 ratio of $[Mn^{III}(TPPS)]^{3-}$/$\{CoNO\}^8$ (**3**). The UV-vis was monitored for 24 h at 298 K (intervals used: 1 min cycles for 1 h; 30 min cycles for the next 19 h). No reaction occurred over the 20-h period based on monitoring of the Soret band (λ_{max} 467 nm).

UV-vis monitor of the reaction of {CoNO}^{8} (3) with [Mn^{III}(TPPS)]$^{3-}$ in the presence of HS$^-$. A 1.2 mM stock solution of $[Mn^{III}(TPPS)]^{3-}$ was prepared in 10 mM PBS (pH 7.4) and the UV-vis spectrum was recorded at 298 K, which was consistent with the literature.[77] No significant changes occurred in the spectrum over 30 min. To the cuvette was then added a 0.020 mL aliquot of a 5.9 mM MeCN stock solution of **5**, yielding a 1:5 ratio of

$[Mn^{III}(TPPS)]^{3-}/\{CoNO\}^{8}$ (**3**). After recording the UV-vis spectrum, a 0.010 mL aliquot of an 11.7 mM PBS stock solution of NaSH was added to the cuvette, yielding a 1:5:5 ratio of $[Mn^{III}(TPPS)]^{3-}/\{CoNO\}^{8}$ (**3**)/HS^-. The UV-vis was monitored for 20 h at 298 K (intervals used: 1 min cycles for 1 h; 5 min cycles for the second 1 h; 30 min cycles for 3 h through 20 h). These reaction conditions were repeated with 10 and 20 equiv of HS^-.

UV-vis monitor of the reaction of $[Mn^{III}(TPPS)]^{3-}$ with 5 and 20 equiv of HS^-. Reaction conditions were prepared in an identical manner as listed above, except using a 0.90 mM PBS stock solution of $[Mn^{III}(TPPS)]^{3-}$ and a 17.59 mM PBS stock solution of NaSH. A 0.005 mL aliquot of the NaSH stock solution was used for a 1:5 ratio of $[Mn^{III}(TPPS)]^{3-}/HS^-$, and a 0.020 mL aliquot of the NaSH stock solution was used for a 1:20 ratio of $[Mn^{III}(TPPS)]^{3-}/HS^-$.

4.9 Supporting Information

X-ray Crystallographic Data Collection and Structure Solution and Refinement. Orange crystals of $[Co(LN_4^{PrIm})(MeCN)_2](BF_4)_2$ (**1**) and purple crystals of $[Co(LN_4^{PrIm})(LN_4^{PrIm}\text{-}\kappa^2\text{-}C,N)]_2(BPh_4)_2$ (**2**) were grown under anaerobic conditions by slow diffusion of Et_2O into an MeCN solution of **1** at -25 °C. Red crystals of $[Co(LN_4^{PrIm})(MeCN)(NO)](BF_4)_2$ (**3**) were grown under anaerobic conditions by slow diffusion of Et_2O into an MeCN solution of **3** at -20 °C. Lastly, yellow crystals of $[Co(LN_4^{PrIm})(MeCN)(NO_2)](BF_4)_2$ (**4**) were grown under anaerobic conditions by slow diffusion of Et_2O into an MeCN solution of **4** at -20 °C. Suitable crystals were mounted on a glass fiber. The X-ray intensity data were measured at 100 K on a Bruker SMART APEX II X-ray diffractometer system with graphite-monochromated Mo Kα radiation (λ = 0.71073 Å) using ω-scan technique controlled by the SMART software package.[86] The data were collected in

1464 frames with 10 second exposure times. The data were corrected for Lorentz and polarization effects[87] and integrated with the manufacturer's SAINT software. Absorption corrections were applied with the program SADABS.[88] Subsequent solution and refinement was performed using the SHELXTL 6.1 solution package operating on a Pentium computer.[89-90] The structure was solved by direct methods using the SHELXTL 6.1 software package.[91] Non-hydrogen atomic scattering factors were taken from the literature tabulations.[92] Selected data and metric parameters for complexes **1**, **2** and **3**, **4** are summarized in Tables 4.S1 and 4.S4 respectively. Selected bond distances and angles for **1** (Table 4.S2), **2** (Table 4.S3), **3** (Table 4.S5), and **4** (Table 4.S5) are also listed in the respective tables. Perspective views of the complexes were obtained using ORTEP.[93]

The structure of **3** was solved by Prof. Marilyn Olmstead in the Department of Chemistry at Univ. of CA-Davis. The structure of **3** contains substitutional disorder that involves mixing one of the axial sites with acetonitrile and nitric oxide. In the other axial group, such disorder was also investigated, but it was too minor to be definitive and it was left as 100% acetonitrile. In the mixed site, there are two different coordinated nitrogens. One (N8a) belongs to the acetonitrile, at a refined occupancy of 65%, and the other (N8b) belongs to nitric oxide at a refined occupancy of 35%. The distances to Co differ. The Co1-N8a distance is 2.216(7) Å, and the Co1-N8b distance is 1.850(11) Å. These distances are within the known range for the two different ligands. Once the N8a:N8b occupancies were determined, two different oxygen positions were considered. Their occupancies were restrained to sum to 0.35. The O1:O2 ratio was then found to be 0.293(6):0.059(6). A N-O distance restraint of 1.15(2) Å was applied. The refined N8b-O1 and N8b-O2 distances are 1.140(11) Å and 1.250(18) Å, respectively. The Co1-N-O angles are non-linear, and the two groups are approximately perpendicular to one another. The solvate acetonitrile molecule exhibits correlated disorder to the nitric oxide disorder. In the major orientation (65%),

nitric oxide must be absent, and in the minor orientation (35%), nitric oxide must be present in order to avoid unusual intermolecular contacts and fill void space, for a total molecular formula of $[Co(L)(acetonitrile)_{1.65}(NO)_{0.35}](BF_4)_2$•acetontrile. During refinement, the minor components of the disorder groups were refined with isotropic displacement parameters.

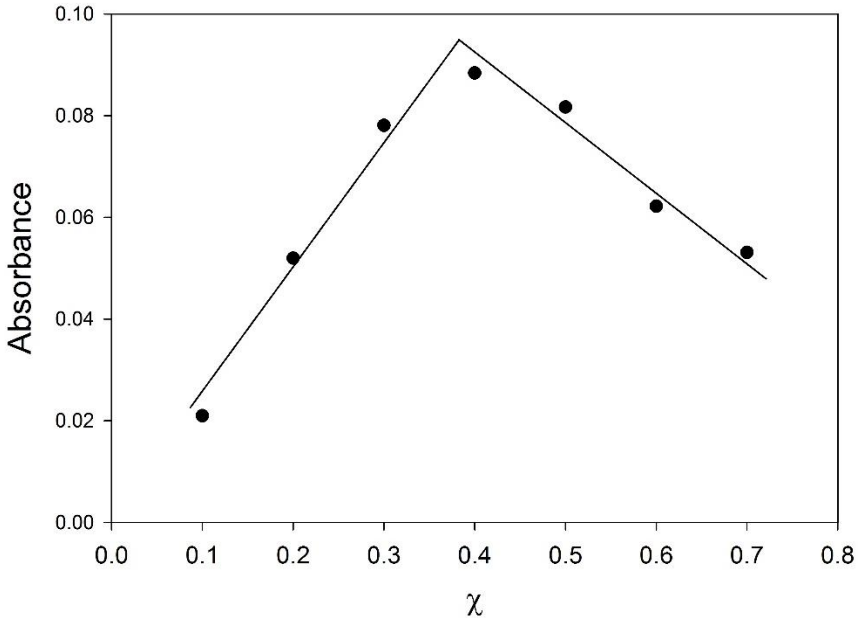

Figure 4.S1. Job's Plot for the method of continuous variation for $[Co(H_2O)_6](BF_4)_2$ and LN_4^{PrIm} in MeCN, indicating a binding stoichiometry of 1:1 to form complex **1**.

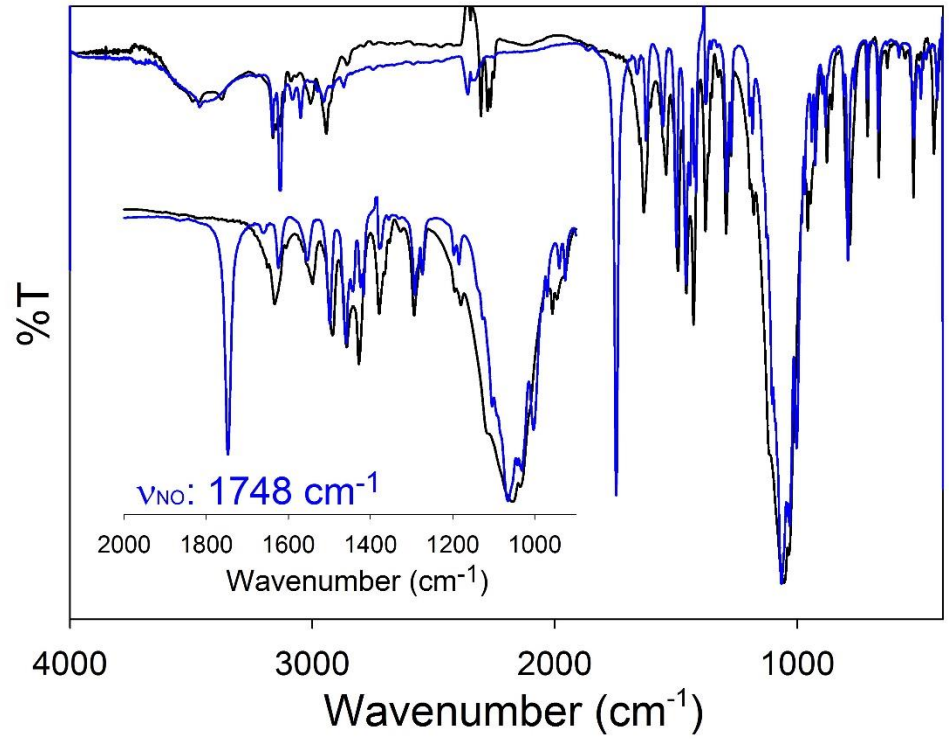

Figure 4.S2. FTIR spectra of $[Co(LN_4^{PrIm})(MeCN)_2](BF_4)_2$ (**1**) (black) and $[Co(LN_4^{PrIm})(MeCN)(NO)](BF_4)_2$ (**3**) (blue) in a KBr matrix.

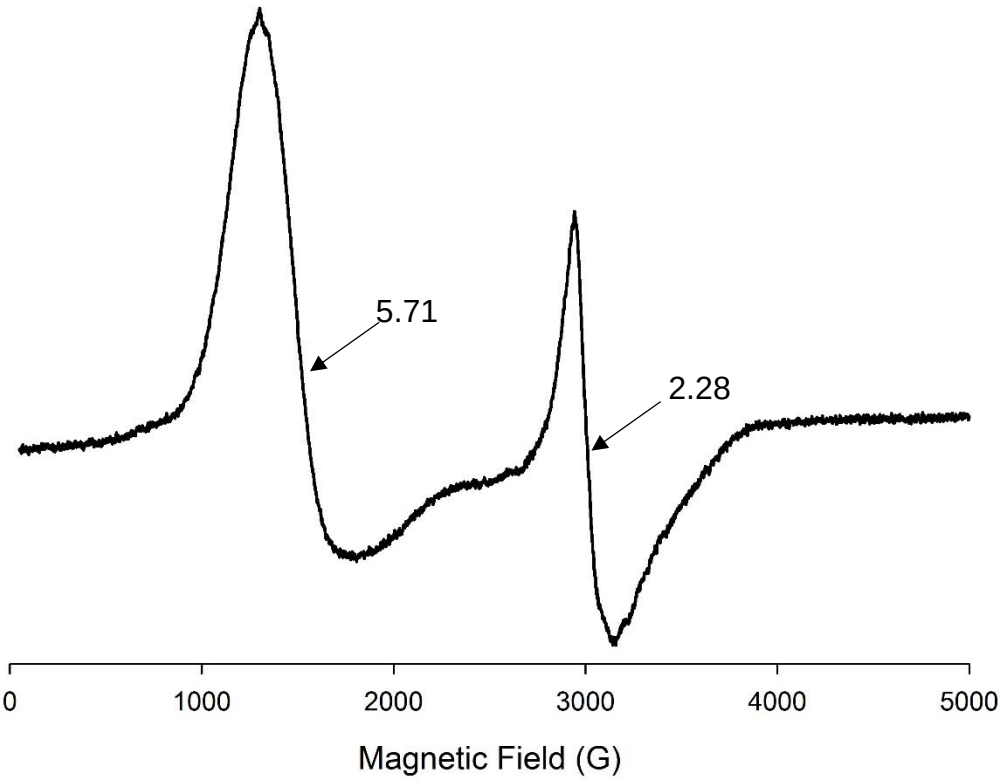

Figure 4.S3. X-band EPR spectrum of $[Co(LN_4^{PrIm})(MeCN)_2](BF_4)_2$ (**1**) at 10 K. Spectrometer settings: microwave frequency, 9.582 GHz; microwave power, 4.0 mW; modulation frequency, 100 KHz; modulation amplitude, 6.477 G.

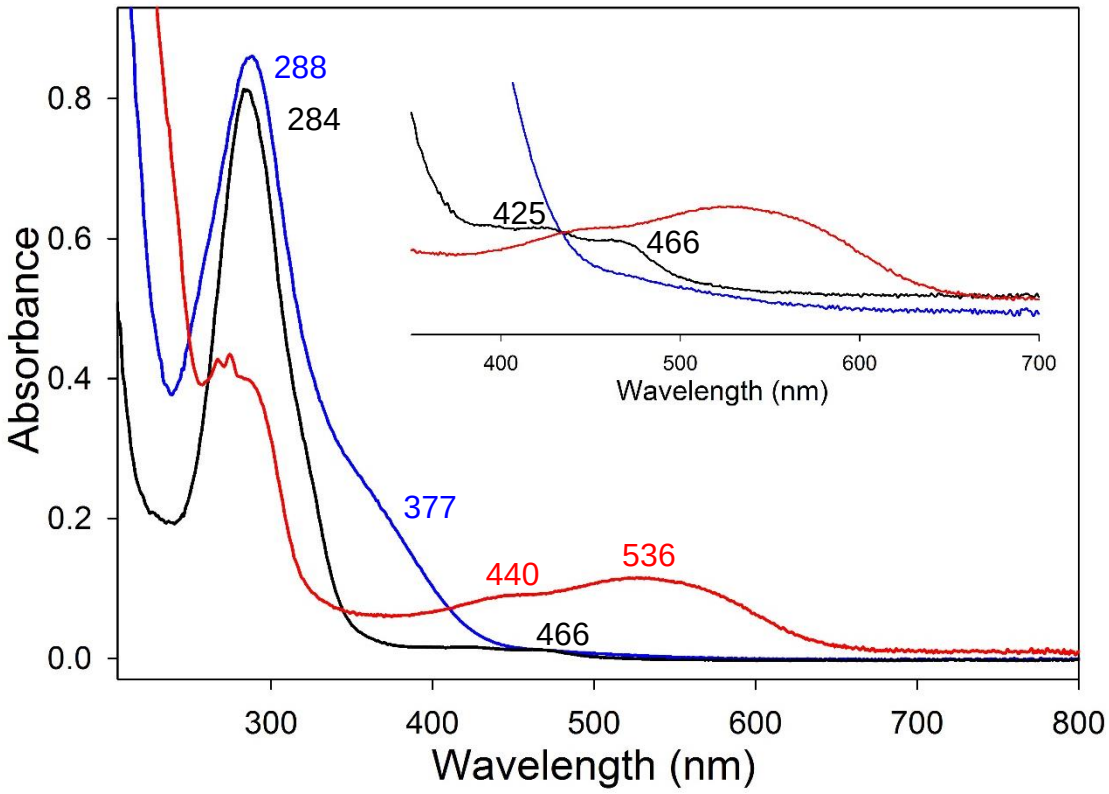

Figure 4.S4. Qualitative UV-vis spectra of $[Co(LN_4^{PrIm})(MeCN)_2](BF_4)_2$ (**1**) (black), $[Co(LN_4^{PrIm})(LN_4^{PrIm}\text{-}\kappa^2\text{-}C,N)]_2(BPh_4)_2$ (**2**) (blue), and $[Co(LN_4^{PrIm})(MeCN)(NO)](BF_4)_2$ (**3**) (red) in MeCN, RT. Color scheme is consistent with the highlighted λ_{max} values (nm).

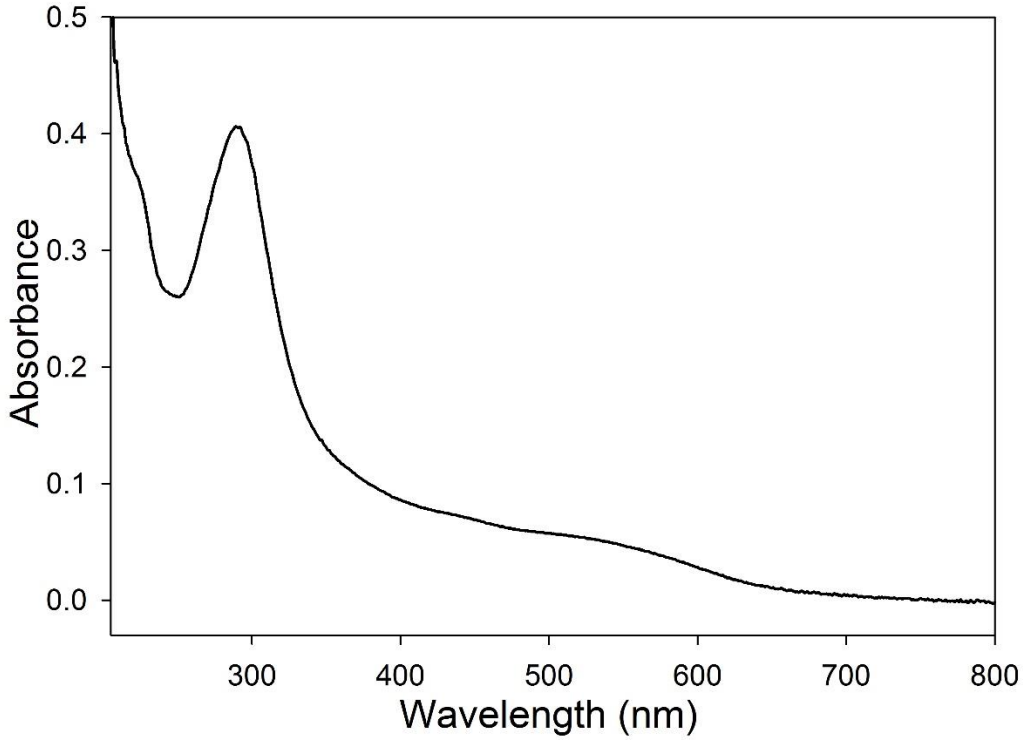

Figure 4.S5. UV-vis spectrum of $[Co(LN_4^{PrIm})(LN_4^{PrIm}\text{-}\kappa^2\text{-}C,N)]_2Cl_2$ (**2**) in 10 mM PBS, pH 7.4 at 298 K.

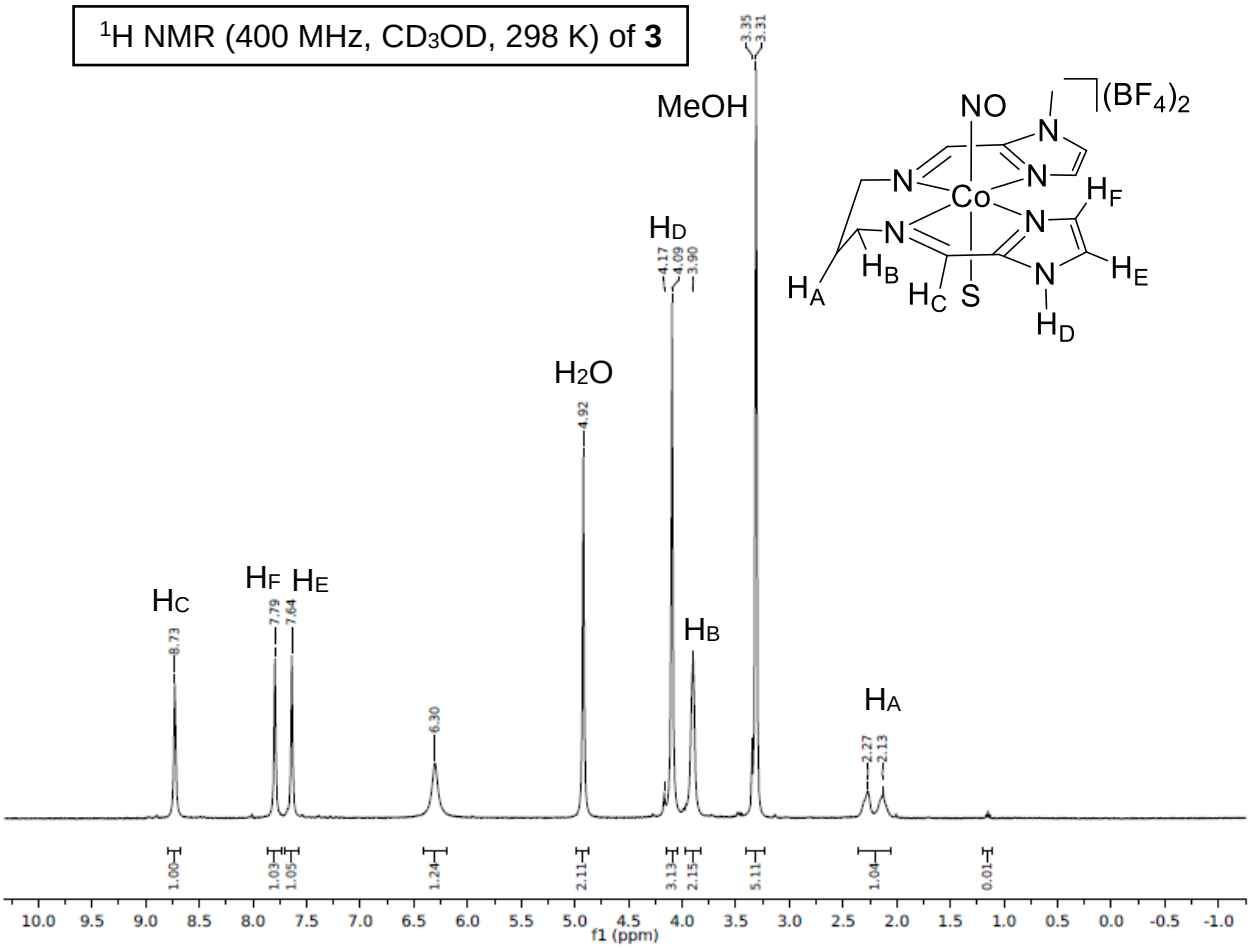

Figure 4.S6. ^{1}H NMR spectrum of [Co(LN_4^{PrIm})(MeOH)(NO)]$(BF_4)_2$ (**3**) in CD_3OD. The peak at 6.30 ppm is unidentified but is consistently present in preparations of **3**.

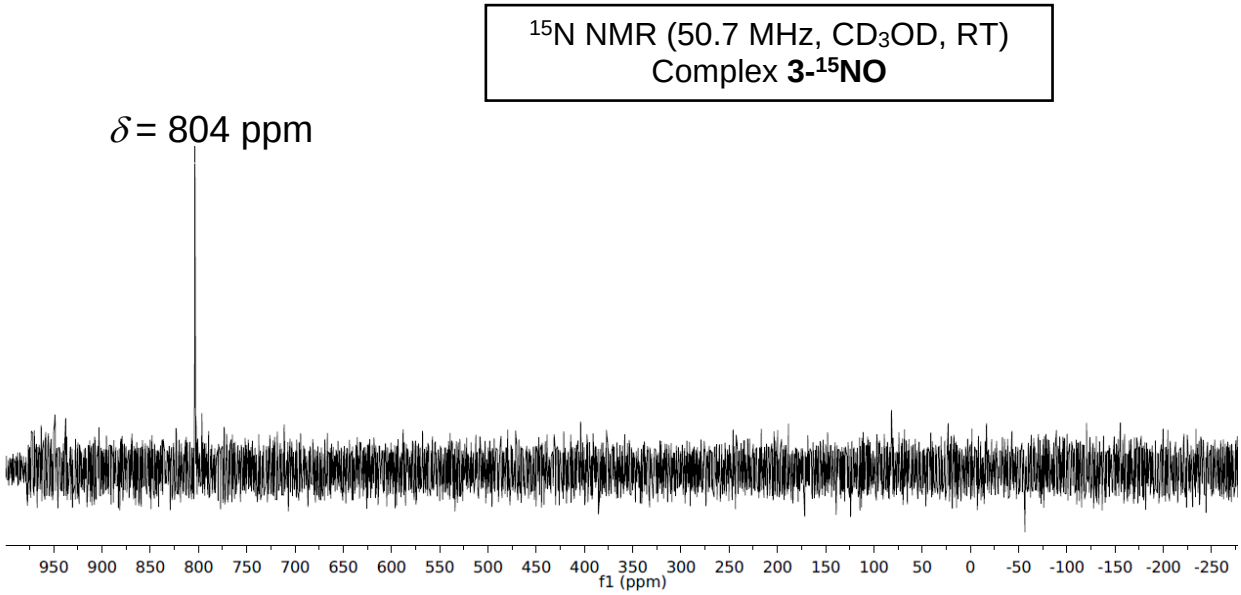

Figure 4.S7. ^{15}N NMR spectrum of $[Co(LN_4^{PrIm})(MeOH)(^{15}NO)](BF_4)_2$ (**3-^{15}NO**) in CD_3OD at RT (vs. external CH_3NO_2).

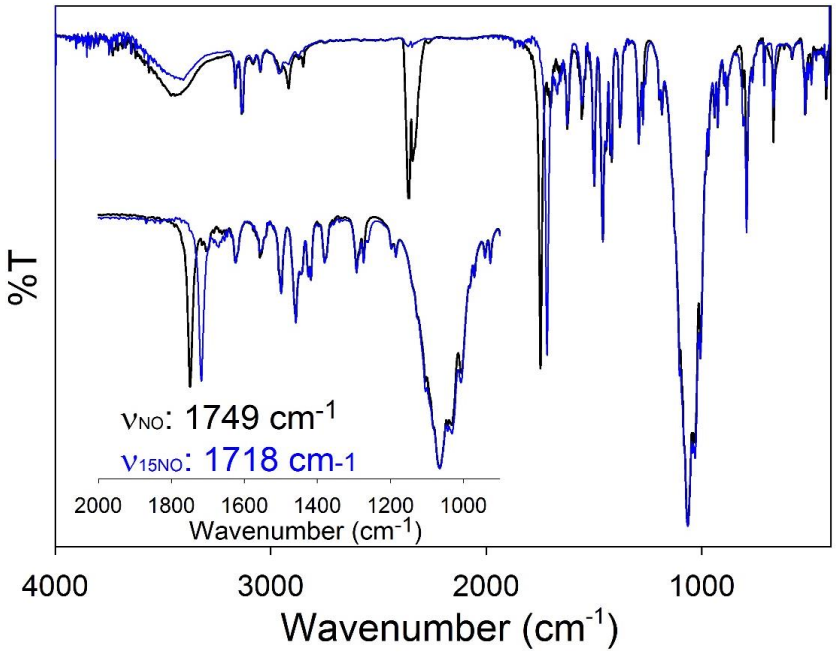

Figure 4.S8. FTIR spectra of $[Co(LN_4^{PrIm})(MeCN)(NO)](BF_4)_2$ (**3**) (black) and $[Co(LN_4^{PrIm})(MeCN)(^{15}NO)](BF_4)_2$ (**3-^{15}NO**) (blue) in a KBr matrix.

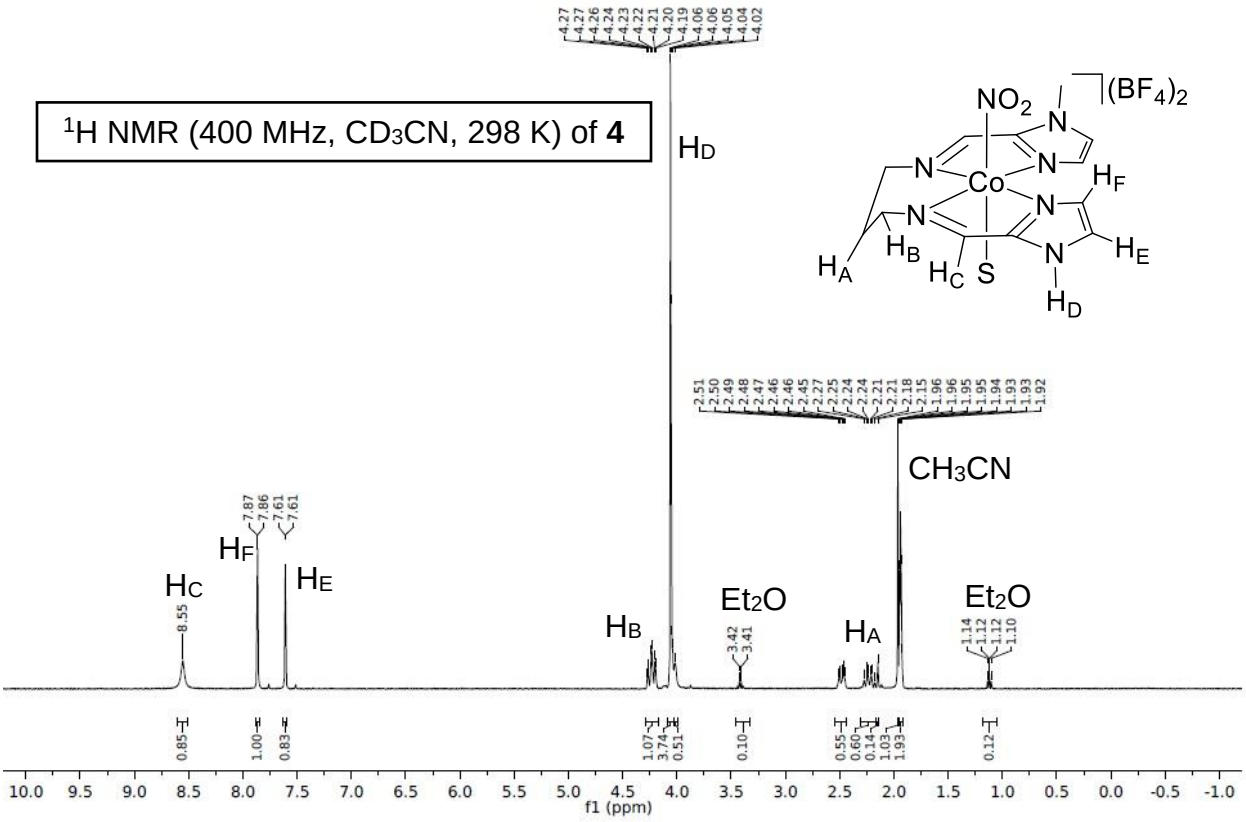

Figure 4.S9. ^{1}H NMR spectrum of [Co(LN$_4^{PrIm}$)(MeCN)(η^1-NO$_2$)](BF$_4$)$_2$ (**4**) in CD$_3$CN.

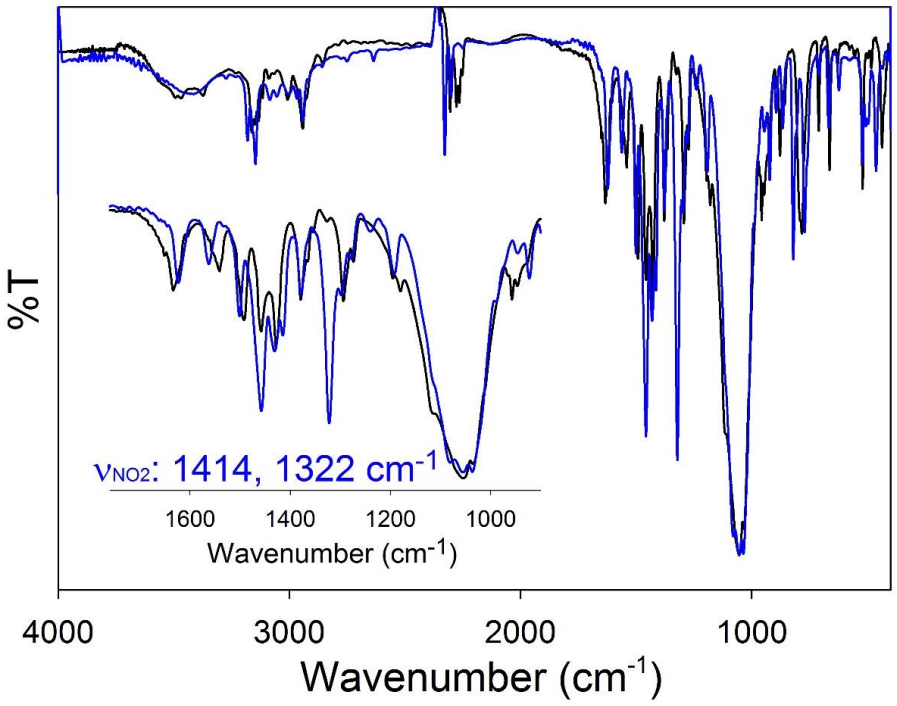

Figure 4.S10. FTIR spectra of $[Co(LN_4^{PrIm})(MeCN)_2](BF_4)_2$ (**1**) (black) and $[Co(LN_4^{PrIm})(MeCN)(NO_2)](BF_4)_2$ (**4**) (blue) in a KBr matrix.

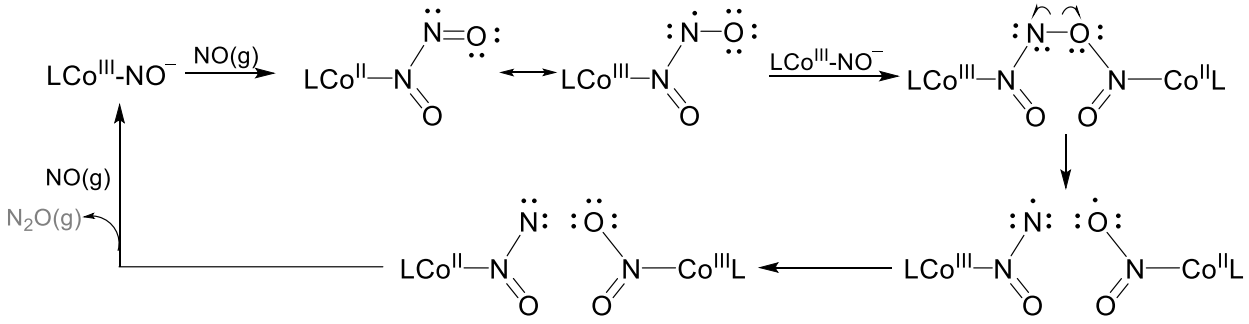

Scheme 4.S1. Proposed mechanism for formation of **4**. Adapted from references 60[60] and 53.[53] The path of disproportionation involves attack of the free NO• on the coordinated NO in $\{CoNO\}^8$ (**3**) to yield a hyponitrito-like intermediate. Further attack of the Co-N_2O_2 moiety by another equivalent of **3** yields **4** and N_2O(g).

Table 4.S1. Summary of crystal data and intensity collection and structure refinement parameters for $[Co(LN_4^{PrIm})(MeCN)_2](BF_4)_2$ (**1**) and $[Co(LN_4^{PrIm})(LN_4^{PrIm}\text{-}\kappa^2\text{-}C,N)]_2(BPh_4)_2$ (**2**).

Parameters	**1**	**2**
Formula	$C_{17}H_{24}B_2CoF_8N_8$	$C_{78}H_{86}N_{12}OB_2Co_2$
Formula weight	572.99	1347.06
Crystal system	Orthorhombic	Monoclinic
Space group	$P2_12_12_1$	C2/c
Crystal color, habit	Orange	Purple
a, Å	10.0163(13)	21.548(4)
b, Å	12.9092(17)	11.516(2)
c, Å	18.175(3)	27.607(5)
α, deg	90	90
β, deg	90	101.501(3)
γ, deg	90	90
V, Å^3	2419.8(6)	6713(2)
Z	4	4
$\rho_{calcd,}$ g/cm^3	1.573	1.333
T, K	100(2)	100(2)
abs coeff, μ (Mo Kα), mm^{-1}	0.794	0.551
θ limits, deg	2.57-30.00	1.929-26.021
total no. of data	7031	38652
no. of unique data	6719	6606
no. of parameters	392	451
GOF of F^2	1.016	1.008
R_1,[a] %	2.90	7.17
wR_2,[b] %	7.39	15.39
max, min peaks, e/Å^3	0.534, -0.285	0.846, -0.385

[a] $R_1 = \Sigma| |F_o| - |F_c| | / \Sigma |F_o|$; [b] $wR_2 = \{\Sigma[w(F_o^2 - F_c^2)^2]/\Sigma[w(F_o^2)^2]\}^{1/2}$

Table 4.S2. Selected bond distances (Å) and bond angles (deg) for $[Co(LN_4^{PrIm})(MeCN)_2](BF_4)_2$ (**1**).

1	
Co1-N1	1.9939(13)
Co1-N3	1.9668(13)
Co1-N4	1.9762(13)
Co1-N5	1.9714(14)
Co1-N7	2.1621(14)
Co1-N8	2.3852(15)
N7-C15	1.132(2)
N8-C17	1.135(2)
N3-Co1-N5	174.05(6)
N4-Co1-N5	81.70(5)
N1-Co1-N3	82.08(5)
N1-Co1-N4	175.76(5)
N1-Co1-N5	101.72(5)
N3-Co1-N7	90.12(5)
N5-Co1-N7	94.27(5)
N4-Co1-N7	89.80(5)
N3-Co1-N4	94.31(5)
C17-N8-Co1	130.78(15)
C15-N7-Co1	170.66(13)

Table 4.S3. Selected bond distances (Å) and bond angles (deg) for [Co(LN_4^{PrIm})(LN_4^{PrIm}-κ^2-*C,N*)]$_2$(BPh_4)$_2$ (**2**).

2			
Co1-N1 (#1)	1.946(4)		
Co1-N3 (#1)	1.941(4)		
Co1-N4 (#1)	1.957(4)		
Co1-N5 (#1)	1.985(4)		
Co1-C9	2.011(5)		
Co1-N4	1.918(4)		
N4-C9	1.425(6)		
N3-C5	1.296(6)		
Co1-Co1 (#1)	2.9790(13)		
N4-Co1-N3 (#1)	158.85(16)	N1 (#1)-Co1-C9	91.79(18)
N4-Co1-N4 (#1)	79.53(16)	N3 (#1)-Co1-C9	118.21(17)
N3 (#1)-Co1-N4 (#1)	96.03(16)	N4 (#1)-Co1-C9	93.60(17)
N4-Co1-N1 (#1)	104.31(15)	N5 (#1)-Co1-C9	135.46(18)
N3 (#1)-Co1-N1 (#1)	81.73(16)	N4 (#1)-Co1-Co1 (#1)	40.25(11)
N4 (#1)-Co1-N1 (#1)	174.59(16)	N1 (#1)-Co1-Co1 (#1)	144.41(12)
N4-Co1-N5 (#1)	94.03(15)	N3 (#1)-Co1-Co1 (#1)	132.03(12)
N3 (#1)-Co1-N1 (#1)	106.20(16)	N4 (#1)-Co1-Co1 (#1)	39.28(11)
N4 (#1)-Co1-N5 (#1)	84.56(15)	N5 (#1)-Co1-Co1 (#1)	89.03(11)
N1 (#1)-Co1-N5 (#1)	91.32(15)	C9-Co1-Co1 (#1)	64.29(14)
N4-Co1-C9	42.44(17)		

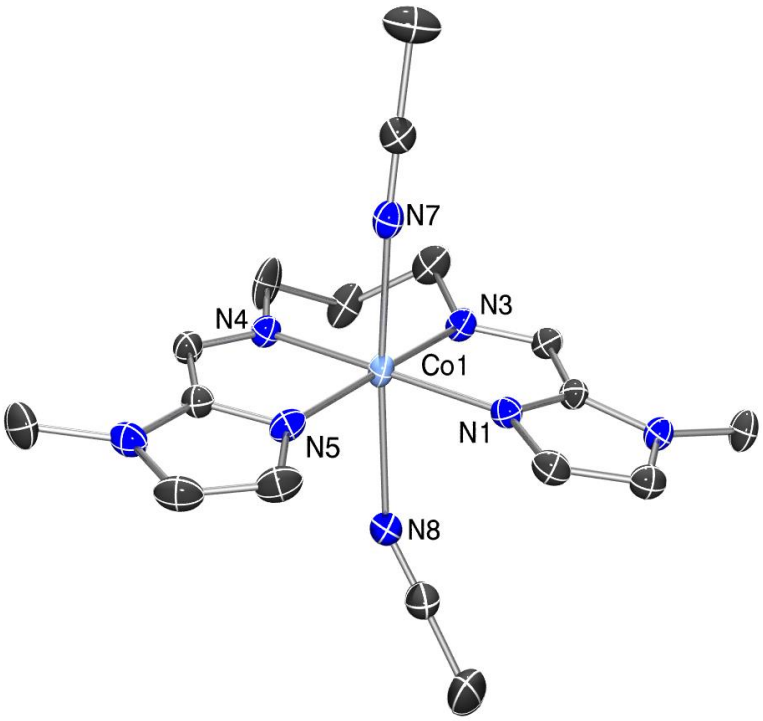

Figure 4.S11. X-ray structure of $[Co(LN_4^{PrIm})(MeCN)_2](BF_4)_2$ (**1**) (50% probability level). H atoms and BF_4^- counteranions omitted for clarity.

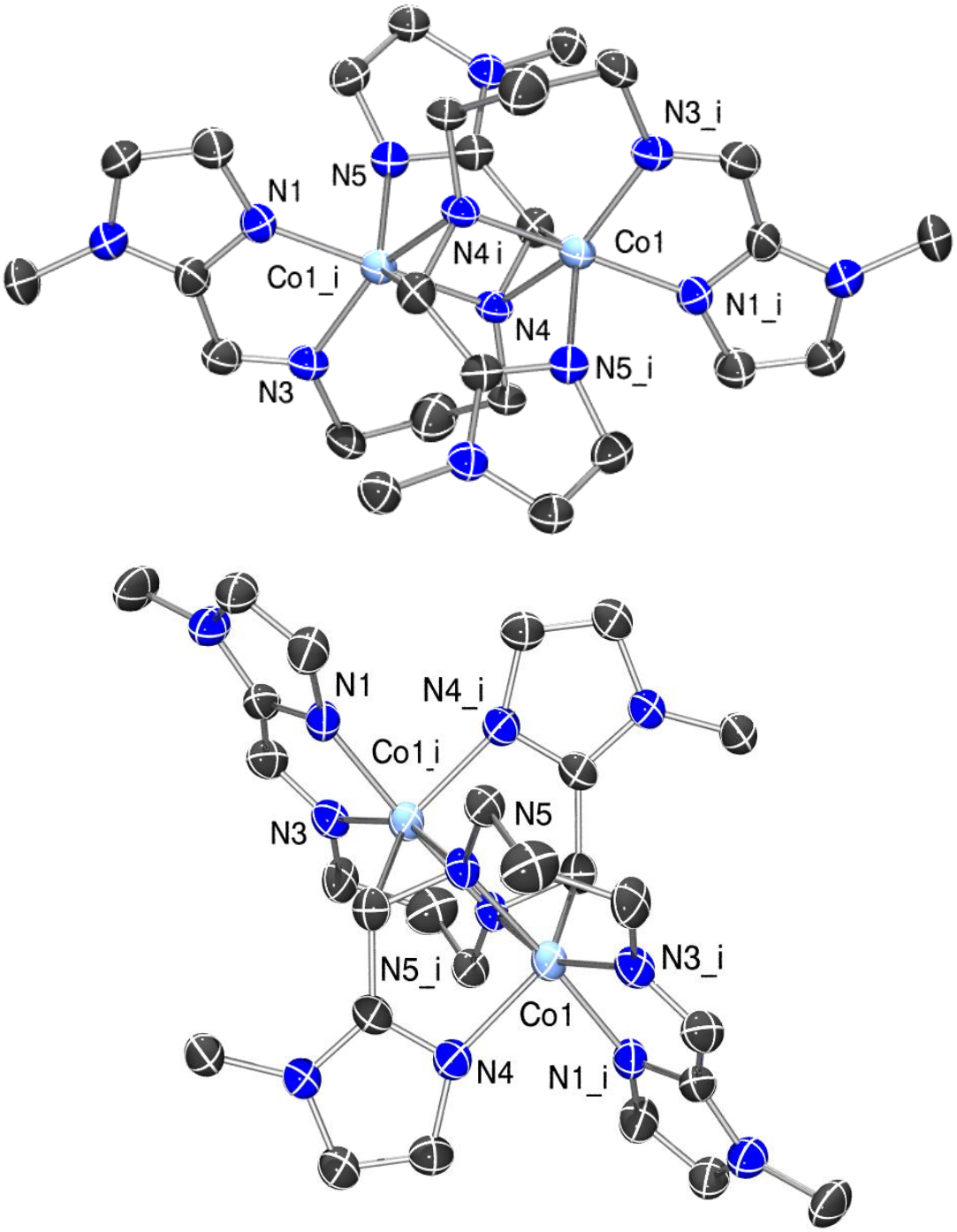

Figure 4.S12. Two views of the X-ray structure of $[Co(LN_4^{PrIm})(LN_4^{PrIm}\text{-}\kappa^2\text{-}C,N)]_2(BPh_4)_2$ (**4**) (50% probability level). H atoms and BPh_4^- counteranions omitted for clarity.

Table 4.S4. Summary of crystal data and intensity collection and structure refinement parameters for $[Co(LN_4^{PrIm})(MeCN)(NO)](BF_4)_2$ (**3**) and $[Co(LN_4^{PrIm})(MeCN)(NO_2)](BF_4)_2$ (**4**).

Parameters	**3**	**4**
Formula	$C_{18.30}H_{25.95}B_2CoF_8N_9O_{0.35}$	$C_{17}H_{24}B_2CoF_8N_9O_2$
Formula weight	610.18	619.00
Crystal system	Monoclinic	Triclinic
Space group	*P*-2_1/n	*P*-1
Crystal color, habit	Red	Red
a, Å	10.7924(12)	10.4508(15)
b, Å	21.373(2)	11.1624(16)
c, Å	11.5982(12)	12.7359(18)
α, deg	90	82.538(2)
β, deg	100.463(2)	77.291(2)
γ, deg	90	64.447(2)
V, Å^3	2630.8(5)	1306.5(3)
Z	4	2
$\rho_{calcd,}$ g/cm^3	1.541	1.573
T, K	100(2)	100(2)
abs coeff, μ (Mo Kα), mm^{-1}	0.737	0.748
θ limits, deg	2.372-27.878	2.49-27.50
total no. of data	34893	16920
no. of unique data	6276	6001
no. of parameters	365	439
GOF of F^2	1.027	1.086
R_1,[a] %	5.57	6.30
wR_2,[b] %	13.33	17.26
max, min peaks, e/Å^3	0.900, -0.623	1.930, -1.016

[a]$R_1 = \Sigma| |F_O| - |F_c| | / \Sigma |F_O|$; [b]$wR_2 = \{\Sigma[w(F_o^2 - F_c^2)^2]/\Sigma[w(F_o^2)^2]\}^{1/2}$

Table 4.S5. Selected bond distances (Å) and bond angles (deg) for $[Co(LN_4^{PrIm})(MeCN)(NO)](BF_4)_2$ (**3**) and $[Co(LN_4^{PrIm})(MeCN)(NO_2)](BF_4)_2$ (**4**).

3			**4**	
Co1-N1	1.961(3)		Co1-N1	1.937(2)
Co1-N3	1.962(3)		Co1-N3	1.940(2)
Co1-N4	1.952(3)		Co1-N4	1.940(2)
Co1-N5	1.977(3)		Co1-N6	1.938(2)
Co1-N7	2.156(3)		Co1-N7	1.991(2)
Co1-N8a	2.216(7)		Co1-N8	1.903(2)
Co1-N8b	1.850(11)		N8-O1	1.203(2)
N7-C14	1.132(5)		N8-O2	1.211(3)
N8a-C16	1.164(1)			
N8b-O1	1.140(11)			
N8b-O2	1.250(18)			
			N3-Co1-N6	177.97(7)
N3-Co1-N5	177.43(1)		N4-Co1-N6	82.61(7)
N4-Co1-N5	82.49(1)		N1-Co1-N3	82.69(6)
N1-Co1-N3	82.07(1)		N1-Co1-N4	175.15(7)
N1-Co1-N4	176.62(1)		N1-Co1-N6	99.33(6)
N1-Co1-N5	100.46(1)		N3-Co1-N7	87.54(7)
N3-Co1-N7	89.18(1)		N6-Co1-N7	92.71(6)
N5-Co1-N7	90.45(1)		N4-Co1-N7	88.40(7)
N4-Co1-N7	88.46(1)		N3-Co1-N4	95.38(7)
N3-Co1-N4	94.97(1)		O1-N8-O2	123.7(2)
C16-N8a-Co1	163.61(6)		O1-N8-Co1	119.0(1)
C14-N7-Co1	176.72(3)		O2-N8-Co1	117.2(1)
O1-N8a-Co1	107.53			
O2-N8a-Co1	101.60			
O1-N8b-Co1	130.87			
O2-N8b-Co1	116.01			

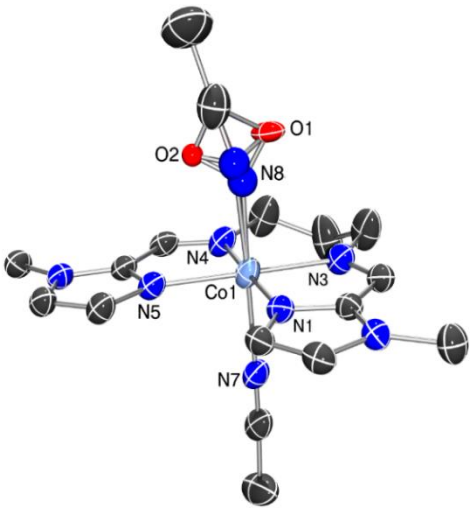

Figure 4.S13. ORTEP perspective of $[Co(LN_4^{PrIm})(MeCN)_{1.65}(NO)_{0.35}](BF_4)_2$•MeCN, which contains $[Co(LN_4^{PrIm})(MeCN)(NO)](BF_4)_2$ (**3**) (50% probability level). This shows both the substitutional disorder of NO and MeCN in one of the axial positions and the disorder of the NO moiety. BF_4^- counteranions, MeCN solvent of crystallization, and H atoms have been omitted for clarity.

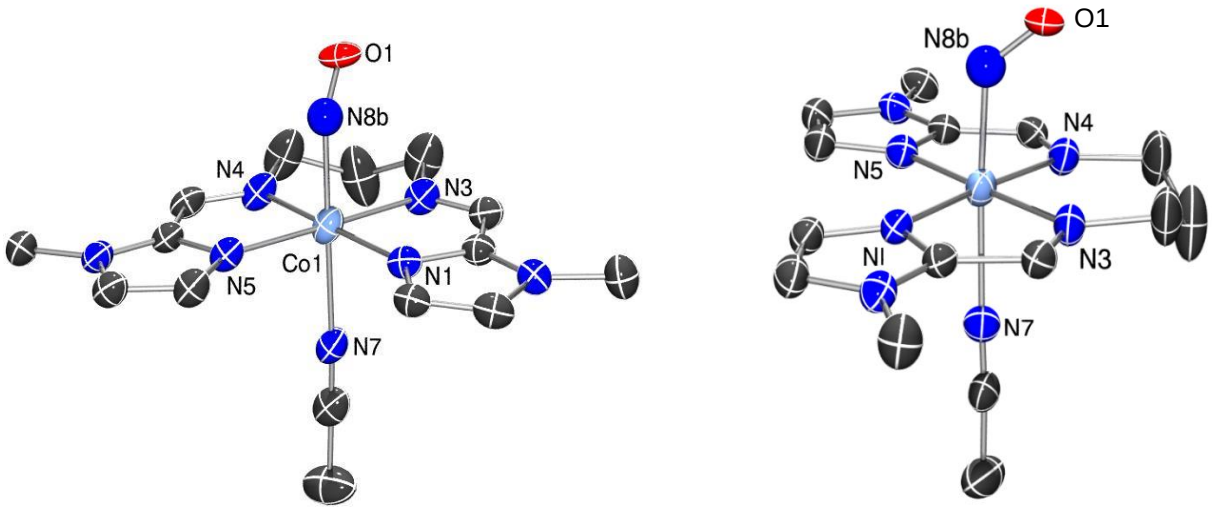

Figure 4.S14. ORTEP views of the NO-containing molecule found in the lattice for $[Co(LN_4^{PrIm})(MeCN)(NO)](BF_4)_2$ (**3**) (50% probability level, vide supra). BF_4^- counteranions, MeCN solvent of crystallization, and H atoms have been omitted for clarity.

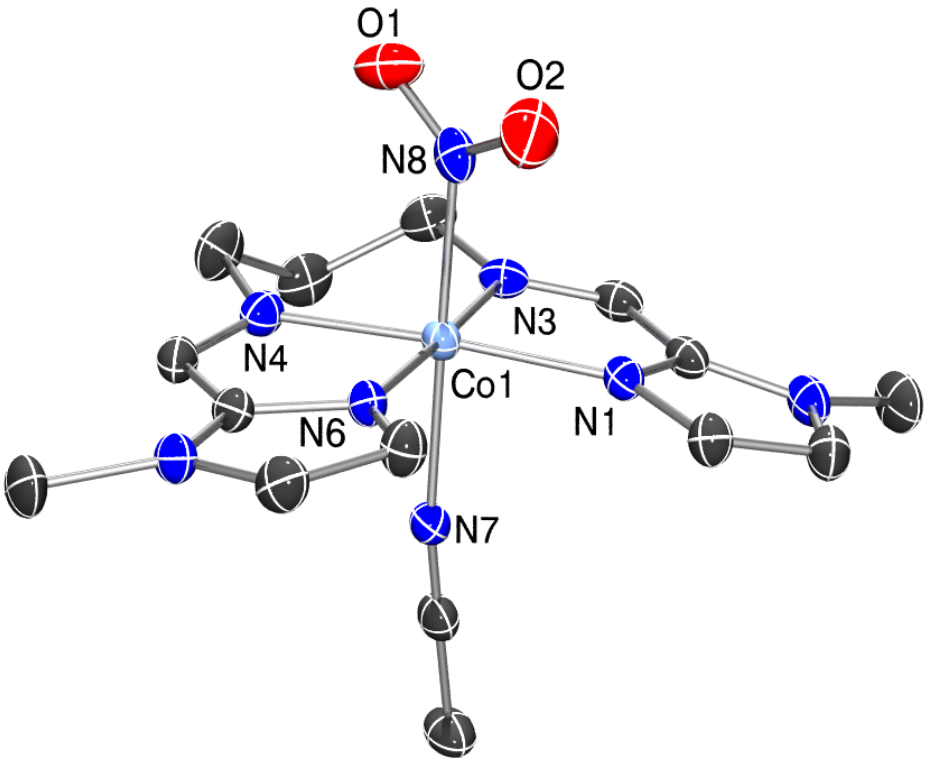

Figure 4.S15. X-ray structure of $[Co(LN_4^{PrIm})(MeCN)(NO_2)](BF_4)_2$ (**4**) (50% probability level). H atoms and BF_4^- counteranions omitted for clarity.

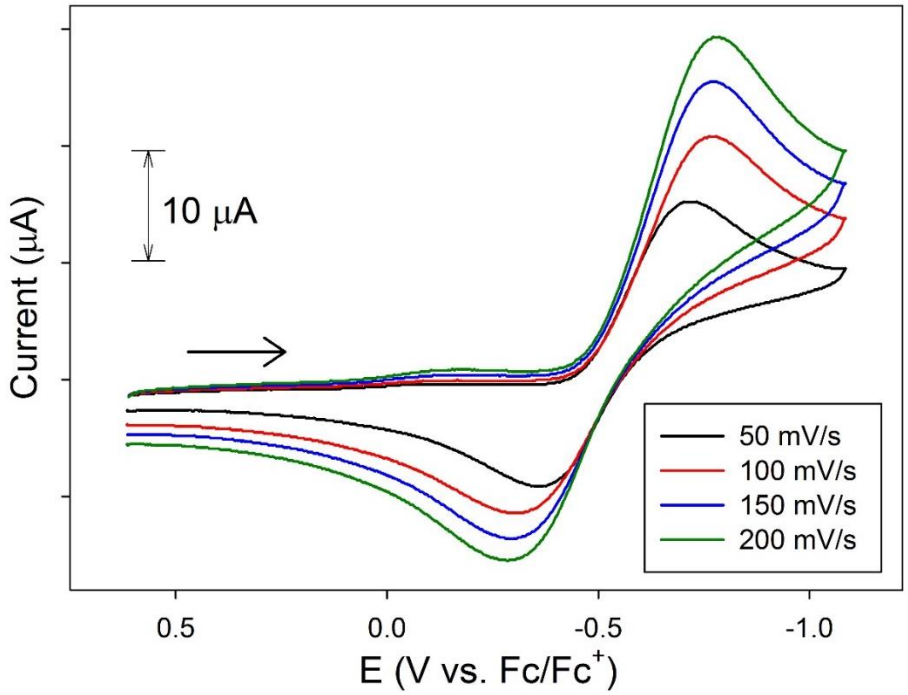

Figure 4.S16. Cyclic voltammogram (CV) of a 4 mM MeCN solution of $[Co(LN_4^{PrIm})(NO)](BF_4)_2$ (**3**) at different scan rates highlighting the $\{CoNO\}^{8/9}$ couple (0.1 M $^nBu_4NPF_6$ supporting electrolyte, glassy carbon working electrode, Pt-wire counter electrode, RT). Arrow displays direction of scan.

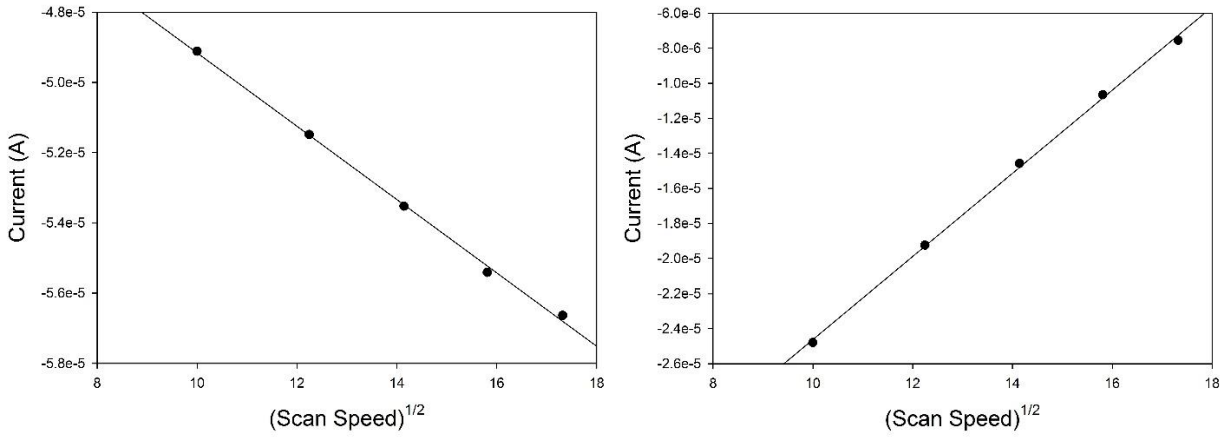

Figure 4.S17. Plots of the anodic, i_{pa}, (*left*, $R^2 = 0.9982$) and cathodic, i_{pc}, (*right*, $R^2 = 0.9989$) peak current versus square root of scan speed for the $\{CoNO\}^{8/9}$ redox couple for complex **3**.

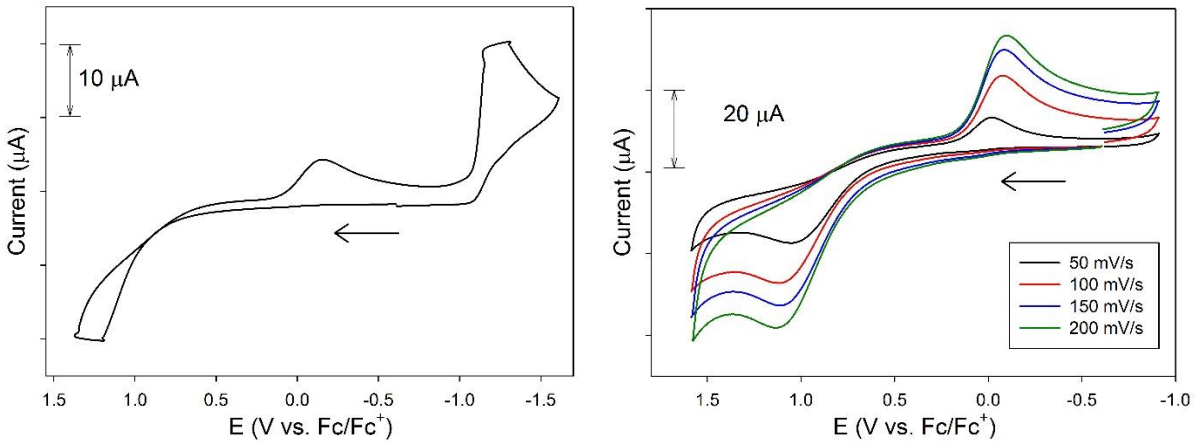

Figure 4.S18. CV of a 5 mM MeCN solution of $[Co(LN_4^{PrIm})(MeCN)_2](BF_4)_2$ (**1**) (*left*), and a truncated version at scan different scan rates (*right*) (0.1 M $^n Bu_4NPF_6$ supporting electrolyte, glassy carbon working electrode, Pt-wire counter electrode, RT). Arrow displays direction of scan.

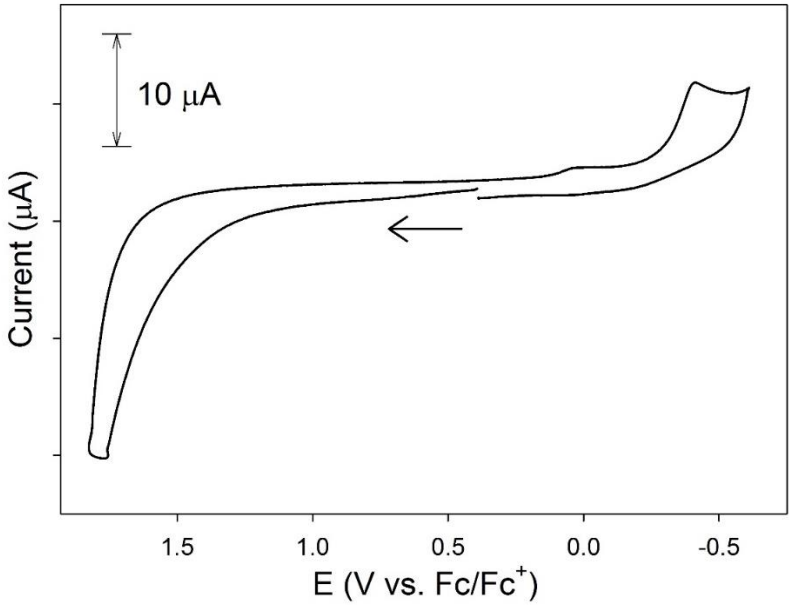

Figure 4.S19. CV of a 3 mM MeCN solution of $[Co(LN_4^{PrIm})(MeCN)(NO_2)](BF_4)_2$ (**4**) (0.1 M $^n Bu_4NPF_6$ supporting electrolyte, glassy carbon working electrode, Pt-wire counter electrode, RT). Arrow displays direction of scan.

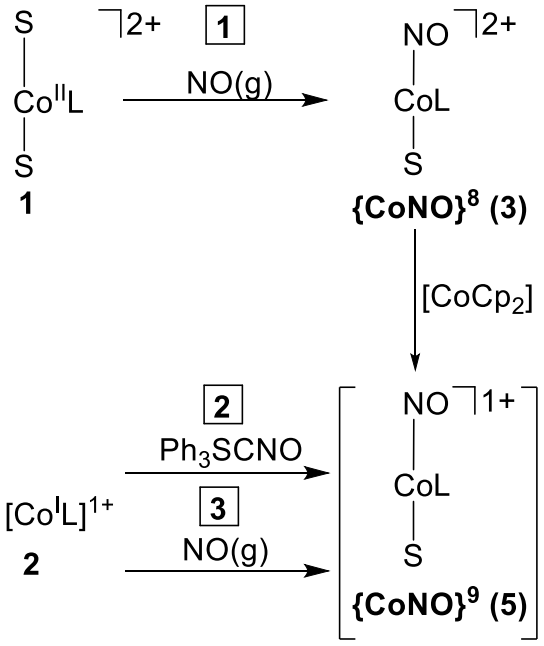

Scheme 4.S2. Attempted synthetic routes for $\{CoNO\}^9$ complex **5**. Brackets denote not yet isolated as clean material.

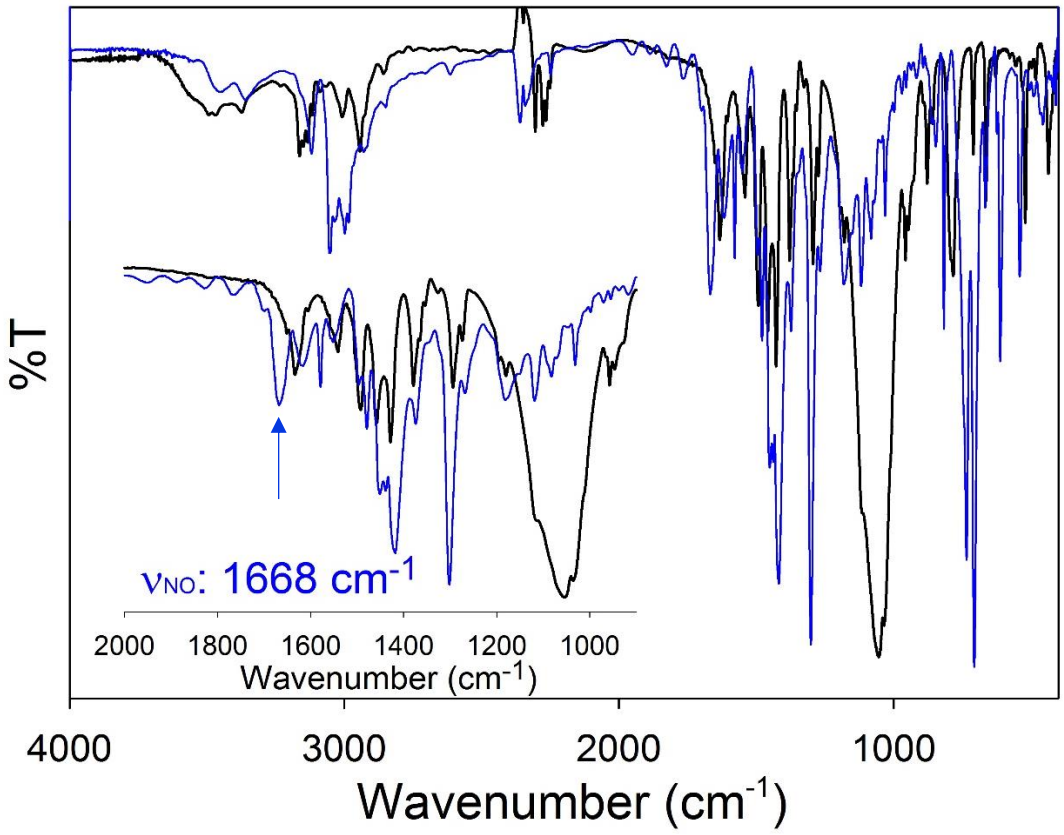

Figure 4.S20. FTIR spectra of $[Co(LN_4^{PrIm})(MeCN)_2](BF_4)_2$ (**1**) (black) and $\{CoNO\}^9$ $[Co(LN_4^{PrIm})(MeCN)(NO)](BPh_4)$ (**5**) (blue) synthesized from route 3 in a KBr matrix.

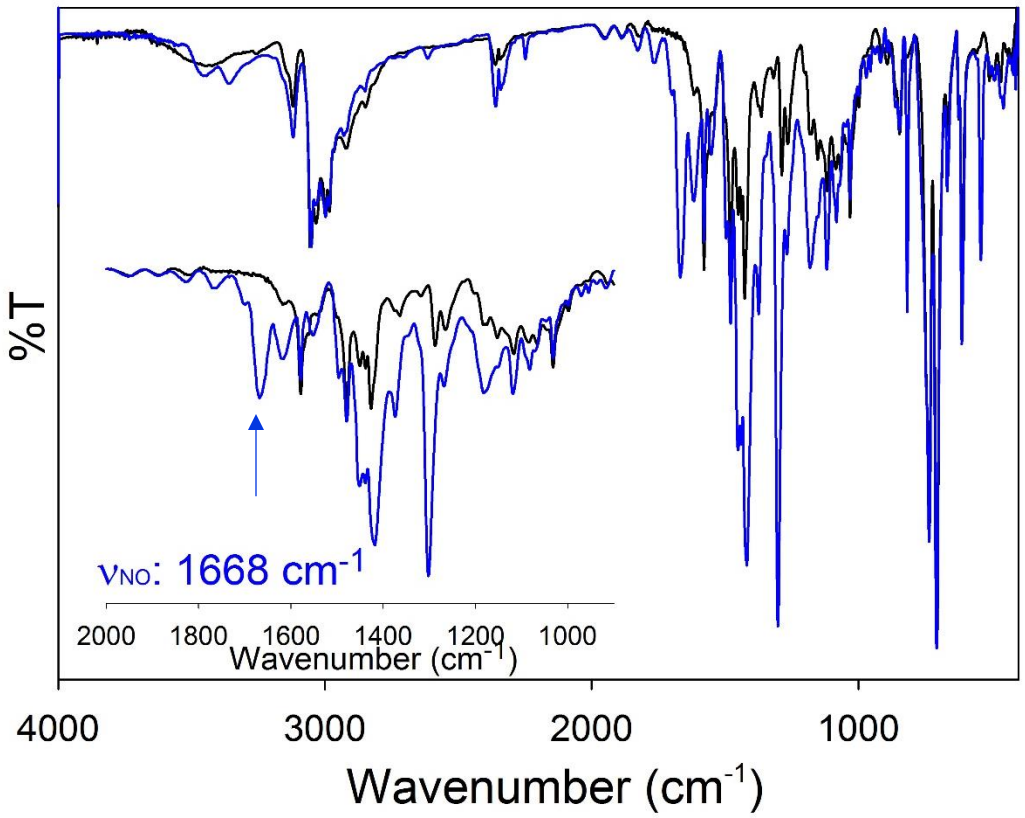

Figure 4.S21. FTIR spectra of $[Co(LN_4^{PrIm})(LN_4^{PrIm}\text{-}\kappa^2\text{-}C,N)]_2(BPh_4)_2$ (**2**) (black) and $\{CoNO\}^9$ $[Co(LN_4^{PrIm})(MeCN)(NO)](BPh_4)$ (**5**) (blue) in a KBr matrix.

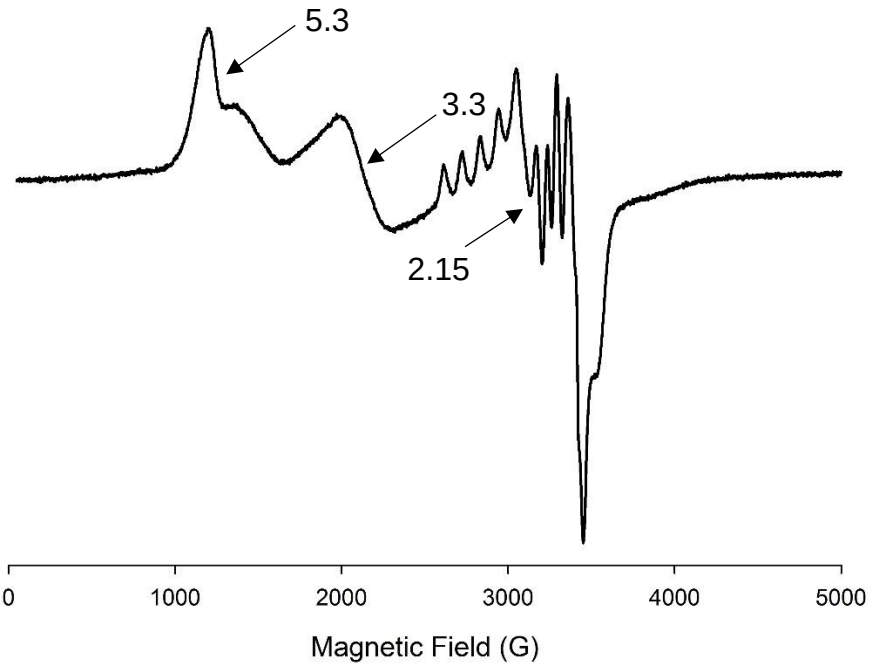

Figure 4.S22. X-band EPR spectrum of [Co(LN_4^{PrIm})(MeCN)(NO)](BPh_4) (**5**) synthesized from route 2 at 10 K. Spectrometer settings: microwave frequency, 9.582 GHz; microwave power, 1.0 mW; modulation frequency, 100 KHz; modulation amplitude, 6.477 G. The higher *g* values are due to by-products such as **1**.

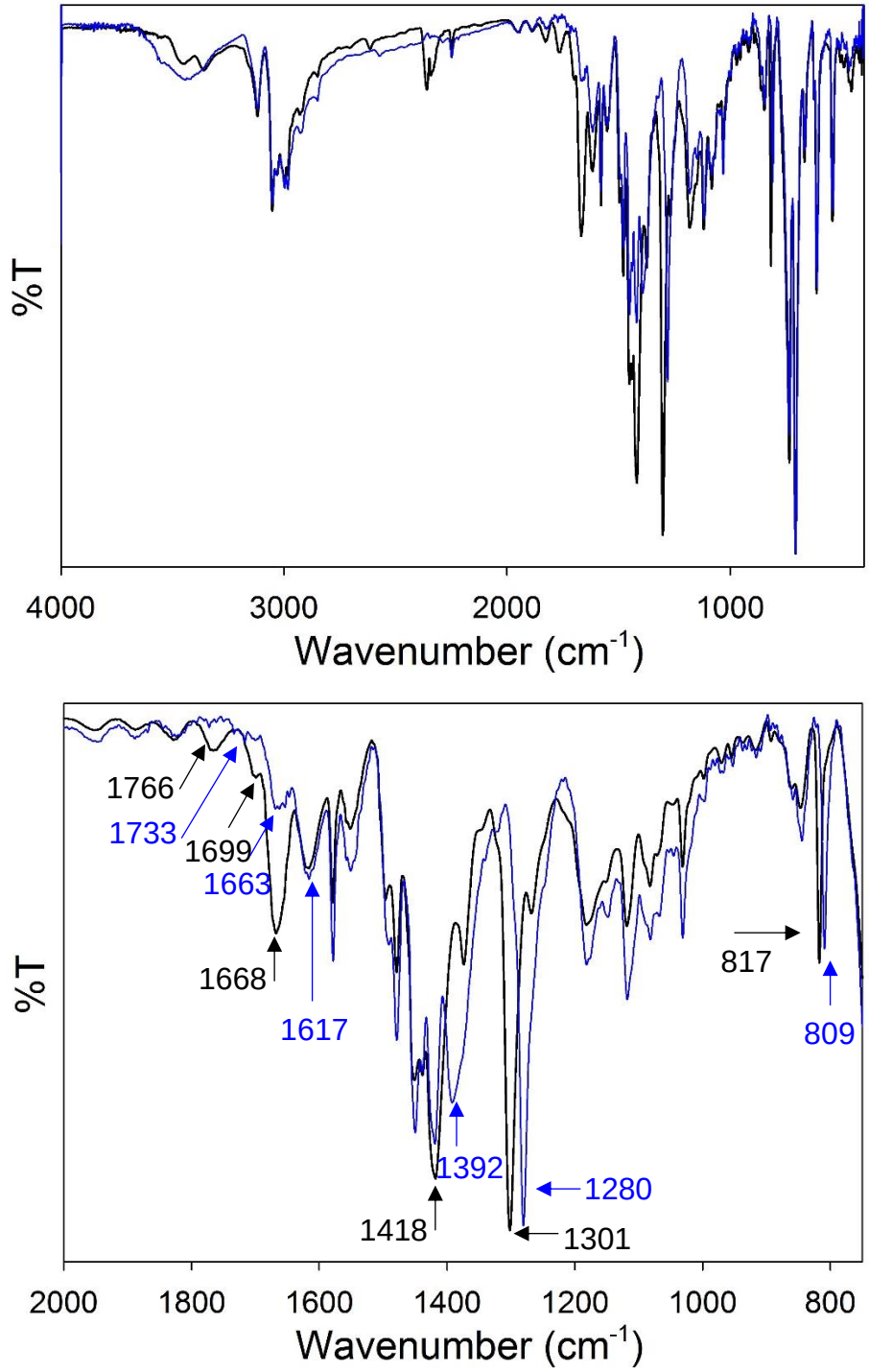

Figure 4.S23. FTIR spectra of [Co(LN$_4^{PrIm}$)(MeCN)(NO)](BPh$_4$) (**5**) (black) and [Co(LN$_4^{PrIm}$)(MeCN)(^{15}NO)](BPh$_4$) (**5-^{15}NO**) (blue) in a KBr matrix.

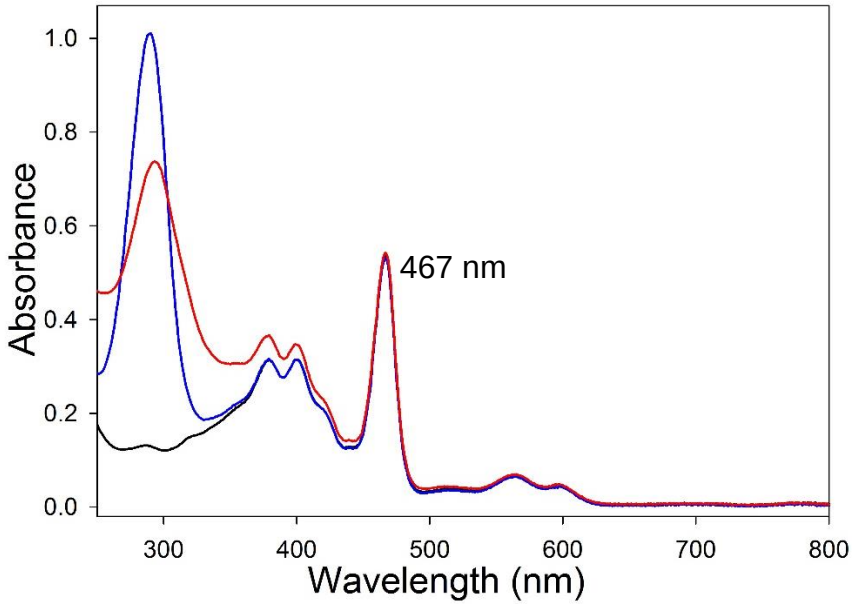

Figure 4.S24. UV-vis spectrum of a 5.98 μM solution of $[Mn^{III}(TPPS)]^{3-}$ before (black line) and after (red line, t = 1 min; blue line, t = 20 h) reaction with $\{CoNO\}^8$ **3** (5 equiv) at 298 K in 10 mM PBS (pH 7.4).

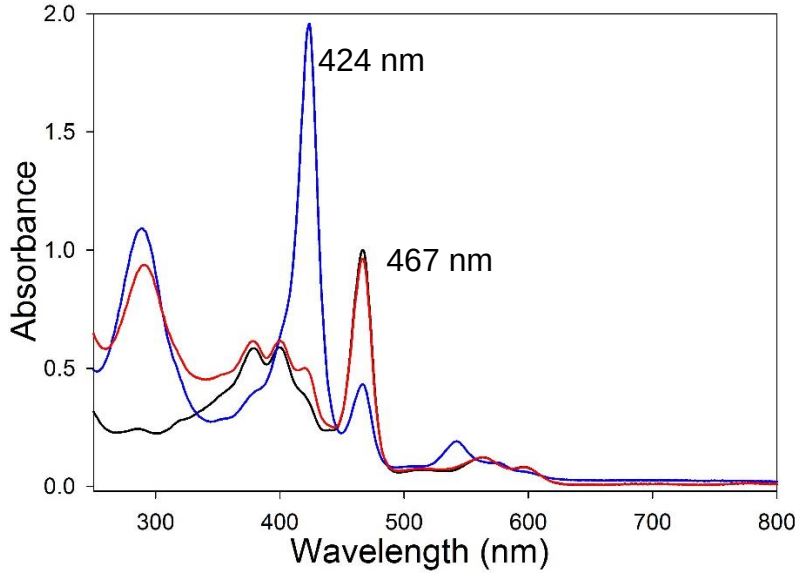

Figure 4.S25. UV-vis spectrum of a 7.77 μM solution of $[Mn^{III}(TPPS)]^{3-}$ (black line) after the addition of $\{CoNO\}^8$ **3** (5 equiv; red line) and after the addition of NaSH (5 equiv; t = 3.5 h: blue line) at 298 K in 10 mM PBS (pH 7.4).

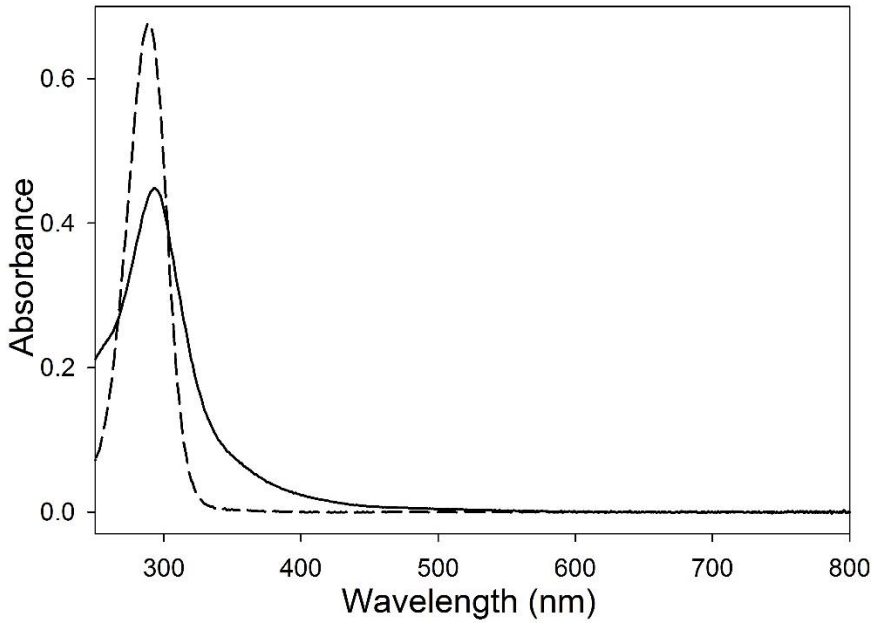

Figure 4.S26. UV-vis spectral monitoring of the stability of a 21.7 μM solution of $[Co(LN_4^{PrIm})(S)(NO)](BF_4)_2$ (**3**) solution (t = 0 min, black; t = 20 h, dash) in 10 mM PBS (pH 7.4), 298 K.

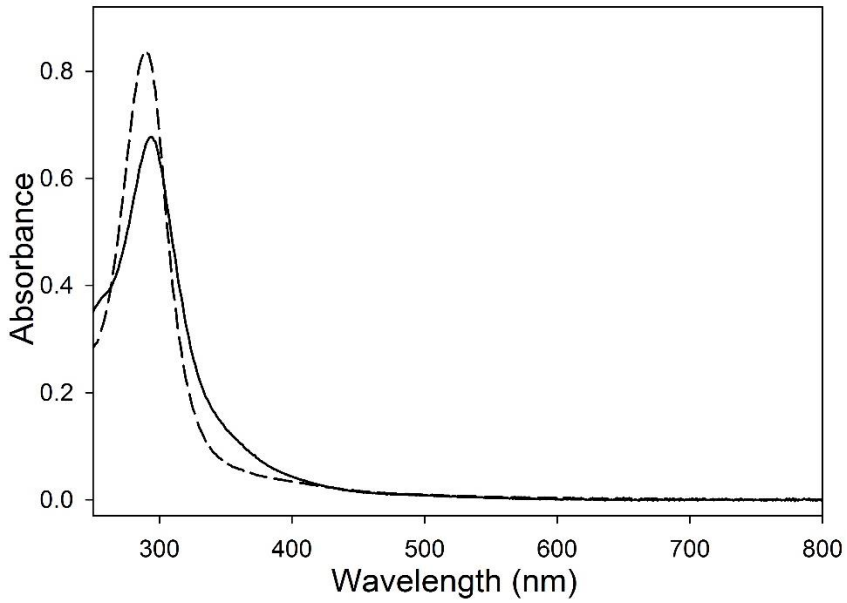

Figure 4.S27. UV-vis spectrum of a 33.1 μM solution of $\{CoNO\}^8$ **3** before (black line) and after (dashed line; t = 20 h) reaction with NaSH (1:1) in 10 mM PBS (pH 7.4), 298 K.

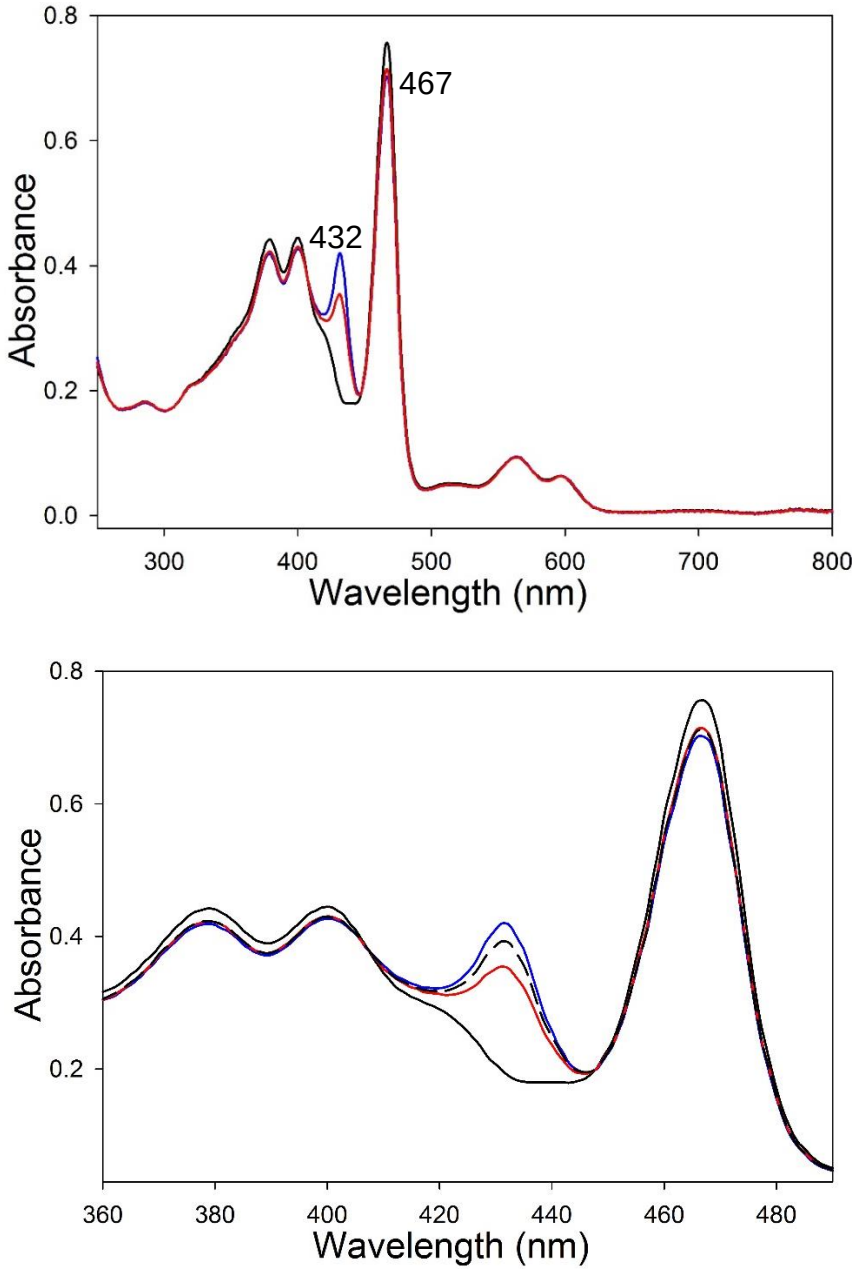

Figure 4.S28. (*Top*) UV-vis spectrum of a 6.53 μM solution of $[Mn^{III}(TPPS)]^{3-}$ (black line) after the addition of NaSH (5 equiv; t = 11.5 h: blue line; t = 20 h: red line) at 298 K in 10 mM PBS (pH 7.4). The band at λ_{max} 432 nm could be a result of HS^- binding to the Mn^{III}-center or to the porphyrin ring.[94] The band at λ_{max} = 432 nm gradually increases over 11.5 h, then decreases for the next 8.5 h. (*Bottom*) Expansion of the Soret band region; black dashed line: t = 2 h after addition of NaSH to the $[Mn^{III}(TPPS)]^{3-}$ solution.

4.10 References

(1) Fukuto, J. M.; Carrington, S. J.; Tantillo, D. J.; Harrison, J. G.; Ignarro, L. J.; Freeman, B. A.; Chen, A.; Wink, D. A. *Chem. Res. Toxicol.* **2012**, *25*, 769.

(2) Li, L.; Moore, P. K. *Biochem. Soc. Trans.* **2007**, *35*, 1138.

(3) Li, Q.; Lancaster, J. R., Jr. *Nitric Oxide* **2013**, *35*, 21.

(4) Meyer, B.; Ward, K.; Koshlap, K.; Peter, L. *Inorg. Chem.* **1983**, *22*, 2345.

(5) Li, L.; Rose, P.; Moore, P. K. *Annu. Rev. Biochem.* **2011**, *51*, 169.

(6) Zhang, X.; Bian, J.-S. *ACS Chem. Neurosci.* **2014**, *5*, 876.

(7) Coletta, C.; Papapetropoulos, A.; Erdelyi, K.; Olah, G.; Módis, K.; Panopoulos, P.; Asimakopoulou, A.; Gerö, D.; Sharina, I.; Martin, E.; Szabo, C. *Proc. Natl. Acad. Sci. U.S.A.* **2012**, *109*, 9161.

(8) Eberhardt, M.; Dux, M.; Namer, B.; Miljkovic, J.; Cordasic, N.; Will, C.; Kichko, T. I.; de la Roche, J.; Fischer, M.; Suárez, S. A.; Bikiel, D.; Dorsch, K.; Leffler, A.; Babes, A.; Lampert, A.; Lennerz, J. K.; Jacobi, J.; Martí, M. A.; Doctorovich, F.; Högestätt, E. D.; Zygmunt, P. M.; Ivanović-Burmazović, I.; Messlinger, K.; Reeh, P.; Filipovic, M. R. *Nature Commun.* **2014**, *5*, 4381.

(9) Filipovic, M. R.; Miljkovic, J. L.; Nauser, T.; Royzen, M.; Klos, K.; Shubina, T.; Koppenol, W. H.; Lippard, S. J.; Ivanović-Burmazović, I. *J. Am. Chem. Soc.* **2012**, *134*, 12016.

(10) Filipovic, M. R.; Eberhardt, M.; Prokopovic, V.; Mijuskovic, A.; Orescanin-Dusic, Z.; Reeh, P.; Ivanović-Burmazović, I. *J. Med. Chem.* **2013**, *56*, 1499.

(11) Salnikov, D. S.; Kucherenko, P. N.; Dereven'kov, I. A.; Makarov, S. V.; van Eldik, R. *Eur. J. Inorg. Chem.* **2014**, 852.

(12) Kaczka, E. A.; Wolf, D. E.; Kuehl, F. A., Jr.; Folkers, K. *J. Am. Chem. Soc.* **1951**, *73*, 3569.

(13) Toohey, J. I. *J. Inorg. Biochem.* **1993**, *49*, 189.

(14) Salnikov, D. S.; Makarov, S. V.; van Eldik, R.; Kucherenko, P. N.; Boss, G. R. *Eur. J. Inorg. Chem.* **2014**, *2014*, 4123.

(15) Strianese, M.; Mirra, S.; Bertolasi, V.; Milione, S.; Pellecchia, C. *New J. Chem.* **2015**, *39*, 4093.

(16) Pleus, R. J.; Waden, H.; Saak, W.; Haase, D.; Pohl, S. *J. Chem. Soc., Dalton Trans.* **1999**, 2601.

(17) Brown, K. L. *Chem. Rev.* **2005**, *105*, 2075.

(18) Banerjee, R.; Ragsdale, S. W. *Annu. Rev. Biochem.* **2003**, *72*, 209.

(19) Pallares, I. G.; Brunold, T. C. *Inorg. Chem.* **2014**, *53*, 7676.

(20) Enemark, J. H.; Feltham, R. D. *Coord. Chem. Rev.* **1974**, *13*, 339. $\{MNO\}^n$ where n = number of metal d + NO π^* electrons.

(21) McCleverty, J. A. *Chem. Rev.* **2004**, *104*, 403 and references therein.

(22) Wyllie, G. R. A.; Scheidt, W. R. *Chem. Rev.* **2002**, *102*, 1067 and references therein.

(23) Wright, A. M.; Hayton, T. W. *Comment Inorg. Chem.* **2012**, *33*, 207 and references therein.

(24) Rhine, M. A.; Rodrigues, A. V.; Bieber Urbauer, R. J.; Urbauer, J. L.; Stemmler, T. L.; Harrop, T. C. *J. Am. Chem. Soc.* **2014**, *136*, 12560.

(25) Ellison, M. K.; Scheidt, W. R. *Inorg. Chem.* **1998**, *37*, 382.

(26) Fujita, E.; Chang, C. K.; Fajer, J. *J. Am. Chem. Soc.* **1985**, *107*, 7665.

(27) Franz, K. J.; Doerrer, L. H.; Spingler, B.; Lippard, S. J. *Inorg. Chem.* **2001**, *40*, 3774.

(28) Kozhukh, J.; Lippard, S. J. *J. Am. Chem. Soc.* **2012**, *134*, 11120.

(29) Hess, J. L.; Conder, H. L.; Green, K. N.; Darensbourg, M. Y. *Inorg. Chem.* **2008**, *47*, 2056.

(30) Uyeda, C.; Peters, J. C. *J. Am. Chem. Soc.* **2013**, *135*, 12023.

(31) Patra, A. K.; Dube, K. S.; Sanders, B. C.; Papaefthymiou, G. C.; Conradie, J.; Ghosh, A.; Harrop, T. C. *Chem. Sci.* **2012**, *3*, 364.

(32) Kumar, P.; Lee, Y.-M.; Hu, L.; Chen, J.; Park, Y. J.; Yao, J.; Chen, H.; Karlin, K. D.; Nam, W. *J. Am. Chem. Soc.* **2016**, *138*, 7753.

(33) Kumar, P.; Lee, Y.-M.; Park, Y. J.; Siegler, M. A.; Karlin, K. D.; Nam, W. *J. Am. Chem. Soc.* **2015**, *137*, 4284.

(34) Doyle, M. P.; Pickering, R. A.; Dykstra, R. L.; Cook, B. R. *J. Am. Chem. Soc.* **1982**, *104*, 3392. The species responsible for release of the NO moiety may be a reduced cobalt nitrosyl given the presence of excess reductant.

(35) Doyle, M. P.; Van Doornik, F. J.; Funckes, C. L. *Inorg. Chim. Acta* **1980**, *46*, L111. $[Co(NH_3)_5(NO)]Cl_2$ reacts with both Fe^{III}- and Fe^{II}-heme proteins.

(36) Ungermann, C. B.; Caulton, K. G. *J. Am. Chem. Soc.* **1976**, *98*, 3862.

(37) Caulton, K. G. *J. Am. Chem. Soc.* **1973**, *95*, 4076.

(38) Blanchard, A. A.; Rafter, J. R.; Adams, W. B., Jr. *J. Am. Chem. Soc.* **1934**, *56*, 16.

(39) Coleman, G. W.; Blanchard, A. A. *J. Am. Chem. Soc.* **1936**, *58*, 2160.

(40) Thyagarajan, S.; Incarvito, C. D.; Rheingold, A. L.; Theopold, K. H. *Inorg. Chim. Acta* **2003**, *345*, 333.

(41) Tomson, N. C.; Crimmin, M. R.; Petrenko, T.; Rosebrugh, L. E.; Sproules, S.; Boyd, W. C.; Bergman, R. G.; DeBeer, S.; Toste, F. D.; Wieghardt, K. *J. Am. Chem. Soc.* **2011**, *133*, 18785.

(42) Sacconi, L.; Ghilardi, C. A.; Mealli, C.; Zanobini, F. *Inorg. Chem.* **1975**, *14*, 1380.

(43) Di Vaira, M.; Ghilardi, C. A.; Sacconi, L. *Inorg. Chem.* **1976**, *15*, 1555.

(44) Chuang, C.-H.; Liaw, W.-F.; Hung, C.-H. *Angew. Chem. Int. Ed.* **2016**, *55*, 5190.

(45) Wasser, I. M.; de Vries, S.; Moënne-Loccoz, P.; Schroder, I.; Karlin, K. D. *Chem. Rev.* **2002**, *102*, 1201.

(46) Butler, A. R.; Megson, I. L. *Chem. Rev.* **2002**, *102*, 1155.

(47) Gass, I. A.; Tewary, S.; Nafady, A.; Chilton, N. F.; Gartshore, C. J.; Asadi, M.; Lupton, D. W.; Moubaraki, B.; Bond, A. M.; Boas, J. F.; Guo, S.-X.; Rajaraman, G.; Murray, K. S. *Inorg. Chem.* **2013**, *52*, 7557.

(48) Vinck, E.; Carter, E.; Murphy, D. M.; Van Doorslaer, S. *Inorg. Chem.* **2012**, *51*, 8014.

(49) Bertini, I.; Luchinat, C. *Adv. Inorg. Biochem.* **1984**, *6*, 71.

(50) Banerjee, R. V.; Matthews, R. G. *FASEB J.* **1990**, *4*, 1450.

(51) King, A. E.; Surendranath, Y.; Piro, N. A.; Bigi, J. P.; Long, J. R.; Chang, C. J. *Chem. Sci.* **2013**, *4*, 1578.

(52) Hu, X. H.; Brunschwig, B. S.; Peters, J. C. *J. Am. Chem. Soc.* **2007**, *129*, 8988.

(53) McCleverty, J. A. *Chem. Rev.* **1979**, *79*, 53.

(54) Mason, J.; Larkworthy, L. F.; Moore, E. A. *Chem. Rev.* **2002**, *102*, 913.

(55) Brouwer, M.; Chamulitrat, W.; Ferruzzi, G.; Sauls, D. L.; Weinberg, J. B. *Blood* **1996**, *88*, 1857.

(56) Gwost, D.; Caulton, K. G. *Inorg. Chem.* **1974**, *12*, 414.

(57) Franz, K. J.; Lippard, S. J. *J. Am. Chem. Soc.* **1998**, *120*, 9034.

(58) Franz, K. J.; Lippard, S. J. *J. Am. Chem. Soc.* **1999**, *121*, 10504.

(59) Trogler, W. C.; Marzilli, L. G. *Inorg. Chem.* **1974**, *13*, 1008.

(60) Clarkson, S. G.; Basolo, F. *Inorg. Chem.* **1973**, *12*, 1528.

(61) Rossi, M.; Sacco, A. *Chem. Commun.* **1971**, 694.

(62) Allen, F. H. *Acta Crystallogr. B* **2002**, *58*, 380.

(63) Bruno, I. J.; Cole, J. C.; Edgington, P. R.; Kessler, M.; Macrae, C. F.; McCabe, P.; Pearson, J.; Taylor, R. *Acta Crystallogr. B* **2002**, *58*, 389.

(64) Allen, F. H.; Kennard, O.; Watson, D. G.; Brammer, L.; Orpen, A. G.; Taylor, R. *J. Chem. Soc. Perkin Trans. II* **1987**, S1.

(65) Dugan, T. R.; Sun, X.; Rybak-Akimova, E. V.; Olatunji-Ojo, O.; Cundari, T. R.; Holland, P. L. *J. Am. Chem. Soc.* **2011**, *133*, 12418.

(66) Mo, Z.; Chen, D.; Leng, X.; Deng, L. *Organometallics* **2012**, *31*, 7040.

(67) The structure contains substitutional disorder that involves mixing one of the axial sites with acetonitrile and nitric oxide. In the other axial group, such disorder was also investigated, but it was too minor to be definitive and it was left as 100% acetonitrile. In the mixed site, there are two different coordinated nitrogens. One (N8a) belongs to the acetonitrile, at a refined occupancy of 65%, and the other (N8b) belongs to nitric oxide at a refined occupancy of 35%. .

(68) Dalby, F. W. *Can. J. Phys.* **1958**, *36*, 1336.

(69) Goodwin, J.; Bailey, R.; Pennington, W.; Rasberry, R.; Green, T.; Shasho, S.; Yongsavanh, M.; Echevarria, V.; Tiedeken, J.; Brown, C.; Fromm, G.; Lyerly, S.; Watson, N.; Long, A.; De Nitto, N. *Inorg. Chem.* **2001**, *40*, 4217.

(70) Böttcher, A.; Takeuchi, T.; Hardcastle, K. I.; Meade, T. J.; Gray, H. B.; Cwikel, D.; Kapon, M.; Dori, Z. *Inorg. Chem.* **1997**, *36*, 2498.

(71) Walter, M. R.; Dzul, S. P.; Rodrigues, A.; Stemmler, T. L.; Telser, J.; Conradie, J.; Ghosh, A.; Harrop, T. C. *Submitted.*

(72) Lim, M. H.; Kuang, C.; Lippard, S. J. *ChemBioChem* **2006**, *7*, 1571.

(73) Crimmin, M. R.; Rosebrugh, L. E.; Tomson, N. C.; Weyhermüller, T.; Bergman, R. G.; Toste, F. D.; Wieghardt, K. *J. Organomet. Chem.* **2011**, *696*, 3974.

(74) Tonzetich, Z. J.; Héroguel, F.; Do, L. H.; Lippard, S. J. *Inorg. Chem.* **2011**, *50*, 1570.

(75) Franz, K. J.; Singh, N.; Spingler, B.; Lippard, S. J. *Inorg. Chem.* **2000**, *39*, 4081.

(76) Kozhukh, J.; Lippard, S. J. *Inorg. Chem.* **2012**, *51*, 9416.

(77) Martí, M. A.; Bari, S. E.; Estrin, D. A.; Doctorovich, F. *J. Am. Chem. Soc.* **2005**, *127*, 4680.

(78) Álvarez, L.; Suarez, S. A.; Bikiel, D. E.; Reboucas, J. S.; Batinić-Haberle, I.; Martí, M. A.; Doctorovich, F. *Inorg. Chem.* **2014**, *53*, 7351.

(79) Doctorovich, F.; Bikiel, D. E.; Pellegrino, J.; Suárez, S. A.; Martí, M. A. *Acc. Chem. Res.* **2014**, *47*, 2907.

(80) Shafirovich, V.; Lymar, S. V. *Proc. Natl. Acad. Sci. U.S.A.* **2002**, *99*, 7340.

(81) Collman, J. P.; Ghosh, S.; Dey, A.; Decréau, R. A. *Proc. Natl. Acad. Sci. U.S.A.* **2009**, *106*, 22090.

(82) Connelly, N. G.; Geiger, W. E. *Chem. Rev.* **1996**, *96*, 877.

(83) Millis, K. K.; Weaver, K. H.; Rabenstein, D. L. *J. Org. Chem.* **1993**, *58*, 4144.

(84) Sanders, B. C.; Hassan, S. M.; Harrop, T. C. *J. Am. Chem. Soc.* **2014**, *136*, 10230.

(85) Harrop, T. C.; Tonzetich, Z. J.; Reisner, E.; Lippard, S. J. *J. Am. Chem. Soc.* **2008**, *130*, 15602.

(86) *SMART v5.626: Software for the CCD Detector System*. Bruker AXS: Madison, WI, 2000.

(87) Walker, N.; Stuart, D. *Acta Crystallogr. A* **1983**, *A39*, 158.

(88) Sheldrick, G. M. *SADABS, Area Detector Absorption Correction*, University of Göttingen: Göttingen, Germany, 2001.

(89) Sheldrick, G. M. *SHELX-97, Program for Refinement of Crystal Structures*, University of Göttingen: Göttingen, Germany, 1997.

(90) Sheldrick, G. M. *Acta Crystallogr. A* **2008**, *A64*, 112.

(91) Sheldrick, G. M. *SHELXTL 6.1, Crystallographic Computing System*, Siemens Analytical X-Ray Instruments: Madison, WI, 2000.

(92) Cromer, D. T.; Waber, J. T., *International Tables for X-Ray Crystallography, Vol. IV, Table 2.2B*. The Kynoch Press: Birmingham, England, 1974.

(93) Burnett, M. N.; Johnson, C. K. *ORTEP-III, Report ORNL-6895*, Oak Ridge National Laboratory: Oak Ridge, TN, 1996.

(94) Román-Morales, E.; Pietri, R.; Ramos-Santana, B.; Vinogradov, S. N.; Lewis-Ballester, A.; López-Garriga, J. *Biochem. Biophys. Res. Commun.* **2010**, *400*, 489.

CHAPTER 5

CONCLUSIONS AND FUTURE OUTLOOK

We have successfully designed and synthesized a family of $\{CoNO\}^{8/9}$ complexes and investigated their reactivity as HNO/NO^- donors. We have shown that cobalt nitrosyls are not inert and in fact can be used as HNO/NO^- donors in a number of capacities. We have also shown that interactions of small molecules/ions (e.g., H^+, O_2, $NO^\bullet$, H_2S/HS^-) with cobalt nitrosyls define their reactivity. In Chapter 1, we highlighted the pharmacological implications of HNO, particularly as they relate to cardiovascular physiology, and the need for the further development of HNO donors. Based on the utility of (reduced) metal nitrosyls (M-NO) for the transformation and liberation of N_yO_x within the global nitrogen cycle, M-NO is a logical avenue for donor molecules. The small molecule approach for developing M-NO provides the ability to design complexes that are synthetically accessible and easily modified in order to tune the electronic nature of the M-NO manifold. Modeling our design off of dianionic heme and monoanionic cobalamin ligands found in nature, the first generation of cobalt nitrosyls employed in our studies bear a diimine/dipyrrolide N_4 donor set with a nitrosyl in the apical position (Chapters 2 and 3).

In Chapter 2, we established the H^+-induced HNO donor properties of such a $\{CoNO\}^8$ complex. Given the typical oxidation state assignment of LS Co^{III}-NO^-, $\{CoNO\}^8$ complexes have been widely viewed as inert, and as such, it was unsurprising when no reaction occurred between the $\{CoNO\}^8$ complex and HNO targets such as $[Fe^{III}(TPP)Cl]$ or Ph_3P. However, in the presence

of stoichiometric protons, it readily reacts to form the corresponding [Fe(TPP)(NO)] or $Ph_3P{=}O$/$Ph_3P{=}NH$ respectively. This reactivity shows that $\{CoNO\}^8$ complexes can serve as HNO/NO^- donors. In the absence of such a target, we showed that $\{CoNO\}^8/H^+$ leads to an equilibrium with the corresponding $\{Co(NO)_2\}^{10}$ and $[Co^{III}L]^+$ complexes via a 3C $\{CoNO\}^8$ intermediate. We also showed that reactivity with O_2 led to the Co-η^1-ONO_2 species, which further demonstrated the nucleophilic nature of NO. In Chapter 3, we explored the reactivity of $\{CoNO\}^9$ through the first report of isolated, structurally characterized 5C $\{CoNO\}^9$ complexes. This is a rare and elusive Enemark-Feltham notation. We showed that these complexes could serve as HNO donors in physiological conditions through quantifying N_2O production and reactivity with water-soluble HNO targets like $[Mn^{III}(TPPS)]^{3-}$ and, for our protein studies, metmyoglobin. Computational efforts further supported the spectroscopic and structural characterization of the isolated $\{CoNO\}^9$ complexes and shed insights into the mechanism of HNO release. We determined that upon protonation, a spin-transition occurs in $\{CoNO\}^9$ from HS Co^{II}-$^3NO^-$ to afford $\{CoHNO\}^9$ as LS Co^{II}-^{1}HNO with an elongated Co-N bond primed for the lability of ^{1}HNO. In the absence of an HNO target, competing reactions exist which together form N_2O, $\{CoNO\}^8$, and $\{Co(NO)_2\}^{10}$ as the predominant products. Although these $\{CoNO\}^{8/9}$ systems with diimine/dipyrrolide N_4 donors provide key spectroscopic, structural, and reactive benchmarks, they exhibit poor water solubility and require organic solvents to help facilitate aqueous solubilization.

In Chapter 4, we investigated cobalt nitrosyls that have a diimine/diimidazole ligand in order to enhance the water solubility and shift the redox potential of the $\{CoNO\}^{8/9}$ couple closer to the biological window (Chapters 2 and 3: $E_{1/2}$ of Co-NO: ~ –1.3 V; Chapter 4: $E_{1/2}$ of Co-NO: ~ –0.5 V vs. Fc^+/Fc). There are significant biological implications of the interactions of small

molecule signaling agents, many of which share biological targets thus placing them in close proximity. We probed the reactivity of a $\{CoNO\}^8$ complex with $NO^{\bullet}$ and H_2S/HS^- in order to determine the fate of such species with a coordinated nitrosyl. The former reaction leads to disproportionation of the coordinated NO by free $NO^{\bullet}$, thus forming the corresponding Co-η^1-ONO. This is an uncommon but not an unprecedented phenomenon. The latter reaction leads to H_2S/HS^--induced release of HNO from an otherwise unreactive $\{CoNO\}^8$ complex, possibly through a Co-HSNO intermediate. This remarkable finding highlights the probable integrated biochemistry of such small molecules facilitated by a metal center. Further studies are required in order to fully understand the by-products and mechanism of this reaction. These exciting results show the importance of investigating the fate of small molecules at a metal center and the resulting downstream signaling cascades that could be occurring in biology and physiology.

There are many avenues that require further exploration. Further analysis is needed with the diimine-/diimidizole platform in order to (i) further examine the mechanism by which H_2S-induced release of HNO is occurring and (ii) isolate $\{CoNO\}^9$ and investigate its properties. Similarly, the crosstalk of small molecule signaling agents such as $NO^{+/\bullet/-}$ with M-bound HS^- is also critical to understanding whether the fate of such reactions differs based on the coordinated molecule. Secondary sphere interactions could be utilized in order to stabilize reactive intermediates/species that form from these reactions. In fact, the Nε of the imidazole provides a modular point for secondary sphere modifications that could incorporate H-bonding donors. Finally, based on the multiple oxidation states that cobalamins traverse in their enzymatic cycles, it would be of great utility to investigate the reaction of $NO^{\bullet}$ and H_2S/HS^- with not only $\{CoNO\}^{8/9}$ but also the corresponding $Co^{III/II/I}$ complexes. Further scrutiny of the integrated biochemistry of small molecule signaling agents at a redox-active metal center will improve our understanding of

the physiological mechanisms of neurotransmission and biology. In summary, we have carefully designed and synthesized two $\{CoNO\}^{8/9}$ families. Their characterization will serve as spectroscopic and structural benchmarks for cobalt nitrosyls. Their reported reactivity highlights the great potential for using such molecules as HNO donors, cardiovascular therapeutics, and as systems that can shed further insights into the crosstalk of signaling agents at a metal center. This work serves as the foundation for realizing the therapeutic capacity of cobalt nitrosyls as well as further elucidating the nature of M-NO traversed in biology.